A systematic study of palmitoylation using the model organism *Caenorhabditis elegans*

Thesis submitted in accordance with the requirements of the University of Liverpool for the degree of Doctor in Philosophy by

Matthew James Edmonds

April 2013

ACKNOWLEDGEMENTS

First and foremost, I would like to thank my supervisor, Prof. Alan Morgan. No matter what set of results I turned up with to his office they always seemed much better when I left! He accommodated my often eccentric working hours and had apparently never-ending patience whilst I prepared this thesis. It was a pleasure to work for him and his support and positivity, especially when nothing seemed to be working, was fully appreciated. I am also grateful to Dr Mary Doherty for kindly performing the mass spectrometry for us and to Tim Frost for helping to collect some of the phenotypic data.

Special thanks go to two people who have been a major force in shaping me over the past four years. I've shared an office with James Johnson from my MRes project on. He imparted his sense of humour and apparently magical ability to clone anything and taught me the majority of the techniques I used during this project. He's also responsible for getting me hooked on Radio 4, audiobooks and all forms of comedy. Then there's Leanne Bloxam. She brought her own special personality into the office and made every day full of laughs. And I know a lot more Bruce Springsteen songs and ways of swearing now…

I owe a lot to the members of Red Block past and present. Thanks to Bob Burgoyne and Jeff Barclay for advice on the project; to Hannah McCue for always being happy to talk and often to share in my rants; to Dayani Rajamanoharan, Xi Chen, Sudhanva Kashyap, Vicky Martin, Pryank Patel, Mimi Ayala, Joanna Wardyn, Sarah Darling, Joe Zeguer, Marie Cawkwell, Margaret Graham, Michèle Riesen, Ciara Walsh, Andy Herbert and Lee Haynes for making the lab such a great environment to work in; also to Helen Barclay and Geoff Williams for solving lab and admin issues as they arose.

Thanks to those people who kindly read and commented on draft chapters of this thesis: Hannah McCue, James Johnson, Martin Smith, and of course Alan Morgan. Special thanks to Martin for being relentlessly enthusiastic and always taking the time to go through talks, posters and writing with me. Martin, his family and Daiva Puraite have given us numerous excellent days out on those rare occasions when we could both get away from the lab!

Finally, the people who helped me through: thanks to Laura, who put up with countless evenings on her own while I stayed in the lab and whose support never wavered; to my parents and in-laws, who were always there for me; to Chris Duncalf, who was an excellent best man and gave me excuses to take days off; to Liz Colby for her empathy during our PhDs; and to all my friends near and far who took the time to ask me how it was going.

ABSTRACT

Palmitoylation is a reversible post-translational modification of proteins which involves the addition of the C16 saturated fatty acid palmitic acid to sulfhydryl groups on cysteine residues, forming a thioester linkage. The addition of palmitate allows proteins to associate with different cellular membranes and membrane subdomains. Palmitoylation is catalysed by the DHHC family of palmitoyl-acyl transferases (PATs), named for their characteristic DHHC motif in a cysteine-rich domain (CRD). Reversibility is conferred by palmitoyl-protein thioesterases (PPTs), which cleave the thioester linkage. The study of palmitoylation has recently gathered pace with the development of methods which allow proteome-scale identification of candidate palmitoyl-proteins.

Despite the importance of model organisms in several key studies in the field, palmitoylation has barely been studied in the simple eukaryote *Caenorhabditis elegans*, the nematode worm. This study commenced with the use of the *C. elegans* genome data to identify its PATs and PPTs, using the DHHC-CRD and homology respectively. The 15 DHHC PATs were officially named using a dhhc-x system and the two previously known PPTs were confirmed as the only ones with homology to other known PPTs. The current knowledge on palmitoylation enzymes and substrates was collated and analysed to predict possible phenotypes resulting from mutation or knockdown of the enzymes and potential substrates.

All available *C. elegans* strains containing a mutation in an individual PAT or PPT were obtained, covering about half of the PATs and both PPTs, and assayed for various gross phenotypes. In addition a complete library of bacteria able to express double-stranded RNA against PAT or PPT genes was sourced and used to perform similar assays using feeding RNA interference (RNAi). A number of small but significant differences were seen both with mutant and RNAi-treated strains, especially in lifespan assays. To test for possible redundancy and compensation amongst the enzymes, double RNAi was performed against selected closely related PATs and both PPTs. This resulted in the largest phenotype seen: a reduction in lifespan after simultaneous knockdown of both *ppt-1* and *ath-1*.

As there are no known palmitoyl-proteins in *C. elegans*, the proteomic approaches acyl-biotin exchange (ABE) and acyl-resin-assisted capture (acyl-RAC) were employed to provide a list of candidates. These were first optimised using rat brain material and the results compared with previous proteomic studies to find that two-thirds of the hits had been previously found. With this validation, both methods were applied to wild-type

C. elegans lysates to give 91 hits as putative palmitoyl-proteins. Mutants for the PPT *ath-1* were also profiled by ABE, showing 33 hits which were not present in the wild-type profile. These are potential ATH-1 substrates whose lack of depalmitoylation in the mutant leads to their enrichment relative to wild-type. However, further repeats of these analyses are required for rigorous statistical testing.

Taken together, this study shows the first characterisation of palmitoylation in *C. elegans*, encompassing all of the DHHC PAT and PPT enzymes, putative palmitoyl-proteins and potential substrates of the PPT enzyme ATH-1.

ABBREVIATIONS

17-ODYA	17-octadecynoic acid
2-BP	2-bromopalmitate
5-HT	5-hydroxytryptamine; serotonin
β4GalNAcTB	β1,4-N-acetylgalactosaminyl-transferase B
β-ME	β-mercaptoethanol
AAP	amino acid permease
AAT	amino acid transporter
ABCA1	ATP-binding cassette transporter A1
ABE	acyl-biotin exchange
ABF	antibacterial factor related
ABT	ABC transporter family
acyl-RAC	acyl-resin-assisted capture
AD	Alzheimer's disease
Ade	adenine-requiring
AF	*Anoplopoma fimbria*
Agp	high affinity glutamine permease
AID	amyloid precursor protein-interacting DHHC
AIP	arsenite inducible RNA associated protein
Akr	ankyrin repeat-containing
ALP	α-actinin-associated LIM protein (ALP)-Enigma family protein
AMPA	α-amino-3-hydroxy-5-methyl-4-isoxazolepropionic acid
ANCL	adult-onset neuronal ceroid lipofuscinosis
ANOVA	analysis of variance
Anr	Avl nine related family
app	approximated
APS	ammonium persulphate
APT	acyl-protein thioesterase
APV	2-amino-5-phosphonovalerate
AR	androgen receptor
ASC	absence of growth suppressor of Cyp1
ASP	aspartyl protease
ATH	acyl-protein thioesterase
ATP	adenosine triphosphate
BAC	bacterial artificial chromosome
BACE1	β-site amyloid precursor protein-cleaving enzyme 1
Bap	branched-chain amino acid permease
BCA	bicinchoninic acid
Bet	blocked early in transport
biotin-BMCC	1-biotinamido-4-[4'-(maleimidomethyl)cyclohexanecarboxamido]butane
biotin-HPDP	N-[6-(biotinamido)hexyl]-3'-(2'-pyridyldithio)propionamide
BLAST	basic local alignment search tool
BOS	bet one suppressor
bp	base pairs
BSA	bovine serum albumin
cAMP	cyclic adenosine monophosphate
caspase	cysteinyl-aspartyl protease
Ccl	C-C motif chemokine
CD	cluster of differentiation
Cdc	cell division cycle
CE	*Caenorhabditis elegans*
Chs	chitin synthase related
CKAP	cytoskeleton-associated protein
CKSAAP	composition of *k*-spaced amino acid pairs
CL3/CaMKIγ	Ca^{2+}/calmodulin-dependent protein kinase CLICK-III/ calmodulin-dependent protein kinase 1γ
CMK	Ca^{2+}/calmodulin-dependent protein kinase
CNQX	6-cyano-7-nitroquinoxaline-2,3-dione
CNS	central nervous system
CoA	coenzyme A
CoASH	unacylated coenzyme A
CON	control sample
COS	CV-1 origin, simian vacuolating virus 40 transformed
CPS	cell death abnormality 3 (CED-3) protease suppressor
CRD	cysteine-rich domain
CSNK	casein kinase
CSP	cysteine string protein
CSS	clustering and scoring strategy
DARPP32	dopamine- and cAMP-regulated phosphoprotein of 32 kDa
DCR-1	dicer related 1
DD	*Dictyostelium discoideum*
DEPC	diethyl pyrocarbonate
DHHC	DHHC domain-containing enzyme; palmitoyl acyl-transferase

Dlg	discs large tumour suppressor
DLG	*Drosophila* discs large homologue (*C. elegans*)
DM	*Drosophila melanogaster*
DNA	deoxyribonucleic acid
DNJ	DnaJ domain-containing protein
dNTP	deoxyribonucleotide triphosphate
Dnz1	DNZDHHC/NEW1 zinc finger protein 11
Dpy	dumpy
DR4	tumour necrosis factor-related apoptosis-inducing ligand receptor 1
DRS	Dent's Ringer solution
dsRNA	double stranded RNA
DTT	dithiothreitol
EARS	glutamyl amino-acyl tRNA synthetase
ECL	enhanced chemiluminescence
EDTA	ethylenediaminetetraacetic acid
Egl	egg-laying defective
EGO	enhancer of abnormal germline proliferation 1 (GLP-1)
EM	electron microscopy
EMB	abnormal embryogenesis
EMS	ethyl methane sulphonate
eNOS	endothelial nitric oxide synthase
Env	late endosome and vacuole interface function
ER	endoplasmic reticulum
ER	oestrogen receptor
Erd	ER retention defective
Erf	effect on Ras function
eri	enhanced RNAi
Ers	Erd suppressor
EXP	experimental sample
FB	fibrous body
FRAP	fluorescence recovery after photobleaching
Frk	fatty acyl-CoA synthetase and RNA processing-associated kinase
FUdR	fluorodeoxyuridine
GABA	γ-amino butyric acid
GABPI	β1,4-N-acetylgalactosaminyl-transferase B pilot
GAD	glutamate decarboxylase
Gap	general amino acid permease
GAP43	growth-associated protein of 43 kDa
GCP16	Golgi complex-associated protein of 16 kDa
GLR	glutamate receptor family (AMPA)
GluT	glucose transporter
Gnp	glutamine permease
GOA	G protein α_o subunit
GOI	gene of interest
Gpa	G-protein α subunit
GPI	glycosylphosphatidylinositol
GRIP	glutamate receptor interacting protein
GTP	guanosine triphosphate
GTPase	guanosine triphosphatase
h	hours
HA	haemagglutinin
HA	hydroxylamine
HB	homogenisation buffer
HD	Huntington's disease
HDFP	hexadecylfluorophosphonate
HEK293	human embryonic kidney cells
Hem	heme biosynthesis
HEPES	4-(2-hydroxyethyl)-1-piperazineethanesulfonic acid
Hhat	Hedgehog acyltransferase
Him	high incidence of males
Hip	huntingtin-interacting protein
Hip (yeast)	histidine permease
HPO	hypersensitive to pore-forming
HRP	horseradish peroxidase
HS	*Homo sapiens*
HSPG	heparan sulphate proteoglycan
Htt	huntingtin
ICAT	isotope coded affinity tag
IMA	importin α family
INA	integrin α
INCL	infantile neuronal ceroid lipofuscinosis
IPTG	isopropyl β-D-1-thiogalactopyranoside
Jnk	c-Jun N-terminal kinase
L	Laemmli
LB	Luria-Bertani broth
LB (ABE)	lysis buffer
LB-T	lysis buffer containing 0.2% Triton X-100
Lcb	long-chain base
Lck	lymphocyte-specific tyrosine kinase
LET	lethal

LFQ	label-free quantification
LGC	ligand-gated ion channel
LIM	domain found in Lin11, Isl-1 and MEC-3
Lpcat1	acyl-CoA: lysophosphatidylcholine acyltransferase 1
LRP	lipoprotein receptor-related protein
Lsb	local anestheticum sensitive (Las) seventeen binding protein
m	minutes
MAGI	membrane associated guanylate kinase inverted homologue
MBOAT	membrane-bound *O*-acyltransferase
MDCK	Madin-Darby canine kidney epithelial cells
mec	mechanosensory abnormality
Meh	multicopy suppressor of Ers1 hygromycin B sensitivity
MeOH	methanol
mEPSC	miniature excitatory postsynaptic current
MGST3	microsomal glutathione *S*-transferase 3
MIP	macrophage inflammatory protein
MKK7	mitogen-activated protein kinase kinase 7
Mlf	multicopy suppressor of leflunomide activity
MM	*Mus musculus*
MMTS	methyl methanethiosulphonate
Mnn	mannosyltransferase
MO	membranous organelle
MosDEL	*Mos1*-mediated targeted deletion
MosSCI	*Mos1*-mediated single copy insertion
MosTIC	*Mos1*-induced transgene-instructed gene conversion
mRNA	messenger RNA
MS	mass spectrometry
Mse	mitochondrial glutamyl-tRNA synthetase
MSP	major sperm protein
MudPIT	multi-dimensional protein identification technology
Munc18	mammalian orthologue of UNC-18
MW	molecular weight
N,N-DMF	N,N-dimethylformamide
NADPH	reduced nicotinamide adenine dinucleotide phosphate
NCAM	neural cell adhesion molecule
NCBI	National Center for Biotechnology Information
NCL	neuronal ceroid lipofuscinosis
Nde1	nuclear distribution protein nudE homologue 1
Ndel1	nuclear distribution protein nudE-like 1
NEM	N-ethylmaleimide
NGM	nematode growth medium
NHR	nuclear hormone receptor
NIDD	nNOS-interacting DHHC domain-containing protein with dendritic mRNA
nNOS	neural nitric oxide synthase
NO	nitric oxide
NPR	neuropeptide receptor family
NR2A/B	N-methyl-D-aspartate receptor subunits 2A/2B
NRDE	nuclear RNAi defective
NSF	NEM-sensitive fusion protein
Nuc	nuclease
NUD	*Aspergillus* nuclear division related
o/n	overnight
OASIS	online application for survival analysis
odr	chemotaxis-defective
ORF	open reading frame
PaCCT	palmitoyltransferase conserved C-terminus
palm	palmitate
PalmPISC	palmitoyl protein identification and site characterisation
PAT	palmitoyl acyl-transferase
PAT	paralysed arrest at two-fold (*C. elegans*)
PBS	phosphate buffered saline
PCR	polymerase chain reaction
PDE	phosphodiesterase
PDZ	PSD-95/Dlg1/zo-1 domain
PEP	carboxypeptidase Y-deficient
Pfa	protein fatty acyltransferase
PI	protease inhibitor cocktail
PI4KIIα	phosphatidylinositol 4-kinase type IIα
PICA	palmitoyl-cysteine isolation capture and analysis

Pin	Psi+ inducibility
PM	plasma membrane
PPI	pre-pulse inhibition
PPT	palmitoyl-protein thioesterase
PR	progesterone receptor
PSD	post-synaptic density
Psr	plasma membrane sodium response
R7BP	regulator of G protein signalling 7 family binding protein
rcf	relative centrifugal force
RGS	regulator of G protein signaling
Rho	Ras homolog
RhoGDI	Rho guanine nucleotide dissociation inhibitor
Ric	resistance to inhibitors of cholinesterase
Rif	repressor activator protein 1-interacting factor
RISC	RNA-induced silencing complex
RNA	ribonucleic acid
RNAi	RNA interference
ROS	reactive oxygen species
rpm	revolutions per minute
Rps11	ribosomal protein S11
rrf	RNA-dependent RNA polymerase family
RT	room temperature
RT-PCR	reverse transcriptase polymerase chain reaction
Sam	*S*-adenosylmethionine metabolism
SAP	shrimp alkaline phosphatase
SB	solubilisation buffer
SC	*Saccharomyces cerevisiae*
Scamp	secretory carrier membrane protein
SC-GT	yeast genetic interaction
SCPL	small C-terminal domain phosphatase-like phosphatase
SDS	sodium dodecyl sulphate
SDS-PAGE	sodium dodecyl sulphate polyacrylamide gel electrophoresis
SEC	secretion mutant
SERZ	Sertoli cell gene with a zinc finger domain
SGD	*Saccharomyces* Genome Database
Shh	Sonic Hedgehog
Shr	suppressor of hyperactive Ras
sid	systemic RNAi defective
SILAC	stable-isotope labeling with amino acids in cell culture
siRNA	small interfering RNA
SLO	slowpoke K^+ channel family
Sna	sensitivity to Na^+
SNAP	soluble NSF-attachment protein
SNAP-25	synaptosome-associated protein of 25 kDa
SNARE	SNAP receptor
SNB	synaptobrevin
Snc	suppressor of the null allele of cyclase associated protein
SNT	synaptotagmin
SOC	super optimal broth with catabolite repression
Sog	short gastrulation
Spe	spermatogenesis deficient
SPHK	sphingosine kinase
SRC	SRC oncogene related
SRU	serpentine receptor, class U
SS	*Salmo salar*
Sso	suppressor of Sec one
SSTR5	somatostatin receptor 5
Ste	sterile
STO	stomatin
STREX	stress-related exon splice variant of large conductance Ca^{2+}- and voltage-activated K^+ channels
Swf	spore wall formation
Syn	syntaxin (*S. cerevisiae*)
SYN	syntaxin (*C. elegans*)
SYX	syntaxin (*C. elegans*)
TAE	Tris acetate EDTA buffer
tag	temporarily assigned gene name
Tat	tyrosine and tryptophan amino acid transporter
Tba	tubulin α
TBC	Tre-2/Bub2/Cdc16 domain family
TBS	Tris-buffered saline
TBS-T	Tris-buffered saline with 0.1% Tween 20
TEMED	N,N,N',N'-tetramethylethylenediamine
TIRFM	total internal reflection fluorescence microscopy
Tlg	t-SNARE affecting a late Golgi compartment
TMD	transmembrane domain

TMP	trimethylpsoralen
tRNA	transfer RNA
TSP	tetraspanin
Tub	tubulin
Tul	transmembrane ubiquitin ligase
TVP	Tlg2-vesicle protein
UB	unbound
Unc	uncoordinated
UTR	untranslated region
UV	ultraviolet light
Vac	vacuole-related
VAM	vacuolar morphogenesis
VAMP	vesicle-associated membrane protein
v-SNARE	vesicle SNARE protein
WHB	worm homogenisation buffer
XLMR	X-linked mental retardation
XT	*Xenopus tropicalis*
YFP	yellow fluorescent protein
YKT-6	yeast Ykt6 v-SNARE homologue
ZDHHC	zinc finger-containing DHHC enzyme
ZM	*Zea mays*
zo	zonula occludens

Chapter 1:

INTRODUCTION

1.1 POST-TRANSLATIONAL LIPID MODIFICATIONS

Proteins are the workhorses of life at the subcellular level. They show an astonishing variety of forms and functions dictated by the physical and chemical properties of their primary amino acid sequence. These properties allow the formation of catalytic sites, channel pores, binding sites and structural units to name but a few. On top of this diverse functionality lies another layer of complexity afforded by post-translational modifications. The addition of chemical adducts to specific parts of proteins allows their function to be regulated with respect to changes in the environment or temporal effects. Phosphorylation, arguably the most studied, involves the addition and removal of phosphate groups and often serves to modulate enzymatic activity. There is, however, a panoply of larger accessory chemical groups which serve as post-translational modifications. These may be based on sugars, as in glycosylation; peptides, as in ubiquitination; and lipids.

The discovery that proteins could have a lipid moiety was made in 1951 with the observation that some protein material could be purified from brain tissue which was insoluble in aqueous solvents but soluble in mixtures of chloroform and methanol (Folch and Lees, 1951). No proteins had previously been observed to be soluble in these mixtures and various protocols for extracting them from tissues were developed (Folch-Pi and Stoffyn, 1972). The main types of protein lipidation which occur in eukaryotes are prenylation, myristoylation and palmitoylation, the subject of this thesis. The first identification of a protein modified with palmitic acid was a vesicular stomatitis virus glycoprotein (Schmidt and Schlesinger, 1979) and the first palmitoylated eukaryotic protein discovered was the transferrin receptor, whose modification was shown to be sensitive to treatment with hydroxylamine (HA) (Omary and Trowbridge, 1981). This chapter will give an introduction to lipid modifications of proteins in general, followed by a discussion of the enzymes required for addition and removal of palmitate and progress in the field to date.

1.1.1 PRENYLATION AND MYRISTOYLATION

Prenylation occurs post-translationally at a C-terminal CaaX motif (where “a” is an aliphatic residue, i.e. one lacking an aromatic ring). An irreversible thioether link is formed between the cysteine residue and a 15-carbon farnesyl or a 20-carbon geranylgeranyl group by farnesyltransferase or geranylgeranyltransferase I respectively before cleavage of the C-terminal aaX (Resh, 2006). The identity of the amino acid at residue X determines whether the protein will be farnesylated or geranylgeranylated: an alanine, cysteine,

glutamine, methionine or serine residue results in farnesylation, whereas a leucine or phenylalanine residue results in geranylgeranylation (Maurer-Stroh and Eisenhaber, 2005). Finally the prenylated cysteine residue is carboxymethylated in the endoplasmic reticulum (ER). Proteins which are commonly prenylated include many signalling proteins, such as Ras proteins (Braun and Fenaux, 2008; Resh, 2006), which may have implications in cancer.

Myristoylation is an irreversible fatty acylation which occurs on approximately 0.5% of proteins (Maurer-Stroh *et al.*, 2002). It is the addition of a 14-carbon saturated or unsaturated fatty acid to glycine residues. The fatty acid used is usually myristate, which was originally discovered as a group blocking Edman degradation of the N-terminus of cyclic adenosine monophosphate (cAMP)-dependent protein kinase (Carr *et al.*, 1982). Its co-translational addition to the N-terminal sequence MGXXX(S/C/T) through an amide bond after removal of the initial methionine by methionine aminopeptidase is catalysed by myristoyl-coenzyme A (CoA):protein *N*-myristoyltransferase (NMT) (Martin *et al.*, 2011), leaving an amide link to the glycine residue. Myristoylation is presumably a fundamentally important modification of some proteins, as fungi require it for viability and one of the vertebrate enzymes, NMT-1, is required for early development and cell division (Resh, 2006; Yang *et al.*, 2005). Myristoylation can also occur post-translationally to internal glycines in the consensus sequence DEVDGXXX(S/C/T) when it is exposed by cysteinyl-aspartyl proteases (caspases) in apoptotic cells, for example on the apoptotic protein Bid (Zha *et al.*, 2000). Although normally occurring on glycine residues, myristoylation has been observed on lysine residues by an amide linkage in the insulin receptor (Hedo *et al.*, 1987) and interleukin 1 subunits (Bursten *et al.*, 1988).

Most lipid modifications serve to attach soluble proteins to cellular membranes. A single farnesyl group on a protein will not lead to a membrane association of more than 1-2 minutes (Peitzsch and McLaughlin, 1993) and the binding energy of a myristoylated peptide to the lipid bilayer is too low for stable association (Peitzsch and McLaughlin, 1993). Additional hydrophobicity is required for a more stable interaction. The two-signal hypothesis argues that a second membrane attachment signal is required for stable membrane attachment. This can be a polybasic domain, such as in the myristoylated tyrosine kinase Src (Murray *et al.*, 1998), or by palmitoylation, for example in myristoylated Gα subunits (Manahan *et al.*, 2000). In the case of Ras, a farnesylated protein, this occurs in the hypervariable region by palmitoylation, either singly as in N-Ras or doubly as in H-Ras (Hancock *et al.*, 1989), or by a polybasic region in K(B)-Ras (Hancock *et al.*, 1990). A subset

of palmitoylated proteins are already irreversibly lipidated in this way and so are called dually lipidated proteins.

Although prenylation and myristoylation are irreversible events there is still scope for regulation of membrane attachment. The myristoyl moiety can undergo conformational changes which allow it either to be available for membrane attachment or hidden within a pocket, a so-called myristoyl switch. The myristoyl switch may often be regulated by binding of a ligand. Examples of proteins whose membrane attachment is regulated in this way include recoverin, a calcium-binding retinal protein (Ames *et al.*, 1996) and c-Abl, a tyrosine kinase which is regulated by phosphotyrosine-containing ligands (Hantschel *et al.*, 2003). An analogous mechanism involving binding of other proteins can also regulate attachment of prenylated proteins to membranes. The guanosine triphosphatase (GTPase) Rho, for example, is geranylgeranylated and is removed from the plasma membrane (PM) by binding to Rho guanine nucleotide dissociation inhibitor (RhoGDI) and maintained in an inactive form in this complex in the cytosol (Hoffman *et al.*, 2000). Despite these switch mechanisms, prenylated and myristoylated proteins retain their lipid moieties indefinitely. Only palmitoylation allows for regulation through addition and removal of the lipid group.

1.1.2 PALMITOYLATION

Palmitoylation of proteins was originally described as a fatty acid which binds to vesicular stomatitis virus glycoprotein (Schmidt and Schlesinger, 1979) and was later found to be a post-translational modification in eukaryotic cells (Omary and Trowbridge, 1981). It has not been demonstrated in bacteria. There are now three forms of palmitoylation which are recognised. *S*-palmitoylation is the addition of the 16-carbon saturated fatty acid palmitic acid to cysteine residues by a thioester bond. It is the major subgroup of the process called *S*-acylation, which includes fatty acids with different lengths of hydrocarbon chain and numbers of unsaturated bonds. This is a reversible process, with *S*-palmitoylation catalysed by the DHHC family of palmitoyl acyl-tranferases (PATs) and depalmitoylation catalysed by palmitoyl-protein thioesterases (PPTs).

A small group of proteins are subject to irreversible *N*-palmitoylation, in which palmitic acid is added to cysteine residues by an amide bond. The protein whose *N*-palmitoylation has been most extensively studied is the mammalian Sonic hedgehog (Shh) protein. Shh is unusual in that it requires dual *N*-palmitoylation and cholesteroylation, a rare C-terminal modification, for its functionality (Ingham, 2001). *N*-palmitoylation is catalysed by the membrane-bound *O*-acyltransferase (MBOAT) family of enzymes, and the MBOAT for

Hedgehog proteins is Hedgehog acyltransferase (Hhat) (Chamoun *et al.*, 2001). The residue which is palmitoylated is a conserved cysteine in the sequence CGPGP, which is revealed by removal of a signal peptide. As it appears that the amino group cannot be directly palmitoylated but a sulfhydryl group is required, the mechanism is thought to consist of an initial thioester bond between the palmitate and cysteine sulfhydryl followed by translocation of the palmitate group to an amide link (Pepinsky *et al.*, 1998). The dual lipidation of Hedgehog proteins has been shown to be required for their function as secreted morphogens, specifically for interactions with heparan sulphate proteoglycans (HSPGs) and the receptor Patched (Callejo *et al.*, 2006). This may prevent it from simply diffusing away. Another protein known to be *N*-palmitoylated is *Drosophila melanogaster* Wingless, a member of the Wnt family of proteins and also secreted, by the MBOAT Porcupine (Franch-Marro *et al.*, 2008).

The first instance of modification of a protein by *O*-palmitoylation was recently identified (Zou *et al.*, 2011). Contrary to the introduction to their paper, *O*-palmitoylation has not strictly been previously demonstrated, as the studies they cite actually relate to *O*-acylation of ghrelin with octanoic acid (Yang *et al.*, 2008) and Wnt proteins by palmitoleic acid (Franch-Marro *et al.*, 2008). The study does find *O*-palmitoylation related to the enzyme acyl-CoA:lysophosphatidylcholine acyltransferase 1 (Lpcat1), which is required for synthesis of pulmonary surfactant in lung epithelia (Zou *et al.*, 2011). Upon a Ca^{2+} stimulus, Lpcat1 translocated to the nucleus where it palmitoylated histone H4. The palmitate group was shown to be insensitive to reduction, and so could not be *S*-palmitoylation. The palmitoylated residue was determined as serine-47 in histone H4. Palmitoylation was much reduced when Lpcat1 histidine-135 was mutated to alanine, suggesting this residue is essential for catalysis. Histone H4 *O*-palmitoylation is thought to be a mechanism regulating RNA synthesis in lung epithelial cells, and there is potential cross-regulation as histone H4 serine residues are also known to be phosphorylated (Zou *et al.*, 2011). There is already an example of phosphorylation of residue close to a palmitoylatable cysteine preventing the *S*-palmitoylation of phosphodiesterase 10A (PDE10A) and thus altering its subcellular localisation (Charych *et al.*, 2010).

S-palmitoylation is the process investigated in this thesis. Unless otherwise stated, the term ‘palmitoylation’ will henceforward refer to *S*-palmitoylation.

1.1.3 PALMITATE SYNTHESIS

Palmitate synthesis in mammals is carried out in the cytosol by fatty acid synthase (Stryer, 1995). The source materials are acetyl-CoA, derived from citrate by adenosine triphosphate (ATP)-citrate lyase, reduced nicotinamide adenine dinucleotide phosphate (NADPH), derived from the pentose phosphate pathway and metabolism of oxaloacetate, and malonyl-CoA, derived from acetyl-CoA by acetyl-CoA decarboxylase. Each monomer of the fatty acid synthase comprises three domains linked by flexible joiners, and the functional enzyme is a dimer of two identical monomers. The first domain of each monomer contains an acetyl transferase, a malonyl transferase and a β-ketoacyl synthase (also called condensing enzyme) region. This first domain of each monomer is physically located opposite the second and third domains of the other monomer (Figure 1.1A). The second domain contains the acyl carrier protein, β-ketoacyl reductase, dehydratase and enoyl reductase; the third domain is a thioesterase. The first step of palmitate synthesis is *O*-linkage of the acetyl of acetyl-CoA and the malonyl of malonyl-CoA to a serine in the active site of the acetyl transferase and malonyl transferase respectively. The acetyl group moves to the β-ketoacyl synthase/condensing enzyme in a cysteine *S*-linkage whilst the malonyl group is transferred to an *S*-linkage on a phosphopantetheinyl group on the acyl carrier protein in the second domain of the other monomer (Figure 1.1B).

Once these initial steps have been performed, elongation of the hydrocarbon chain takes place. A condensation reaction transfers the acetyl group onto two of the three malonyl group carbons to form an acetoacetyl-*S*-phosphopantetheinyl group with the third malonyl carbon released in carbon dioxide. This intermediate is reduced to a butyryl group by the β-ketoacyl reductase, dehydratase and enoyl reductase portions of the second domain. The butyryl group is transferred back to the cysteine residue in the β-ketoacyl synthase/condensing enzyme in the first domain. Another malonyl group is added to the acyl carrier protein and is used to provide a further two-carbon section for a condensation reaction (Figure 1.1C). The cycle continues until the C_{16} palmitate is produced. The thioesterase moiety in the third domain cleaves this from the β-ketoacyl synthase/condensing enzyme in the first domain (Stryer, 1995). Palmitoyl-CoA, which is the substrate for palmitoylation, is produced by palmitoyl-CoA synthetase from palmitate, ATP and unacylated CoA (CoASH) (Brandes *et al.*, 1973).

The process of palmitate synthesis is similar in *Saccharomyces cerevisiae*. The fatty acid synthase complex has a molecular weight of 2400 kDa and is composed of two different subunits in the arrangement $\alpha_6\beta_6$. In this context, the α subunit contains the acyl carrier

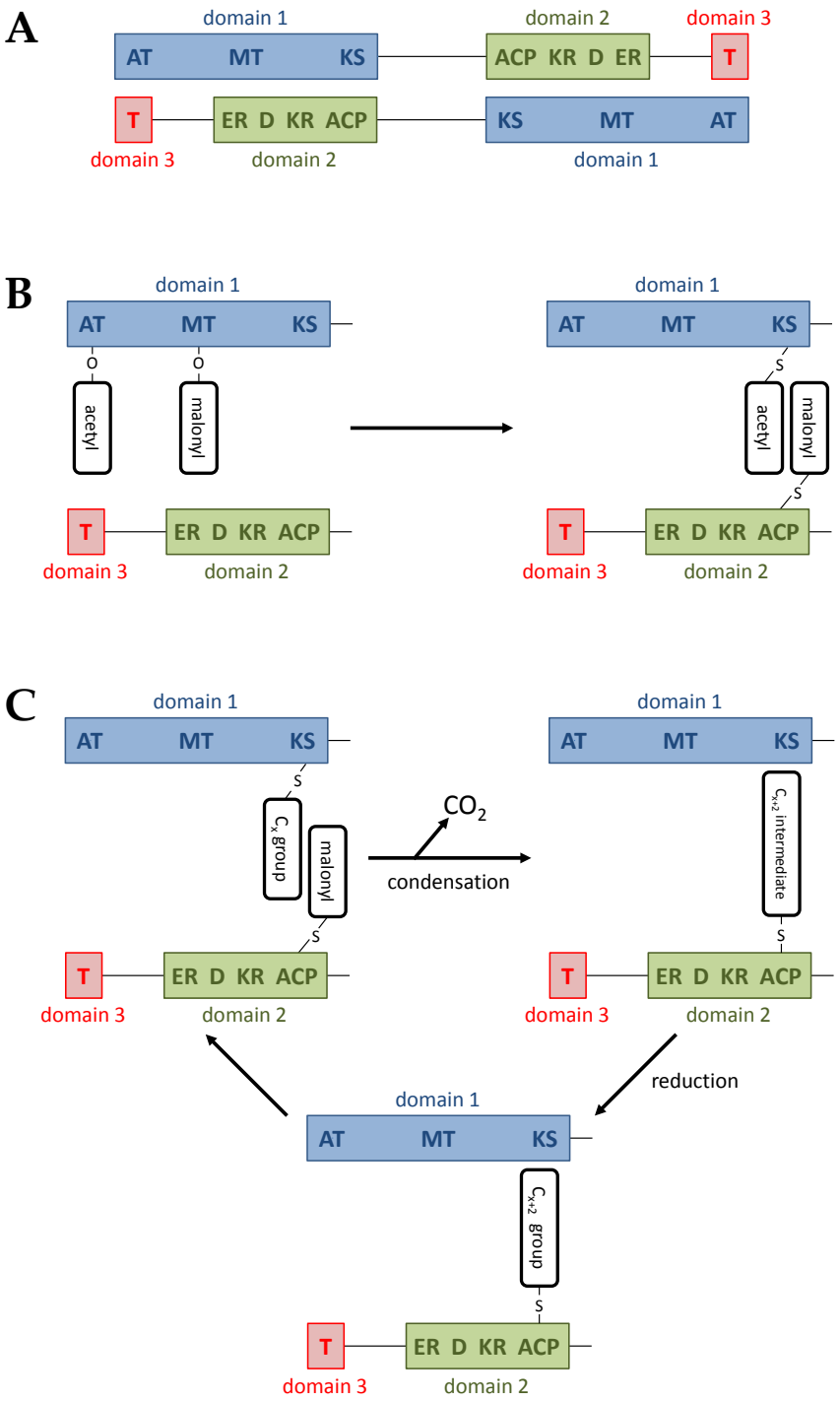

FIGURE 1.1: Schematic of palmitate synthesis

(A) Schematic showing the arrangement of two fatty acid synthase monomers into a functional dimer. Each monomer is situated so domain 1 is adjacent to domains 2 and 3 of the other monomer. (B) The initial steps of synthesis. An acetyl group is *O*-linked to the acetyl transferase and a malonyl group to malonyl transferase on domain 1 of one monomer. The acetyl group is transferred to an *S*-linkage to the β-ketoacyl synthase while the malonyl group becomes *S*-linked to the acyl carrier protein on domain 2 of the opposing monomer. (C) The elongation cycle. A condensation reaction between the C_2 malonyl group and the existing chain (C_2 acetyl initially) gives an intermediate which is then reduced to give a saturated hydrocarbon chain extended by two carbons. The elongation cycle continues until C_{16} palmitate is produced. It is cleaved from the enzyme by the thioesterase domain. ACP, acyl carrier protein; AT, acetyl transferase; D, dehydratase; ER, enoyl reductase; KR, β-ketoacyl reductase; KS, β-ketoacyl synthase; MT, malonyl transferase; T, thioesterase.

protein, condensing enzyme and β-ketoacyl reductase; the β subunit contains the acetyl transacylase, malonyl transacylase, β-hydroxyacyl dehydratase and enoyl reductase moieties (Stryer, 1995).

1.2 DHHC PALMITOYL ACYL-TRANSFERASES

1.2.1 DISCOVERY OF DHHCS

It took a long time for the enzymes responsible for *in vivo* palmitoylation to be identified. *In vitro* palmitoylation assays assessing palmitoyl-CoA incorporation into known palmitoyl-proteins were clouded by nonenzymatic palmitoylation. Spontaneous palmitoylation was observed on $G\alpha_{i1}$, $G\alpha_o$ and $G\alpha_z$ and, at a slower rate, $G\alpha_s$ and $G\alpha_q$ (Duncan and Gilman, 1996) and in synaptosomal-associated protein of 25 kDa (SNAP-25) when it was bound to syntaxin-1 (Veit, 2000). This also raised the question as to whether enzymes were required at all for protein palmitoylation. Indeed, there is evidence that palmitoylation of the *S. cerevisiae* protein blocked early in transport 3 (Bet3) occurs autocatalytically *in vivo*. Bet3 is palmitoylated nonenzymatically *in vitro* (Kummel *et al.*, 2010) and structural studies performed using Bet3 purified from *S. cerevisiae* (Turnbull *et al.*, 2005) and overexpressed in *Escherichia coli* (Kim *et al.*, 2005) found it to be palmitoylated at cysteine-68 but that the palmitate moiety was submerged in a hydrophobic pocket, orientated inwards. The finding in *E. coli* is particularly surprising as there is no evidence of bacteria being able to acylate proteins and they lack the necessary enzymes. In addition Bet3 palmitoylation was not found to be diminished in any mutant *S. cerevisiae* strains deficient for PATs (Roth *et al.*, 2006). Even after the DHHC group of enzymes was identified as PATs, *in vitro* palmitoylation assays tended to fail due to the poor activity of these transmembrane proteins *in vitro*.

The first identifications of palmitoylating enzymes were made using similar methods in *S. cerevisiae* and were published more-or-less concurrently. Palmitoylation of Ras2 had been observed to be deficient in strains carrying mutations in the effect on Ras function 2 (*ERF2*) (Bartels *et al.*, 1999) and *ERF4*/suppressor of hyperactive Ras 5 (*SHR5*) (Jung *et al.*, 1995) genes. This was studied further to determine their roles in Ras palmitoylation (Lobo *et al.*, 2002). A strain carrying a mutant form of Ras2 with a polybasic domain instead of a farnesylated CaaX motif, which therefore required its palmitoylation for viability, showed that both Erf2 and Erf4 were needed for palmitoylation of Ras2. Palmitoylation of yeast casein kinase 2 (Yck2) was investigated in relation to the protein ankyrin repeat-containing protein 1 (Akr1) based on the observation that localisation of Yck2 is altered in an *akr1Δ*

strain from the plasma membrane to the cytoplasm (Roth *et al.*, 2002). Yck2 incorporated [^{3}H]-palmitate in wild-type cells but not in *akr1Δ* cells, and [^{3}H]-palmitate was also incorporated into Ras2 providing Erf2 and Erf4 were present. Mutation of two C-terminal cysteine residues of Yck2 to serine abolished this labelling and replicated the mislocalisation in wild-type cells. The only sequence homology shared by Akr1 and Erf2 was in a domain containing a motif first described as a potential zinc finger through computational analysis of the *S. cerevisiae* genome (Bohm *et al.*, 1997). This domain, originally called a NEW1 domain, contains several conserved cysteine residues and an aspartic acid-histidine-histidine-cysteine (DHHC) motif. Both studies tested the importance of this motif. Mutants of the first histidine residue (to alanine) and the conserved cysteine residue (to serine) of the DHHC motif of Erf2 were tested (Lobo *et al.*, 2002). Two similar mutant forms of Akr1 were also engineered: one with the aspartic acid and first histidine residues mutated to alanine and the other with the cysteine residue mutated to alanine (Roth *et al.*, 2002). None of these mutants was able to palmitoylate its substrate, and so the DHHC cysteine-rich domain (DHHC-CRD) was shown to be a defining feature of PATs responsible for *S*-palmitoylation. This family of PATs is often referred to as the DHHCs.

The identification of the DHHC-CRD as the unifying motif of the PAT enzymes responsible for *S*-palmitoylation allowed rapid identification of the complete family in some organisms, comprising eight putative members in *S. cerevisiae* (Mitchell *et al.*, 2006) and 23 in *Homo sapiens* (Korycka *et al.*, 2012) and *Mus musculus* (Fukata and Fukata, 2010). In addition there are certain structural similarities which are found in the DHHCs, such as the presence of at least four transmembrane domains (TMDs) with the DHHC-CRD positioned on the cytoplasmic face of the membrane, usually between TMD2 and -3 (Fukata and Fukata, 2010; Kihara *et al.*, 2005; Korycka *et al.*, 2012; Mitchell *et al.*, 2006). Most of the DHHCs appear to be ER- or Golgi-localised (Ohno *et al.*, 2006). Interestingly the mammalian orthologue of Erf2, DHHC9, also requires the orthologue of Erf4/Shr5, Golgi complex-associated protein of 16 kDa (GCP16), for its palmitoyltransferase activity towards H- and N-Ras (Swarthout *et al.*, 2005). None of the other DHHCs have yet been shown to need an accessory protein for function like this, suggesting Erf4/Shr5 and GCP16 are needed more for substrate specificity than catalysis. Whilst the partner protein is required for activity, it is Erf2 and DHHC9 which have been shown to be responsible for the palmitate transfer (Lobo *et al.*, 2002; Swarthout *et al.*, 2005). Conversely the mammalian PAT for R-Ras, DHHC19, does not have a binding partner for function and is itself prenylated at its CaaX motif (Baumgart *et al.*, 2010). This is an example of how the DHHC enzymes can be

particularly specific in some cases, with different Ras family members being palmitoylated by different enzymes. Although individual tissues display individual profiles of DHHC expression, many may be present at once. The messenger RNA (mRNA) of 19 and 18 DHHCs was detected in human testis and liver respectively (Ohno *et al.*, 2006), and the cervical cancer HeLa cell line expresses 20 DHHCs (Lakkaraju *et al.*, 2012). Similarities and differences between DHHCs are discussed further in Chapter 3.

1.2.2 REACTION MECHANISM

The studies which identified Erf2/Erf4 and Akr1 as DHHCs using [^{3}H]-palmitate labelling of Ras2 and Yck2 respectively also observed labelling of Erf2 and Akr1 themselves (Lobo *et al.*, 2002; Roth *et al.*, 2002). Several other DHHCs were also observed to incorporate palmitate, including *H. sapiens* DHHC9 (Swarthout *et al.*, 2005) and DHHC15 (Fukata *et al.*, 2004). Initial proteomic scale studies in *S. cerevisiae* also identified Akr1 as a palmitoyl-protein (Roth *et al.*, 2006) and the first mammalian proteomic study found DHHC17/huntingtin-interacting protein 14 (HIP14) to be palmitoylated (Kang *et al.*, 2008). These observations led to the hypothesis that palmitoylation of substrates proceeded by formation of a palmitoyl-enzyme intermediate followed by transfer of palmitate to the substrate. A reaction mechanism of palmitoylation by Erf2 was recently elucidated (Mitchell *et al.*, 2010). Generation of deletion mutants showed that only the DHHC-CRD of Erf2 was required for autopalmitoylation and palmitoylation of Ras2. Mutation of any of the cysteine residues and some of the histidine residues in the DHHC-CRD were shown to give loss-of-function in Erf2 through a complementation assay. This would account for the high conservation of these residues in the DHHC enzymes (see Chapter 3). Study of the reaction kinetics found that palmitoyl-Erf2 is formed within five seconds in burst kinetics consistent with one active site per Erf2/Erf4 complex. In the absence of the substrate, there was found to be gradual hydrolysis resulting in release of the palmitate group. However if Ras2 was present then its association with the Erf2/Erf4 complex resulted in palmitate transfer to the substrate. The presence of Ras2 also appeared to stimulate Erf2/Erf4 activity. Palmitoylation of Ras2 did not occur when the first histidine or the cysteine residue of the DHHC motif was mutated, consistent with earlier reports (Lobo *et al.*, 2002; Roth *et al.*, 2002).

Thus, the following reaction mechanism is currently proposed (Mitchell *et al.*, 2010). The enzyme undergoes autopalmitoylation with burst kinetics by formation of a thioester to the cysteine residue in the DHHC motif, the single catalytic site. Palmitoyl-CoA undergoes nucleophilic attack by the cysteine residue, which is first deprotonated. This is regulated by

one ionisable group with a pK_a of 7.2, thought to be the first histidine in the DHHC motif, or there may be enough of a change in pH of the microenvironment of the residue to promote it directly. The palmitoyl-enzyme intermediate then either transfers the palmitoyl moiety to the substrate or releases it through a reaction with water. The kinetics of the autopalmitoylation step presumably means that the palmitoyl-enzyme is regenerated quickly.

1.3 PALMITOYL-PROTEIN THIOESTERASES

Palmitoylation is a reversible modification, with depalmitoylation mediated by the PPTs. These are understudied compared with the DHHCs and palmitoylated proteins themselves. This is partly due to the difficulty in identifying the physiological PPTs for specific proteins and the lack of any unifying sequence which can be used to search genomic data for new candidates. The known PPTs were purified based on assays to remove [^{3}H]-palmitate from well-known palmitoyl-proteins. Unlike the integral membrane DHHC proteins, the PPTs are soluble. PPT1 was identified through its ability to depalmitoylate H-Ras, $G\alpha_o$, $G\alpha_i$ and $G\alpha_s$ *in vitro* (Camp and Hofmann, 1993), although it is localised within lysosomes and, in neurons, synaptic vesicles so its physiological substrates are more likely to be secreted or outward-facing proteins (Camp *et al.*, 1994; Hellsten *et al.*, 1996; Lehtovirta *et al.*, 2001; Verkruyse and Hofmann, 1996). The lysosomal localisation may be important in the role of PPT1 in lysosomal storage disorders (Hellsten *et al.*, 1996; Verkruyse and Hofmann, 1996). Mutations in *PPT1* have been shown to cause the neurodegenerative disease infantile neuronal ceroid lipofuscinosis (INCL) (Vesa *et al.*, 1995), which is discussed below. There is evidence that PPT1 contributes to the catabolism of acylated proteins in the lysosome and that dysfunction of this pathway is responsible for the build up of lipids inside lysosomes found in INCL (Lu *et al.*, 1996). An analysis of rat tissue expression showed *PPT1* is highly expressed in the spleen, brain and testes but not in pancreas, lung, muscle tissues, liver or kidney (Camp and Hofmann, 1993).

When PPT1 was originally identified, a sensitivity to diethylpyrocarbonate (DEPC) was noted, which is consistent with a catalytic histidine residue (Camp and Hofmann, 1993). The catalytic triad of a serine, an aspartate and a histidine residue was later confirmed in a crystal structure (Bellizzi *et al.*, 2000) and is common to other members of the PPT enzyme family and indeed to thioesterases in general (Calero *et al.*, 2003; Devedjiev *et al.*, 2000). PPT1 was shown to be specific to thioesters, being unable to depalmitoylate many oxyester-linked substrates, and even to specific thioesters, as it could depalmitoylate

palmitoyl-CoA but not palmitoyl-carnitine (Camp and Hofmann, 1993). An enzyme with homology to PPT1 has been named PPT2, although it only appears to be able to remove palmitate from palmitoyl-CoA and not palmitoyl-proteins (Calero *et al.*, 2003; Soyombo and Hofmann, 1997).

A separate branch of the PPT family is the acyl-protein thioesterases (APTs). Interestingly *S. cerevisiae* only has one known PPT enzyme, which is APT1 (Duncan and Gilman, 2002), although another yeast, *Schizosaccharomyces pombe*, does have a PPT1 orthologue (Cho and Hofmann, 2004). APT1 is a cytosolic enzyme which was purified by its depalmitoylation of $G\alpha_{i1}$ (Duncan and Gilman, 1998). The enzyme was shown to be specific for depalmitoylation as [^{3}H]-myristate was not removed. APT1 also has lysophospholipase activity but was shown to have a strong preference for deacylating proteins. Other substrates demonstrated in this study were Ras and $G\alpha_s$. This enzyme is more likely than PPT1 to be the main physiological PPT as its cytosolic localisation would give it access to more palmitoyl-proteins (Duncan and Gilman, 1998). Indeed, a study was published soon afterwards identifying APT1 as the PPT for endothelial nitric oxide synthase (eNOS) (Yeh *et al.*, 1999). Interestingly, a recent palmitoyl-proteomics study pulled out APT1 as one of its hits and its palmitoylation was verified by Western blot and studies using 2-bromopalmitate (2-BP), which inhibits palmitoylation by preventing palmitate synthesis (Yang *et al.*, 2010). This has potential importance in giving APT1 access to many palmitoylated proteins which will be membrane-associated and also gives scope for direct regulation of depalmitoylating activity by the palmitoylation machinery. The other family member, APT2, has been identified by homology to APT1. APT1, but not APT2, has recently been shown to regulate the depalmitoylation of large conductance Ca^{2+}-activated K^+ (BK) channels, which are palmitoylated on their intracellular S0-S1 loop (Tian *et al.*, 2012). The identification of further PPTs and substrates for specific enzymes is an area of the field requiring considerable research. As with phosphatases in phosphorylation and deubiquitinases in ubiquitination, knowledge of their workings will provide a much more complete picture of palmitoylation.

1.4 INVESTIGATING PALMITOYLATION

1.4.1 CLASSICAL STUDIES

Initial characterisations of palmitoylation usually involved labelling of proteins with [^{3}H]-palmitate. Indeed, the first report of a palmitoylated protein from a virus used this method (Schmidt and Schlesinger, 1979), as did the first characterisation of a eukaryotic

palmitoyl-protein, the transferrin receptor (Omary and Trowbridge, 1981). A study observing for the first time palmitoylation of the β_2 adrenergic receptor using [^{3}H]-palmitate showed that mutation of cysteine-341 to glycine abolished palmitoylation and had functional consequences, including uncoupling of the receptor from G_s (O'Dowd *et al.*, 1989). An important study examining postsynaptic density protein of 95 kDa (PSD-95) found its hydrophobic partitioning in rat brain and CV-1 origin, simian vacuolating virus 40 transformed (COS) cell membranes was due to its palmitoylation (Topinka and Bredt, 1998). The intensity of PSD-95 labelling with [^{3}H]-palmitate was very high, indicating it is a major palmitoyl-protein in rat brain. PSD-95 palmitoylation was also shown to be important for its interaction with the K^+ channel Kv1.4, uncovering a major functional role for palmitoylation at the synapse.

After the identification of Erf2 and Akr1 as PATs, the main focus of research was to confirm the PAT activity of the other DHHC-CRD-containing proteins in *S. cerevisiae*. The next DHHC to be confirmed was spore wall formation 1 (Swf1) which was shown to palmitoylate several soluble N-ethylmaleimide (NEM)-sensitive fusion protein (NSF) attachment protein (SNAP) receptor (SNARE) proteins (Valdez-Taubas and Pelham, 2005). Palmitoylation of the synaptobrevin homologue suppressor of the null allele of cyclase-associated protein 1 (Snc1) was examined using the shift in its mobility on a polyacrylamide gel when palmitate is removed using HA. Snc1 migrated at the unpalmitoylated molecular weight in a *swf1Δ* strain and when its juxtamembrane (and only) cysteine residue was mutated to alanine. The syntaxin 8 homologue Syn8 was also shown to be palmitoylated by Swf1 in this way. A different approach was taken for target SNARE (t-SNARE) affecting a late Golgi compartment 1 (Tlg1) as the mobility shift was small and labelling with [^{3}H]-palmitate was unsuccessful. Instead, the cell lysate was treated with a biotin construct which selectively labels thioreactive groups on unpalmitoylated cysteine residues. Unpalmitoylated Tlg1 was detected in *swf1Δ* cells but not in wild-type cells. A complementary experiment detecting palmitoylated proteins by blocking free thiols with NEM, treating with HA and labelling the revealed thiols, similar to the acyl-biotin exchange (ABE) assay discussed below, detected Tlg1 only in the wild-type cells.

The first demonstration of palmitoyltransferase activity from the *S. cerevisiae* enzyme protein fatty acyltransferase 3 (Pfa3) arose from the observation that stressed *pfa3Δ* cells give a fragmented vacuolar morphology similar to cells lacking vacuole protein 8 (Vac8) (Smotrys *et al.*, 2005). Pfa3 was found to be localised to the vacuolar membrane and vacuolar fusion depended upon its catalytic cysteine residue. Pfa3 could incorporate

[^{3}H]-palmitate into Vac8 *in vitro* and levels of [^{3}H]-palmitoylated Vac8 were reduced by 80% in *pfa3Δ* cells compared with wild-type levels. A similar screen for phenotypes similar to a strain lacking chitin synthase-related 3 (Chs3) found Pfa4 to be responsible for its palmitoylation (Lam *et al.*, 2006). This regulated Chs3 exit from the ER and subsequent chitin synthesis.

As discussed above, the identification of Erf2/Erf4 and Akr1 as PATs in *S. cerevisiae* was conducted by examining incorporation of [^{3}H]-palmitate into Ras2 and Yck2 respectively under different conditions (Lobo *et al.*, 2002; Roth *et al.*, 2002), and allowed this methodology to be used to investigate broader relationships in palmitoylation. Shortly after the identification of the first DHHCs in *S. cerevisiae* came studies which examined them in a mammalian context. A total of 23 proteins containing the DHHC-CRD were found in the *M. musculus* genome and were co-expressed in COS-7 cells with the known palmitoyl-protein PSD-95 to see which enzymes would promote its palmitoylation (Fukata *et al.*, 2004). They found that DHHC2/reduced expression in metastasis (REAM), DHHC3/Golgi-associated DHHC zinc finger-containing protein (GODZ), DHHC7/Sertoli cell gene with a zinc finger domain (SERZ), and DHHC15 were responsible for palmitoylating PSD-95 and this was blocked in a dose-dependent manner by 2-BP, an inhibitor of palmitate synthesis. The palmitate modification was sensitive to both dithiothreitol (DTT) and HA treatment. An examination of the specificities of the DHHCs responsible for palmitoylating PSD-95 using the known palmitoyl-proteins growth associated protein of 43 kDa (GAP43/neuromodulin), Lck, SNAP-25b and H-Ras showed distinct but overlapping specificities within the mammalian enzymes. A similar screen in *S. cerevisiae* using overexpression of DHHCs and biotin labelling as in ABE below found several known substrates are palmitoylated by many DHHCs. For example, Vac8 was palmitoylated by Akr1, Erf2, Pfa3, Pfa4 and Pfa5 (Hou *et al.*, 2009).

The effects of palmitoylation on dynamics of association with membranes can be assessed using live cell imaging techniques. A screen of the mammalian DHHC enzymes in HeLa cells found that DHHC3/GODZ and DHHC7/SERZ were responsible for palmitoylation of Gα subunits in the Golgi (Tsutsumi *et al.*, 2009). Total internal reflection fluorescence microscopy (TIRFM) was used to examine the localisation of Gα subunits to the PM. As a proof-of-principle, inhibition of overall palmitoylation with 2-BP and mutation of the palmitoylated cysteine residues to serine abolished membrane localisation of green fluorescent protein (GFP)-tagged $G\alpha_q$ whereas $G\alpha_q$ artificially targeted to the PM with a polybasic domain was unaffected. Small inhibiting RNA (siRNA) knockdown of DHHC3 or -7

reduced the intensity of GFP fluorescence at the PM indicating reduced $G\alpha_q$ localisation there. A fluorescence recovery after photobleaching (FRAP) approach was also taken. Recovery of fluorescence at the Golgi was shown to be dependent on palmitoylation of $G\alpha_q$ by use of 2-BP and cycloheximide. siRNA-mediated knockdown of DHHC3 or -7 resulted in a diffuse cytoplasmic localisation of $G\alpha_q$, showing these enzymes are required for trapping of $G\alpha_q$ at the Golgi membrane from which it is trafficked to the PM. Palmitoylation of Gα subunits was also shown to be required for coupling of G-protein coupled receptors to downstream effects (Tsutsumi *et al.*, 2009). This study shows how live cell imaging has the potential to elucidate the function of palmitoylation of specific proteins in detail.

The study of proteins which may undergo rapid palmitate turnover can be facilitated by the use of PPT inhibitors to prevent depalmitoylation. These can provide a complementary perturbation to the use of 2-BP, which inhibits palmitate synthesis and therefore the rate of palmitoylation. An example of the use of PPT inhibitors is in the study of H- and N-Ras. These normally undergo a cycle of different membrane localisations based on their palmitoylation status. Unpalmitoylated (but always farnesylated) Ras is distributed between the cytosol and endomembranes. Palmitoylation at the Golgi traps Ras there, committing it to the bulk-flow exocytotic pathway which traffics it to the PM. Ras can then be removed from the PM by depalmitoylation (Rocks *et al.*, 2005). A protein structure similarity clustering strategy, which compares the tertiary structures of similar proteins, was used to design potential selective inhibitors of APT1, resulting in the chemical palmostatin B which covalently modifies the active site of both APT1 and -2 (Dekker *et al.*, 2010; Rusch *et al.*, 2011). This inhibited depalmitoylation of H- and N-Ras, altering their Golgi and PM distribution to endomembranes in general. This effect was replicated by siRNA-mediated knockdown of APT1. In this way, inhibitors were used to confirm the model above. PPT inhibitors can also be used to study the dynamics of palmitoylation. A recent proteomic study using click chemistry (discussed below) in T cells found the PPT1 inhibitor hexadecylfluorophosphonate (HDFP) (Martin *et al.*, 2012). A pulse-chase experiment showed proteins with rapid palmitate turnover. Treatment with HDFP gave a time-dependent enhancement of palmitoylation of proteins and, using HDFP as the chase in pulse-chase experiments, uncovered a subset of these proteins which were stabilised by HDFP but depalmitoylated in control cells. Among proteins identified as having PPT1-regulated rapid palmitate turnover were H- and N-Ras and $G\alpha_s$ (Martin *et al.*, 2012).

1.4.2 PALMITOYL-PROTEOMICS

The limitations of classical methods of examining palmitoylation, such as immunoprecipitation of the protein in question, and therefore prior knowledge of its likely palmitoylation, and the autoradiograph exposure times of weeks to months (Drisdel and Green, 2004) led to the development of techniques which could be used on a larger scale and with extracts from tissues. These methods rely on the cleavage of the relatively labile thioester bond between cysteine residues and palmitate molecules by neutral HA. In ABE the revealed sulfhydryl groups are labelled with a thioreactive biotin construct followed by pulldown on streptavidin- or neutravidin-conjugated beads (Drisdel and Green, 2004; Kang *et al.*, 2008; Roth *et al.*, 2006), whereas in acyl-resin-assisted capture (acyl-RAC) they are bound directly to thioreactive sepharose (Forrester *et al.*, 2011). An alternative to these cysteine-centric approaches is a palmitate-centric approach relying on metabolic labelling. Instead of [^{3}H]-palmitate, the palmitate analogues 17-octadecynoic acid (17-ODYA) (Martin and Cravatt, 2009; Martin *et al.*, 2012) or alk-16 (Yount *et al.*, 2010) can be used. The proteins labelled with these reagents are reacted with azide reporters using so-called click chemistry (Speers and Cravatt, 2004) allowing overall visualisation by fluorescence in polyacrylamide gels and purification for mass spectrometric analysis. However, this method is perhaps best used in cell culture whereas ABE and acyl-RAC enable purification of palmitoyl-proteins from any protein mixture, which can be derived from animal tissues. The dynamics of palmitoylation are more easily studied by click chemistry methods, for example in pulse-chase experiments.

The power of this proteomic approach was demonstrated in the first two studies to use it. An analysis of *S. cerevisiae* using ABE found 47 palmitoyl-proteins, including 12 of the 15 known at the time (Table 1.1) (Roth *et al.*, 2006). This unbiased approach could therefore rapidly identify many more palmitoyl-proteins than classical methods. An analysis of rat embryonic neurons soon afterwards found 50 known palmitoyl-proteins and 113 novel candidates (Kang *et al.*, 2008). 21 of these candidates were confirmed by [^{3}H]-palmitate labelling, which remains the gold standard for verifying new palmitoyl-proteins from such studies. The number of organisms, tissues and cell lines which have been subjected to proteomic analysis is rising as the field gains momentum (Table 1.1). Part of the value of this approach is that it may prompt researchers to consider the effects of palmitoylation on their protein of interest.

Study	Method	Source material	No. hits	Notes
(Roth *et al.*, 2006)	ABE	*Saccharomyces cerevisiae*	47	
(Kang *et al.*, 2008)	ABE	rat cultured embryonic neurons and synaptosomes	163	
(Zhang *et al.*, 2008)	PICA	HeLa cells	50	probed DHHC2 substrates
(Martin and Cravatt, 2009)	click chemistry: 17-ODYA	Jurkat T cells	125	
(Yang *et al.*, 2010)	ABE, PalmPISC	DU145 human prostate cancer cells	169	408 total hits from lipid rafts; 112 from rest of membrane; 273 in common
(Yount *et al.*, 2010)	click chemistry: alk-16	mouse D2.4 dendritic cells	60	
(Dowal *et al.*, 2011)	ABE, PalmPISC	human platelets	215	
(Merrick *et al.*, 2011)	ABE	RAW 264.7 macrophages	80	
(Forrester *et al.*, 2011)	acyl-RAC	bovine brain membranes and HEK293 cells	88	site-specific analysis
(Martin *et al.*, 2012)	click chemistry: 17-ODYA	mouse T cell hybridomas	415	coupled to SILAC; PPT inhibitors used to study dynamics
(Ivaldi *et al.*, 2012)	ABE	human B lymphocytes	95	
(Marin *et al.*, 2012)	ABE	human EA.hy 926 endothelial cells	184	
(Hemsley *et al.*, 2012)	ABE	*Arabidopsis thaliana*	581	

TABLE 1.1: Findings from published palmitoyl-proteomic analyses

All published palmitoyl-proteomic studies to date are listed along with the method used, source material and number of high confidence palmitoyl-proteins identified. 17-ODYA, 17-octadecynoic acid; ABE, acyl-biotin exchange; acyl-RAC, acyl-resin-assisted capture; PalmPISC, palmitoyl protein identification and site characterisation; PICA, palmitoyl-cysteine isolation capture and analysis; PPT, palmitoyl-protein thioesterase; SILAC, stable isotope labelling of amino acids in cell culture.

1.4.3 PALMITOYLATION SITES

Palmitoylation of eukaryotic proteins has been known for nearly 30 years (Magee and Courtneidge, 1985) but there remains a lack of a consensus motif for determining which cysteine residues will be palmitoylated and which will not. This is in contrast to the specific consensus for myristoylation of MGXXX(S/C/T) and which is mediated by only two vertebrate myristoyltransferases, and the CaaX motif for prenylation by farnesyltransferase or geranylgeranyltransferase. It has been hypothesised that this very lack of a consensus for palmitoylation may be the reason for having such a relatively large number of PATs (Greaves *et al.*, 2009). Nonetheless there are some programs which use previously gathered information on palmitoylation sites to try to predict potential palmitoylation sites from a primary amino acid sequence. One such program is clustering and scoring strategy (CSS)-palm (http://csspalm.biocuckoo.org/) (Ren *et al.*, 2008), which has recently been updated to version 3.0. This uses a manually curated set of 439 palmitoylation sites on 194 proteins as its source. Another program called composition of *k*-spaced amino acid pairs (CKSAAP)-palm uses a different algorithm which appears to detect some types of palmitoyl-protein which CSS-palm does not (http://doc.aporc.org/wiki/CKSAAP-Palm) (Wang *et al.*, 2009). Whilst these pieces of software may be useful for finding potential palmitoylation sites in proteins, they are no substitute for finding or confirming the relevant sites experimentally.

The most common way to identify the palmitoylated cysteine residues in a protein is a protein-centric approach. Usually palmitoylation of a protein has been confirmed by [^{3}H]-palmitate incorporation. The use of truncations can be used to refine which region contains the palmitoylated residue(s) and abolition of [^{3}H]-palmitate labelling after mutation of the candidate cysteine(s) to alanine or serine, which cannot be palmitoylated, confirms the site. This method has been used to identify palmitoylated residues on many proteins. Examples of this approach include the discovery of palmitoylation of cysteine-181 and -184 in H-Ras and cysteine-181 in N-Ras (Hancock *et al.*, 1989), PSD-95 on cysteine-3 and -5 (Topinka and Bredt, 1998), and cysteine-3 in $G\alpha_o$ (Parenti *et al.*, 1993).

With the advent of proteomic techniques for assessing protein palmitoylation, some groups have modified these methods to try to identify not only the proteins but also their palmitoylation sites at the same time. The first to adopt this kind of approach was a technique dubbed palmitoyl-cysteine isolation capture and analysis (PICA) (Zhang *et al.*, 2008). The principle of this assay is labelling of formerly palmitoylated sites with heavy or light isotope coded affinity tag (ICAT) reagents, digestion with trypsin and mass

spectrometric analysis. The differences in mass allowed identification of cytoskeleton-associated protein 4 (CKAP4/p63) as a substrate for DHHC2, which palmitoylates it on cysteine-100. A technique called palmitoyl protein identification and site characterisation (PalmPISC) used a similar principle by treating two samples to label both chemically on palmitoylation sites. The chemical was eluted in one sample and the mass shift used to identify the palmitoylation site in a mass spectrometric analysis. PalmPISC was used to detect 143 putative palmitoylation sites in samples from lipid raft and non-raft membrane subdomains (Yang *et al.*, 2010) and 103 putative palmitoyl-proteins in platelets (Dowal *et al.*, 2011). The most recently published method, acyl-RAC, also assessed palmitoylation sites by omitting the elution step and digesting the proteins on the resin. Comparison of the heavy-labelled experimental sample with the light-labelled control allowed identification of palmitoylated cysteine residues on 84 peptides from HEK293 cells (Forrester *et al.*, 2011). Novel palmitoylation sites on ribosomal protein S11 (Rps11), the secretory pathway protein Sec61b and microsomal glutathione *S*-transferase 3 (MGST3) were validated by comparison of wild-type and cysteine-to-serine mutations. Proteomic scale techniques such as these offer a promising way to generate new leads in discovery of palmitoylation sites.

In an attempt to classify DHHCs based on their preferences for certain types of substrate, an assay system was developed by expressing the *H. sapiens* DHHCs in *S. cerevisiae* (Ohno *et al.*, 2012). The types of proteins which are palmitoylated can be roughly grouped into categories based on their properties or the location of the palmitoylated cysteine residue(s) (Table 1.2) (Ohno *et al.*, 2012; Resh, 1999; Roth *et al.*, 2006). Model substrates representing each of these groups were Myc-tagged and co-expressed with FLAG-tagged *S. cerevisiae* or *H. sapiens* DHHC proteins in *S. cerevisiae* strains optimised so each substrate underwent no background palmitoylation. The enzymes which palmitoylated each model substrate are shown in Table 1.2. There were some DHHCs which were not observed to palmitoylate any of the model substrates or sometimes even to form palmitoyl-enzyme intermediates. The authors attributed this to the possible specificity of these enzymes to substrates not used in this system – for example DHHC6 has been previously shown to palmitoylate calnexin on two cysteine residues adjacent to its single transmembrane domain (TMD) (Lakkaraju *et al.*, 2012) but did not palmitoylate the model substrate of this category, *S. cerevisiae* suppressor of Sec one (Sso1). This system has promise as a way of assessing the broad specificities of the DHHC families of other organisms and may be

Region	Example substrate	Example DHHCs (Ohno *et al.*, 2012)	
		S. cerevisiae	***H. sapiens***
N-terminal region of soluble proteins	PSD-95: Cys-3 and Cys-5 (Topinka and Bredt, 1998)	Akr1, Pfa4, Pfa5	DHHC2, 3, 7, 8, 15, 17
C-terminal region of soluble proteins	Yck1: two Cys residues at the extreme C-terminus (Roth *et al.*, 2002)	Akr1, Pfa3, Pfa4, Pfa5	DHHC2, 3, 5, 6, 7, 8, 9, 11, 14, 15, 17, 18, 20, 21
internal regions of soluble proteins	SNAP-25b: Cys-85, Cys-88, Cys-90, Cys-92 (Lane and Liu, 1997)		DHHC3, 7, 17
dually lipidated proteins: near *N*-myristoylation or C-terminal prenylation	Gpa2: N-terminally myristoylated (Harashima and Heitman, 2005)	Akr1, Erf2, Pfa3, Pfa5	DHHC1, 2, 3, 5, 6, 7, 8, 9, 11, 12, 14, 15, 17, 18, 20, 21
cytosolic region adjacent to the TMD of singly membrane-spanning proteins	Sso1 (Roth *et al.*, 2006)	Pfa3, Swf1	DHHC2, 20
cytosolic regions adjacent to a TMD in multiply membrane-spanning proteins	Agp1 (Roth *et al.*, 2006)	Pfa4	DHHC2, 3, 7, 11, 15, 20, 21

TABLE 1.2: Grouping of palmitoylated proteins by site of palmitoylation

Palmitoylated proteins can be grouped based on commonalities in the location of the palmitoylated residue(s). The example substrates and enzymes able to palmitoylate them are shown (Ohno *et al.*, 2012). N.B. The gene-based nomenclature for the *H. sapiens* DHHCs is used here for consistency with the rest of the thesis. An alternative protein nomenclature is used in (Ohno *et al.*, 2012). Agp, high affinity glutamine permease; Akr, ankyrin repeat-containing; Erf, effect on Ras function; Gpa, G protein α subunit; Pfa, protein fatty acyltransferase; PSD, postsynaptic density; SNAP-25, synaptosomal protein of 25 kDa; Sso, suppressor of Sec one; Swf, spore wall formation; TMD, transmembrane domain; Yck, yeast casein kinase.

improved by including another model substrate in each group to try to eliminate false negatives.

1.5 FUNCTIONS OF PALMITOYLATION

1.5.1 MEMBRANE TARGETING

The classical function of lipid modifications of proteins is to mediate attachment of soluble proteins to cellular membranes. This is also the case for palmitoylation, which can also occur on TMD-containing proteins and may regulate their association with different subcellular membranes. Data on many of the palmitoyl-proteins from *S. cerevisiae* would support the role of palmitoylation in membrane targeting. Erf2 with Erf4/Shr5 was responsible for proper membrane attachment and function of Ras2 (Lobo *et al.*, 2002). Mislocalisation of Yck2 is seen in *akr1Δ* mutants (Roth *et al.*, 2002). Swf1 was observed to prevent ubiquitination and subsequent degradation of Tlg1 by transmembrane ubiquitin ligase 1 (Tul1), maintaining its proper localisation to the *trans*-Golgi network and ER (Valdez-Taubas and Pelham, 2005). Pfa3 is responsible for palmitoylation of the vacuole protein Vac8, and disruption of this event leads to a vacuole fractionation phenotype (Smotrys *et al.*, 2005). Palmitoylation by Pfa4 is necessary for the exit of Chs3 from the ER and therefore its correct trafficking (Lam *et al.*, 2006). Well-studied examples in mammals are the palmitoylation-dependent localisation of Ras, discussed above (Rocks *et al.*, 2005), and of PSD-95 and its regulation of cell surface levels of α-amino-3-hydroxy-5-methyl-4-isoxazolepropionic acid (AMPA) receptors (El-Husseini Ael *et al.*, 2002; Fukata *et al.*, 2004; Topinka and Bredt, 1998). In some cases, expression of DHHCs on specific endomembranes may serve to tether proteins there, as may happen with Pfa3 and Vac8 at the vacuole. Some of the Golgi-based DHHCs have a much broader substrate specificity, such as DHHC2/REAM, -3/GODZ and -17/HIP14 (Ohno *et al.*, 2006), and may serve to palmitoylate proteins more generally in trafficking pathways.

One of the interesting questions in palmitoylation research is why TMD-containing proteins would be palmitoylated. One of the possibilities which has been proposed is the resolution of hydrophobic mismatching (Charollais and Van Der Goot, 2009; Greaves *et al.*, 2009). Membrane systems within the cell differ in their thickness due to their particular composition of protein and lipid components. For example, a study in rat polarised hepatocytes reported membrane thicknesses of 42.5 Å and 35.6 Å for the apical and basolateral PM respectively, 39.5 Å for the Golgi and 37.5 Å for the ER (Mitra *et al.*, 2004). This means that a TMD which is the right length for the thickness of one membrane system

may not be for another. If the TMD is too short, there is a negative mismatch; if it is too long there is a positive mismatch (Figure 1.2). An example of a protein affected by this is lipoprotein receptor-related protein 6 (LRP6), which traffics from the ER to the PM and whose palmitoylation on a juxtamembrane cysteine residue is required for exit from the ER (Abrami *et al.*, 2008). Shortening of the 23 residue TMD by two amino acids allowed an unpalmitoylatable LRP6 mutant to traffic to the PM. Given this corresponds to a reduction in TMD length by roughly the same proportion as the difference between the apical PM and ER membrane thicknesses, this suggests that palmitoylation allows resolution of what would otherwise be a positive hydrophobic mismatch at the ER membrane. A study in model membranes suggested that palmitoylation could accommodate a positive mismatch by allowing the TMD to tilt in the membrane (Figure 1.2B) (Abrami *et al.*, 2008; Joseph and Nagaraj, 1995). This may then induce a negative hydrophobic mismatch for LRP6 once it has reached the PM. This new mismatch could be resolved by depalmitoylation by a PPT enzyme, or possibly by some physical alternatives to accommodate the palmitate group which have been suggested (Greaves *et al.*, 2009): palmitoylated LRP6 may segregate into a relatively disordered membrane subdomain; it may be associated with another protein which stabilises its membrane configuration; a relatively ordered membrane subdomain may prevent TMD tilting; or hydrophobic forces within the membrane may dominate and palmitoylation only contributes when there is a mismatch and subsequent TMD destabilisation.

Negative hydrophobic mismatches could be resolved by palmitoylating a juxtamembrane cysteine residue to increase the effective TMD length (Figure 1.2A). Palmitoylation may also allow transmembrane proteins to associate with more ordered lipid microdomains (Figure 1.2C) (Uittenbogaard and Smart, 2000). This can result from TMDs containing residues with a large number of bulky side groups, such as aromatic rings, which tend to associate preferentially with disordered membrane subdomains. Palmitoylation of a juxtamembrane cysteine in these circumstances allow the TMD to localise in more ordered subdomains. A proteome scale study which examined palmitoyl-protein abundance in lipid rafts in human prostate cancer cells found a subset localised to lipid raft fractions, although more were found in non-raft fractions (Yang *et al.*, 2010).

1.5.2 PALMITATE TURNOVER

Palmitoylation has the distinguishing feature of being a reversible process, unique among the lipid modifications of proteins. As such, some studies have looked at the implications of palmitoylation and depalmitoylation cycles beyond simple targeting to different

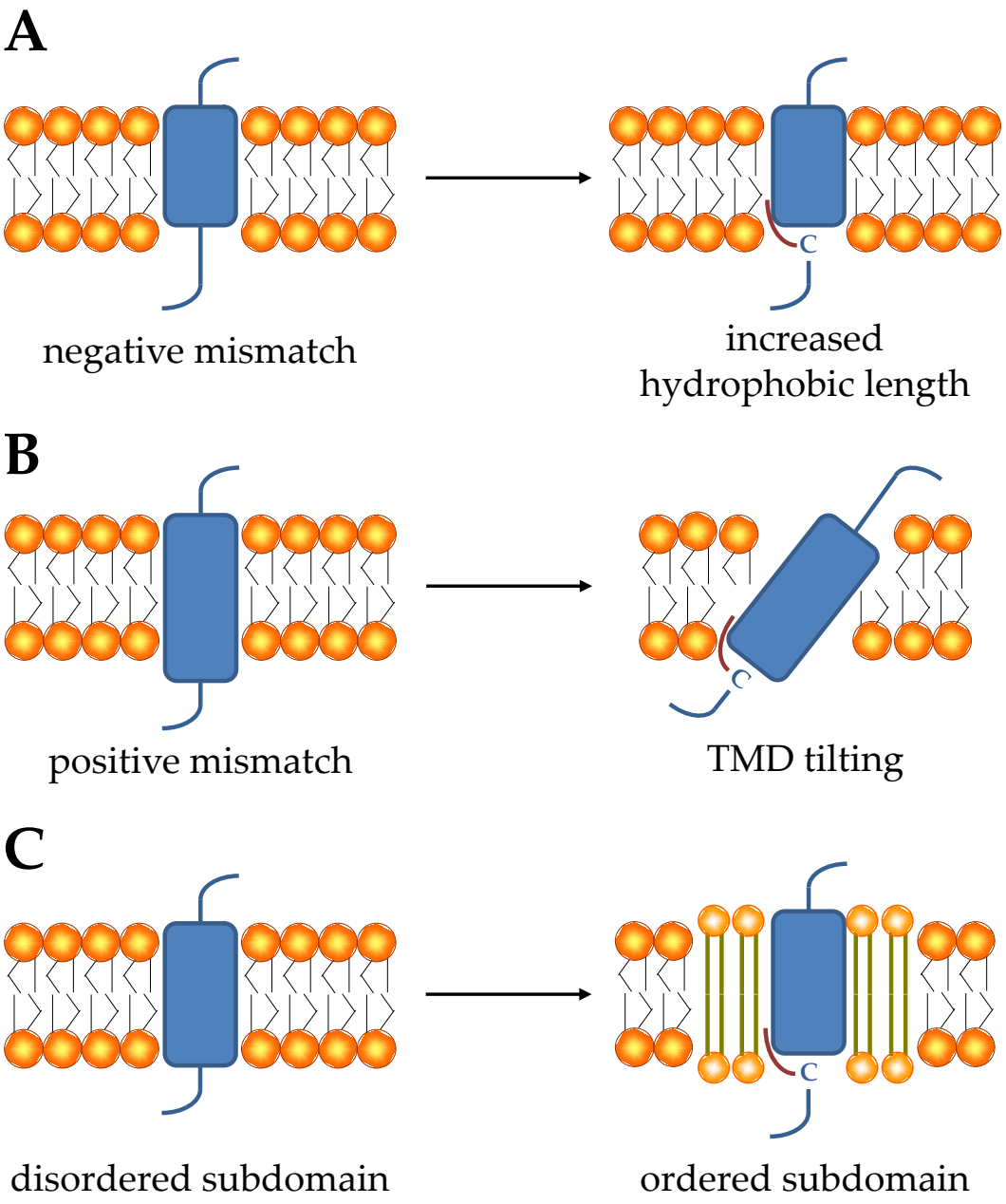

FIGURE 1.2: Resolution of hydrophobic mismatching by palmitoylation

Hydrophobic mismatching occurs when the length of a TMD is different from the thickness of the membrane in which it resides. This can be resolved by palmitoylation (red line) of a juxtamembrane cysteine residue on the cytosolic side of the membrane. (A) A negative hydrophobic mismatch occurs when the TMD is too short. Palmitoylation increases the effective hydrophobic length of the TMD. (B) A positive hydrophobic mismatch occurs when the TMD is too long. Palmitoylation induces a tilt in the TMD to accommodate it in the membrane. (C) TMDs with many bulky side groups preferentially associate with more disordered regions of the membrane. Palmitoylation can alter this preference and allow association with more ordered subdomains. C, cysteine residue; TMD, transmembrane domain.

membranes. One of the classic examples is palmitate turnover on the important signalling molecule $G\alpha_s$. [^{3}H]-palmitate labelling showed that palmitoylated $G\alpha_s$ is present solely in the particulate (i.e. membrane-bound) fraction of S49 *cyc*$^-$ mouse lymphoma cells expressing haemagglutinin (HA)-tagged $G\alpha_s$ (Wedegaertner and Bourne, 1994). In contrast, $G\alpha_s$ carrying the activating mutation R201C exhibited considerably less palmitoylation and was almost entirely present in the soluble fraction. Pulse-chase experiments showed [^{3}H]-palmitate on activated $G\alpha_s$ had a half-life of about two minutes, compared with 90 minutes in the wild-type protein. This was consistent with results from an experiment using isoproterenol, a β-adrenoreceptor agonist, which showed near-maximal palmitate incorporation within five minutes of treatment and a half-life of about two minutes. This was a result of receptor activation rather than a downstream effect, as the stimulation of cAMP production by forskolin had no effect on palmitate turnover. In addition, another $G\alpha_s$ mutant G226A, which cannot dissociate from the βγ subunit, abolished the effect of isoproterenol on palmitate turnover. This study was intriguing because it gave a possible mechanism of desensitisation of this signaling pathway mediated by the G protein itself rather than the receptor. As receptors are activated by agonists, the α subunit dissociates from the βγ subunit which allows it to be depalmitoylated, presumably by APT1 (Duncan and Gilman, 1998). Receptor activation also stimulates palmitoylation of $G\alpha_s$, which would make it available to receptors, and this step is potentially open to regulation from other signals which may affect the activity of PATs.

Another key study on the importance of dynamic palmitoylation examined its role on PSD-95 (El-Husseini Ael *et al.*, 2002). Treatment of cultured DIV 14 hippocampal neurons with the palmitate synthesis inhibitor 2-BP reduced PSD-95 palmitoylation and shifted a proportion of it into the soluble fraction. In addition, synaptic clusters of both PSD-95 and the related protein PSD-93 were dispersed with 2-BP treatment. Pharmacological blockade of glutamate receptors with kynurenic acid (targeting ionotropic receptors), 6-cyano-7-nitroquinoxaline-2,3-dione (CNQX) (AMPA receptors) or 2-amino-5-phosphonovalerate (APV) (N-methyl-D-aspartate (NMDA) receptors) prevented this effect. Removal of extracellular Ca^{2+} also reversed 2-BP-induced declustering, suggesting Ca^{2+} entry may be involved. The normal half-life of palmitate on PSD-95 was found to be approximately two hours, which increased to four hours upon treatment with kynurenic acid. This regulation of PSD-95 was shown to have an effect on synaptic responsivity, as AMPA receptor GluR1 subunit clustering was also reduced by 2-BP treatment, with a concurrent reduction in both amplitude and frequency of miniature excitatory postsynaptic currents (mEPSCs). Thus

palmitoylation can have an effect on synaptic strength through regulation of clustering of postsynaptic receptor subunits. Interestingly, a recent study shows that the palmitoylated cysteine residues in PSD-95, Cys-3 and -5, are also sites of *S*-nitrosylation. 2-BP treatment was shown to increase nitrosylation of these residues, raising the possibility of competing modifications providing a fine-tuning mechanism on PSD-95 function (Ho *et al.*, 2011).

Different palmitoyl-proteins undergo different dynamics of depalmitoylation. To investigate this, cultured neurons were treated with 2-BP for five hours and a proteomic analysis was performed (Kang *et al.*, 2008). If there is rapid turnover of palmitate on a protein, it will be depalmitoylated but then cannot be repalmitoylated, so should disappear from the list of palmitoyl-proteins when compared with untreated neurons. On the other hand, proteins undergoing little or no palmitate turnover will remain palmitoylated and therefore still be detected. This analysis showed that PSD-95, Ras isoforms, RhoA and -B, cell division cycle 42 (Cdc42) and syntaxin 1b are subject to rapid palmitate turnover; SNAP25, syntaptotagmin 1, secretory carrier membrane protein 1 (Scamp1), glucose transporter type 1 (GluT-1) and calnexin were stably palmitoylated (Kang *et al.*, 2008). To investigate whether palmitoylation dynamics could play a part in physiological and pathophysiological situations, the same analysis was performed after treating the neurons with glutamate, an excitatory neurotransmitter, and kainate, which promotes seizure-like activity. The general trend in these situations was in opposite directions. For example, glutamate decreased levels of palmitate on PSD-95, Ras and Cdc42, whereas kainate increased palmitoylation of these proteins (Kang *et al.*, 2008).

1.5.3 DISEASE ASSOCIATIONS

A number of links have been demonstrated between palmitoylation and various disease states. Some of the DHHC enzymes have been directly implicated in disease association studies. The region containing the *ZDHHC2/REAM* gene contains potential tumour suppressor genes (Qin, 2002) and mutations in it are linked with different cancers (Oyama *et al.*, 2000). *ZDHHC9* is upregulated in colon cancer (Mansilla *et al.*, 2007) and *ZDHHC20* is overexpressed in many types of cancer (Draper and Smith, 2010). In addition *ZDHHC14* has been identified as a possible oncogene in diffuse B cell lymphomas and post-transplant lymphoproliferative disorders (Rinaldi *et al.*, 2006) and gain of function of *ZDHHC11* is associated with bladder cancer (Yamamoto *et al.*, 2007). Knockdown of DHHC8 by siRNA in a mouse mesothelioma model has recently been shown to enhance sensitivity to X-rays to suppress proliferation (Sudo *et al.*, 2012). Overexpression of *ZDHHC20* has also been

shown to enhance cellular transformation, a hallmark of tumour formation (Draper and Smith, 2010).

Associations have been found between X-linked mental retardation (XLMR) and both the *ZDHHC9* (Raymond *et al.*, 2007) and *ZDHHC15* genes (Mansouri *et al.*, 2005). There is also a tentative link between the *ZDHHC8* gene and schizophrenia. This is controversial, having been found in some studies (Chen *et al.*, 2004; Mukai *et al.*, 2004; Shin *et al.*, 2010) but not others (Faul *et al.*, 2005; Glaser *et al.*, 2005; Otani *et al.*, 2005; Xu *et al.*, 2010) and remains to be resolved.

There are implications of a strong role of aberrant palmitoylation in neurodegenerative diseases. Many proteins known to be involved in such conditions are substrates of DHHC enzymes. AMPA receptor subunits, palmitoylated by DHHC3/GODZ and DHHC17/HIP14 and NMDA receptor subunits, palmitoylated by DHHC3/GODZ (Hayashi *et al.*, 2009; Huang *et al.*, 2009), are both involved in glutamate-induced excitotoxicity. The enzyme β-site amyloid precursor protein-cleaving enzyme 1 (BACE1), which is associated with Alzheimer's disease (AD) is palmitoylated by DHHC3/GODZ, -4, -7/SERZ, and -15 (Vetrivel *et al.*, 2009). Huntingtin (Htt), the protein involved in Huntington's disease (HD), is palmitoylated by DHHC13/HIP14-like (HIP14L) and DHHC17/HIP14 (Huang *et al.*, 2009). The strength of the interaction between DHHC17/HIP14 and Htt is inversely correlated with the length of the polyglutamine repeat region (Singaraja *et al.*, 2002) and knockout mice for both DHHC17/HIP14 (Singaraja *et al.*, 2011) and DHHC13/HIP14L (Sutton *et al.*, 2012) display symptoms similar to a mouse model of HD, suggesting a prominent role of palmitoylation in its pathogenesis.

A group of neurodegenerative disorders in which palmitoylation appears to play a particularly prominent role is the neuronal ceroid lipofuscinoses, or Batten disease. This is a group of lysosomal storage disorders related to different genes which is characterised by an autofluorescent storage material which gradually accumulates over time (Cooper, 2010). The gene associated with the earliest-onset form, INCL, is PPT1 (Vesa *et al.*, 1995). This is a lysosomal enzyme, which fits in with the broad grouping of lysosomal storage disorders. There are a number of different mutations which can result in lack of mRNA expression, a distorted palmitate binding pocket or lack of enzymatic activity (Das *et al.*, 2001). Dysfunctional PPT1 may contribute to the lysosomal pathology of INCL by allowing build-up of lipids in lysosomes (Lu *et al.*, 1996). Disruption of either PPT1 or PPT2 in mice causes neuronal ceroid lipofuscinosis-like symptoms (Gupta *et al.*, 2001). A knockout mouse for

Ppt1 has been made and showed a progressive synaptic pathology with loss of SNAP25 immunoreactivity correlating with neuron loss in some brain regions and globular synaptobrevin aggregates around surviving neurons (Bible *et al.*, 2004; Kielar *et al.*, 2009). There was also very high expression of the inflammatory protein C-C motif chemokine 3 (Ccl3)/macrophage inflammatory protein 1α (MIP-1α) in the thalamus suggesting an increased inflammatory response which may cause or be a response to the neuronal loss (Kielar *et al.*, 2009). *S. cerevisiae* does not have a homologue of PPT1, but the yeast *S. pombe* requires its PPT1 homologue for viability and the knockout can be rescued with human PPT1 (Cho and Hofmann, 2004). Rescue of the lethal phenotype with mutant PPT1 constructs gave phenotypes similar to lysosomal storage disorders, such as sensitivity to high extracellular pH (Cho and Hofmann, 2004). *D. melanogaster* Ppt1 is also required for development and mutants show similar pathologies to INCL, including accumulation of an abnormal storage material and reduced lifespan (Buff *et al.*, 2007; Chu-LaGraff *et al.*, 2010; Hickey *et al.*, 2006; Korey and MacDonald, 2003; Saja *et al.*, 2010). *Caenorhabditis elegans ppt-1* mutants, however, show only a mild mitochondrial defect, suggesting other important contributing factors to INCL pathology may not be present in this model organism (Porter *et al.*, 2005).

Another neuronal ceroid lipofuscinosis, an adult-onset variant (ANCL) has recently been linked to mutations in the gene encoding cysteine string protein (CSP) (Benitez *et al.*, 2011; Noskova *et al.*, 2011; Velinov *et al.*, 2012), a protein which has the most known palmitoylated cysteine residues (Gundersen *et al.*, 1994). Mutants of CSP show a neurodegenerative phenotype both in mice (Fernandez-Chacon *et al.*, 2004) and in *D. melanogaster* (Zinsmaier *et al.*, 1994). In addition, palmitoylation of *D. melanogaster* CSP by its palmitoyltransferase Hip14 was shown to target it to synaptic vesicles and was required for synaptic functionality (Ohyama *et al.*, 2007). In *H. sapiens*, CSP is also palmitoylated by DHHC17/HIP14 among other DHHCs (Greaves *et al.*, 2008), giving a possible role for its palmitoylation in ANCL.

1.6 MODEL ORGANISMS

The use of model organisms has been instrumental in the study of palmitoylation. The relatively simple organism *S. cerevisiae* was used to identify the first confirmed PATs and through their common DHHC-CRD opened the study of similar enzymes in other organisms (Lobo *et al.*, 2002; Roth *et al.*, 2002). There have been relatively few studies in *D. melanogaster* (Bannan *et al.*, 2008), but the importance of CSP and SNAP-25

palmitoylation by Hip14 in synaptic transmission has been elucidated (Ohyama *et al.*, 2007; Stowers and Isacoff, 2007). CSP had previously been shown to be an important protein as its mutation induced paralysis and shortened survival times (Zinsmaier *et al.*, 1994). Hip14 was also shown to be important for the correct membrane localisation and secretion of short gastrulation (Sog) (Kang and Bier, 2010). A *D. melanogaster* model of INCL has also been made by mutating the *Ppt1* gene and reproduces the progressive neurodegeneration of the disease (Buff *et al.*, 2007; Chu-LaGraff *et al.*, 2010; Glaser *et al.*, 2003; Hickey *et al.*, 2006; Korey and MacDonald, 2003). Studies in knockout mice have also informed about the physiological roles of some of the enzymes involved in palmitoylation. The knockouts of the DHHCs HIP14 and HIP14L show pathological features similar to a mouse model of HD, for example (Singaraja *et al.*, 2011; Sutton *et al.*, 2012; Young *et al.*, 2012). The mouse knockouts of PPT1 (Bible *et al.*, 2004; Gupta *et al.*, 2001; Kielar *et al.*, 2009) and PPT2 (Gupta *et al.*, 2001; Gupta *et al.*, 2003) have replicated the phenotype of INCL and given clues as to the potential mechanisms of neurodegeneration in this disorder.

1.6.1 *C. ELEGANS*

A useful model organism whose use has been neglected so far in palmitoylation research is the nematode worm, *Caenorhabditis elegans*. *C. elegans* is a simple eukaryotic organism whose ease of genetic manipulation makes it ideal for screening mutations of genes with linked function (Brenner, 1974). Originally this was phenotype driven, performed by looking for common phenotypes in animals exposed to a mutagen. The publication of the *C. elegans* genome, the first of a multicellular animal (*C. elegans* Sequencing Consortium, 1998), allowed such screens to be performed based on genes belonging to the same biochemical families as well.

C. elegans was first isolated as a free-living organism in soil which feeds on bacteria and can be cheaply and conveniently cultured in the laboratory (Brenner, 1974). They are mostly hermaphrodites which self-fertilise and give rise to genetically identical progeny, making maintenance of strains containing mutant alleles particularly easy. Males do occur spontaneously at a proportion of roughly one male per 5000 hermaphrodites and offer a way to introduce new alleles by crossing (Fay). Both the hermaphrodite and male cell lineages have been precisely mapped, with hermaphrodites having 810 somatic cells and males 970 (Sulston and Horvitz, 1977). Mutants can often result in behavioural phenotypes which can be readily scored against wild-type behaviour, such as unco-ordinated locomotion (Unc) or mechanosensation defective (Mec). Rescue or modulation of these phenotypes with other mutants can give insights into the function of the proteins involved.

Similarly, related or highly similar phenotypes can give evidence for proteins which are involved in the same pathway or cellular process.

Studies using mutant animals can be complemented by using RNA interference (RNAi), which was originally developed in *C. elegans*. Some genes are required for viability so RNAi can also be used to probe the function of these genes, as surviving animals by definition have high enough expression for viability but not necessarily for normal function. The RNAi concept originated from the observation of reduced expression of a herpes simplex virus gene in a mouse cell line when complementary antisense transcripts were injected (Izant and Weintraub, 1984). This was further developed in *C. elegans* with the design of antisense RNAs against the *unc-22* and *unc-54* genes. Injection of these constructs into the gonads of adult wild-type hermaphrodites induced a phenotype similar to the mutants of those genes in their progeny (Fire *et al.*, 1991). Its utility as a tool for quickly reducing gene expression *in vivo* was enhanced by the discovery that use of double-stranded RNA (dsRNA) increases efficacy by an order of magnitude (Fire *et al.*, 1998). RNAi in *C. elegans* has become particularly easy to perform with the development of protocols which enable feeding of bacteria expressing dsRNAs to the animals rather than having to inject them with the constructs (Timmons *et al.*, 2001). This is made possible by the ability of the gut to absorb the dsRNAs which are then distributed to most other tissues (Fischer, 2010) although some tissues, such as most neurons, are refractory to RNAi (Asikainen *et al.*, 2005). Libraries of bacteria carrying vectors expressing dsRNA directed against the majority of the predicted and confirmed genes in *C. elegans* have been constructed (Kamath *et al.*, 2001). The use of RNAi gives a relatively easy method of disrupting gene function without having to produce and validate mutant strains. Results obtained through RNAi can also complement those from mutant strains, giving higher confidence that the phenotypes observed are not due to secondary mutations arising from the mutagenesis procedure.

Studies on palmitoylation in *C. elegans* have been rare. An attempt to create a model of INCL by characterising *ppt-1* mutants had mixed success. At a cellular level only a mild mitochondrial defect was observed, not as severe as INCL models in other organisms. The ability of the group to perform many behavioural and phenotypic analyses on the animals is an example of how mutant strains can be quickly characterised. Some mild phenotypes were found, including a delay in the moult from the final larval stage to adult animals and in onset of egg-laying behaviour, but not in brood size or lifespan (Porter *et al.*, 2005). Only one of the DHHC enzymes in *C. elegans*, spermatogenesis deficient 10 (SPE-10), has been studied. However these studies mainly occurred before the identification of its DHHC-CRD

and focused on a defect in fusion of an organelle with the PM which affected spermatogenesis (Gleason *et al.*, 2006; Shakes and Ward, 1989). This strain also showed increased stress resistance and an increase in maximum lifespan (Cypser and Johnson, 1999).

The lack of other studies investigating palmitoylation in this important and useful model organism is surely unjustified. *C. elegans* has the advantage of being a simple multicellular organism in which many fundamental processes are conserved with higher mammals, such as neurotransmission. This means it combines many of the advantages of unicellular organisms and higher organisms. The relatively easy genetics allows screens of mutations in whole gene families to be performed easily when compared with the expense and time involved in creating rodent knockouts and models, whilst still maintaining relevance to similar pathways in higher organisms. The application of RNAi in this organism, both against individual genes and combinations also allows rapid screening of many genes which may only be possible in a similar way in mammals by use of cell lines. Data obtained from experiments using *C. elegans* will complement those already obtained in *S. cerevisiae* and *D. melanogaster* and help inform further studies in the mammalian context.

1.7 AIMS AND OBJECTIVES

Since the discovery a decade ago of the first enzymes responsible for palmitoylating proteins, the field of palmitoylation has gradually gained pace, helped by the identification of the DHHC-CRD as their characteristic feature. The study of specific enzyme-substrate interactions was mainly restricted to *S. cerevisiae* and mammalian cell lines. The development of proteomic scale technology has allowed candidate palmitoyl-proteins to be found in an ever-increasing number of different cell lines, tissues and organisms. However, the model organism *C. elegans* has yet to have any such analyses performed on it. This thesis aims to address this gap in palmitoylation research with the following objectives:

1. To determine the enzymes involved in palmitoylation in *C. elegans* and their phylogenetic relationships through *in silico* resources and predict potential interactions and phenotypes using data from other organisms.

2. To use mutants and RNAi to disrupt each *C. elegans* enzyme in order to uncover resulting phenotypes.

3. To adapt the ABE and acyl-RAC proteomic approaches for use with *C. elegans* and thereby produce the first palmitoyl-proteome of a whole multicellular organism.

Chapter 2:

MATERIALS AND METHODS

2.1 MATERIALS

2.1.1 REAGENTS

All chemicals and primers were obtained from Sigma (Dorset, UK) unless otherwise specified.

Absolutely RNA Microprep Kit was obtained from Agilent Technologies (Stockport, UK). Diethyl pyrocarbonate-treated water was obtained from Ambion (Life Technologies, Paisley, UK). BioScript reverse transcriptase and its buffer and isopropyl β-D-1-thiogalactopyranoside (IPTG) were obtained from Bioline (London, UK). Phusion DNA polymerase and its buffers were obtained from Finnzymes (Vantaa, Finland; part of Thermo Scientific). Antibiotics were obtained from Formedium (Hunstanton, UK). The 30% ProtoGel, 4X ProtoGel resolving buffer, ammonium persulphate (APS), N,N,N',N'-tetramethylethylenediamine (TEMED), ProtoGel stacking buffer, Pre-stained Protein Ladder and ProtoBlue Safe were obtained from Geneflow (Fradley, UK). SYBR® Safe DNA Gel Stain, RNase OUT, BP clonase™ II, LR clonase™ II, T4 DNA ligase and its buffer and NuPAGE® 12% Bis-Tris Gels were obtained from Invitrogen (Life Technologies, Paisley, UK). IRBlue gel stain was obtained from Licor (Lincoln, NE, USA). HighRanger Plus 100bp DNA Ladder was obtained from Norgen Biotek (Thorold, ON, Canada). Restriction endonucleases and their buffers were obtained from New England Biolabs (Hitchin, UK). Shrimp alkaline phosphatase (SAP) was obtained from Promega (Madison, WI, USA). Complete Mini EDTA-free Protease Inhibitor Cocktail (PI) tablets were obtained from Roche (Mannheim, Germany). Frozen rat brains were obtained from Seralab (Barnet, UK). The GenElute™ Plasmid Miniprep Kit, GenElute™ Gel Extraction Kit, 425-600 µm acid-washed glass beads and thiopropyl Sepharose® 6B were obtained from Sigma. The Pierce® Bicinchoninic Acid (BCA) Protein Assay Kit, EZ-link® biotin-HPDP and NeutrAvidin® UltraLink® Resin were obtained from Thermo Scientific (Rockford, IL, USA). DH5α *Escherichia coli* cells were made in-house.

Primary antibodies used were: mouse anti-synaptosome-associated protein of 25 kDa (SNAP-25) and rabbit anti-Munc18 (BD Transduction Laboratories, Ireland); mouse anti-syntaxin 1 (HPC1) and rabbit anti-syntaxin-3 (Synaptic Systems, Göttingen, Germany); rabbit anti-vesicle-associated membrane protein 2 (VAMP-2) (a gift from M. Takahashi); anti-cysteine string protein (CSP) raised in rabbit as previously described (Chamberlain and Burgoyne, 1996). Horseradish peroxidase (HRP)-coupled secondary antibodies used were: anti-mouse-HRP and anti-rabbit-HRP (Sigma).

2.1.2 NEMATODE STRAINS AND MATERIALS

All *C. elegans* strains were obtained from the *Caenorhabditis* Genetics Center (University of Minnesota, Twin Cities, MN, USA) except tm4272, which was obtained from the National Bioresource Project for the Experimental Animal "Nematode *C. elegans*" based in the lab of Dr Shohei Mitani (Tokyo Women's Medical University, Tokyo, Japan).

E. coli OP50 was obtained from the *Caenorhabditis* Genetics Center. The Vidal *C. elegans* Open Reading Frame (ORF) RNAi feeding library was obtained from Source Bioscience (Nottingham, UK) (Rual *et al.*, 2004). Culture plates were obtained from Appleton Woods (Birmingham, UK). 2 ml round-bottom cryogenic vials used for homogenisation of worms were obtained from Corning (Amsterdam, the Netherlands).

2.2 *IN SILICO* WORK

2.2.1 DATABASE MINING

Initial searches for putative worm DHHC enzymes were conducted on WormBase (http://www.wormbase.org/) using the Pfam tag of DHHC zinc-finger domain (PF01529). Palmitoyl-protein thioesterases (PPTs) were found by BLAST searching (http://blast.ncbi.nlm.nih.gov/) using the known human PPT sequences; no characteristic PPT domain has been found.

H. sapiens, *D. melanogaster* and *S. cerevisiae* DHHCs and PPTs were found by searching the NCBI databases (http://www.ncbi.nlm.nih.gov/). The numbers of enzymes found in all organisms were verified by reference to figures existing in the literature.

2.2.2 SEQUENCE ANALYSIS

Sequence alignments were performed using the Clustal Omega online program (http://www.ebi.ac.uk/Tools/msa/clustalo/). Colour highlighting of salient domains was manually applied.

Phylogenetic trees were generated using the Phylip v3.69 suite of programs (http://evolution.genetics.washington.edu/phylip/getme.html). The output was uploaded to the Interactive Tree of Life server (http://itol.embl.de/index.shtml) (Letunic and Bork, 2007) and manipulated to obtain the trees presented here.

2.3 NEMATODE WORK

2.3.1 NOMENCLATURE

The official names for all genes and proteins were used, using the source Wormbase (http://www.wormbase.org/). Unnamed genes were named according to official conventions.

2.3.2 CULTURE

For normal maintenance, *C. elegans* were cultured in 60mm plates on nematode growth medium agar (NGM; 2% (w/v) agar, 0.3% (w/v) NaCl, 0.25% (w/v) peptone, 1 mM $CaCl_2$, 5 µg ml^{-1} cholesterol, 25 mM KH_2PO_4, 1 mM $MgSO_4$) at 20 °C, seeded with 30 µl *E. coli* OP50 culture as a food source, using standard methods (Brenner, 1974). For proteomic studies, *C. elegans* were grown in liquid culture.

2.3.3 FROZEN STOCKS

C. elegans can survive freezing, which is convenient for long term storage. The best plates for freezing are slightly starved and contain many L1 and L2 larvae. The plate was washed off with 1.5 ml M9 buffer (5 g l^{-1} NaCl, 3 g l^{-1} KH_2PO_4, 6 g l^{-1} Na_2HPO_4, 1 mM $MgSO_4$). 1.5 ml freezing solution (100 mM NaCl, 50 mM KH_2PO_4, 30% (w/v) glycerol, 5.5 mM NaOH, 3 mM $MgSO_4$) was added and mixed well. The mixture was split evenly between four cryovials, and put in a -80 °C freezer packed in a polystyrene box wrapped in tissue to achieve a slower freezing rate of approximately 1 °C per minute. One of the aliquots was thawed the following day and plated to check there were surviving worms. Working populations of worms were refreshed from frozen stocks periodically to combat any genetic drift from normal strain maintenance.

2.3.4 FEEDING RNAI

RNAi feeding experiments were conducted using bacteria from the Vidal *C. elegans* ORF RNAi Library (Rual *et al.*, 2004) where available, or were cloned in-house. All RNAi feeding bacteria were *E. coli* strain HT115 carrying the pG-L4440 vector containing the relevant insert.

Plates of NGM containing 25 µg ml^{-1} carbenicillin and 1 mM IPTG were poured 4-7 days before seeding with 50 µl of the relevant bacterial strain. RNAi plates were always kept in the dark, as IPTG is light sensitive. The bacteria were allowed to induce overnight. Ten L3-L4 stage worms were transferred to each plate. Once the next generation of worms had reached young adult stage, three adults were moved onto individual replica plates, allowed

to lay eggs and removed the following day. These progeny were used in the assays once they had reached adulthood.

2.3.5 MORPHOLOGY

Morphology of individual worms was assessed using a microscope stage controlled by computer through an Optiscan II box (Prior) with a video feed transmitted by a DinoEye Eyepiece Camera (ANMO Electronics Corporation). WormTracker software (http://www.mrc-lmb.cam.ac.uk/wormtracker/; v2.0.3.1) was used to track the worms and collect data over a two minute period. Data were analysed in Worm Analysis Toolbox software (v1.9) and Microsoft® Office Excel® 2007.

2.3.6 LIFESPAN

To synchronise a worm strain, a relatively full plate of gravid adults was collected and treated by bleaching to release eggs which were transferred to the edge of a seeded plate. These worms were picked onto lifespan plates once they reached adulthood, defined as day 0. Plates were checked every 1-2 days to determine survival and worms were transferred to a fresh plate if necessary.

2.3.7 BEHAVIOURAL ASSAYS

Behaviour was assessed using assays testing locomotory ability in liquid and on solid media, locomotory ability with age in liquid and mechanosensation using standard methods outlined in Section 4.2.3.

2.3.8 STATISTICAL ANALYSIS

If two data sets were being directly compared, Student's *t*-test was used. For comparison of multiple data sets in one analysis, a one-way analysis of variance (ANOVA) was used. These tests were performed in Microsoft Office® Excel® 2007 and SigmaPlot (Systat Softare, Inc.; v.12.2.0.45).

Lifespan analyses were performed using the Online Application for the Survival Analysis of Lifespan Assays (OASIS; http://sbi.postech.ac.kr/oasis/introduction/) (Yang *et al.*, 2011). Mean lifespans were compared using the log-rank (Mantel-Cox) test, and mortality at more specific time points was compared using Fisher's exact test. Age-dependent thrashing was compared using one-way analysis of covariance (ANCOVA) in Microsoft Office® Excel® 2007.

2.4 MOLECULAR BIOLOGY

2.4.1 DNA PURIFICATION AND VERIFICATION

E. coli containing the relevant plasmid were cultured overnight in 5 ml LB containing a selection antibiotic at 37 °C, 250 rpm. 2 ml culture was pelleted in an Eppendorf tube in a microcentrifuge at 14000 rpm for one minute. The supernatant was discarded and the DNA extracted from the bacterial pellet using a GenElute™ HP Plasmid Miniprep Kit following the manufacturer's guidelines.

The identity of purified DNA was confirmed either with digestion using restriction endonucleases and separation by agarose gel electrophoresis or by sequencing by DNA Sequencing & Services at the University of Dundee, UK.

2.4.2 GATEWAY™ CLONING

To form a complete library of RNAi feeding bacteria clones for the DHHCs, it was necessary to clone some vectors. Complementary DNA (cDNA) was first synthesised from wild-type *C. elegans* total RNA extract. Reverse transcriptase polymerase chain reaction (RT-PCR) was performed using custom-designed primers to generate an attB-flanked DNA sequence. The BP reaction was performed to transfer this DNA into the attR-containing vector pDONR201. Successful incorporation into the vector was verified by transforming into DH5α cells, miniprepping and performing test digests. This generated attL-flanked DNA sequences which were transferred into the attR-containing vector pG-L4440 using the LR reaction. Successful incorporation into the pG-L4440 vector was verified by transforming into DH5α cells, miniprepping and performing test digests. The vectors were then transformed into HT115 cells for consistency with the Vidal RNAi library.

2.5 PROTEIN BIOCHEMISTRY

2.5.1 PREPARATION OF LYSATES

2.5.1.1 RAT BRAIN

10 ml homogenisation buffer (HB; 0.32 M sucrose, 10 mM HEPES pH 7.4) containing one Complete Mini EDTA-free PI tablet was made up and pre-chilled on ice. An adult female Sprague Dawley rat brain, snap-frozen, was thawed on ice in about 5 ml HB. The brain was cut into pieces that were as small as possible using dissection scissors on a glass plate. The brain was transferred to a specialised glass tube, the remaining HB added and processed using an electric homogeniser (Janke & Kunkel K.G., now IKA®-Werke GmbH & Co. K.G., Staufen, Germany) until homogeneous. The homogenate was spun at 3500 rcf at 4 °C for

five minutes to remove debris. The supernatant was split into 1 ml aliquots in Eppendorf tubes and SDS added to 2% final concentration. These were rotated for 10-20 minutes at room temperature and spun at 14000 rpm, 4 °C for five minutes. The remainder of the supernatant was transferred to a 15 ml Falcon tube.

2.5.1.2 NEMATODES

Worm pellets were frozen at -80 °C and thawed on ice before use. Up to 500 µl worms and an equal volume of worm homogenisation buffer (WHB: 140 mM KCl, 1 mM ethylenediaminetetraacetic acid (EDTA), 50 mM HEPES pH 7.4, 2% SDS) with PIs were put in a 2 ml round-bottom cryogenic vial. 425-600 µm acid-washed glass beads were added up to the meniscus using a tip box lid. Tubes were shaken in a Mikro-Dismembrator S (B. Braun Biotech International, Melsungen, Germany) at 2000 rpm for two minutes. Three holes were made in the base of each tube with a BD Microlance™ 3 25G (Becton Dickinson & Co. Ltd, Ireland). The tube was placed in a 15ml Falcon and spun at 5000 rpm, 4 °C for five minutes. The lysate was transferred to Eppendorfs and spun at 13000 rpm, 4 °C for 20 minutes. The supernatant was transferred to fresh tubes and used immediately.

2.5.2 PURIFICATION OF PALMITOYL-PROTEINS

Palmitoyl-proteins were purified from rat brain and *C. elegans* homogenates using two methods: acyl-biotin exchange (ABE) and acyl-resin-assisted capture (acyl-RAC). These are summarised below, with full protocols outlined in Sections 5.2.2.4 and 5.2.2.5.

2.5.2.1 ACYL-BIOTIN EXCHANGE

Methyl methanethiosulphonate (MMTS) was added to 20 mM to the lysate to block free thiols and incubated at room temperature for two hours. The sample was split into three 15 ml Falcon tubes and a methanol precipitation performed as follows:

- a three-times volume of -20 °C methanol was added and the tubes vortexed and spun at 3500 rcf, 4 °C for two minutes
- the supernatant was discarded and the pellet resuspended in 1 ml solubilisation buffer (SB; 4% SDS, 50 mM Tris.HCl, 5 mM EDTA, pH 7.4) and incubated at 37 °C, 220 rpm for 30 minutes
- the solution was made up to 4 ml total volume with lysis buffer (LB; 150 mM NaCl, 50 mM Tris.HCl, 5 mM EDTA, pH 7.4) + 0.2% Triton X-100 (LB-T)
- the methanol precipitation was repeated three times in total

The combined volume was split into two 15 ml Falcons. Hydroxylamine (HA) was added to 1 M to the experimental tube to cleave thioester bonds between cysteine residues and palmitate molecules. Tris.HCl was added to 1M to the control tube. EZ-link® N-[6-(biotinamido)hexyl]-3'-(2'-pyridyldithio)propionamide (biotin-HPDP) was added to both tubes to 0.5 mM to label revealed thiols. Samples were incubated at room temperature on a rocker overnight.

Each sample was methoanol precipitated three times. The final time, 250 µl SB was used for resuspension and was made up to 10 ml with LB-T before incubating on a rocker at room temperature for 30 minutes. Meanwhile, 600 µl NeutrAvidin® UltraLink® Resin per tube, which binds to the biotin-HPDP-labelled protein, was washed three times in 10 ml LB-T and spun at 3500 rcf, 4 °C for two minutes between washes. The samples were spun at 3500 rcf, 4 °C for two minutes and the supernatant was added to the washed beads and incubated at room temperature on a rocker for 90 minutes. After spinning at 3500 rcf, 4 °C for two minutes, the pellet was washed four times with 10 ml LB-T + 0.1% SDS, spinning at 3500 rcf, 4 °C for two minutes between washes. Proteins were eluted in 3 ml LB-T + 1% β-mercaptoethanol (β-ME) by incubating at 37 °C for one hour with occasional agitation. The samples were spun at 3500 rcf, 4 °C for two minutes, and the supernatant split into 0.3 ml aliquots in Eppendorfs to allow a methanol precipitation with a 10000 rpm spin at 4 °C for five minutes. The pellets were resuspended serially in 250µl 4X Laemmli buffer (8% SDS, 40% glycerol, 20% β-ME, 0.008% bromophenol blue, 0.25 M Tris.HCl, pH 6.8). 1 ml 4X Laemmli was added to the bead pellet, which was resuspended and boiled. The supernatant was taken off and stored at -20 °C (Laemmli elution).

2.5.2.2 ACYL-RESIN-ASSISTED CAPTURE

A bicinchoninic acid (BCA) assay was performed on all samples to determine their concentrations. Each sample was diluted to 2 mg ml^{-1} with blocking buffer (100 mM HEPES, 1 mM EDTA, 2.5% SDS, pH 7.4). MMTS was added to 0.5% to block free thiols and the samples incubated at 40 °C for one hour with frequent vortexing. The samples were methanol precipitated three times; the final time, instead of resuspending in SB, the samples were resuspended in 1 ml binding buffer (100 mM HEPES, 1 mM EDTA, 1% SDS, pH 7.4) and incubated at 37 °C, 220 rpm for 30 minutes. Meanwhile, 0.25g thiopropyl Sepharose® 6B beads per sample were washed in 20 ml distilled water for 15 minutes. These beads bind directly to revealed thiols. The beads were spun at 3500 rcf, 4 °C for two minutes, the supernatant removed and an equal volume of binding buffer added to the settled slurry. Each sample was split into two and 1 ml slurry added to each. HA was added

to 1 M to the experimental tube and Tris.HCl to 1 M to the control tube and a PI tablet added. Samples were incubated on a rocker at room temperature overnight.

The following day, samples were spun at 3500 rcf, 4 °C for two minutes. The bead pellet was washed five times with 5 ml binding buffer, spinning at 3500 rcf, 4 °C for two minutes between washes. Proteins were eluted in 3 ml LB-T + 1% β-ME by incubating at 37 °C for one hour with occasional agitation. The samples were spun at 3500 rcf, 4 °C for two minutes, and the supernatant split into 0.3 ml aliquots in Eppendorfs to allow a methanol precipitation with a 10000 rpm spin at 4 °C for five minutes. The pellets were resuspended serially in 250µl 4X Laemmli buffer (8% SDS, 40% glycerol, 20% β-ME, 0.008% bromophenol blue, 0.25 M Tris.HCl, pH 6.8). 1 ml 4X Laemmli was added to the bead pellet, which was resuspended and boiled. The supernatant was taken off and stored at -20 °C (Laemmli elution).

2.5.3 SDS-PAGE

Separation of protein samples was performed using SDS-polyacrylamide gel electrophoresis (SDS-PAGE). Samples were prepared by boiling in Laemmli buffer at 95 °C for five minutes. Gels were cast in the Mini PROTEAN 3 system (BioRad, Hemel Hempstead, UK). Two 15% resolving gels were made by mixing 6.25 ml 30% ProtoGel, 3.13 ml 4X ProtoGel resolving buffer and 3 ml distilled H_2O. Polymerisation was initiated by adding 125 µl 10% APS and 12.5 µl TEMED and mixing. 5 ml gel was transferred into the 1 mm space between two glass plates held in a casting frame. The remaining volume was filled with distilled H_2O and the gel allowed to set. For the 4% stacking gel, 1.3 ml 30% ProtoGel, 2.5 ml ProtoGel stacking buffer and 6.1 ml distilled H_2O were mixed. Polymerisation was initiated by adding 50 µl 10% APS and 10 µl TEMED and mixing. The water was poured out of the casting apparatus and remaining drops soaked up with filter paper. The apparatus was filled to the top with stacking gel and a comb inserted and the gel allowed to set. Pre-cast NuPAGE® 12% Bis-Tris Gels were also used.

Gels were put into gel tanks which were filled with running buffer (0.025 M Tris, 0.192 M glycine, 0.1% SDS). Combs were removed from the gels and samples were loaded alongside 5 µl pre-stained protein ladder. Gels were run at 180-200 V until the dye reached the bottom of the gel. Gels were visualised by staining with Coomassie Blue, ProtoBlue Safe or IRBlue, or by silver staining. Gels were imaged in a ChemiDoc XRS with Quantity One software.

2.5.4 WESTERN BLOTTING

Proteins were transferred to nitrocellulose submerged in transfer buffer (0.025 M Tris, 0.192 M glycine, 20% methanol) in a BioRad Trans-blot Electrophoresis Transfer Cell, either at 100 V for one hour with an ice pack or 20 V overnight. Nitrocellulose was blocked for one hour in Tris-buffered saline (TBS; 20 mM Tris, 140 mM NaCl, pH 7.4) with 0.1% Tween 20 (TBS-T) and 5% (w/v) dried skimmed milk. The primary antibody was applied at an appropriate dilution in TBS-T supplemented with 5% (w/v) BSA and incubated on a rocker for either one hour at room temperature or at 4 °C overnight. The nitrocellulose was washed three times in TBS-T for five minutes before incubation in an appropriate HRP-conjugated secondary antibody at 1:2000 dilution for one hour on a rocker. The nitrocellulose was rinsed with TBS-T and visualised using enhanced chemiluminescence (ECL) reagents A (2.5 mM luminol, 400 µM *p*-coumaric acid, 100 mM Tris.HCl pH 8.5) and B (0.018% H_2O_2, 100 mM Tris.HCl pH 8.5) mixed 1:1. Imaging was performed in a ChemiDoc XRS using Quantity One software.

2.5.5 MASS SPECTROMETRY

The β-ME or Laemmli eluates were sent to Dr Mary Doherty (University of the Highlands and Islands, Inverness, UK) who kindly analysed them by liquid chromatography-tandem mass spectrometry (LC-MS/MS) was performed using a Thermo LTQ-Orbitrap XL LC-MS^n mass spectrometer equipped with a nanospray source and coupled to a Waters nanoAcquity ultra performance liquid chromatography (UPLC) system.

The data were subsequently analysed using Proteome Discoverer software (Thermo Scientific, Rockford, IL, USA) and MaxQUANT (http://maxquant.org/index.htm) and searched against a locally implemented MASCOT server (v2.3.01). Results were processed by discarding contaminants. The ratio of experimental:control scores was taken and any with a ratio of less than five were discarded (Martin and Cravatt, 2009). A control value of 0.2 was given to proteins present only in the experimental samples to avoid dividing by zero (Dowal *et al.*, 2011; Roth *et al.*, 2006; Yang *et al.*, 2010). Results were considered higher confidence if identified from multiple unique peptides and lower confidence if identified from a single unique peptide. Unfortunately there were insufficient repeats to perform robust statistical analysis of the mass spectrometry output.

Chapter 3:

IN SILICO ANALYSIS

3.1 INTRODUCTION

3.1.1 INVESTIGATION OF PALMITOYL ACYL-TRANSFERASES IN DIFFERENT ORGANISMS

3.1.1.1 IDENTIFICATION OF PALMITOYL ACYL-TRANSFERASES

Although palmitoylation as a post-translational modification in eukaryotic cells had been known about for many years (Omary and Trowbridge, 1981), it was not until relatively recently that the enzymes involved were identified (Bohm *et al.*, 1997; Fukata *et al.*, 2004; Mitchell *et al.*, 2006; Roth *et al.*, 2002). The realisation that these palmitoyl acyl-transferases (PATs/DHHCs) shared the eponymous aspartic acid-histidine-histidine-cysteine (DHHC) motif in a cysteine-rich domain (CRD) allowed easy searching of whole genome data for putative DHHCs. This method has allowed the prediction of 23 such genes in humans (*Homo sapiens*) and 24 in mice (*Mus musculus*) (Fukata *et al.*, 2004; Fukata and Fukata, 2010), 22 in fruit flies (*Drosophila melanogaster*) (Bannan *et al.*, 2008) and eight predicted, of which seven are confirmed, in yeast (*Saccharomyces cerevisiae*) (Roth *et al.*, 2002). Whilst the DHHC-CRD consensus has been refined from the initial NEW1 motif to $Cx_2Cx_3(R/K)PxRx_2HCx_2Cx_2Cx_4DHHCxW(V/I)xNC(I/V)Gx_2Nx_3F$, there is some tolerance to substitutions within this sequence (Mitchell *et al.*, 2006). The *S. cerevisiae* DHHCs Akr1, Akr2 and Pfa5 have a DHYC motif instead of DHHC, for example (Mitchell *et al.*, 2006). Furthermore, the eighth *S. cerevisiae* DHHC, YNL155W, is more distantly related and so its status as a *de facto* palmitoyltransferase is uncertain (Mitchell *et al.*, 2006). The motif is also the active site of these enzymes (Mitchell *et al.*, 2010) and many, though not all, of the predicted DHHCs have since been validated experimentally as having palmitoyltransferase enzymatic activity (Ohno *et al.*, 2012), giving high confidence that genes identified using this consensus sequence are likely to be genuine.

In the case of the nematode worm *Caenorhabditis elegans*, there has been some confusion in the literature, with figures of 15 (Fukata and Fukata, 2010), 16 (Mitchell *et al.*, 2006) and 17 (Gleason *et al.*, 2006) DHHC genes being quoted. However, there has been no analysis of these putative enzymes in terms of their palmitoylating activity. Given the suitability of *C. elegans* as a model system for probing questions about both development and neuronal function (Brenner, 1974; Chalfie and Sulston, 1981), coupled with the importance of palmitoylation in these systems (Fukata and Fukata, 2010; Porter *et al.*, 2005; Prescott *et al.*, 2009), a more thorough analysis could open up new areas of research within the field.

3.1.1.2 PREDICTION OF THE PROPERTIES OF PALMITOYL ACYL-TRANSFERASES

Numerous proteome-scale studies in recent years have enabled the identification of proteins which undergo palmitoylation in different cell types and organisms (Dowal *et al.*, 2011; Kang *et al.*, 2008; Marin *et al.*, 2012; Merrick *et al.*, 2011; Roth *et al.*, 2006; Yang *et al.*, 2010). However, there is comparatively little known about which DHHC enzyme(s) palmitoylate which substrate(s). This is partly due to the workload in characterising individual enzymes or substrates to obtain very specific information. A proteomic scale analysis gives much more information in terms of identifying many palmitoylated proteins but teasing out enzyme-substrate data is not so easily done. A study investigating DHHC2 substrates only found a handful of new candidates (Zhang *et al.*, 2008). However, these whole genome studies and some apparent general rules can give a headstart in predicting potential substrates for a DHHC enzyme before investigating it experimentally.

Several attempts have been made to group the DHHC enzymes into sub-families based on various parameters. A phylogenetic analysis to group enzymes based on their relatedness can be done to gain an initial overview of information on the DHHCs within individual organisms and also with a wider perspective by including families from many organisms. A comparison of the *S. cerevisiae* DHHCs with the *H. sapiens* DHHCs showed several broad sub-families (Mitchell *et al.*, 2006). DHHC enzymes have a common structure of at least four transmembrane domains (TMDs), with the DHHC motif found in the cytoplasmic loop between TMD2 and TMD3 (Fukata and Fukata, 2010; Kihara *et al.*, 2005; Korycka *et al.*, 2012; Mitchell *et al.*, 2006). Some sub-families can be explained by the presence of common domains that are not in the majority of the enzymes. For example, the *S. cerevisiae* enzymes Akr1 and Akr2 cluster with the *H. sapiens* enzymes DHHC17 (also called huntingtin-interacting protein 14 (HIP14)) and DHHC13 (also called HIP14-like (HIP14L)). All of these proteins have ankyrin repeat domains N-terminal of their first TMD. Other groups were observed to contain one *S. cerevisiae* DHHC and a handful of *H. sapiens* DHHCs (Mitchell *et al.*, 2006). A similar analysis was done including the *D. melanogaster* genes (Bannan *et al.*, 2008). The ankyrin repeat containing proteins in *D. melanogaster* clustered within that same group as above. A large group of enzymes with no homology to *S. cerevisiae* or *H. sapiens* DHHCs was also present. They hypothesised that this was the result of duplications during the evolution of different *Drosophila* species (Bannan *et al.*, 2008). Whether these have a species-specific role would be interesting to find out. There may be a high level of redundancy among this sub-group. Whilst proteins grouped using phylogenetics are not necessarily direct homologues, the function, localisation and

substrates of the enzymes in one organism could be used as a starting point for investigating proteins in another. This approach will be taken with the *C. elegans* family of enzymes.

Some tools for large scale prediction of enzyme properties are available in *S. cerevisiae*. Whilst these are not the result of careful individual protein analysis and have the caveats associated with many genome-wide methods, they can be useful predictors of broad properties. Among these are the green fluorescent protein (GFP) tagging project and various interaction studies, which are collated online via http://yeastgfp.yeastgenome.org/ and the *Saccharomyces* Genome Database (SGD). In addition, there has been a project to identify interacting proteins in *C. elegans* through yeast two-hybrid experiments which is collated online at http://www.functionalnet.org/wormnet/about.html. These resources may be used to give an idea of the localisation of different DHHCs and of possible classes of proteins which could interact with each enzyme. These could be very broad, as in the classes of palmitoyltransferase substrates based on the location of the palmitoylated cysteine residue(s) (Ohno *et al.*, 2012; Resh, 1999). It may even be possible to predict phenotypes in knockouts of individual DHHCs from the classes of protein with which they interact.

3.1.2 DISCOVERY OF PALMITOYL-PROTEIN THIOESTERASES

The palmitoyl-protein thioesterases (PPTs) present more of a challenge to study systematically due to the present lack of a common identifying motif (see Section 1.3). The mammalian cytosolic PPT acyl-protein thioesterase 1 (APT1) was originally discovered through its action in removing [^{3}H]-palmitate from Gα subunits (Duncan and Gilman, 1998). Another gene, APT2, has been found by homology to APT1 but has barely been studied. PPT1 was also discovered through biochemical activity against palmitoylated H-Ras (Camp and Hofmann, 1993) and has been shown to be lysosomal rather than cytoplasmic (Verkruyse and Hofmann, 1996), although in neurons it is localised to synaptic vesicles and synaptosomes instead (Lehtovirta *et al.*, 2001). This is likely to limit its physiological substrates. A second lysosomal enzyme, PPT2, was found through homology to PPT1 (Soyombo and Hofmann, 1997). It shares 26% identity with PPT1 and the ability to depalmitoylate palmitoyl-coenzyme A (palmitoyl-CoA), although it cannot depalmitoylate proteins (Calero *et al.*, 2003; Soyombo and Hofmann, 1997). Despite the lack of a consensus motif to find new PPT candidates within genomes, many of the methods described above can still be used to give information on localisation and possible substrates.

As DHHCs have not been studied in detail in *C. elegans* and the literature on its PPTs is limited to *ppt-1*, this chapter set out to perform a thorough characterisation of these enzyme families using various computational tools. The members of the DHHC family will be confirmed through the presence of the DHHC-CRD. Phylogenetic analyses will be performed on both the DHHC and PPT families to identify patterns both within the families and in the context of other important organisms in which they are known. This will be combined with the available information in various online databases to provide predictions which may help with the direction and interpretation of *in vivo* studies.

3.2 METHODS

3.2.1 DATABASE MINING

Initial searches for putative *C. elegans* DHHC enzymes were conducted on WormBase (http://www.wormbase.org/) using the Pfam tag of DHHC zinc-finger domain (PF01529). Palmitoyl-protein thioesterases (PPTs) were found by basic local alignment search tool (BLAST) searching (http://blast.ncbi.nlm.nih.gov/) using the known *H. sapiens* PPT sequences; no characteristic PPT domain has been found.

Basic information known about the *H. sapiens*, *D. melanogaster* and *S. cerevisiae* DHHCs and PPTs were found by searching the NCBI databases (http://www.ncbi.nlm.nih.gov/). In addition, the following organism-specific resources were used: *Saccharomyces* Genome Database (SGD) (http://www.yeastgenome.org/); FlyBase (http://flybase.org/); WormBase. Protein interaction data were obtained from SGD and from the WormNet website (http://www.functionalnet.org/wormnet/about.html). The localisation data for *S. cerevisiae* proteins were obtained from the *S. cerevisiae* GFP tagging project (http://yeastgfp.yeastgenome.org/).

3.2.2 SEQUENCE ANALYSIS

BLAST searches to identify potential orthologues were conducted using the amino acid sequence of the relevant protein. The "non-redundant protein sequences" database was searched with results restricted to the species of interest, depending on the analysis being performed.

Sequence alignments were performed using the Clustal Omega online program (http://www.ebi.ac.uk/Tools/msa/clustalo/). Colour highlighting of salient features was manually applied. The colouring of the sequences in the PPT alignments was applied using the Clustal Omega program and are the standard property-based colours.

The domain structure diagram was constructed principally from information predicted by the InterProScan program (http://www.ebi.ac.uk/interpro/). Where transmembrane domains were low confidence or ambiguous, additional evidence was sought from the TMpred program (http://www.ch.embnet.org/software/TMPRED_form.html). Information on the palmitoyltransferase conserved C-terminus (PaCCT) was obtained from a published analysis (Gonzalez Montoro *et al.*, 2009).

3.2.3 PHYLOGENETIC ANALYSIS

To generate phylogenetic trees, alignments were first generated using BioEdit (Isis Pharmaceuticals; v6.0.5) and saved in .phy format. This was used as the "infile" for Seqboot, a program in the suite of programs Phylip v3.69 (http://evolution.genetics.washington.edu/phylip/getme.html). 2000 bootstraps were generated and used as the "infile" for Proml, another Phylip program, using no outgroups and set to unrooted tree. 10 jumbles were used if computing power sufficed, otherwise one jumble was used. The "outtree" output file was used as the "intree" file for the Consense part of the Phylip suite. This final "outtree" file was uploaded to the Interactive Tree of Life server (http://itol.embl.de/index.shtml) (Letunic and Bork, 2007). Trees were formatted to display as unrooted and labels and clades were coloured using the tool provided.

Due to limitations in computing power, the analysis of the DHHCs containing all those from *S. cerevisiae*, *D. melanogaster*, *C. elegans* and *H. sapiens* was conducted using the conserved DHHC-CRD region only. All other analyses could be performed with the full length sequences.

3.3 RESULTS

3.3.1 EXPLORATION OF THE DHHC ENZYME FAMILY

3.3.1.1 IDENTIFICATION AND NAMING OF THE *C. ELEGANS* DHHC ENZYMES

Before exploring palmitoylation in *C. elegans*, it was first necessary to confirm its DHHC enzymes and find what is already known about them and their counterparts in other organisms. The online database WormBase (http://www.wormbase.org/) contains all the known genomic, transcript, protein and functional data associated with *C. elegans* and is frequently updated. A search of WormBase (version WS207) for the Pfam tag assigned to the DHHC motif uncovered 15 genes. Four of these 15 were previously named: *dhhc-1*, *dhhc-2*, *tag-233* and *spe-10*. The remainder were annotated only with their gene code.

These were renamed in line with official conventions using the *dhhc-x* nomenclature already started. *tag-233*, a temporarily assigned gene name, was also renamed. Where possible, the number assigned to the *dhhc-x* nomenclature was based on homology to the *H. sapiens* DHHCs. The *spe-10* name is based upon a published spermatogenesis defect phenotype (Cypser and Johnson, 1999; Gleason *et al.*, 2006; Shakes and Ward, 1989) and so was not altered to avoid confusion within the literature. The old and new gene names and their respective codes are shown in Table 3.1. The proposal to the WormBase gene naming committee was accepted, and as a result the number of *dhhc* genes increased from two to 14 as of release WS235 of WormBase.

3.3.1.2 CHARACTERISTICS OF THE *C. ELEGANS* DHHC ENZYMES

A sequence alignment of the primary sequence of the 15 *C. elegans* DHHCs was performed (Figure 3.1). This confirms that all of them contain the DHHC motif required for enzymatic activity within a cysteine-rich region. The positions of these cysteines relative to the DHHC motif are absolutely conserved and correspond to those originally observed in this domain (Bohm *et al.*, 1997). To assess whether the *C. elegans* DHHCs conform to the common structure found in this family, a domain structure diagram was constructed using domains predicted from the primary sequence (Figure 3.2). In general, DHHCs have been found to have four TMDs, though some have more, and the DHHC-CRD is normally located in a cytoplasmic loop between the second and third TMDs (Fukata and Fukata, 2010; Kihara *et al.*, 2005; Korycka *et al.*, 2012; Mitchell *et al.*, 2006). The majority of the *C. elegans* DHHCs fit this description, although there are some exceptions. DHHC-11 has no TMDs preceding the DHHC-CRD, while DHHC-13 and -14 have five and three TMDs respectively preceding the DHHC-CRD. The final TMD of DHHC-9 is nearly double the length that would be expected at 34 residues. Closer inspection of the sequence at this point shows a prolonged region containing a high proportion of hydrophobic residues. Presumably this stretch contains a TMD within it, but the prediction software is unable to determine exactly where. DHHC-13 and -14 are the only *C. elegans* DHHCs which contain multiple ankyrin repeats in the N-terminal section of the sequence. Three enzymes, DHHC-5 and -8 and SPE-10, also contain a palmitoyltransferase conserved C-terminal (PaCCT) motif. This motif is only present in a subset of DHHC enzymes, but has been shown to be required for the activity of the *S. cerevisiae* DHHCs Swf1 and Pfa3 (Gonzalez Montoro *et al.*, 2009).

The protein sequences were next subjected to a phylogenetic analysis. Some of the features of the resulting phylogenetic tree (Figure 3.3) correlate well with the domain

Gene	Previous Name/Gene Code
dhhc-1	*dhhc-1* (F09B12.2)
dhhc-2	*dhhc-2* (Y47H9C.2)
dhhc-3	F33D11.12
dhhc-4	ZK757.4
dhhc-5	R13F6.5
dhhc-6	M18.8
dhhc-7	C17D12.1
dhhc-8	Y39E4B.7
dhhc-9	C43H6.7
dhhc-10	K02G10.1
dhhc-11	T22E7.2
dhhc-12	F59C6.2
dhhc-13	H32C10.3
dhhc-14	*tag-233* (D2021.2)
spe-10	*spe-10* (AC3.10)

TABLE 3.1: DHHC genes in *C. elegans*

Listed are the 15 DHHC genes found in *C. elegans* by searching for the conserved DHHC motif. *dhhc-1*, *dhhc-2*, *tag-233* and *spe-10* were the only ones with existing names. The remaining genes were named *dhhc-3* to *dhhc-13* and *tag-233* renamed as *dhhc-14*. Where possible, homology to human DHHC proteins was taken into account. *spe*, spermatogenesis deficient; *tag*, temporarily assigned gene name.

```
DHHC-1   VIKPGYKHCHSCHSMSPLRAHHCPVCDVCILRRDHHCSFGAVCVGHFNQRYFVAAVINLF 156
DHHC-2   GEHVKMKYCTTCRLYRPPRCSHCAICDNCVLMFDHHCPWVGNCIGLRNYTYFYRFVFCLS 253
DHHC-3   -GQQTIYKCQKCASIKPDRAHHCSVCERCIRRMDHHCPWVNNCVGEGNQKFFVLFTMY-- 135
DHHC-4   GFDHGIRFCDKCCCIKPDRSHHCSMCEQCVLKFDHHCPWVNNCVNFGNYKYFILFLAYGF 185
DHHC-5   DKEIKEDVCQLCNYRKPPRWHHCRRCNLCVHRMDHHCPILQLCIHSGNHKYFLLFLVWPL 135
DHHC-6   ADEKKLQFCVPCNGFKVPRSHHCSKCDRCCMKMDHHCPWINNCVGHRNHQYFLRFLFFSV 159
DHHC-7   SSATEWTMCTRCDSLRPPRAHHCRVCKRCVRKMDHHCPWVNNCVGEYNQKWFLQFIFY-- 164
DHHC-8   GITVRMKWCVTCKFYRPPRSSHCSVCNRCIETFDHHCPWVHNCVGKRNYRYFFFFLCSLS 156
DHHC-9   PGEEGDSFCSKCNYWKSDNAHHCSVCEKCVLGMDHHCIWINQCVGLHNHRHFFLFIANLT 161
DHHC-10  ANESGSKFCFTCNKEAPQRSHHCPLCKMCVLRKDHHCFITGACVGLGNQRYFMVFLFWCA 184
DHHC-11  RHVITNSFCSICEVRTYRETKHCKRCNFCIDDFDHHCVWLNNCIGGKNYRPFVVLVICVN 90
DHHC-12  PGTPSDSFCIKCNNWKGPSTSHCKACDKCIYRMDHHCPHIGQCVGAHNQSHFFLFLFYLQ 164
DHHC-13  EEKQIDRYCFTCWIPKTSSSHHCSQCDKCVDGFDHHCPWIHKCVYRKNLRAFVFFCLTIF 594
DHHC-14  GIQHQQKYCFTCFIRKMDHTKHCAVCGFCVNNFDHHCPWLNSCVTRRNMREFIMFVIS-- 450
SPE-10   DQVGRLKYCYECGHIKPDRARHCSSCGKCCIKYDHHCPWINMCVTHVNYKYFLLYIIYTS 207
                  *  *          **  *  *    ****     *:   *   *
```

FIGURE 3.1: Alignment of the cysteine-rich domains of the DHHC enzymes in *C. elegans*

The primary sequence of each protein is shown around the cysteine-rich domain, and the position of the final residue of the line shown on the right. Absolutely conserved residues are indicated by an asterisk and a colon indicates residues with similar properties, in this case small hydrophobic residues. The characteristic DHHC motif is highlighted in green and the nearby conserved cysteine residues in cyan.

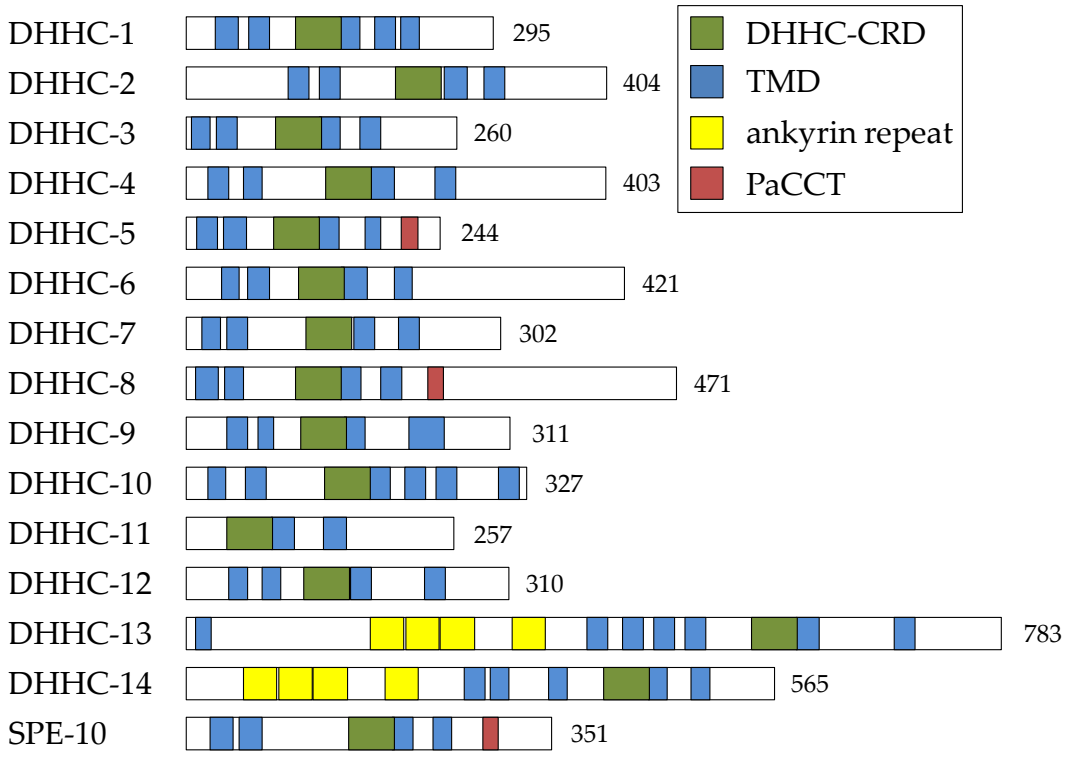

FIGURE 3.2: Domain structure of the *C. elegans* DHHC enzymes

The *C. elegans* DHHC enzymes are represented as diagrams to scale of the protein sequence. The DHHC-CRD (green), TMDs (blue), ankyrin repeats (yellow) and PaCCT motifs (red) are shown. The numbers to the right indicate the length of the sequence. CRD, cysteine-rich domain; PaCCT, palmitoyltransferase conserved C-terminal; TMD, transmembrane domain.

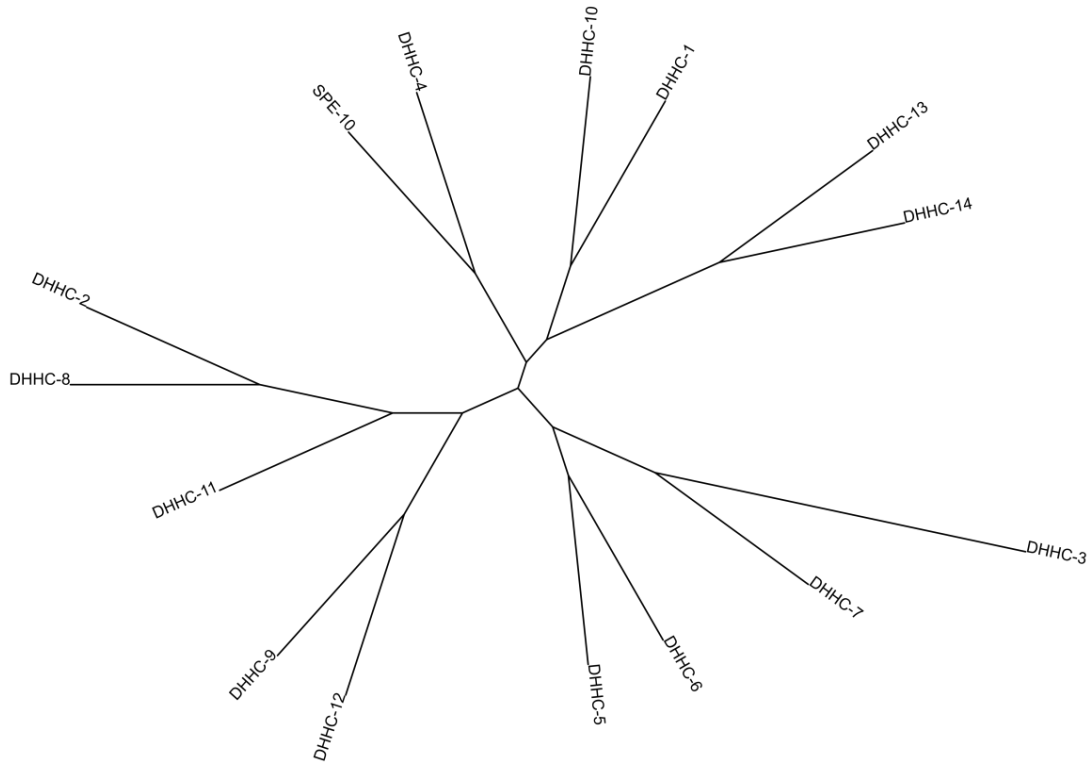

FIGURE 3.3: Phylogenetic tree of the DHHC enzymes in *C. elegans*

The 15 *C. elegans* DHHCs were subjected to phylogenetic analysis and the resulting tree was plotted using the Interactive Tree of Life (http://itol.embl.de) (Letunic and Bork, 2007).

structure shown in Figure 3.2. The enzymes mostly form pairs which are closely related. The ankyrin repeat-containing proteins DHHC-13 and -14 are one such pair. The exception is DHHC-11, which can probably be accounted for by its lack of two N-terminal TMDs compared with the rest of the family. The pairs of closely related enzymes branch off from broader sub-families in a similar way to phylogenetic trees constructed in other species (Bannan *et al.*, 2008; Fukata and Fukata, 2010; Korycka *et al.*, 2012; Mitchell *et al.*, 2006). The three PaCCT motif-containing proteins, DHHC-5 and -8 and SPE-10, appear on distant branches of the phylogenetic tree and so the presence of this motif would seem to have arisen independently in each.

There are no published data on any of the *C. elegans dhhc* genes, apart from *spe-10* (Cypser and Johnson, 1999; Gleason *et al.*, 2006; Shakes and Ward, 1989). There is, however, a small amount of information available on WormBase from large scale studies which is summarised in Table 3.2. In addition the presence of a PaCCT domain as assessed by (Gonzalez Montoro *et al.*, 2009) and shown in Figure 3.2 is indicated along with its precise position in the protein sequence. Most of the available information is quite vague and this is consistent with an enzyme family whose study has been neglected so far in *C. elegans*.

3.3.1.3 COMPARISON OF THE DHHC FAMILIES IN DIFFERENT ORGANISMS

3.3.1.3.1 *S. CEREVISIAE*

The single-celled organism *S. cerevisiae* has seven well-characterised DHHCs and one putative DHHC enzyme. Table 3.3 contains a summary of the information available in SGD and from other sources about these enzymes. Most of these proteins have been studied to some extent with the exception of YNL155W. Four of the eight enzymes contain the PaCCT motif, including the two in which it was characterised, Swf1 and Pfa3. There is a large amount of data available as a result of whole-genome or -proteome analyses in *S. cerevisiae*. One of these studies involved tagging every *S. cerevisiae* protein with green fluorescent protein (GFP) and observing its localisation (Huh *et al.*, 2003). Unfortunately, for five of these enzymes there were no or ambiguous results, but some further localisation analysis has been done as part of studies into substrate specificity (Hou *et al.*, 2009; Ohno *et al.*, 2006; Valdez-Taubas and Pelham, 2005). Pfa3 showed localisation to the vacuole, which is consistent with its known function in vacuolar membrane fusion and its substrate Vac8. Akr1 showed Golgi and early Golgi localisation. This would be consistent with many *H. sapiens* DHHCs shown to localise to the Golgi (Table 3.5).

Gene	Chromosome	Protein ID(s)	Gene Expression	PaCCT motif	Phenotypes	Other Information
dhhc-1	X	NP_510510.1				
dhhc-2	I	NP_493007.2				
dhhc-3	I	NP_491702.1				
dhhc-4	III	a: NP_001023032.1 b: NP_001023033.1 c: NP_001122751.1 d: NP_001255040.1 e: NP_001255041.1 f: NP_001255038.1 g: NP_001255039.1	ubiquitous			isoforms a-d have the DHHC motif; part of the C-terminal region is in all isoforms
dhhc-5	III	NP_498488.2	excretory cell, intestine (weak)	a.a. 208-223	embryonic/post-embryonic development variant (RNAi)	
dhhc-6	IV	NP_502302.2	head neurons (larva), intestine (adult)		sterile, embryonic lethal, larval arrest, reduced brood size (RNAi)	
dhhc-7	I	a: NP_492960.1 b: NP_492961.1				isoform b has an N-terminal truncation before the DHHC region
dhhc-8	III	NP_499713.3		a.a 234-248	embryonic/post-embryonic development variant (RNAi)	predicted protein binding motif
dhhc-9	X	NP_508435.2				
dhhc-10	X	NP_508805.3	ubiquitous, stronger in anterior pharynx			
dhhc-11	I	NP_491675.3	spermathecal valve (L3/L4), head neurons			
dhhc-12	I	NP_492753.2	possibly in two head and one tail neurons			
dhhc-13	IV	NP_500889.1			fat content variant/reduced (RNAi)	
dhhc-14	X	a: NP_001024514.2 b: NP_001024515.1	generalised, possibly neuronal			isoform b has an N-terminal truncation before the DHHC region
spe-10	V	NP_001021339.1		weak: a.a. 287-301	transgene induced cosuppression (RNAi); hermaphrodite sterile; unfertilised eggs laid; increased lifespan; increased stress resistance	

TABLE 3.2: Collated information on *C. elegans* DHHC enzymes

Information was collected from WormBase, the National Center for Biotechnology Information (NCBI) website (http://www.ncbi.nlm.nih.gov) and (Gonzalez Montoro *et al.*, 2009). PaCCT, palmitoyltransferase conserved C-terminus.

Gene	Description	Protein ID	PaCCT Motif	Localisation	Notes
AKR1	palmitoyl transferase involved in protein palmitoylation; acts as a negative regulator of pheromone response pathway; required for endocytosis of pheromone receptors; involved in cell shape control; contains ankyrin repeats	NP_010550.1		Golgi; early Golgi[1,2]	
AKR2	ankyrin repeat-containing protein similar to Akr1p; member of a family of putative palmitoyltransferases containing an Asp-His-His-Cys-cysteine rich (DHHC-CRD) domain; possibly involved in constitutive endocytosis of Ste3p	NP_014677.1		ambiguous[1]; Golgi[2]	
ERF2	subunit of a palmitoyltransferase, composed of Erf2p and Shr5p, that adds a palmitoyl lipid moiety to heterolipidated substrates such as Ras1p and Ras2p through a thioester linkage; mutants partially mislocalise Ras2p to the vacuole	NP_013347.1	a.a. 307-322	ER[2,3]	
PFA3	palmitoyltransferase for Vac8p, required for vacuolar membrane fusion; contains an Asp-His-His-Cys-cysteine rich (DHHC-CRD) domain; autoacylates; required for vacuolar integrity under stress conditions	NP_014073.1	a.a. 248-263	vacuole[1-3]	
PFA4	palmitoyltransferase with autoacylation activity, required for palmitoylation of amino acid permeases containing a C-terminal Phe-Trp-Cys site; required for modification of Chs3p; member of the DHHC family of putative palmitoyltransferases	NP_014640.1		ER[2,3]	
PFA5	palmitoyltransferase with autoacylation activity; likely functions in pathway(s) outside Ras; member of a family of putative palmitoyltransferases containing an Asp-His-His-Cys-cysteine rich (DHHC-CRD) domain	NP_010747.1	a.a. 285-300	PM[2,3]; vacuole-vacuole junctions[2]	
SWF1	palmitoyltransferase that acts on the SNAREs Snc1p, Syn8p, Tlg1p and likely on all SNAREs; member of a family of putative palmitoyltransferases containing an Asp-His-His-Cys-cysteine rich (DHHC-CRD) domain; may have a role in vacuole fusion	NP_010411.1	a.a. 321-336	ER[4]	
YNL155W	putative protein of unknown function, contains DHHC domain, also predicted to have thiol-disulfide oxidoreductase active site	NP_014244.1		cytoplasm; nucleus[1]	closest *C. elegans* match is AIP-1; closest DHHC is DHHC-14 (e value 0.24)

[1]http://yeastgfp.yeastgenome.org/
[2](Ohno *et al.*, 2006)
[3](Hou *et al.*, 2009)
[4](Valdez-Taubas and Pelham, 2005)

TABLE 3.3: Collated information on *S. cerevisiae* DHHC enzymes

Information was collected from the *Saccharomyces* Genome Database (SGD; http://www.yeastgenome.org/), the NCBI website, (Gonzalez Montoro *et al.*, 2009) and the yeast GFP fusion localization database (http://yeastgfp.yeastgenome.org/). AIP, arsenite inducible RNA associated protein; *AKR*, ankyrin repeat-containing; Chs, chitin synthase-related; ER, endoplasmic reticulum; *ERF*, effect on Ras function; HPO, hypersensitive to pore-forming toxin; *PFA*, protein fatty acyltransferase; PM, plasma membrane; Shr, suppressor of hyperactive Ras; Snc, suppressor of the null allele of cyclase associated protein; Ste, sterile; *SWF*, spore wall formation; Syn, syntaxin; Tlg, t-SNARE affecting a late Golgi compartment; Vac, vacuole-related.

The putative DHHC, YNL155W, contains the conserved cysteine residues and the DHHC motif, adding to the confidence that it is a real palmitoylating enzyme. It shows only distant homology to a *C. elegans* DHHC, DHHC-14. However, the basis of this is a short stretch of sequence which includes the DHHC-CRD. It remains to be seen whether YNL155W has palmitoyltransferase activity.

3.3.1.3.2 *D. MELANOGASTER*

The fruit fly *D. melanogaster* has 22 DHHCs, listed in Table 3.4. Most of these have not been studied in detail, other than their developmental expression pattern (Bannan *et al.*, 2008). The exception is huntingtin-interacting protein 14 (Hip14), which when mutated leads to defects in photoreceptor synaptic transmission (Ohyama *et al.*, 2007; Stowers and Isacoff, 2007) and in larval neuromuscular axon guidance (Kraut *et al.*, 2001). This was found to be due to loss of proper function of two synaptic proteins which were found to be substrates of Hip14: cysteine string protein (CSP) and synaptosomal-associated protein of 25 kDa (SNAP-25) (Ohyama *et al.*, 2007; Stowers and Isacoff, 2007).

Many of the *D. melanogaster* DHHCs have multiple isoforms, raising the possibility of either highly specific roles or a reasonable level of redundancy within the system. It is possible that there are large differences in isoform expression depending on the tissue and developmental stage. The analysis of developmental expression did not cover different isoforms of any of the DHHCs (Bannan *et al.*, 2008). Another feature of these DHHCs is that all but three of them contain a PaCCT motif. The significance of this abundance remains to be seen. It will be interesting to see whether this is a quirk of the *D. melanogaster* DHHCs or important for their function. Potentially more interesting is whether there is any difference between the three which lack the PaCCT motif and the rest of the family at a functional level.

3.3.1.3.3 *H. SAPIENS*

Humans have 23 DHHCs encoded by the gene family named *ZDHHC* based on the initial observation of a zinc finger domain as well as the DHHC-CRD (Fukata and Fukata, 2010; Korycka *et al.*, 2012). These are numbered 1-24 as *ZDHHC10* was later found to be identical to *ZDHHC9* and was removed from this classification. In addition there is a predicted DHHC, *ZDHHC11B*, which has high homology to *ZDHHC11* but has not been officially recognised as yet.

An overview of the *H. sapiens* DHHCs is shown in Table 3.5. Palmitoyltransferase activity has been observed in all of these except DHHC1, -11, -16, and -24 (Ohno *et al.*, 2012), and

Gene	Protein ID(s)	Isoforms/Variants	PaCCT Motif	Notes
app (*CG42318/ CG5620/ CG17144*)	H: NP_001137938.2 I: NP_001137939.2 J: NP_996065.2 K: NP_648561.2 L: NP_001137936.1 M: NP_001137937.1 O: NP_001246732.1 P: NP_001246733.1 Q: NP_001246731.1	9 isoforms; all contain DHHC motif	isoform H: a.a. 283-298 isoform L: a.a. 283-298	
CG1407	A: NP_724868.2 B: NP_610544.1 C: NP_724869.2 D: FBpp0303357	4 isoforms; all contain DHHC motif	isoform A: a.a. 265-279 isoform B: a.a. 265-279	
CG4483	NP_648294.1		a.a. 246-260	
CG4676	NP_610853.1		a.a. 235-249	
CG4956	NP_651428.2		weak; a.a. 258-272	
CG5196	A: NP_650191.1 B: NP_996201.1	2 isoforms; both contain DHHC motif	isoform A: a.a. 244-258 isoform B: a.a. 212-246	
CG5880	NP_651539.3		a.a. 327-341	
CG8314	NP_611070.1			
CG10344	A: NP_726201.1 B: NP_611671.1	2 isoforms; both contain DHHC motif	isoform B: a.a. 234-246	
CG13029	C: NP_648928.1 D: FBpp0304948	2 isoforms; only isoform C contains DHHC motif	isoform C: a.a. 241-255	
CG17075	A: NP_608508.1 B: NP_001245821.1	2 isoforms; CDS identical		
CG17195	NP_651427.2		weak; a.a. 239-263	
CG17196	A: NP_651426.1 B: NP_001163735.1	2 isoforms; only isoform B contains DHHC motif	isoform A: a.a. 232-246 isoform B: a.a. 207-221	
CG17197	NP_651425.2		a.a. 233-247	contains DRHC instead of DHHC
CG17198	NP_651424.3		weak; a.a. 255-269	
CG17287	NP_611197.1		weak; a.a. 258-272	
CG18810	NP_652670.2		weak; a.a. 243-257	
CG34449	A: NP_727339.3 B: NP_001096921.1 C: NP_001096922.1 D: NP_001245592.1 E: FBpp0303736	5 isoforms; all contain DHHC motif	isoform A: weak; a.a. 225-239 isoform B: weak; a.a. 225-239 isoform C: weak; a.a.225-239	
Dnz1 (*CG6627*)	NP_477449.1			
GABPI (*CG17257*)	A: NP_722869.1 B: NP_608741.1			contains DHHS instead of DHHC
Hip14 (*CG6017*)	A: NP_648824.1 B: FBpp0303194 C: FBpp0305754	3 listed isoforms; isoforms A and C are identical; all contain DHHC motif	isoforms A/C: a.a. 573-587	
patsas (*CG6618*)	NP_723724.1		a.a. 553-567	

TABLE 3.4: Collated information on *D. melanogaster* DHHC enzymes

Information was collected from FlyBase (http://flybase.org/), the NCBI website and (Gonzalez Montoro *et al.*, 2009). *app*, approximated; *Dnz1*, DNZDHHC/NEW1 zinc finger protein 11; *GABPI*, β1,4-N-acetylgalactosaminyltransferase B pilot; *Hip*, huntingtin-interacting protein.

Gene	Protein ID(s)	Isoforms/ Variants	PaCCT Motif	Localisation	Notes
ZDHHC1	NP_037436.1			ER[1]	
ZDHHC2	NP_057437.1			ER[1]; Golgi[1]	also called REAM; deleted in many cancers; putative tumour suppressor
ZDHHC3	1: NP_001128651.1, 2: NP_057682.1	2 isoforms; both contain DHHC		Golgi[1]	also called GODZ; mediates membrane Ca^{2+} transport[3]
ZDHHC4	1: NP_001127859.1, 2: NP_001127860.1, 3: NP_060576.1, 4: NP_001127861.1	4 variants in the 5'-UTR; protein sequence identical	a.a. 317-331	Golgi[1]	
ZDHHC5	NP_056272.2		a.a. 230-254	PM[1]	
ZDHHC6	NP_071939.1			ER[1]	
ZDHHC7	1: NP_001139020.1, 2: NP_060210.2	2 isoforms; both contain DHHC		Golgi[1]	also called SERZ
ZDHHC8	NP_037505.1		a.a. 230-254	Golgi[1]	may be associated with risk of schizophrenia[4]
ZDHHC9	1: NP_057116.2, 2: NP_001008223.1	2 variants: 2 has alternate and shorter 5'-UTR		ER[1]; Golgi[1]	*ZDHHC10* was found to be identical to *ZDHHC9*; upregulated in colon cancer[5]; mutated in XLMR[6]
ZDHHC11	NP_079062.1			ER[1]	gain of function in bladder cancer[7]
ZDHHC11B	P0C7U3.1, XP_003403828.2, XP_003118580.3				predicted gene; similar to *ZDHHC11*
ZDHHC12	NP_116188.2		a.a. 229-253	ER[1]; Golgi[1]	also called AID
ZDHHC13	1: NP_061901.2, 2: NP_001001483.1	2 isoforms; both contain DHHC	isoform 1: a.a. 574-588	ER[1]; Golgi[1]	also called HIP14L; chanzyme involved in Mg^{2+} transport[8]
ZDHHC14	1: NP_078906.2, 2: NP_714968.1	2 isoforms; both contain DHHC	isoform 1: a.a. 299-315	ER[1]	putative oncogene in lymphomas[9]
ZDHHC15	1: NP_659406.1, 2: NP_001139728.1, 3: NP_001139729.1	3 isoforms; all contain DHHC		Golgi[1]	loss of expression associated with XLMR[10]; isoform 3 has no DHHC motif
ZDHHC16	1: NP_115703.2 (NP_932163.1), 2: NP_932160.1, 3: NP_932161.1, 4: NP_932162.1	4 isoforms; 1 has two accessions; all contain DHHC		ER[2]	also called Aph-2
ZDHHC17	NP_056151.2		a.a. 584-598	Golgi[1]	also called HIP14; chanzyme involved in Mg^{2+} transport[8]
ZDHHC18	NP_115659.1			Golgi[1]	
ZDHHC19	NP_001034706.1		a.a. 237-251	ER[1]	
ZDHHC20	NP_694983.2		a.a. 257-271	PM[1]	overexpressed in many tumours[11]
ZDHHC21	NP_848661.1			PM[1]; ER[1]	
ZDHHC22	NP_777636.2				
ZDHHC23	NP_775841.2			ER[1]	also called NIDD
ZDHHC24	NP_997223.1			ER[1]	

[1](Ohno *et al.*, 2006) [2](Li *et al.*, 2002) [3](Hines *et al.*, 2010) [4](Faul *et al.*, 2005)
[5](Mansilla *et al.*, 2007) [6](Raymond *et al.*, 2007) [7](Yamamoto *et al.*, 2007) [8](Goytain *et al.*, 2008)
[9](Rinaldi *et al.*, 2006) [10](Mansouri *et al.*, 2005) [11](Draper and Smith, 2010)

TABLE 3.5: Collated information on *H. sapiens* DHHC enzymes

Information was collected from the NCBI website, (Gonzalez Montoro *et al.*, 2009) and literature searches. AID, amyloid precursor protein-interacting DHHC; Aph, Abl-philin; ER, endoplasmic reticulum; GODZ, Golgi-associated DHHC zinc finger protein; HIP, huntingtin-interacting protein; HIP14L, HIP14-like; HPO, hypersensitive to pore-forming toxin; NIDD, neural nitric oxide synthase-interacting DHHC domain-containing protein with dendritic mRNA; PM, plasma membrane; REAM, reduced expression associated with metastasis; SERZ, Sertoli cell gene with a zinc finger domain; UTR, untranslated region; XLMR, X-linked mental retardation.

as stated above DHHC11B is not normally viewed as a DHHC enzyme. As with the *S. cerevisiae* DHHCs, most of the *H. sapiens* family show localisation to intracellular membranes – 11 to the Golgi, 13 to the endoplasmic reticulum (ER) – and three also show localisation to the plasma membrane. Interestingly, DHHC3, -13 and -17 have been shown to also act in ion transport (Goytain *et al.*, 2008; Hines *et al.*, 2010) and all show Golgi localisation. The dual properties of ion channel and enzyme qualify these proteins as chanzymes (Montell, 2003). Nine *H. sapiens* DHHCs contain a PaCCT motif, roughly similar in proportion to the *S. cerevisiae* family. Again, the significance of this motif has not been explored outside of the *S. cerevisiae* proteins (Gonzalez Montoro *et al.*, 2009).

Many of the disease associations shown in Table 3.5 are the result of genome-wide association studies. However DHHC17/HIP14 was found to have an interaction with huntingtin (Htt) which inversely correlates with the length of the Htt expanded polyglutamine repeat region (Singaraja *et al.*, 2002). The same study found that DHHC17/HIP14 is expressed in a specific subset of mouse striatal neurons affected in Huntington's disease (HD): those which project to the globus pallidus. DHHC17/HIP14 has been found to palmitoylate Htt at cysteine-214, close to the polyglutamine tract, and this is also reduced with an expanded polyglutamine region (Huang *et al.*, 2004; Yanai *et al.*, 2006). It is directly involved in the pathogenesis of HD, as in mouse neurons expressing both wild-type and polyglutamine-expanded Htt downregulation of DHHC17/HIP14 by small interfering RNA (siRNA) increased formation of inclusions, whereas overexpression reduced inclusions (Yanai *et al.*, 2006). DHHC17/HIP14 is currently the only DHHC for which a disease association has been so thoroughly explored. Recently the relationship of the similar enzyme DHHC13/HIP14-like (HIP14L) to Htt was also investigated in a knockout mouse (see Section 3.4.1.3) (Sutton *et al.*, 2012).

3.3.1.3.4 SEQUENCE ANALYSIS

Given the lack of experimental information on the vast majority of the *C. elegans* DHHCs, a comparison with the DHHCs in the organisms named above may provide some insight. First of all, it would be helpful to see how the *C. elegans* DHHCs fit in evolutionarily with these other families. To do this, the protein sequences of DHHC enzymes from *S. cerevisiae*, *D. melanogaster* and *H. sapiens* were combined with the *C. elegans* sequences for a large scale phylogenetic analysis (Figure 3.4). Only the conserved DHHC-CRDs were compared in this analysis in order to make the computation more manageable. Comparing the locations of the *C. elegans* DHHCs on this tree with the previous one containing only the *C. elegans* family (Figure 3.3) shows that the pairs are maintained, although their precise position in

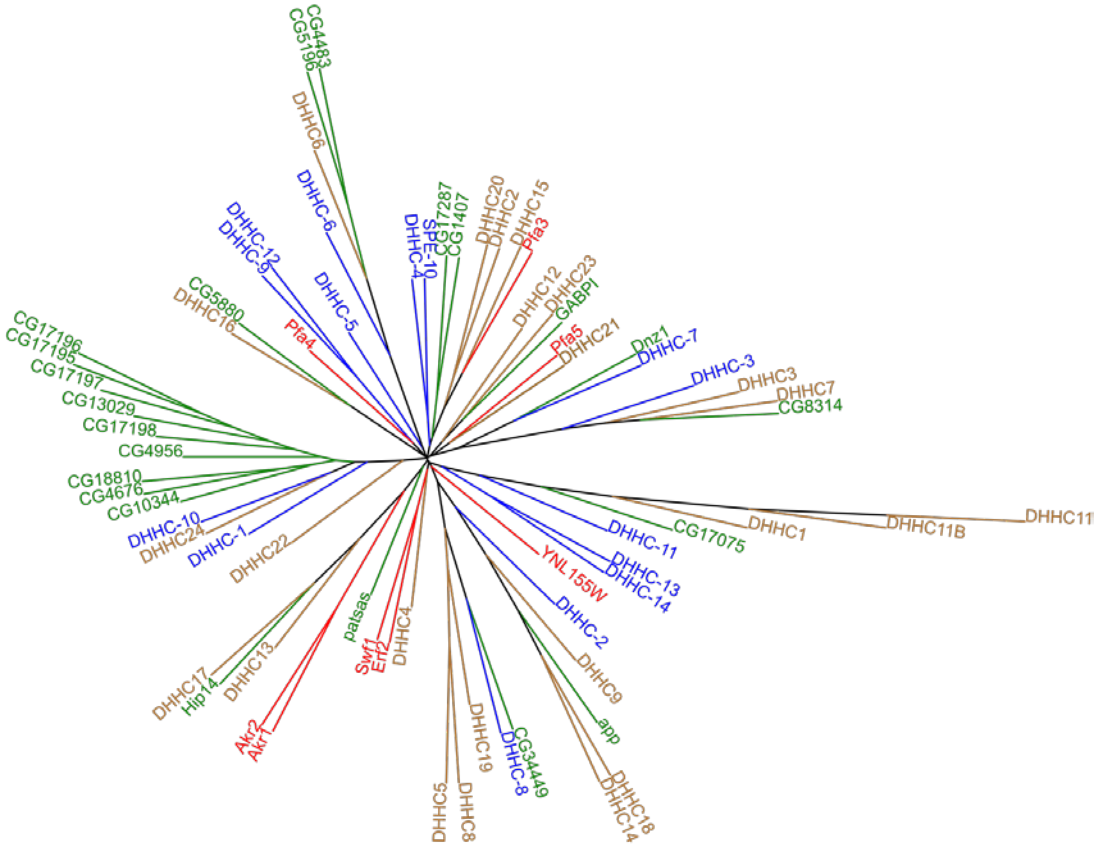

FIGURE 3.4: Phylogenetic tree of known and putative DHHC enzymes in evolutionarily important organisms

The conserved cysteine-rich domain containing the DHHC motif in *S. cerevisiae* (red), *C. elegans* (blue), *D. melanogaster* (green) and *H. sapiens* (brown) were subjected to phylogenetic analysis. The resulting tree was rendered and coloured using Interactive Tree of Life (Letunic and Bork, 2007).

relation to each other has changed in some cases. This may reflect differing areas of similarity around the DHHC-CRD compared with the N- and C-termini of the full length sequence used for the earlier analysis. The *C. elegans* DHHCs also appear mostly to be related, albeit distantly in some cases, to proteins in other organisms, allowing predictions to be made based on knowledge from other organisms. The most distant proteins are DHHC-5 and the pair DHHC-13 and -14 so these may show more functional divergence from other organisms.

A feature of the phylogenetic tree which stands out is the cluster of nine *D. melanogaster* DHHCs which seem to have only one close relation in *H. sapiens* (DHHC24) and in *C. elegans* (DHHC-10). These genes are highly expressed in the *D. melanogaster* adult testes according to FlyAtlas (Chintapalli *et al.*, 2007). Of these nine, *CG17195*, *CG17196*, *CG17197*, *CG17198* and *CG4956* are arranged concurrently in the 96F2 region of chromosome III. They are believed to be the result of a gene duplication event which occurred after the split between the *melanogaster* and *obscura* groups in the *Sophophora* subgenus with *CG4956* as the original gene as it is the only one with orthologues in all the *Drosophila* species (Bannan *et al.*, 2008). This accounts for their high relatedness and thus their clustering on the phylogenetic tree.

Whilst the consensus sequence for DHHCs is quite precisely defined, it has been noted that there are variations within it which seem to be tolerated (Mitchell *et al.*, 2006). With this in mind, the enzyme sequences from the organisms of interest were aligned with the focus on the region containing the full consensus sequence (Figure 3.5). There does indeed seem to be variation in how important individual residues in the consensus sequence are. The only residues which are absolutely conserved are the aspartate of the DHHC motif and the asparagine which is the penultimate residue in the sequence. Although absolutely conserved among the *C. elegans* DHHCs, many of the cysteine residues which form the CRD are missing from some enzymes. The most obvious are the *S. cerevisiae* DHHCs Akr1 and -2 and the *H. sapiens* DHHC22, which are missing five and two cysteines respectively. Four other residues at the N-terminal end of the consensus are also absent from DHHC22. These residues do seem to be less critical and one or more of them are also missing from the *C. elegans* DHHC-1, -6, -9 and -11 to -14. Even the DHHC motif, required for enzymatic activity, is not absolutely conserved. The *S. cerevisiae* DHHCs Akr1, Akr2 and Pfa5 have a tyrosine instead of a histidine residue in the third position, although these enzymes retain their palmitoyltransferase activity (Mitchell *et al.*, 2006). The histidine residue in the second position is changed to an arginine in *D. melanogaster* CG17197 and glutamine in

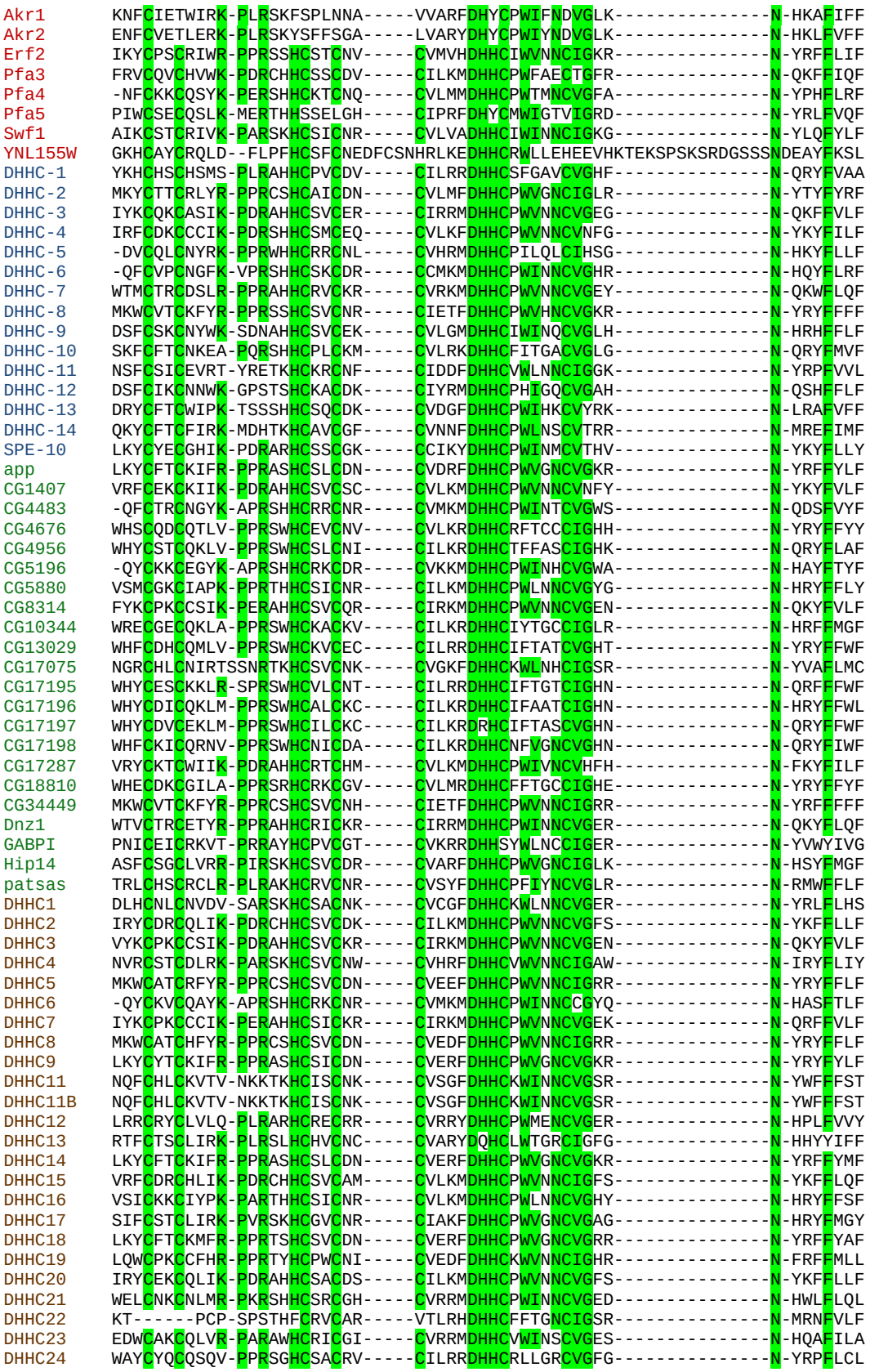

FIGURE 3.5: Alignment of the conserved region of the DHHC enzymes in organisms of interest

An alignment highlighting the consensus $Cx_2Cx_3(R/K)PxRx_2HCx_2Cx_2Cx_4DHHCxW(V/I)xNC(I/V)Gx_2Nx_3F$. The DHHC enzymes in *S. cerevisiae* (red lettering), *C. elegans* (blue), *D. melanogaster* (green) and *H. sapiens* (brown) are shown.

H. sapiens DHHC13/HIP14L. Again, while the former has not been studied, HIP14L is known to have palmitoyltransferase activity (Huang *et al.*, 2009). The cysteine in the DHHC motif is changed to a serine residue in the *D. melanogaster* DHHC β1,4-N-acetylgalactosaminyl-transferase B pilot (GABPI). Given that this cysteine residue is required to form the palmitoyl-enzyme intermediate (Mitchell *et al.*, 2010) and its mutation to serine is a common way to inactivate DHHCs, it is likely that GABPI has no palmitoyltransferase activity *in vivo*.

In addition to the DHHC-CRD, there are two other regions of relatively high sequence conservation which have been observed in DHHCs. There is an aspartate-proline-glycine (DPG) motif commonly next to TMD2 and a threonine-threonine-x-glutamate (TTxE) motif commonly next to TMD4 (Mitchell *et al.*, 2006). The DPG motif can be found in *C. elegans* DHHC-2, -3, -5 and -7, and the TTxE motif in *C. elegans* DHHC-3, -4, -6 and -10 and SPE-10. The functional significance of these motifs is not yet known.

In addition to the phylogenetic analysis and the sequence alignments, the sequences of the *C. elegans* DHHC enzymes were inputted into basic local alignment search tool (BLAST) searches to identify possible orthologues in the other species discussed here (Table 3.6). This will provide additional evidence which may add confidence to any putative orthologues. As might be expected, there is some variety as to how closely related these proteins are to those in other species. Generally speaking, the lowest confidence hits occur in the *S. cerevisiae* family. This may be attributed to the small size of the family in *S. cerevisiae* and indicates that expansion of the family over evolutionary time has not been limited to gradual changes to existing genes. It also agrees with the phylogenetic analysis, in which few of the *C. elegans* DHHCs are positioned particularly close to the *S. cerevisiae* DHHCs. *S. cerevisiae* Pfa4 is positioned close to *C. elegans* DHHC-5, -9 and -12 on the phylogenetic tree, yet of these three only DHHC-12 shows Pfa4 as its closest match. This may be because the phylogenetic tree was constructed using only the DHHC-CRD region of the sequences, whereas the BLAST searches were conducted with the full sequence. A similar explanation accounts for the fact that DHHC-13 and -14, which have N-terminal ankyrin repeat regions, show Akr1 and -2 as their closest matches respectively but have a relatively distant position on the phylogenetic tree. Indeed these are the highest confidence matches amongst the *S. cerevisiae* proteins. Two isoforms of *C. elegans* DHHC-4 do not match up to *S. cerevisiae* DHHC proteins presumably because they lack the exon containing the DHHC motif. However, they do still show DHHC proteins as their closest

C. elegans DHHC	*S. cerevisiae*			*D. melanogaster*			*H. sapiens*		
	Protein	**E value**	**Identity**	**Protein**	**E value**	**Identity**	**Protein**	**E value**	**Identity**
DHHC-1	Pfa3	8e-14	28%	CG10344B	1e-24	26%	DHHC24	6e-23	32%
DHHC-2	Erf2	3e-30	31%	AppH	7e-86	46%	DHHC14 isoform 2	9e-94	42%
DHHC-3	Pfa3	2e-22	37%	CG8314	2e-86	50%	DHHC3 isoform 1	4e-98	56%
DHHC-4a	Pfa3	2e-20	26%	CG1407A	2e-78	38%	DHHC2	1e-79	38%
DHHC-4b	Pfa3	1e-20	26%	CG1407A	2e-78	38%	DHHC2	7e-80	38%
DHHC-4c	Pfa3	6e-21	26%	CG1407A	1e-75	42%	DHHC2	2e-77	39%
DHHC-4d	Pfa3	2e-23	28%	CG1407A	5e-81	39%	DHHC2	2e-83	40%
DHHC-4e	Frk1	0.037	25%	CG1407A	1e-20	36%	DHHC2	5e-21	49%
DHHC-4f	Ade5,7	0.035	27%	CG1407A	1e-09	30%	DHHC2	4e-09	49%
DHHC-5	Pfa3	8e-16	29%	CG8314	4e-20	30%	DHHC21	7e-22	30%
DHHC-6	Pfa4	2e-19	34%	CG5196A	5e-81	36%	DHHC6	1e-86	35%
DHHC-7a	Pfa3	5e-17	35%	Dnz1	7e-80	42%	DHHC7 isoform 2	7e-49	34%
DHHC-7b	Pfa3	8e-18	32%	Dnz1	2e-60	44%	DHHC3 isoform 1	6e-34	35%
DHHC-8	Erf2	4e-23	31%	CG34449D	2e-76	51%	DHHC8 isoform 2	5e-75	50%
DHHC-9	Erf2	3e-17	26%	CG5880	3e-35	29%	DHHC16 isoform 2	1e-31	34%
DHHC-10	Pfa4	6e-15	41%	CG10344B	1e-18	44%	DHHC24	3e-15	31%
DHHC-11	Swf1	1e-15	33%	CG17075A	6e-19	38%	DHHC11	3e-20	28%
DHHC-12	Pfa4	4e-16	42%	CG5196B	1e-17	27%	DHHC16 isoform 2	3e-17	29%
DHHC-13	Akr1	2e-33	28%	Hip14	3e-43	31%	DHHC17	5e-42	28%
DHHC-14a	Akr2	1e-35	24%	Hip14	1e-68	29%	DHHC17	2e-72	30%
DHHC-14b	Swf1	1e-14	31%	AppO	6e-21	27%	DHHC17	6e-25	33%
SPE-10	Pfa3	1e-17	27%	CG1407B	3e-43	31%	DHHC2	3e-37	31%

TABLE 3.6: Orthologues of *C. elegans* DHHC enzymes in other organisms

BLAST searches were conducted using the protein sequences of each of the *C. elegans* DHHC enzymes. The closest matches in *S. cerevisiae*, *D. melanogaster* and *H. sapiens* are shown along with relevant parameters. Ade, adenine-requiring; BLAST, basic local alignment search tool; Frk, fatty acyl-CoA synthetase and RNA processing-associated kinase.

matches in *D. melanogaster* and *H. sapiens*, showing DHHC-4 has relatively high homology to these proteins outside of the DHHC-CRD.

The *C. elegans* DHHCs show somewhat higher confidence comparisons with the *D. melanogaster* family. The highest confidence orthologues are between DHHC-2 and approximated (App) and between DHHC-3 and CG8314, both of which show high relatedness on the phylogenetic tree. Two pairs which stand out on the phylogenetic tree, DHHC-7 with DNZDHHC/NEW1 zinc finger protein 11 (Dnz1) and DHHC-8 with CG34449, also come out as orthologues with a high degree of confidence through BLAST searching. The ankyrin repeat-containing proteins DHHC-13 and -14 again come closest to one of the *D. melanogaster* ankyrin repeat-containing proteins, Hip14 (the other is Patsas). The lowest confidence hits come from *C. elegans* DHHC-10, -11 and -12. In the case of DHHC-10 this is somewhat surprising given its position on the phylogenetic tree adjacent to a large subfamily of *D. melanogaster* proteins, even though the closest *D. melanogaster* protein is the same in both cases. This suggests the DHHC-CRD is highly similar but there may be a large degree of divergence outside of this domain. A similar explanation may account for the relatively low confidence between DHHC-11 and CG17075 despite appearing quite closely related on the phylogenetic tree.

The highest overall confidence for orthologues of the *C. elegans* DHHCs comes from the *H. sapiens* family. Again the highest confidence comes from the *C. elegans* proteins DHHC-2 and -3, homologous to *H. sapiens* DHHC14 and -3/GODZ respectively. Another group has previously found DHHC-3 to be the *C. elegans* orthologue of DHHC3/GODZ and the most closely related *D. melanogaster* protein to be CG8314 (Uemura *et al.*, 2002). Other high confidence hits include *C. elegans* DHHC-4 with *H. sapiens* DHHC2, DHHC-6 with DHHC6, DHHC-8 with DHHC8 and DHHC-14 with DHHC17/HIP14. The other ankyrin repeat-containing protein DHHC-13 is also most homologous to *H. sapiens* DHHC17/HIP14. Interestingly, when just the DHHC-CRD is analysed as in the phylogenetic tree (Figure 3.4), the ankyrin-repeat containing proteins from *S. cerevisiae*, *D. melanogaster* and *H. sapiens* form a subgroup even though the region is not included in the analysis. The *C. elegans* counterparts are placed elsewhere on the tree, suggesting a degree of genetic separation compared with the other species. As *C. elegans* are predominantly hermaphrodites and have genetically identical progeny, this may be a result of genetic drift from a gradual accumulation of mutations. The lowest confidence comparisons between *C. elegans* and *H. sapiens* DHHCs again come from *C. elegans* DHHC-10, -11 and -12. This suggests these enzymes may have arisen in *C. elegans* independently.

3.3.1.3.5 ENZYME-SUBSTRATE INTERACTIONS

As there is no information available for substrates of the *C. elegans* DHHCs, some insight may be gained by studying the known enzyme-substrate pairs in the other organisms. These are listed in Table 3.7. By far the most is known about the substrates of *H. sapiens* DHHCs. Most of these studies have focused on finding the DHHCs responsible for palmitoylating a particular protein. Some enzymes seem to have a particularly broad specificity and appear in many studies, for example DHHC3/GODZ, DHHC7/SERZ and DHHC17/HIP14. DHHC3/GODZ and DHHC7/SERZ in particular seem to have many substrates in common with each other. This may be a result of their high level of relatedness as seen in phylogenetic trees of just the DHHC-CRD (Figure 3.4) and the entire sequence (Korycka *et al.*, 2012). However many of the substrates of DHHC17/HIP14 do not seem to be shared with the similar enzyme DHHC13/HIP14L. It is possible this is a result of different subcellular localisations. DHHC17/HIP14 has been shown to be mainly localised to the Golgi (Huang *et al.*, 2004; Singaraja *et al.*, 2002). The *D. melanogaster* orthologue Hip14 also localises to presynaptic vesicles and the plasma membrane in neurons (Ohyama *et al.*, 2007; Stowers and Isacoff, 2007), although *H. sapiens* DHHC17/HIP14 did not colocalise with synaptophysin, a presynaptic marker, in rat hippocampal neurons (Huang *et al.*, 2009). DHHC13/HIP14L, in contrast, is localised to the ER. Some proteins are palmitoylated by a variety of enzymes, for example SNAP-25 is palmitoylated by DHHC2/reduced expression associated with metastasis (REAM), DHHC3/GODZ, DHHC7/SERZ, DHHC8, DHHC13/HIP14L and DHHC17/HIP14. Alternatively some enzyme-substrate pairs seem to be highly specific, such as DHHC19 and R-Ras and DHHC17/HIP14 and synaptotagmin-1.

In order to try to predict possible palmitoyl-proteins in *C. elegans*, BLAST searches were conducted to find orthologues of the known palmitoyl-proteins from *S. cerevisiae* (Table 3.8). These comprised the proteins identified using a proteomic analysis (Roth *et al.*, 2006) and those identified as substrates of specific DHHCs (Table 3.7). There is a large variation in the confidence of these hits. Some of the higher confidence orthologues include the casein kinases (Yck1-3 in *S. cerevisiae*; CSNK-1 in *C. elegans*), tubulin and G protein α subunits (Gpa1/2 in *S. cerevisiae*; GOA-1 in *C. elegans*). A similar analysis was done using the mammalian proteins with known substrates identified in Table 3.7 (Table 3.9). Although proteome scale analyses of palmitoyl-proteins exist in many mammalian tissues and cell types, the lists of identified proteins stretch to hundreds. For this reason it was decided only to find orthologues for proteins whose DHHC partners are known. The *C. elegans*

DHHC enzyme	Species	Substrate(s)	Evidence
Akr1	*S. cerevisiae*	Anr2, Env7, Lcb4, Meh1, Rho3, Sna4, Vac8, Yck1, Yck2, Yck3, Ypl199c	(Hou *et al.*, 2009; Kihara *et al.*, 2005; Pasula *et al.*, 2010; Roth *et al.*, 2002; Roth *et al.*, 2006; Wu and Brennwald, 2010)
Erf2[1]	*S. cerevisiae*	Gpa2, Ras1, Ras2, Rho2, Rho3, Vac8, Yck3	(Hou *et al.*, 2009; Lobo *et al.*, 2002; Roth *et al.*, 2006)
Pfa3	*S. cerevisiae*	Vac8, Yck3	(Hou *et al.*, 2009; Hou *et al.*, 2005; Smotrys *et al.*, 2005)
Pfa4	*S. cerevisiae*	Agp1, Bap2, Chs3, Gap1, Gnp1, Hip1, Rif1, Tat1, Tat2 Vac8, Yck3	(Hou *et al.*, 2009; Lam *et al.*, 2006; Park *et al.*, 2011; Roth *et al.*, 2006)
Pfa5	*S. cerevisiae*	Vac8, Yck3	(Hou *et al.*, 2009)
Swf1	*S. cerevisiae*	Mnn11, Pin2, Snc1, Sso1, Sso2, Ste18, Syn8, Tlg1, Ypl199c	(Roth *et al.*, 2006; Valdez-Taubas and Pelham, 2005)
Hip14	*D. melanogaster*	CSP, Sog	(Kang and Bier, 2010; Ohyama *et al.*, 2007)
DHHC2/ REAM	*H. sapiens*	ABCA1, CD9, CD151, CKAP4/p63, eNOS, Lck, Nde1, Ndel1, PI4KIIα, PSD-95, R7BP, SNAP-23, SNAP-25, stathmin 2-4	(Fernandez-Hernando *et al.*, 2006; Fukata *et al.*, 2004; Greaves *et al.*, 2010; Jennings *et al.*, 2009; Jia *et al.*, 2011; Levy *et al.*, 2011; Lu *et al.*, 2012; Sharma *et al.*, 2008; Shmueli *et al.*, 2010; Singaraja *et al.*, 2009; Zhang *et al.*, 2008)
DHHC3/ GODZ	*H. sapiens*	AMPA receptor subunits GluR1/2, BACE1, CL3/CaMKIγ, CSP, DR4, eNOS, $G\alpha_{i2}$, $G\alpha_q$, $G\alpha_s$, $GABA_A$ receptor γ2 subunit, GAD65, integrin α6β4, NCAM, Nde1, Ndel1, NR2A/B, PI4KIIα, PSD-95, RGS4, SNAP-23, SNAP-25, stathmin 2-4, STREX	(Fernandez-Hernando *et al.*, 2006; Fukata *et al.*, 2004; Greaves *et al.*, 2010; Greaves *et al.*, 2008; Hayashi *et al.*, 2009; Huang *et al.*, 2009; Keller *et al.*, 2004; Levy *et al.*, 2011; Lu *et al.*, 2012; Oh *et al.*, 2012; Ponimaskin *et al.*, 2008; Sharma *et al.*, 2012; Takemoto-Kimura *et al.*, 2007; Tian *et al.*, 2010; Tsutsumi *et al.*, 2009; Vetrivel *et al.*, 2009; Wang *et al.*, 2010)
DHHC4	*H. sapiens*	BACE1	(Vetrivel *et al.*, 2009)
DHHC5	*H. sapiens*	flotillin-2, GRIP1, SSTR5, stathmin 2, STREX	(Kokkola *et al.*, 2011; Levy *et al.*, 2011; Li *et al.*, 2012; Thomas *et al.*, 2012; Tian *et al.*, 2010)
DHHC6	*H. sapiens*	calnexin	(Lakkaraju *et al.*, 2012)
DHHC7/ SERZ	*H. sapiens*	AR, BACE1, CSP, eNOS, ER, $G\alpha_{i2}$, $G\alpha_q$, $G\alpha_s$, $GABA_A$ receptor γ2 subunit, GAP43, NCAM, Nde1, Ndel1, PDE10A2, PI4KIIα, PR, PSD-95, RGS4, SNAP-23, SNAP-25, sortilin, stathmin 2-4, STREX	(Charych *et al.*, 2010; Fang *et al.*, 2006; Fernandez-Hernando *et al.*, 2006; Fukata *et al.*, 2004; Greaves *et al.*, 2010; Greaves *et al.*, 2008; Levy *et al.*, 2011; Lu *et al.*, 2012; McCormick *et al.*, 2008; Pedram *et al.*, 2012; Ponimaskin *et al.*, 2008; Tian *et al.*, 2010; Tsutsumi *et al.*, 2009; Vetrivel *et al.*, 2009; Wang *et al.*, 2010)
DHHC8	*H. sapiens*	ABCA1, eNOS, GAD65, GRIP1, paralemmin-1, PSD-93, PSD-95, SNAP-25	(Fernandez-Hernando *et al.*, 2006; Huang *et al.*, 2009; Mukai *et al.*, 2008; Singaraja *et al.*, 2009; Thomas *et al.*, 2012)
DHHC9[2]	*H. sapiens*	H-Ras, N-Ras, STREX	(Swarthout *et al.*, 2005; Tian *et al.*, 2010)
DHHC12/ AID	*H. sapiens*	ABCA1	(Singaraja *et al.*, 2009)
DHHC13/ HIP14L	*H. sapiens*	GAD65, Htt	(Huang *et al.*, 2009)
DHHC14	*H. sapiens*	PI4KIIα	(Lu *et al.*, 2012)
DHHC15	*H. sapiens*	ABCA1, BACE1, CD151, CI-MPR, CSP, GAP43, PI4KIIα, PSD-95, SNAP-25, sortilin, stathmin 2-4	(Fukata *et al.*, 2004; Greaves *et al.*, 2010; Greaves *et al.*, 2008; Levy *et al.*, 2011; Lu *et al.*, 2012; McCormick *et al.*, 2008; Sharma *et al.*, 2008; Singaraja *et al.*, 2009; Vetrivel *et al.*, 2009)
DHHC17/ HIP14	*H. sapiens*	AMPA receptor subunits GluR1/2, CSP, GAD65, H-Ras, Htt, Lck, N-Ras, PSD-95, SNAP-23, SNAP-25, stathmin 2, STREX, synaptotagmin-1	(Ducker *et al.*, 2004; Fukata *et al.*, 2004; Greaves *et al.*, 2010; Greaves *et al.*, 2008; Huang *et al.*, 2009; Huang *et al.*, 2004; Levy *et al.*, 2011; Tian *et al.*, 2010)
DHHC18	*H. sapiens*	Lck, H-Ras	(Fukata *et al.*, 2004)
DHHC19	*H. sapiens*	PDE10A2, R-Ras	(Baumgart *et al.*, 2010; Charych *et al.*, 2010)
DHHC20	*H. sapiens*	ABCA1, BACE1	(Singaraja *et al.*, 2009; Vetrivel *et al.*, 2009)
DHHC21	*H. sapiens*	ABCA1, AR, eNOS, ER, Fyn, Lck, PI4KIIα, PR, stathmin 2-4	(Fernandez-Hernando *et al.*, 2006; Levy *et al.*, 2011; Lu *et al.*, 2012; Mill *et al.*, 2009; Pedram *et al.*, 2012; Singaraja *et al.*, 2009; Tsutsumi *et al.*, 2009)
DHHC22	*H. sapiens*	BK channel	(Tian *et al.*, 2012)
DHHC23	*H. sapiens*	BK channel	(Tian *et al.*, 2012)

[1] Requires Erf4/Shr5 for enzymatic activity (Lobo *et al.*, 2002)

[2] Requires GCP16 for enzymatic activity (Swarthout *et al.*, 2005)

orthologues of mammalian proteins generally speaking have higher confidence. Proteins with close orthologues include: large conductance Ca^{2+}-activated K^+ (BK) channels (*C. elegans* SLO-1), Fyn (SRC-2), glutamine decarboxylase GAD65 (UNC-25), G protein α subunits (GOA-1, EGL-30, GSA-1), glutamate receptor subunits (GLR-1), phosphodiesterase 10A2 (PDE-5), phosphatidylinositol 4-kinase IIα (ZC8.6), postsynaptic density proteins PSD-93 and -95 (DLG-1) and synaptotagmin-1 (SNT-1). The two *D. melanogaster* proteins known to be palmitoylated by Hip14, CSP and Sog, correspond to DnaJ domain-containing protein 14 (DNJ-14, 3e-23) and cysteine-rich motor neuron protein homologue 1 (CRM-1, 7e-11) in *C. elegans*.

Many large-scale interaction studies have been performed in *S. cerevisiae*. These can provide another level of analysis on top of the known enzyme-substrate pairs and some examples are shown in Table 3.10. This resource included some, but not all, of the known substrates. The soluble N-ethylmaleimide (NEM)-sensitive fusion protein (NSF)-attachment protein (SNAP) receptors (SNAREs) Vac8, Snc1 and Syn8 in *S. cerevisiae* and SNAP-23 and -25 in *H. sapiens* are known palmitoyl-proteins, suggesting the other SNARE proteins listed in Table 3.10 are plausible candidates as substrates. The proteins Snc2, Sso1 and Tlg2 have

TABLE 3.7: Known DHHC enzyme-substrate pairs

Experimentally confirmed substrates for specific DHHC enzymes were found by literature searching. ABCA1, ATP-binding cassette transporter A1; Agp, high affinity glutamine permease; AMPA, α-amino-3-hydroxy-5-methyl-4-isoxazolepropionic acid; Anr, Avl nine related family; AR, androgen receptor; BACE1, β-site amyloid precursor protein-cleaving enzyme 1; Bap, branched-chain amino acid permease; BK, large conductance Ca^{2+}-activated K^+ channel; CD, cluster of differentiation; Chs, chitin synthase-related; CI-MPR, cation-independent mannose 6-phosphate receptor; CKAP, cytoskeleton-associated protein; CL3/CaMKIγ, Ca^{2+}/calmodulin-dependent protein kinase CLICK-III/calmodulin-dependent protein kinase 1γ; CSP, cysteine string protein; DR4, tumour necrosis factor-related apoptosis-inducing ligand receptor 1; eNOS, endothelial nitric oxide synthase; Env, late endosome and vacuole interface function; ER, oestrogen receptor; GABA, γ-amino butyric acid; GAD, glutamate decarboxylase; Gap, general amino acid permease; GAP43, growth-associated protein of 43 kDa; Gnp, glutamine permease; Gpa, G protein α subunit; GRIP, glutamate receptor interacting protein; Lcb, long-chain base; Hip (yeast), histidine permease; Htt, Huntingtin; Lck, lymphocyte-specific tyrosine kinase; Meh, multicopy suppressor of endoplasmic reticulum retention defective (Erd) suppressor 1 (Ers1) hygromycin B sensitivity; Mnn, mannosyltransferase; NCAM, neural cell adhesion molecule; PR, progesterone receptor; Nde1, nuclear distribution protein nudE homologue 1; Ndel1, nuclear distribution protein nudE-like 1; NR2A/B, N-methyl-D-aspartate receptor subunits 2A/2B; PDE10A2, phosphodiesterase 10A2; PI4KIIα, phosphatidylinositol 4-kinase type IIα; Pin, Psi+ inducibility; PSD, post-synaptic density; R7BP, regulator of G protein signalling 7 family binding protein; REAM, reduced expression associated with metastasis; RGS, regulator of G protein signaling; Rho, Ras homolog; Rif, repressor activator protein 1 (Rap1)-interacting factor; Sna, sensitivity to Na^+; SNAP, synaptosomal-associated protein of 25 kDa; Snc, suppressor of the null allele of cyclase associated protein; Sog, short gastrulation; Sso, suppressor of Sec one; SSTR5, somatostatin receptor 5; Ste, sterile; STREX, stress-regulated exon splice variant of large conductance Ca^{2+}- and voltage-activated K^+ channels; Swf, spore wall formation; Syn, syntaxin; Tat, tyrosine and tryptophan amino acid transporter; Tlg, t-SNARE affecting a late Golgi compartment; Vac, vacuole related; Yck, yeast casein kinase.

Palmitoyl protein	DHHC(s)	*C. elegans* orthologue	E value
Agp1	Pfa4	AAT-1	3e-08
Akr1		DHHC-13	3e-29
Anr2	Akr1	T14D7.1	0.039
Bap2	Pfa4	B0454.6	6e-09
Bet3		ZK1098.5	7e-31
Chs3	Pfa4	CHS-1	2e-18
Env7	Akr1	D2045.7	5e-20
Gap1	Pfa4	AAT-2	3e-08
Gnp1	Pfa4	AAT-3	0.007
Gpa1		GOA-1	7e-80
Gpa2	Erf2	GOA-1	4e-87
Hem14		UNC-86	4e-04
Hip1	Pfa4	C50D2.2	3e-13
Lcb4	Akr1	SPHK-1	9e-14
Lsb6		ZC8.6	6e-50
Meh1	Akr1	T11B7.1	0.020
Mlf3		M02B7.5	2.1
Mnn1		C44C10.4	0.73
Mnn10		F28G4.3	0.069
Mnn11	Swf1	Y47G6A.9	0.13
Mse1		EARS-2	3e-80
Nuc1		CPS-6	2e-60
Pin2	Swf1	ABF-5	0.011
Psr1		SCPL-1	6e-57
Psr2		SCPL-1	4e-58
Ras1	Erf2	LET-60	7e-59
Ras2	Erf2	RAP-1	9e-58
Rho2	Erf2	RHO-1	2e-62

Palmitoyl protein	DHHC(s)	*C. elegans* orthologue	E value
Rho3	Akr1, Erf2	RHO-1	3e-57
Rif1	Pfa4	F41H10.4	7e-06
Sam3		AAT-1	0.006
Sna4	Akr1	ALP-1	0.17
Snc1	Swf1	SNB-1	3e-13
Snc2		SNB-1	7e-17
Sso1	Swf1	UNC-64	2e-26
Sso2	Swf1	UNC-64	8e-28
Ste18	Swf1	TBC-7	3.3
Syn8	Swf1	T14G8.3	0.001
Tat1	Pfa4	B0454.6	3e-10
Tat2	Pfa4	F23F1.6	3e-05
Tlg1	Swf1	SYX-6	8e-04
Tlg2		SYN-16	7e-24
Tub1		TBA-2	0.0
Tvp18		SRU-22	0.049
Vac8	Akr1, Erf2, Pfa3, Pfa4, Pfa5	IMA-3	5e-10
Vam3		SYX-5	3e-06
Ybr016w		-	-
Yck1	Akr1	CSNK-1	9e-108
Yck2	Akr1	CSNK-1	1e-109
Yck3		CSNK-1	9e-92
Ycp4		Y79H2A.3	3.9
Ygl108c		T05E11.7	0.18
Ykt6		YKT-6	1e-56
Ylr001c		C11E4.7	3.8
Ylr326w		F07C4.6	2.4
Ypl199c	Akr1, Swf1	Y32B12C.1	0.001

TABLE 3.8: Orthologues of *S. cerevisiae* palmitoyl-proteins in *C. elegans*

BLAST searches were performed using the protein sequences above to find *C. elegans* orthologues. The *S. cerevisiae* proteins and the DHHC(s) responsible for their palmitoylation are from Table 3.7 and (Roth *et al.*, 2006). Abbreviations are as in Table 3.7 except: AAT, amino acid transporter; ABF, antibacterial factor related; ALP, α-actinin-associated LIM protein (ALP)-Enigma family protein; Bet, blocked early in transport; CPS, cell death abnormality 3 (CED-3) protease suppressor; CSNK, casein kinase; EARS, glutamyl amino-acyl tRNA synthetase; GOA, G protein α_o subunit; Hem, heme biosynthesis; IMA, importin α family; LET, lethal; Lsb, local anestheticum sensitive (Las) seventeen binding protein; Mlf, multicopy suppressor of leflunomide activity; Mse, mitochondrial glutamyl-transfer-RNA synthetase; Nuc, nuclease; Psr, plasma membrane sodium response; Sam, *S*-adenosylmethionine metabolism; SCPL, small C-terminal domain phosphatase-like phosphatase; SNB, synaptobrevin; SPHK, sphingosine kinase; SRU, serpentine receptor class U; SYN, syntaxin; SYX, syntaxin; TBA, tubulin α; TBC, Tre-2/Bub2/Cdc16 domain family; Tub, tubulin; Tvp, Tlg2-vesicle protein; UNC, uncoordinated; Vam, vacuolar morphogenesis; YKT-6, yeast Ykt6 v-SNARE homologue.

Palmitoyl-protein	DHHC(s)	*C. elegans* orthologue	E value
ABCA1	DHHC2/REAM, DHHC8, DHHC12/AID, DHHC15, DHHC20, DHHC21	ABT-2	1e-114
AR	DHHC7/SERZ, DHHC21	NHR-69	7e-24
BACE1	DHHC3/GODZ, DHHC4, DHHC7/SERZ, DHHC15, DHHC20	ASP-4	3e-24
BK channel	DHHC22, DHHC23	SLO-1	0.0
CD9	DHHC2/REAM	TSP-8	2e-21
CD151	DHHC2/REAM, DHHC15	TSP-7	5e-21
CI-MPR	DHHC15	ZK1307.8	0.51
CKAP4/p63	DHHC2/REAM	UNC-15	2e-09
CL3/CaMKIγ	DHHC3/GODZ	CMK-1	4e-134
CSP	DHHC3/GODZ, DHHC7/SERZ, DHHC15, DHHC17/HIP14	DNJ-14	7e-31
DR4	DHHC3/GODZ	F47C12.1	0.45
eNOS	DHHC2/REAM, DHHC3/GODZ, DHHC7/SERZ, DHHC8, DHHC21	EMB-8	3e-64
ER	DHHC7/SERZ, DHHC21	NHR-91	6e-31
flotillin-2	DHHC5	STO-5	0.31
Fyn	DHHC21	SRC-2	0.0
$GABA_A$ receptor γ2 subunit	DHHC3/GODZ, DHHC7/SERZ	LGC-37	5e-90
GAD65	DHHC3/GODZ, DHHC8, DHHC13/HIP14L, DHHC17/HIP14	UNC-25	0.0
GAP43	DHHC7/SERZ, DHHC15	UNC-73	1.5
GluR1	DHHC3/GODZ, DHHC17/HIP14	GLR-1	1e-180
GluR2	DHHC3/GODZ, DHHC17/HIP14	GLR-1	2e-178
GRIP1	DHHC5, DHHC8	MAGI-1	6e-17
$G\alpha_{i2}$	DHHC3/GODZ, DHHC7/SERZ	GOA-1	0.0
$G\alpha_q$	DHHC3/GODZ, DHHC7/SERZ	EGL-30	0.0
$G\alpha_s$	DHHC3/GODZ, DHHC7/SERZ	GSA-1	0.0
H-Ras	DHHC9, DHHC17/HIP14, DHHC18	LET-60	2e-93
Htt	DHHC13/HIP14L, DHHC17/HIP14	F21G4.6	3e-06
integrin α6	DHHC3/GODZ	INA-1	2e-78
integrin β4	DHHC3/GODZ	PAT-3	8e-135
Lck	DHHC2/REAM, DHHC17/HIP14, DHHC18, DHHC21	SRC-2	6e-157
NCAM	DHHC3/GODZ, DHHC7/SERZ	HIM-4	1e-38
Nde1	DHHC2/REAM, DHHC3/GODZ, DHHC7/SERZ	NUD-2	6e-07
Ndel1	DHHC2/REAM, DHHC3/GODZ, DHHC7/SERZ	NUD-2	8e-05
N-Ras	DHHC9, DHHC17/HIP14	LET-60	1e-92
paralemmin-1	DHHC8	Y80D3A.8	4.6
PDE10A2	DHHC7/SERZ, DHHC19	PDE-5	6e-161
PI4KIIα	DHHC2/REAM, DHHC3/GODZ, DHHC7/SERZ, DHHC14, DHHC15, DHHC21	ZC8.6	7e-131
PR	DHHC7/SERZ, DHHC21	NHR-69	2e-25
PSD-93	DHHC8	DLG-1	9e-135
PSD-95	DHHC2/REAM, DHHC3/GODZ, DHHC7/SERZ, DHHC8, DHHC15, DHHC17/HIP14	DLG-1	1e-155
R7BP	DHHC2/REAM	Y116A8C.37	0.46
RGS4	DHHC3/GODZ, DHHC7/SERZ	RGS-2	3e-34
R-Ras	DHHC19	RAS-1	2e-71
SNAP-23	DHHC2/REAM, DHHC3/GODZ, DHHC7/SERZ, DHHC17/HIP14	RIC-4	7e-57
SNAP-25	DHHC2/REAM, DHHC3/GODZ, DHHC7/SERZ, DHHC8, DHHC15, DHHC17/HIP14	RIC-4	4e-67
sortilin	DHHC7/SERZ, DHHC15	F45H11.5	2.5
SSTR5	DHHC5	NPR-24	9e-42
stathmin-2	DHHC2/REAM, DHHC3/GODZ, DHHC5, DHHC7/SERZ, DHHC15, DHHC17/HIP14, DHHC21	F34D10.4	1.6
stathmin-3	DHHC2/REAM, DHHC3/GODZ, DHHC7/SERZ, DHHC15, DHHC21	E01A2.2	0.077
stathmin-4	DHHC2/REAM, DHHC3/GODZ, DHHC7/SERZ, DHHC15, DHHC21	DPY-6	0.21
STREX	DHHC3/GODZ, DHHC5, DHHC7/SERZ, DHHC9, DHHC17/HIP14	NHR-173	0.66
synaptotagmin-1	DHHC17/HIP14	SNT-1	4e-143

TABLE 3.9: Orthologues of *H. sapiens* palmitoyl-proteins in *C. elegans*

BLAST searches using the proteins above were performed to find orthologues in *C. elegans*. The *H. sapiens* proteins and the DHHC(s) responsible for their palmitoylation are from Table 3.7. Abbreviations are as in Table 3.7 except: ABT, ABC transporter family; ASP, aspartyl protease; CMK, Ca^{2+}/calmodulin-dependent protein kinase; DLG, Drosophila discs large homologue; DNJ, DnaJ domain containing protein; DPY, dumpy; EGL, egg-laying defective; EMB, abnormal embryogenesis; GLR, glutamate receptor family (α-amino-3-hydroxy-5-methyl-4-isoxazolepentaenoic acid (AMPA)); GOA, G protein α_o subunit; GSA, G protein α_s subunit; HIM, high incidence of males;

high confidence of being genuine substrates. In addition, G protein γ subunits are candidate substrates, as the Gγ protein Ste18 has been shown to be palmitoylated by Swf1 (Roth *et al.*, 2006). There have also been some large-scale studies using *C. elegans* proteins which can be used to determine possible substrates through known interactions. These interactions are collated through WormNet (http://www.functionalnet.org/wormnet/) and some are presented in Table 3.11. These have been selected because they are orthologues of known palmitoyl-proteins in *S. cerevisiae* and mammals (Table 3.7). The objective of Table 3.10 and Table 3.11 was to use the known data on palmitoyl-proteins and their cognate enzymes in other organisms to predict possible substrates and their likely enzyme partners in *C. elegans*. Hopefully these analyses will help to direct future studies on palmitoyl-proteins in *C. elegans* and increase the confidence in hits which also appear in these tables.

3.3.2 THE PALMITOYL-PROTEIN THIOESTERASE ENZYME FAMILY

As discussed in the introduction to this chapter, there are no unifying motifs in the PPTs which allow easy genomic searches. This limits the process of finding PPTs in unexplored genomes to searching for orthologues of known PPTs. The two known sub-families of PPTs, the PPTs and the APTs, are well represented across diverse organisms, although not many have both types of PPT. There is generally a reasonable degree of sequence conservation within orthologues of each individual protein, as can be seen in sequence alignments (Figure 3.6, Figure 3.7). However, there is no one conserved region in common between the two sequences. In *C. elegans* there are two PPTs: PPT-1 and ATH-1, which are orthologues of *H. sapiens* PPT1 and APT1 respectively.

The complete sequences of the PPTs in *S. cerevisiae*, *C. elegans*, *D. melanogaster* and *H. sapiens* were subjected to phylogenetic analysis and a phylogenetic tree was constructed (Figure 3.8). The tree shows a clear divide between the PPT and APT sub-families. The APT sub-family seems to be derived from the *S. cerevisiae* thioesterase enzyme Apt1, whereas the PPT sub-family is only present in the more complex organisms.

Some of the resources used for the DHHCs above can also provide some insight into the function of the PPTs. The *S. cerevisiae* PPT Apt1 is shown by the GFP-tagging study

LGC, ligand-gated ion channel; INA, integrin α; LET, lethal; MAGI, membrane associated guanylate kinase inverted homologue; NHR, nuclear hormone receptor; NPR, neuropeptide receptor family; NUD, *Aspergillus* nuclear division related; PAT, paralysed arrest at two-fold; PDE, phosphodiesterase; RIC, resistance to inhibitors of cholinesterase; RGS, regulator of G protein signaling; SLO, slowpoke K^+ channel family; SNT, synaptotagmin; SRC, SRC oncogene related; STO, stomatin; TSP, tetraspanin.

DHHC enzyme	No. of interactors	Selected interactors		
		Gene	Type	Experiment
Akr1	145	***AKR1***	**physical**	**PCA**
		ENV9	genetic	negative genetic
		GNP1	**genetic**	**negative genetic**
		GPA1	**genetic**	**synthetic lethality**
		LCB4	**physical**	**biochemical activity**
		MEH1	**physical**	**biochemical activity**
		PEP12	genetic	negative genetic
		PEP12	physical	affinity capture-MS
		PIN2	**physical**	**PCA**
		RAS1	**physical**	**two-hybrid**
		STE4	genetic	dosage rescue
		STE4	physical	two-hybrid (2), affinity capture-MS (3)
		STE18	**physical**	**two-hybrid (2)**
		TLG2	**physical**	**co-purification**
		YCK1	**physical**	**PCA, two-hybrid**
		YCK2	**genetic**	**negative genetic**
		YCK2	**physical**	**biochemical activity, co-localisation, two-hybrid**
		YKT6	**physical**	**affinity capture-MS**
Akr2	21	***LCB4***	**physical**	**affinity capture-Western, two-hybrid**
		TAT2	**genetic**	**negative genetic**
		VAM7	physical	two-hybrid
Erf2	60	***AGP1***	**genetic**	**negative genetic**
		RAS2	**genetic**	**synthetic lethality, synthetic rescue**
		RAS2	**physical**	**biochemical activity, co-localisation**
		VAC8	**physical**	**biochemical activity**
		VAM7	**genetic**	**negative genetic (2)**
Pfa3	11	***MEH1***	**physical**	**biochemical activity**
		VAC8	**physical**	**affinity capture-Western, biochemical activity (2), co-fractionation, co-localisation**
Pfa4	64	*BOS1*	genetic	negative genetic
		CHS3	**physical**	**affinity capture-Western**
		RIF2	genetic	phenotypic enhancement
Pfa5	15	***YGL108C***	**physical**	**biochemical activity**
Swf1	237	*ASC1*	genetic	negative genetic
		SEC9	genetic	negative genetic
		SEC22	genetic	negative genetic
		SNC1	**genetic**	**negative genetic (2)**
		SNC2	**genetic**	**synthetic lethality**
		SNC2	genetic	synthetic lethality
		SSO1	**genetic**	**synthetic lethality**
		TLG2	**genetic**	**negative genetic (2), synthetic growth defect**
YNL155W	29	***YCK2***	**physical**	**biochemical activity**

TABLE 3.10: Interaction data for the *S. cerevisiae* DHHC enzymes

Data from genome- and proteome-scale protein interaction studies in *S. cerevisiae* are collated on the SGD website. Shown is the total number of interactors for each DHHC enzyme, along with a selection of those which may be of interest to this study. Numbers in parentheses in the Experiment column indicate how many different experiments give evidence for the interaction. Known palmitoyl-proteins are shown in bold. *AGP*, high affinity glutamine permease; *ASC*, absence of growth suppressor of Cyp1; *BOS*, bet one suppressor; *CHS*, chitin synthase; *ENV*, late endosome and vacuole interface function; *GNP*, glutamine permease; *GPA*, G protein α subunit; *LCB*, long-chain base; *MEH*, multicopy suppressor of endoplasmic reticulum retention defective (Erd) suppressor 1 (Ers1) hygromycin B sensitivity; MS, mass spectrometry; PCA, protein-fragment complementation assay; *PEP*, carboxypeptidase Y-deficient; *PIN*, Psi+ inducibility; *RIF*, repressor activator protein 1 (Rap1)-interacting factor; *SEC*, secretory; *SNC*, suppressor of the null allele of cyclase associated protein; *SSO*, suppressor of Sec one; *STE*, sterile; *TAT*, tyrosine and tryptophan amino acid transporter; *TLG*, t-SNARE affecting a late Golgi compartment; *VAC*, vacuole-related; *VAM*, vacuolar morphogenesis; *YCK*, yeast casein kinase.

Gene	No. of interactors	Selected interactors			
		Gene	Name	Description	Evidence
dhhc-1	81				
dhhc-2	109	*let-60*	lethal	Ras family small GTPase	SC-GT
		ras-1	R-Ras related	small GTPase	SC-GT
dhhc-3	6				
dhhc-4	70				
dhhc-6	354				
dhhc-8	10				
dhhc-9	18				
dhhc-11	5				
dhhc-12	230				
dhhc-13	74	*goa-1, gpa-3, -4, -7, -16, odr-3*	G-protein α subunits	signal transduction	SC-GT
dhhc-14	28	*unc-64*	syntaxin-1	exocytosis	SC-GT

TABLE 3.11: Interaction data for the *C. elegans* DHHC enzymes

The online database WormNet (http://www.functionalnet.org/wormnet/) was searched for interactors with the *C. elegans* DHHC enzymes. The total number of interactors found and some interactors of potential interest are presented here. *dhhc-13* was found to interact with three other DHHC enzymes: *dhhc-2*, *dhhc-4* and *dhhc-14*. The genes *dhhc-5*, *dhhc-7*, *dhhc-10* and *spe-10* were not present in WormNet. *odr*, chemotaxis-defective; SG-GT, yeast genetic interaction; *unc*, uncoordinated.

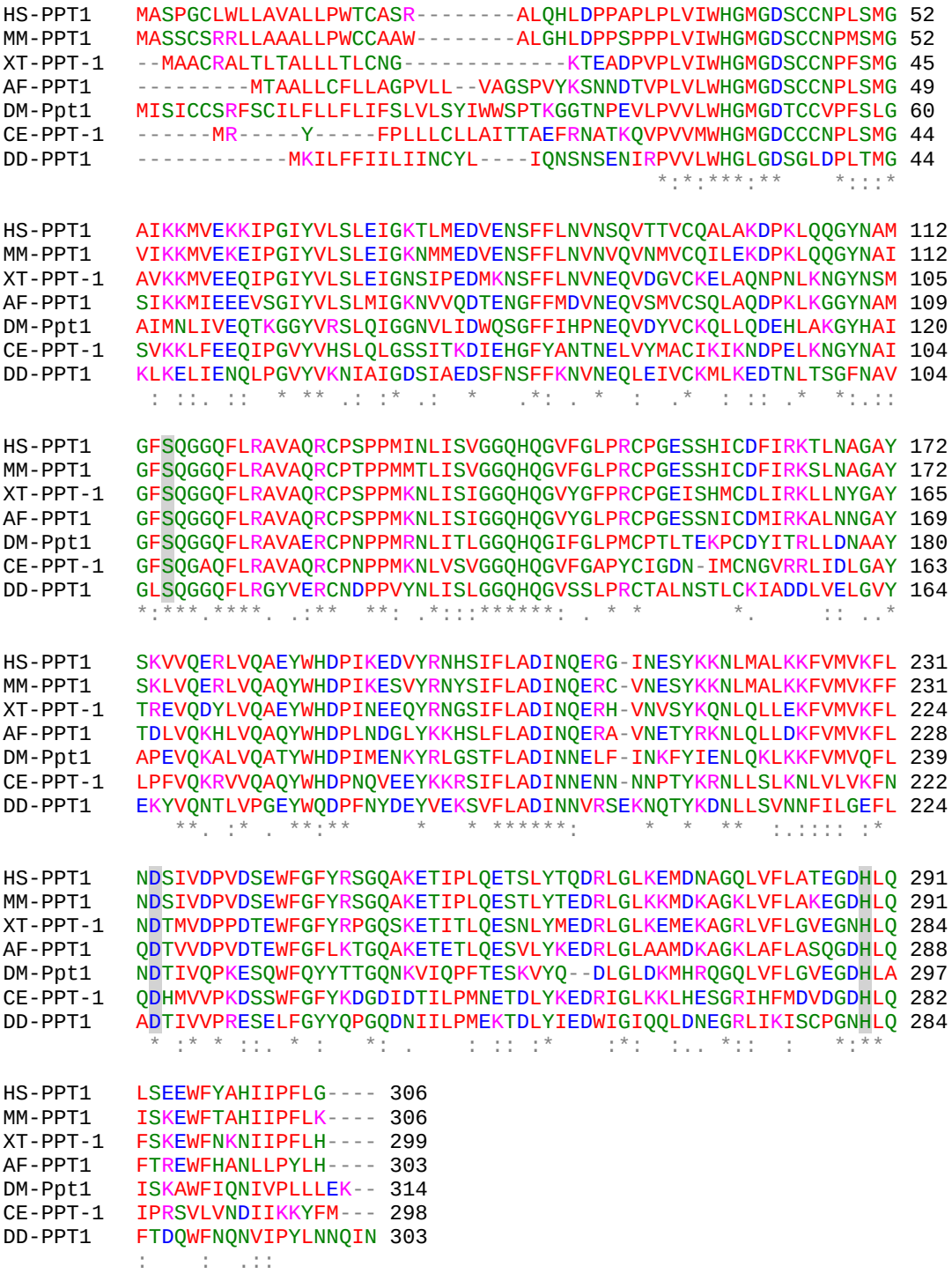

FIGURE 3.6: Alignment of homologues of PPT1 in diverse species

This alignment shows short regions of homology between the PPT1 sequences of different species amongst more divergent stretches of sequence. The catalytic triad (Bellizzi *et al.*, 2000) is shaded in grey. Absolutely conserved residues are indicated by an asterisk, a colon indicates residues with highly similar properties and a period indicates residues with less similar properties. AF, *Anoplopoma fimbria*; CE, *Caenorhabditis elegans*; DD, *Dictyostelium discoideum*; DM, *Drosophila melanogaster*; HS, *Homo sapiens*; MM, *Mus musculus*; XT, *Xenopus tropicalis*.

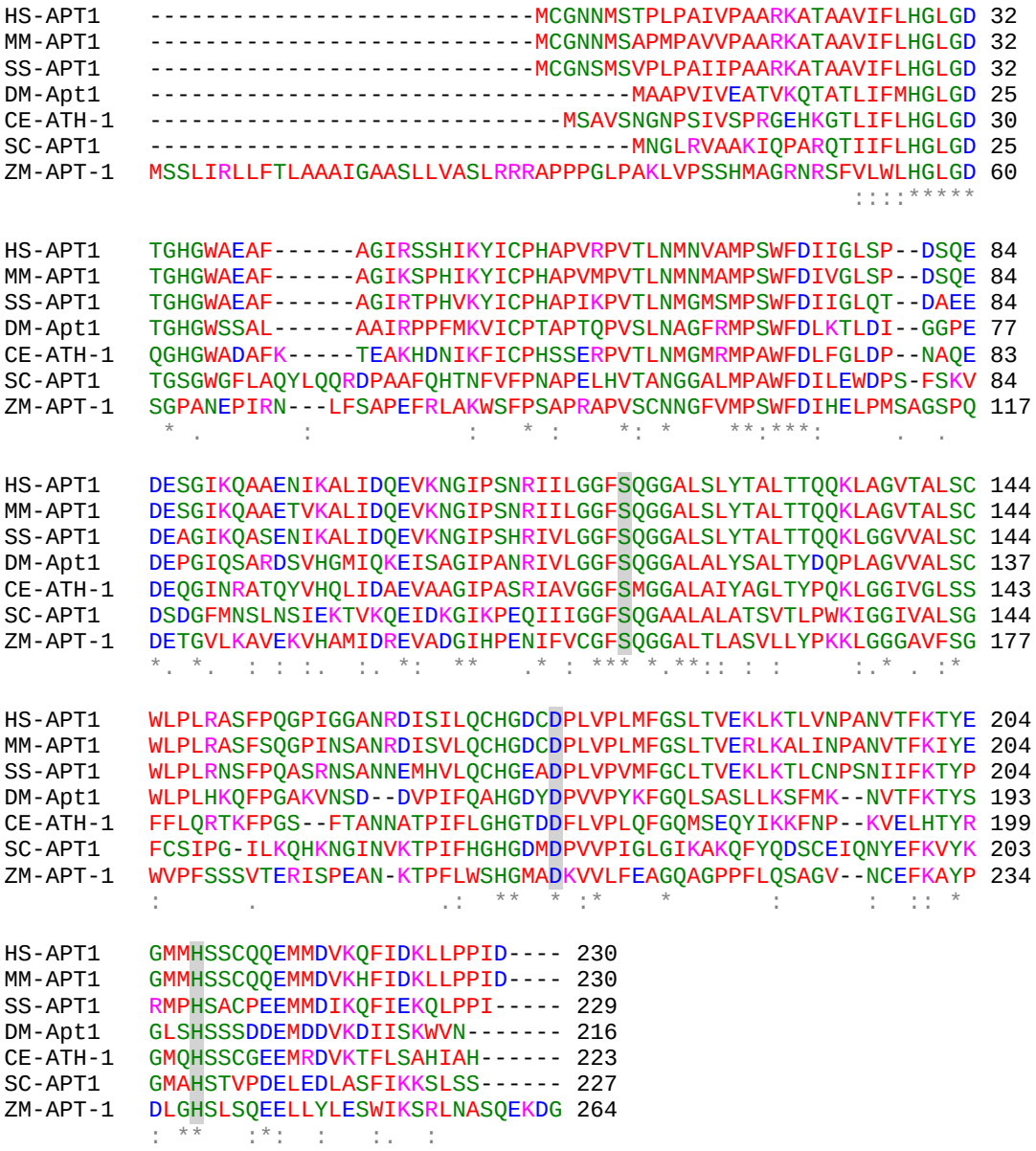

FIGURE 3.7: Alignment of homologues of APT1 in diverse species

This alignment shows relatively few regions of absolute homology. The catalytic triad (Devedjiev *et al.*, 2000) is shaded in grey. Absolutely conserved residues are indicated by an asterisk, a colon indicates residues with highly similar properties and a period indicates residues with less similar properties. CE, *Caenorhabditis elegans*; DM, *Drosophila melanogaster*; HS, *Homo sapiens*; MM, *Mus musculus*; SC, *Saccharomyces cerevisiae*; SS, *Salmo salar*; ZM, *Zea mays*.

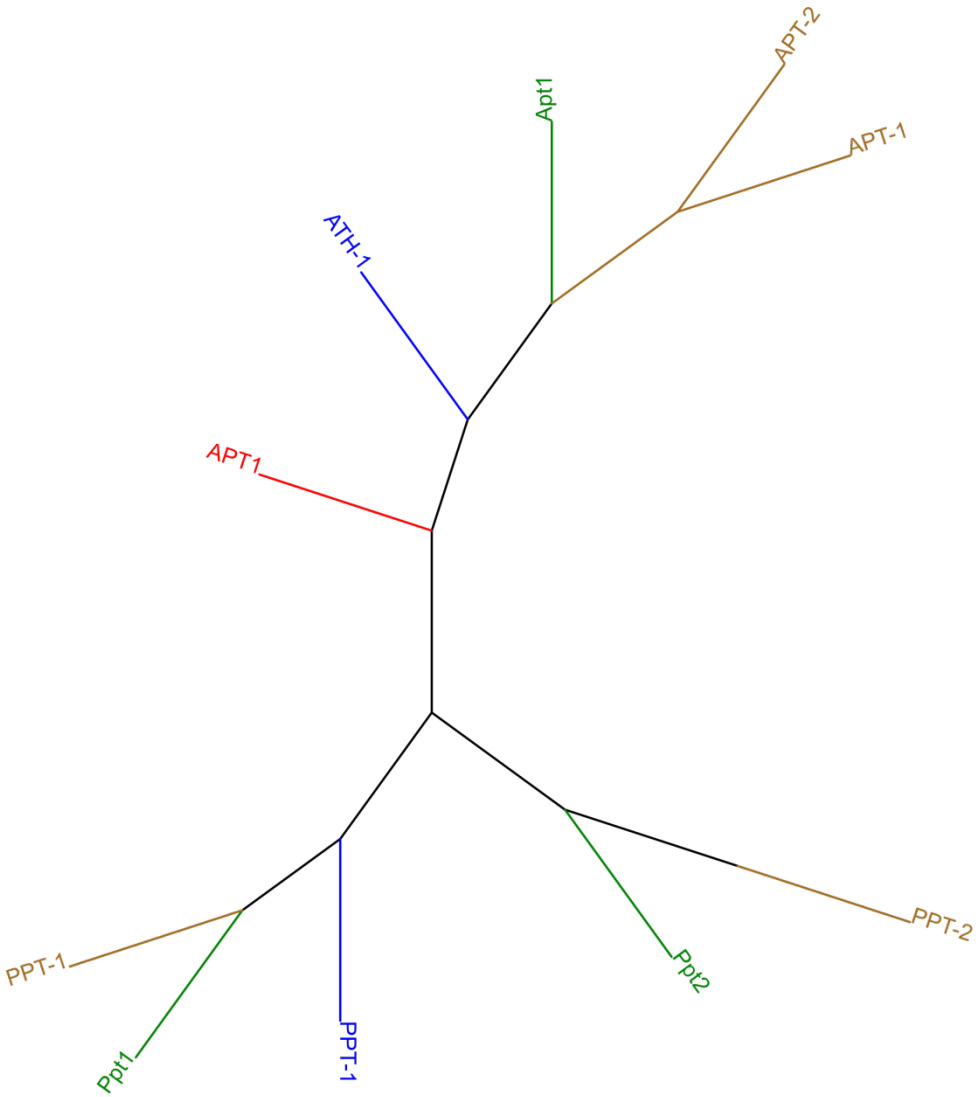

FIGURE 3.8: Phylogenetic tree of PPT enzymes from evolutionarily important organisms

The complete sequences of the known PPT family enzymes in *S. cerevisiae* (red), *C. elegans* (blue), *D. melanogaster* (green) and *H. sapiens* (brown) were subjected to phylogenetic analysis. The resulting tree was rendered and coloured using Interactive Tree of Life (Letunic and Bork, 2007).

(Huh *et al.*, 2003) to be localised to the cytoplasm and nucleus. This is consistent with the known localisation of *H. sapiens* APT1 in the cytoplasm (Duncan and Gilman, 1998), compared with PPT1 and -2, which are lysosomal (Soyombo and Hofmann, 1997; Verkruyse and Hofmann, 1996).

The *S. cerevisiae* and *C. elegans* interaction studies may also uncover potential substrates of the PPTs. According to SGD, *S. cerevisiae* Apt1 has 23 interactors, although none of them are known palmitoyl-proteins (Roth *et al.*, 2006). A search of the WormNet resource shows that PPT-1 has 19 interactors and ATH-1 has 169. A few of the ATH-1 interactors are likely palmitoyl-proteins, including G protein α subunits (GOA-1, GPA-3, -4, -7, -16) and regulators of G protein signaling (RGS-1, -2). Known substrates of *H. sapiens* PPT1 include H-Ras (Camp and Hofmann, 1993), and *H. sapiens* APT1 can remove palmitate from $G\alpha_s$, H- and N-Ras, eNOS, ghrelin and BK channels (Dekker *et al.*, 2010; Duncan and Gilman, 1998; Satou *et al.*, 2010; Tian *et al.*, 2012; Yeh *et al.*, 1999). N-Ras is a substrate for both APT1 and -2 (Rusch *et al.*, 2011).

A crystal structure of *H. sapiens* PPT1 showed it acts as a monomer with an α/β hydrolase fold and three catalytic residues: serine-115, aspartate-233 and histidine-289 (Bellizzi *et al.*, 2000). A comparison with the crystal structure of PPT2 showed a similar structure – an α/β hydrolase fold and the catalytic residues serine-111, aspartate-228 and histidine-283 – although a much smaller lipid-binding groove in PPT2 accounts for its inability to remove palmitate from proteins (Calero *et al.*, 2003). The crystal structure of APT1 again shows an α/β hydrolase fold with the catalytic residues serine-114, aspartate-169 and histidine-203, but forms a dimer which hides the active site. This would mean the dimer would have to dissociate for the enzyme to be active (Devedjiev *et al.*, 2000). These catalytic triads are absolutely conserved amongst orthologues in different species (Figure 3.6, Figure 3.7). Although substrates of the PPTs are not generally known, there has been a disproportionate amount of research conducted on the function of PPT1 since it was discovered to be mutated in the disease infantile neuronal ceroid lipofuscinosis (INCL) (Vesa *et al.*, 1995). PPT1 was found to be expressed developmentally in the rat brain and retina, correlating with the clinical manifestation of early loss of vision followed by neuronal deterioration in INCL (Zhang *et al.*, 1999). The most common mutations of PPT1 in INCL cause decreased enzymatic activity, different palmitate binding and reduced protein levels (Das *et al.*, 2001). PPT1 is also known to be glycosylated at asparagine-197 and asparagine-232 which is a requirement for its activity, transport to the lysosome and prevention of its lysosomal degradation (Hellsten *et al.*, 1996; Lyly *et al.*, 2007; Verkruyse

and Hofmann, 1996). Interest in this disease has led to INCL models in diverse organisms, including *M. musculus* (Gupta *et al.*, 2001), *D. melanogaster* (Glaser *et al.*, 2003; Hickey *et al.*, 2006), the yeast *Schizosaccharomyces pombe* (Cho and Hofmann, 2004) and *C. elegans* (Porter *et al.*, 2005). The *C. elegans* model showed the least severe phenotype – a mild developmental and reproductive phenotype resulting from a mitochondrial defect (Porter *et al.*, 2005). Deficiency of PPT2 has been shown to produce a lysosomal storage disorder with distinct effects from PPT1 in a mouse model (Gupta *et al.*, 2003).

D. melanogaster has also been used for research into the PPTs, especially Ppt1. Loss-of-function mutations in Ppt1 replicated the abnormal storage of autofluorescent material and reduced lifespan seen in INCL but not the neurodegeneration (Hickey *et al.*, 2006). *Drosophila* Ppt1 has been found to be involved in various synaptic functions, and its overexpression in the visual system resulted in neurodegeneration (Buff *et al.*, 2007; Chu-LaGraff *et al.*, 2010; Korey and MacDonald, 2003; Saja *et al.*, 2010). Although Ppt2 was seen to have a small amount of thioesterase activity, its overexpression was not able to rescue phenotypes seen in a Ppt1 knockout (Bannan *et al.*, 2008). Apt1 was found to be expressed at high levels throughout embryonic development, with neural enrichment in both the larval and adult central nervous system (CNS). Consistent with the *H. sapiens* protein, Apt1 was cytoplasmic with a possible enrichment in an endosomal compartment (Bannan *et al.*, 2008).

3.4 DISCUSSION

3.4.1 DHHCS

3.4.1.1 DHHC ENZYMES

In comparison with other organisms important to research, palmitoylation has been neglected as a field of study in the model organism *C. elegans*. Database mining using the conserved DHHC-CRD clarified the confusion in the literature showing there are 15 DHHCs in *C. elegans*. This contrasts with varying published figures of 15 (Fukata and Fukata, 2010), 16 (Mitchell *et al.*, 2006) and 17 (Gleason *et al.*, 2006) DHHCs. It may be that the source of confusion is the occasional duplications which can occur in genome databases and which are removed as they are curated. Confusion has occurred in other organisms as well. For example, 20 *D. melanogaster* DHHCs were quoted in one study (Ohyama *et al.*, 2007) but this family has since been confirmed to comprise 22 members (Bannan *et al.*, 2008). A systematic naming procedure of *dhhc-x* was applied to the unnamed *C. elegans* genes and their products in this family. An exception was made for *spe-10*, as this has been the

subject of published research and so a renaming might cause confusion (Cypser and Johnson, 1999; Gleason *et al.*, 2006; Shakes and Ward, 1989). Sequence analysis confirmed that all of these proteins contained the requisite DHHC-CRD which is the active site (Lobo *et al.*, 2002; Mitchell *et al.*, 2010). Although palmitoyltransferase activity is yet to be directly observed with these enzymes, the overall structure as presented in Figure 3.2 is in line with enzymes whose activity has been confirmed and can be considered of very high confidence, justifying an initial characterisation of this family in *C. elegans*. An obvious discrepancy occurs with DHHC-11, which omits the two TMDs normally found before the DHHC-CRD and is a little isolated on the phylogenetic tree (Figure 3.3). It is possible that these TMDs are missing as a result of a mutation producing a protein truncated at the N-terminus. Alternatively, palmitoylation of one of the cysteine residues upstream of the first TMD could mediate membrane attachment of the N-terminus of the protein, compensating for the lack of TMDs in this region. It is also possible that the missing TMDs are present in the genome on an exon which has been incorrectly annotated.

Several similar pairs of *C. elegans* DHHCs emerged from a phylogenetic analysis of the family (Figure 3.3). Interestingly, some of these pairs also share high homology with the same protein in other organisms, suggesting they may have arisen from duplications in the past (Table 3.6). DHHC-1 and -10 are both on chromosome X and are closest to *D. melanogaster* CG10344 and *H. sapiens* DHHC24 but distinct *S. cerevisiae* proteins: Pfa3 and Pfa4 respectively. DHHC-4 and SPE-10 share homology to *S. cerevisiae* Pfa3, *D. melanogaster* CG1407 and *H. sapiens* DHHC2. DHHC-9 and -12 are closest to *H. sapiens* DHHC16. This similarity in these pairs suggests that they may share common substrates and functions within the cell.

A large proportion of the *D. melanogaster* DHHCs, including Hip14, contain the PaCCT motif identified in the *S. cerevisiae* DHHCs Swf1 and Pfa3 (Gonzalez Montoro *et al.*, 2009). The PaCCT motif is also present in all the DHHCs which make up the cluster of *D. melanogaster* DHHCs seen in the phylogenetic tree (Figure 3.4), which may partially explain why the proportion containing the motif is particularly high compared with the other organisms presented. Although this motif was shown to be critical for the function of these two *S. cerevisiae* DHHCs, the mechanism is not clear and no further research has been published. For this reason it remains to be seen whether the PaCCT motif is particularly important to the *D. melanogaster* DHHCs. The presence of the PaCCT motif in only three of the *C. elegans* DHHCs suggests it does not have widespread significance in this species.

3.4.1.2 PREDICTION OF SUBSTRATES

The *H. sapiens* DHHCs seem to vary widely in their promiscuity, although this may partly be a function of which enzymes have been focused on. DHHC3/GODZ, DHHC7/SERZ and DHHC17/HIP14 have the most substrates listed in Table 3.7, ranging from neurotransmitter receptors and ion channels to G proteins and structural molecules. This broad specificity does not appear to be so much the case in *S. cerevisiae*, where Swf1 appears to be responsible for palmitoylating SNARE proteins and Pfa4 the amino acid permeases (AAPs) for example. The subcellular localisation of DHHC enzymes has been studied in *S. cerevisiae* and *H. sapiens* (Table 3.3, Table 3.5). They show varying locations within the cell, which may contribute to spatio-temporal specificity. However DHHC3/GODZ, DHHC7/SERZ and DHHC17/HIP14 are all Golgi-localised, so the substrates they share may be regulated by distinct expression of the DHHCs in different cell types or during development. Alternatively, it may be a source of redundancy in the system.

Some of the substrates may be suitable candidates for studying in more detail in a model system such as *C. elegans*. Both DHHC3/GODZ and DHHC17/HIP14 have close orthologues in *C. elegans* – DHHC-3 and DHHC-14 respectively (Table 3.6). Their substrates synaptotagmin-1 and ATP-binding cassette transporter A1 (ABCA1), for example, also have close orthologues in SNT-1 and ABT-2 respectively (Table 3.9). Given the genetic tractability of *C. elegans* compared with mammalian systems, it would be a logical system in which these predicted enzyme-substrate pairs could be confirmed and refined down to which cysteine residues are palmitoylated. The reverse process could also be put into action, using *C. elegans* to inform studies of *H. sapiens* DHHCs. The *C. elegans* enzymes DHHC-2 and -6 are close matches for *H. sapiens* DHHC14 and -6 respectively, neither of which have been characterised. The closest *C. elegans* orthologues to known *S. cerevisiae* palmitoyl-proteins were also investigated (Table 3.8). Predictions made using this method would have the highest confidence where close orthologues exist, so perhaps they are better from the *H. sapiens* list as the matches are generally better both in enzymes and substrates. Of course, all of the organisms investigated are representative of different types of organism, so these links may not be definitive. For example, the substrates and interactors of *S. cerevisiae* Erf2 include Ras and Rho proteins. DHHC-13 is the most closely related *C. elegans* enzyme, and it may therefore be predicted to be responsible for palmitoylation of *C. elegans* Ras and Rho proteins. However, the main Ras orthologue in *C. elegans* is LET-60, which is most closely related to K-Ras(B). K-Ras(B) is not palmitoylated because it lacks the requisite cysteine residue in the hypervariable region (Hancock *et al.*, 1989) and

instead associates with membranes through its polybasic domain (Hancock *et al.*, 1990). LET-60 also lacks cysteine residues in its hypervariable region and so it is unlikely that LET-60 would be palmitoylated. Table 3.7 shows *H. sapiens* CSP is known to be palmitoylated by DHHC3/GODZ, DHHC7/SERZ, DHHC15 and DHHC17/HIP14, and the *D. melanogaster* version by its Hip14. It is therefore possible that the *C. elegans* orthologue of CSP, DnaJ domain-containing protein 14 (DNJ-14), might be palmitoylated by DHHC-3, DHHC-7, DHHC-13 or -14, the most highly related enzymes (Table 3.6).

S. cerevisiae was the model organism in which the first experiments to probe DHHC function and substrates were performed and the first proteome-scale analysis of palmitoylated proteins was conducted (Roth *et al.*, 2006). There is a wealth of information available from genome-wide interaction studies in *S. cerevisiae*, both about *S. cerevisiae* proteins and those from other species studied using systems such as yeast two-hybrid (Table 3.10, Table 3.11). This information should be used with caution, as many of the known *S. cerevisiae* substrates are not found in this list. The predictive power of a similar analysis of *C. elegans* interactions is probably quite low, as four of the 15 DHHCs are not represented at all, and those that are show very few proteins of the kinds shown in Table 3.7.

An interaction between a DHHC and another protein does not necessarily mean that the protein is a substrate. There have been reported interactions away from the DHHC-CRD which have been shown to modulate the function of the enzyme. The *S. cerevisiae* DHHC Akr1 interacts with Ste4, a G protein β subunit (Table 3.10). This has been shown to be dependent on the ankyrin repeat region of Akr1 and independent of the acyltransferase activity. The ankyrin repeat region partially contributed to the cell morphology phenotype (Hemsley and Grierson, 2011). This study also showed that in addition to autopalmitoylation, Akr1 can palmitoylate other Akr1 molecules in *trans* at sites away from the DHHC-CRD. Another *S. cerevisiae* enzyme, Swf1, has also been found to regulate actin cytoskeleton organisation independently of the DHHC domain (Dighe and Kozminski, 2008). In human embryonic kidney (HEK293) cells, the *H. sapiens* enzyme DHHC17/HIP14 was found to interact with c-Jun N-terminal kinase isoform 3 (Jnk3) in the ankyrin repeat region, especially within the second repeat, with a resulting increase in phosphorylation and activity of Jnk3. This was mediated by recruitment of mitogen-activated protein kinase kinase 7 (MKK7). Palmitoylation of postsynaptic density protein 95 (PSD-95) by DHHC17/HIP14 inhibited the interaction with Jnk3, and this was reversed by sequestration of PSD-95 by N-methyl-D-aspartate receptors (NMDARs) induced by excitotoxicity. The

particular binding motif in the second ankyrin repeat was unique to DHHC17/HIP14 (Yang and Cynader, 2011). The *H. sapiens* enzyme DHHC23/neuronal nitric oxide synthase (nNOS)-interacting DHHC domain-containing protein with dendritic mRNA (NIDD) has been shown to interact with a PSD-95/*Drosophila* discs large tumour suppressor (Dlg1)/zonula occludens-1 protein (zo1) (PDZ) domain in nNOS through a glutamate-aspartate-isoleucine-valine (EDIV) motif at its C-terminus. This resulted in an increase in nitric oxide (NO) formation by nNOS (Saitoh *et al.*, 2004). Another study found that the four C-terminal amino acids (glutamate-isoleucine-serine-valine (EISV)) of DHHC5 mediate an interaction with the third PDZ domain of PSD-95 (Li *et al.*, 2010). In *D. melanogaster*, GABPI has been shown to interact with β1,4-N-acetylgalactosaminyltransferase B (β4GalNAcTB) and regulate its exit from the ER, an effect which is presumably independent of palmitoylation as GABPI lacks the requisite cysteine of the DHHC motif (Johswich *et al.*, 2009). It is therefore likely that some proteins identified in large-scale interaction studies are modulators rather than substrates.

3.4.1.3 PREDICTION OF PHENOTYPES

There is very little information available on the DHHCs in *C. elegans*, and the few phenotypes which are reported are mostly the results of large-scale RNA interference (RNAi) screens. These are fairly vague, such as “development variant”, which offers little insight. The one mutant which has been studied is that of *spe-10* (Cypser and Johnson, 1999; Gleason *et al.*, 2006; Shakes and Ward, 1989). However, these studies showed how it is involved in the process of spermatogenesis in *C. elegans*, and that the mutant has a general increase in stress resistance and lifespan. Neither of them provided new information in terms of the palmitoyltransferase activity of SPE-10 or potential substrates. On the basis of this relative dearth of information, it was useful to investigate what is known about DHHC functions in other organisms.

As *S. cerevisiae* has the fewest members of its DHHC family, some phenotypes relating to fundamental processes may be expected. Indeed null strains for some of the DHHCs have been shown to have specific phenotypes. Akr1 mutants are misshapen, show slow growth, do not survive at 37 °C and have defects in their pheromone response (Givan and Sprague, 1997; Kao *et al.*, 1996; Pryciak and Hartwell, 1996). Swf1 mutants also show a significant growth phenotype (Roth *et al.*, 2006) and are unable to grow in conditions of high salinity or with lactate as the sole carbon source (Gonzalez Montoro *et al.*, 2009). However, the fundamental importance of palmitoylation can be questioned given that a deletion strain of five of the *S. cerevisiae* DHHCs (*akr1Δ akr2Δ pfa3Δ pfa4Δ pfa5Δ*) is viable (Hou *et al.*, 2009;

Roth *et al.*, 2006). This strain can even tolerate an additional conditional depletion of Swf1 or Erf2, though not absolute deletions (Roth *et al.*, 2006). Of course, this may still be explained by overlapping specificities of the enzymes, which could lead to functional redundancy. In the large phylogenetic tree (Figure 3.4), the *S. cerevisiae* DHHCs Akr1 and Akr2 and Swf1 and Erf2 form two sets of closely related pairs. Given there are also several *C. elegans* DHHCs which form pairs in the phylogenetic analysis, it is possible that similar difficulties will appear when handling single knockouts. However there are also several *C. elegans* DHHCs which are on their own in the phylogenetic tree, such as DHHC-2 and DHHC-8. These may be more promising leads for knockout phenotypes.

Although the DHHC enzymes of *D. melanogaster* have not been extensively studied, there have been some important insights using this model organism. The DHHC Hip14 was shown to be responsible for palmitoylation and proper functionality of CSP, the most palmitoylated protein known (Ohyama *et al.*, 2007). This study showed that Hip14 is located both pre- and postsynaptically and is required for proper exocytosis of synaptic vesicles. This was found to be a result of mislocalisation of CSP away from the synapse and was replicated by expression of an unpalmitoylatable version of CSP. A chimeric version of CSP which is forced into synaptic vesicles rescued a Hip14 temperature-sensitive phenotype. Thus palmitoylation of CSP by Hip14 targets it to synaptic vesicles where it promotes proper synaptic function. Hip14 palmitoylation of SNAP-25 and its localisation were found to be independent of CSP, and the lack of effect of SNAP-25 mislocalisation is thought to be due to compensation by SNAP-24 (Vilinsky *et al.*, 2002). Another paper showed the developmentally secreted chordin homologue short gastrulation (Sog) as another substrate of Hip14 (Kang and Bier, 2010). Hip14 and Sog were found to be localised to the Golgi in the *Drosophila* embryonic S2 cell line, where they interact. Palmitoylation of Sog on cysteine-27 and cysteine-28 by Hip14 was found to promote its secretion. These studies illustrate how a single DHHC can have diverse substrates and functions depending on the tissues and cell types in which it is expressed.

The relationship between *H. sapiens* DHHC17/HIP14 and Htt has led to interest in this particular enzyme in mammals and as a result a knockout mouse has been made (Singaraja *et al.*, 2011). These mice showed a neuropathology very similar to their HD mouse model (YAC128), including reduced brain weight, decreased striatal medium spiny neuron number and reduced striatal, cerebral cortex, hippocampal and white matter volume. These changes were observed in *Hip14*$^{-/-}$ mice but not *Hip14*$^{+/-}$ mice, showing complete lack of *Hip14* is necessary for these changes. In addition, there were fewer excitatory

(i.e. glutamatergic) synapses per neuron. Astrocyte and microglial numbers were unchanged. The neuropathology was found not to be progressive but to result from increased cell death later in development, between embryonic days 14.5 and 17.5, which is different from YAC128 mice, which have no evidence of neuropathology until three months of age. A reduction in dopamine- and cyclic adenosine monophosphate (cAMP)-regulated phosphoprotein of 32 kDa (DARPP32) and enkephalin, which is a hallmark of even mild HD, is also seen in these mice. Behavioural measures were also disrupted as in YAC128 mice in motor co-ordination, dark-phase open-field and pre-pulse inhibition (PPI) tests. There was no change in Htt palmitoylation between wild-type and knockout mice, and the closely related enzyme HIP14L appears to be responsible for this. HIP14 showed reduced autopalmitoylation, suggesting mutant Htt alters its activity. Expression of human DHHC17/HIP14 in these mice using a bacterial artificial chromosome (BAC) strategy rescued the anatomical, neurochemical and behavioural deficiencies (Young *et al.*, 2012). The only phenotype not rescued in the BAC mice was overall body weight. This may be a result of the relatively low expression level (around 35% of wild-type), or an artefact of expressing human DHHC17/HIP14 in mice. The same group has also produced a mouse knockout of *Hip14l* (Sutton *et al.*, 2012). Unlike the *Hip14*$^{-/-}$ mice, the *Hip14l*$^{-/-}$ mice showed a progressive reduction in brain weight and the volume of the striatum, cortex, thalamus, globus pallidus and corpus callosum. The same reduction of DARPP32 and enkephalin but not substance P was seen as in the *Hip14*$^{-/-}$ and YAC128 mice. There were some differences in the phenotypes observed in the *Hip14l*$^{-/-}$ mice compared with the *Hip14*$^{-/-}$ mice. Anatomically, the *Hip14l*$^{-/-}$ mice suffered mild hypotrichosis and alopecia. Behaviourally, they showed hypoactivity and deficits in learning but normal motor function. SNAP-25 showed a 33% reduction in palmitoylation in *Hip14l*$^{-/-}$ mice, which is interestingly large given there are six other DHHCs which can palmitoylate it (Table 3.7). Given Htt is a substrate for both DHHC17/HIP14 and DHHC13/HIP14L, and expanded Htt affects the activity of both enzymes, it seems likely that a reduction of function of both enzymes is involved in HD pathogenesis. It will be interesting to see what further insight can be gained from these mouse models and whether mouse knockouts of other DHHC enzymes also show disease-like phenotypes.

Palmitoylation as a post-translational modification in humans is relatively understudied and much of the information available on some of the less studied family members is in the form of associations from large-scale studies on specific diseases. *C. elegans* is often used to study development and neuronal function, processes which are involved in the most

common associations – cancers and neurodegenerative diseases. Whilst studies in *C. elegans* may not be able to shed further light on associations with some human diseases such as X-linked mental retardation (XLMR), it can be a useful proxy for more fundamental processes underlying these conditions. Some of the *H. sapiens* DHHC enzymes have also been shown to have functions away from the DHHC-CRD active site, such as the involvement of DHHC3, DHHC13/HIP14L and DHHC17/HIP14 in ion transport (Goytain *et al.*, 2008; Hines *et al.*, 2010). This phenomenon has not been reported for DHHCs from other organisms as yet. It would be interesting to investigate whether this function is more widespread and if it is independent of the palmitoyltransferase activity or whether they modulate each other. *C. elegans* is in many ways an ideal system in which to investigate these aspects of the DHHC enzymes further, using these predictions as a guide to interpret the observations.

3.4.2 PALMITOYL-PROTEIN THIOESTERASES

The lack of any conserved motifs has limited the known PPTs to two sub-families: PPTs and APTs. Despite this, crystal structures of *H. sapiens* PPT1, PPT2 and APT1 show the same basic structure of an α/β hydrolase fold and a catalytic triad of serine, aspartate and histidine residues (Bellizzi *et al.*, 2000; Calero *et al.*, 2003; Devedjiev *et al.*, 2000). It is surprising that some organisms only have one of these enzymes given the relative abundance of different DHHCs. Analogous reversible post-translational modifications do not have quite this extreme a ratio of enzymes. The human genome contains around 500 kinases (Manning *et al.*, 2002) compared with approximately 200 phosphatases (Sacco *et al.*, 2012). Similarly, in the ubiquitin system there are about 600 E3 ligases (Li *et al.*, 2008) and nearly 90 deubiquitinases (Clague *et al.*, 2012). It is possible that there are other PPTs which are yet to be discovered, otherwise mutants lacking them would be expected to have more severe phenotypes than are observed. Deletion of the only *S. cerevisiae* enzyme, Apt1, does not lead to any gross phenotype (Duncan and Gilman, 2002). Inhibition of APT1 by palmostatin B in Madin-Darby canine kidney epithelial (MDCK) cells prevented N-Ras depalmitoylation and altered its subcellular localisation from the plasma membrane and Golgi to all cellular membranes (Dekker *et al.*, 2010). Despite this mislocalisation of an important signaling molecule, the cells showed no obvious phenotype. Similarly, a study identifying APT1 as the PPT for BK channels reported no phenotypes despite the channels becoming trapped in the ER (Tian *et al.*, 2012). If Apt1 is the only PPT in *S. cerevisiae* and it is responsible for depalmitoylation of substrates such as Gα and Ras then it seems likely

there is some compensatory mechanism which prevents manifestation of a severe phenotype, and an as-yet-undiscovered set of PPTs is a possible explanation.

Although a cause of the disease INCL has been traced to a mutation in the human PPT1 gene (Vesa *et al.*, 1995), *ppt-1* mutants in *C. elegans* show only a mild mitochondrial defect (Porter *et al.*, 2005). Perhaps more success has been seen in *D. melanogaster* mutants. It has been shown that *D. melanogaster* requires Ppt1 for normal neuronal development, and that defects resulting from its mutation are similar to those seen in INCL (Buff *et al.*, 2007; Chu-LaGraff *et al.*, 2010; Korey and MacDonald, 2003; Saja *et al.*, 2010). Overexpression of Ppt2 in *Ppt1* mutants failed to rescue the phenotypes, suggesting there are distinct specificities (Bannan *et al.*, 2008). The disruption of both PPTs in *C. elegans* and the comparison of palmitoyl-proteomes of wild-type and PPT mutants may help shed light on the roles the PPTs play. This will be potentially valuable in expanding the knowledge of PPT substrates and help to answer the question of whether PPTs have distinct sets of substrates or whether there is an overlap.

This chapter has identified the DHHC enzymes in *C. elegans* and set out the currently available information about both DHHCs and PPTs in three important organisms: *S. cerevisiae*, *D. melanogaster* and *H. sapiens*. As palmitoylation is essentially unexplored in *C. elegans*, the information presented here should act as a platform for assessing data collected in this model organism. Furthermore, these data may be used to predict possible outcomes from known phenotypes in *C. elegans*. For example, the *C. elegans* orthologue of synaptotagmin-1, SNT-1, has a deficit in locomotion resulting from impaired synaptic release (Nonet *et al.*, 1993). The only known DHHC for synaptotagmin-1 is DHHC17/HIP14 (Table 3.7), so mutants lacking the similar enzymes DHHC-13 or -14 may also show locomotion defects. Mutants for the *C. elegans* orthologue of CSP, DNJ-14, show a reduction in lifespan and an age-dependent locomotion defect (unpublished data). This phenotype may be harder to observe among DHHC mutants as many share CSP as a substrate in *H. sapiens*. EGL-30, the orthologue of the important cell signaling molecule $G\alpha_q$, gives phenotypes of disrupted viability, egg-laying and locomotion when deleted (Brundage *et al.*, 1996). *H. sapiens* $G\alpha_q$ is palmitoylated by DHHC3/GODZ and DHHC7/SERZ, so disruption of the similar *C. elegans* proteins DHHC-3 or DHHC-7 may recapitulate some of these phenotypes. This examination of the effects of disruption of individual enzymes on *C. elegans* at both phenotypic and proteomic levels will complement the current knowledge and hopefully provide additional insights into the nature of palmitoylation.

Chapter 4:

PHENOTYPIC ANALYSIS IN *C. ELEGANS*

4.1 INTRODUCTION

4.1.1 PROBING GENE FUNCTION IN *C. ELEGANS*

4.1.1.1 MUTATIONS

The nematode worm *Caenorhabditis elegans* is a useful experimental tool for probing functions of genes in well conserved processes using simple assays. There are a variety of mutagenesis methods which can be used on *C. elegans*, traditionally including treatment with chemical agents such as trimethylpsoralen (TMP) and ethyl methane sulphonate (EMS) (Barstead and Moerman, 2006; Gengyo-Ando and Mitani, 2000), using electromagnetic spectrum radiation such as ultraviolet (UV) light and X-rays (Gengyo-Ando and Mitani, 2000; Sigurdson *et al.*, 1984), and more recently using more precise transposon based approaches (Bessereau *et al.*, 2001). As most existing strains were made using random mutagenesis, there is a chance that mutations exist in genes other than the gene of interest which could contribute to any phenotypes observed. This can be counteracted by outcrossing a mutant strain to wild-type N2 males several times, or alternatively several strains containing different alleles disrupting the same gene can be compared for common phenotypes.

4.1.1.2 RNAI

An alternative to creating mutant strains is to knock down expression from specific genes using RNA interference (RNAi). In most *C. elegans* tissues, double stranded RNA (dsRNA) molecules are taken up into cells where they are processed into primary small interfering RNA (siRNA) molecules of about 22 nucleotides. This is mediated by the RNase III enzyme dicer related 1 (DCR-1), which cleaves long dsRNA molecules sequentially, working along their length (Fischer, 2010). The target messenger RNA (mRNA) of the siRNA fragments acts as a template for amplification. This process, called transitive RNAi, is mediated by enhancer of abnormal germline proliferation one (EGO-1) in the germline (Smardon *et al.*, 2000) and by RNA-dependent RNA polymerase family 1 (RRF-1) in somatic cells (Sijen *et al.*, 2001). The helicase dicer related helicase 3 (DRH-3) is required for the production of secondary siRNAs. Most RNAi then occurs in the cytoplasm, where the RNA-induced silencing complex (RISC) mediates degradation of the target mRNA (Fischer, 2010). There is also an element of nuclear RNAi in *C. elegans*, where degradation of pre-mRNAs is mediated by nuclear RNAi defective 3 (NRDE-3) (Guang *et al.*, 2008).

RNAi was initially performed by injecting dsRNA into the animals (Fire *et al.*, 1998), although the observation of the spread of RNAi effects to most tissues led to simpler and

more cost-effective protocols based on soaking animals in dsRNA solutions (Tabara *et al.*, 1998) or feeding animals with bacteria expressing dsRNAs (Kamath *et al.*, 2001; Timmons and Fire, 1998). Despite the effectiveness of RNAi in many tissues, *C. elegans* neurons in particular are refractory to its effects (Fire *et al.*, 1998). The sensitivity of different types of neurons has been dissected, with γ-amino butyric acid (GABA)-ergic and some dopaminergic neurons particularly resistant and cholinergic, glutamatergic, touch sensitive and the remaining dopaminergic neurons less so (Asikainen *et al.*, 2005). These effects were seen with injection, soaking and feeding methods of dsRNA administration. Several strains have been produced which partially overcome this to provide a degree of knockdown in neurons. A strain deficient for *rrf-3*, which suppresses amplification of secondary siRNAs, shows a general increase in sensitivity to RNAi, including in neurons (Simmer *et al.*, 2002). The *rrf-3* mutant strain had complete sensitivity to RNAi in all neuronal types except dopaminergic neurons, which still had a marked improvement in sensitivity (Asikainen *et al.*, 2005). A deficiency in the exonuclease enhanced RNAi 1 (*eri-1*) also gives an organism-wide increase in RNAi sensitivity (Kennedy *et al.*, 2004). The systemic RNAi defective 1 (SID-1) protein was found to be responsible for passive uptake of dsRNA molecules into cells (Winston *et al.*, 2002). It has recently been shown to enhance the effects of feeding RNAi in neurons alone by its specific expression under a pan-neuronal promoter (Calixto *et al.*, 2010). A similar strategy which involves expressing the dsRNAs against the gene of interest under control of a promoter specific to the cell type of interest has also been used, although this requires injection of the construct (Esposito *et al.*, 2007).

4.1.2 KNOWN PHENOTYPES

The only member of the DHHC family of enzymes which has been studied in *C. elegans* is SPE-10. The *spe-10* gene was named after a spermatogenesis defect (Spe) which was first described in detail in this context before the DHHC-cysteine-rich domain (CRD) containing protein family was identified (Shakes and Ward, 1989). In wild-type spermatogenesis, primary spermatocytes exist in a syncitium associated with a common cytoplasmic core called the rachis. During spermatocyte maturation, fibrous bodies (FBs) made of major sperm protein (MSP) mature within membranous organelles (MOs). Mature primary spermatocytes bud off and undergo two rounds of meiosis to produce four spermatids and a residual body. The FBs disperse into the cytoplasm and the MOs move adjacent to the plasma membrane (PM). As each spermatid differentiates into a spermatozoon, the MOs fuse with the PM and secrete their contents, leaving a permanent fusion pore. In *spe-10* mutants, FB-MO complexes tend to break down before the spermatids have budded from

the rachis, resulting in FBs which do not disperse in the residual body and instead sometimes bud off as cytoplasts (Shakes and Ward, 1989). The MOs tend to become large and vacuolated, which is visible under Nomarski optics as a cratered appearance in spermatids which budded from residual bodies containing FB defects. These spermatids also have an off-centre nucleus, are smaller in size and resulting spermatozoa do not show the characteristic crawling motion of wild-type spermatozoa (Shakes and Ward, 1989). A later study found that *spe-10* is only expressed in animals undergoing spermatogenesis and most, but not all, SPE-10 protein immunofluorescence staining co-localises with an FB-MO marker (Gleason *et al.*, 2006). This study makes reference to another *C. elegans* DHHC-CRD containing protein, SPE-21, which also shows a spermatogenesis defect. However, no trace of the *spe-21* gene can be found on WormBase (http://www.wormbase.org/) or in any published literature, so it is unknown whether this gene corresponds to any of the *C. elegans* DHHC-CRD family members identified in Chapter 3. The final study to examine *spe-10* mutant strains looked at stress resistance (Cypser and Johnson, 1999). They found an increase in lifespan in some, though not all, experiments and increased resistance to UV exposure and high temperature (35 °C) but not paraquat, a reactive oxygen species (ROS) generator.

An initial characterisation of the *C. elegans* palmitoyl-protein thioesterase 1 (PPT-1) protein was performed with a view to gaining insight into the inherited disease infantile neuronal ceroid lipofuscinosis (INCL), also known as Haltia-Santavuori disease (Porter *et al.*, 2005), which is caused by mutations in the human PPT1 gene (Vesa *et al.*, 1995). An adapted assay for human PPT1 activity showed *C. elegans* PPT-1 can act on the same substrate, and that the mutant strains MN1 and VC184 had tenfold lower activity. A number of mild phenotypes were catalogued in this study. There was a three hour delay in the developmental moult from the final larval stage, L4, into adults. Onset of egg-laying was also delayed by four hours and continued two days after wild-type animals had stopped laying, although the total brood size was unchanged. This coincided with an increased frequency of bagging, whereby eggs hatch inside the parent animal. There was no difference in lifespan and there was a lack of accumulation of autofluorescent material which is seen in the human disease. Electron microscopy (EM) showed defects in mitochondria in energetically active tissues, including neurons. There were higher numbers of smaller mitochondria resulting in a decrease in mitochondrial area in cross-sections and their morphology was altered. Instead of an inner membrane folded into cristae, the inner membrane formed whorls in one-day-old adults. Fewer whorls were observed in

six-day-old adults although there was evidence of autophagy and lysosomal degeneration. Despite these changes, these mutants were observed to have a much milder phenotype when compared with the severe deficits in human INCL (Porter *et al.*, 2005).

4.1.3 PREDICTIONS FROM *IN SILICO* ANALYSIS

This chapter will give an initial phenotypic analysis of *C. elegans* strains in which DHHC or PPT family genes have either been mutated or had their expression reduced with the aim of characterising processes in which they may be involved. By relating any phenotypes which are uncovered back to the *in silico* analyses in Chapter 3, it is hoped *C. elegans* will be validated as a model in which palmitoylation can be studied in more depth with relation to specific enzymes. In turn the *in silico* analyses can also be used to provide predictions which can be tested using phenotypic assays. For example the lack of fusion of MOs in *spe-10* spermatogenesis described above (Shakes and Ward, 1989) could result from altered palmitoylation of proteins which are important in fusion. The most closely related enzymes in other organisms are protein fatty acyltransferase 3 (Pfa3) in *Saccharomyces cerevisiae* and DHHC2/reduced expression associated with metastasis (REAM) in *Homo sapiens* (Table 3.6). Pfa3 is one of the palmitoyl acyl-transferases (PATs) responsible for palmitoylating the vacuolar fusion protein Vac8 and DHHC2/REAM palmitoylates the membrane fusion proteins synaptosomal-associated protein of 23 kDa (SNAP-23) and SNAP-25 (Table 3.7). In addition, Pfa3 resides on the vacuole (Table 3.3). SPE-10 was shown to reside on MO membranes (Gleason *et al.*, 2006), so may palmitoylate fusion proteins present there, leading to fusion of the MO with the PM. The *S. cerevisiae* DHHC spore wall formation 1 (Swf1) is responsible for palmitoylating many proteins involved in membrane fusion. Similarly, the mammalian DHHC17/Huntingtin-interacting protein 14 (HIP14) palmitoylates many proteins involved in synaptic fusion and postsynaptic receptors which have orthologues in *C. elegans* (Table 3.7, Table 3.9). Both Swf1 and DHHC17/HIP14 are the orthologues of *C. elegans* DHHC-14 in their respective species, so disruption of *dhhc-14* may give phenotypes which result from abnormal membrane fusion, such as uncoordinated (Unc) phenotypes or maybe phenotypes derived from malfunction of subsets of neurons, such as mechanosensation (Mec) phenotypes. However, this approach is limited by the information available in other organisms. For example, *C. elegans* DHHC-1 is most closely related to *S. cerevisiae* Pfa3, whose only known substrate is Vac8, *Drosophila melanogaster* CG10344 and *H. sapiens* DHHC24, neither of which have any known substrates (Table 3.6, Table 3.7). This chapter aims to help elucidate some of the possible

pathways regulated by each enzyme by performing behavioural assays and lifespan analysis on available mutant strains and complement these findings using an RNAi approach.

4.2 METHODS

4.2.1 NEMATODE HUSBANDRY

4.2.1.1 STRAINS

All *C. elegans* strains were obtained from the *Caenorhabditis* Genetics Center (CGC; University of Minnesota, Twin Cities, MN, USA) except tm4272, which was obtained from the National Bioresource Project for the Experimental Animal "Nematode *C. elegans*" based in the lab of Dr Shohei Mitani (Tokyo Women's Medical University, Tokyo, Japan).

The Vidal *C. elegans* Open Reading Frame (ORF) RNAi feeding library was obtained from Source Bioscience (Nottingham, UK) (Rual *et al.*, 2004).

4.2.1.2 CULTURE

C. elegans were cultured in 60 mm plates on nematode growth medium agar (NGM; 2% (w/v) agar, 0.3% (w/v) NaCl, 0.25% (w/v) peptone, 1 mM $CaCl_2$, 5 µg ml^{-1} cholesterol, 25 mM KH_2PO_4, 1 mM $MgSO_4$) at 20 °C, seeded with 30 µl *E. coli* OP50 culture (CGC) as a food source, using standard methods (Brenner, 1974).

4.2.2 RNAI

4.2.2.1 FEEDING RNAI

The procedure for conducting feeding RNAi in *C. elegans* is summarised in Figure 4.1. RNAi feeding experiments were conducted using bacteria from the Vidal *C. elegans* ORF RNAi Library (Rual *et al.*, 2004) where available, or were cloned in-house. All RNAi feeding bacteria were *E. coli* strain HT115, which lacks the dsRNA-specific RNase III but contains an isopropyl β-D-1-thiogalactopyranoside (IPTG)-inducible T7 RNA polymerase (Timmons *et al.*, 2001), carrying the pG-L4440 vector containing the relevant insert. The negative control for most experiments was feeding of HT115 carrying the pG-L4440 vector without an insert (L4440). *hsp-1* was used as a positive control, as it gives a sterile phenotype (Simmer *et al.*, 2003).

10 cm plates of Luria-Bertani (LB) agar (1% tryptone, 0.5% yeast extract, 1% NaCl, 1.5% agar) with 100 µg ml^{-1} ampicillin were poured. Bacterial strains were streaked on separate plates and incubated overnight at 37 °C. Two discrete colonies from each plate were each grown in 3 ml LB containing 100 µg ml^{-1} ampicillin overnight at 37 °C, 220 rpm. DNA was

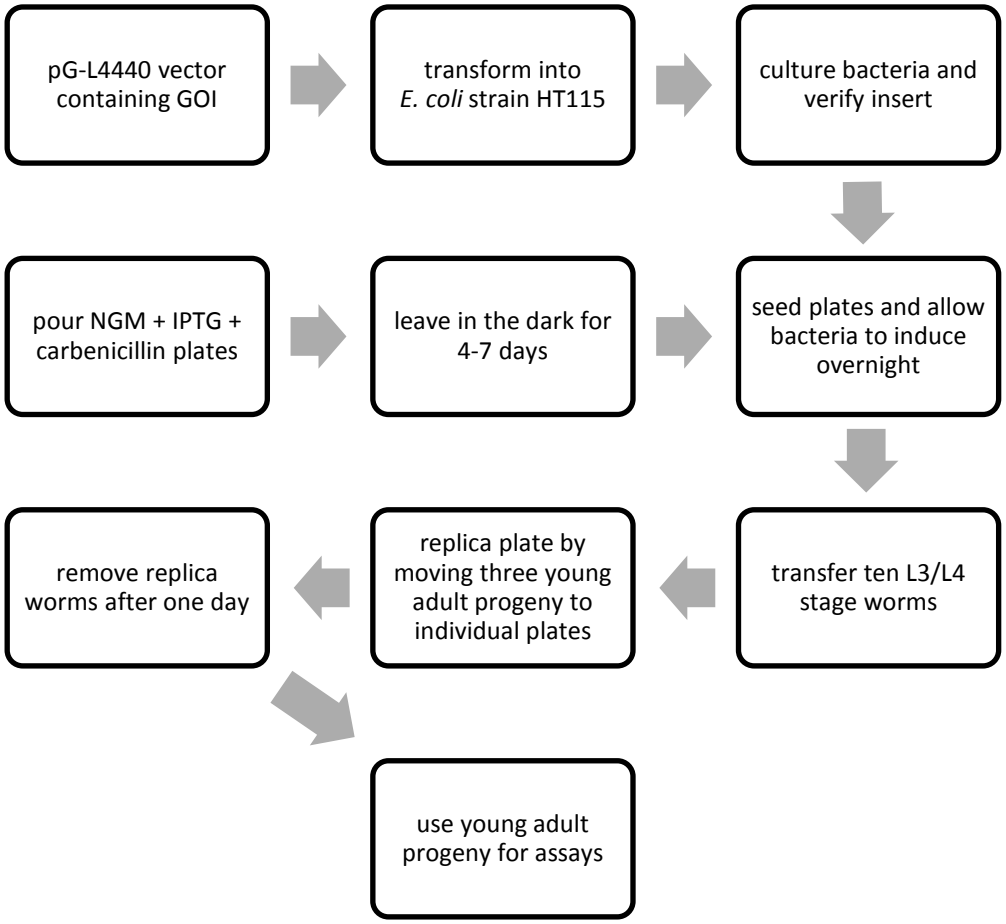

FIGURE 4.1: Schematic of feeding RNAi in *C. elegans*

A flow diagram showing the procedure for the feeding RNAi screen. GOI, gene of interest; IPTG isopropyl β-D-1-thiogalactopyranoside; NGM, nematode growth medium.

isolated using a miniprep kit and the correct insert verified by restriction endonuclease digest or by sequencing if necessary.

For RNAi, plates of NGM containing 25 µg ml^{-1} carbenicillin and 1 mM IPTG were poured 4-7 days before seeding with 50 µl of the relevant bacterial strain. RNAi plates were always kept in the dark, as IPTG is light sensitive. The dsRNA was induced overnight before ten L3-L4 stage worms were transferred to each plate. Once the next generation of worms had reached young adult stage, three adults were moved onto individual replica plates, allowed to lay eggs and removed the following day. These progeny were used in the assays once they had reached adulthood.

4.2.2.2 CONFIRMATION OF RNAI LIBRARY STRAINS

4.2.2.2.1 DNA PURIFICATION

E. coli containing the relevant plasmid were streaked onto LB agar plates containing a selection antibiotic and cultured overnight at 37 °C. Two discrete colonies were cultured in 5 ml LB each containing a selection antibiotic at 37 °C, 250 rpm overnight. 2 ml of culture was pelleted in an Eppendorf tube in a microcentrifuge at 14000 rpm for one minute. The supernatant was discarded and the DNA extracted from the bacterial pellet using a GenElute™ HP Plasmid Miniprep Kit following the manufacturer's guidelines.

4.2.2.2.2 RESTRICTION ENDONUCLEASE DIGESTION

Restriction digests were used to confirm the identity of purified DNA. 5 µl miniprep DNA was added to 0.5 µl restriction enzyme and 1X reaction buffer in 20 µl total reaction volume. The reaction was incubated at 37 °C for at least one hour. The resulting fragments were combined with 6X DNA loading buffer (0.35% (w/v) orange G, 0.1% (w/v) bromophenol blue, 30% (w/v) sucrose) and separated by gel electrophoresis using a 0.8% (w/v) agarose gel containing SYBR® Safe DNA Gel Stain (Life Technologies). Electrophoresis was carried out in Tris-acetate-EDTA buffer (40 mM Tris, 20 mM acetic acid, 1mM EDTA) at 90 V for 45-60 minutes. 10 µl HighRanger Plus 100bp DNA ladder (Norgen Biotech) was run alongside the samples as a size reference. Gels were visualised under UV light in a ChemiDoc XRS (BioRad, Hemel Hempstead, UK) with Quantity One software (BioRad; v4.6.3).

4.2.2.2.3 DNA SEQUENCING

If there was ambiguity in restriction digest results, purified DNA was sent for sequencing by DNA Sequencing & Services at the University of Dundee, UK. Two tubes were sent containing 5 µl template miniprep DNA. The first contained 0.2 µM pL4440 Seq Rev primer

and was made up to 32 µl total volume. The second was made up to 30 µl for the M13 For primer to be added by the company. The results were analysed using VectorNTI (Invitrogen; v11.0) or BioEdit software and basic local alignment search tool (BLAST) searches.

4.2.2.3 GATEWAY™ CLONING

4.2.2.3.1 POLYMERASE CHAIN REACTION

To form a complete library of RNAi feeding bacteria clones for the DHHCs, some vectors needed to be cloned. cDNA was first synthesised. 2 µg total RNA from wild-type worms extracted using an Absolutely RNA Microprep Kit (Agilent) was made up to 16.45 µl with diethylpyrocarbonate-treated (DEPC)-H_2O. 0.8 µl 50 µM oligo(dT) primer was added and incubated at 70 °C for ten minutes, then on ice for two minutes. 5 µl Bioscript reaction buffer, 1.25 µl 10 mM dNTPs, 0.5 µl RNase OUT and 1 µl BioScript (Bioline) were added and reverse transcription performed under the following conditions: 25 °C (10 minutes), 42 °C (60 minutes), 90 °C (2 minutes). 75 µl DEPC-H_2O was added to the products and stored at -20 °C.

Reverse transcriptase PCR (RT-PCR) was performed using custom-designed primers, listed in Table 4.1. 5 µl cDNA, 2 µl 10 µM forward primer, 2 µl 10 µM reverse primer, 1 µl 10 mM dNTPs, 10 µl 5X high fidelity (HF) or GC-rich-optimised (GC) buffer and 0.5 µl Phusion DNA polymerase were made up to a total reaction volume of 50 µl with DEPC-H_2O. The PCR conditions were as follows: 98 °C (2 minutes); 30-35 cycles of 98 °C (15 s), 60 or 62 °C (30 s), 72 °C (15-30 s); 72 °C (5 minutes); 4 °C store.

4.2.2.3.2 BP REACTION

This reaction was performed to transfer the required attB-flanked DNA sequence into an attP-containing vector. 7 µl PCR product, 1 µl pDONR201 (150 ng μl^{-1}) and 2 µl BP clonase™ II were mixed and incubated at 25 °C for at least one hour. 1 µl proteinase K was added and incubated at 37 °C for ten minutes to digest the BP clonase enzyme. Successful incorporation into the vector was verified by transforming into DH5α cells, miniprepping and performing test digests.

4.2.2.3.3 LR REACTION

This reaction was performed to transfer the required attL-flanked DNA into an attR-containing vector, in this case pG-L4440. 3 µl entry vector miniprep, 3 µl pG-L4440 and 2 µl LR clonase™ II was made up to 10 µl and incubated at 25 °C overnight. 1 µl proteinase K was added and incubated at 37 °C for ten minutes. Successful incorporation into the

Primer name	Primer sequence
dhhc-3 Fwd	5′-***GGGGACAAGTTTGTACAAAAAAGCAGGCT***TGGTCACTTGGTTGCTGGTATC-3′
dhhc-3 Rev	5′-***GGGGACCACTTTGTACAAGAAAGCTGGG***CAAACAGAATACTCGAAAGTTGGTCTC-3′
dhhc-4 Fwd	5′-***GGGGACAAGTTTGTACAAAAAAGCAGGCT***TGTCTTGTCGGGATTGCACAAG-3′
dhhc-4 Rev	5′-***GGGGACCACTTTGTACAAGAAAGCTGGG***TTACGCCGTCACCGAGTCATGTC-3′
dhhc-6 Fwd	5′-***GGGGACAAGTTTGTACAAAAAAGCAGGCT***GGATTGGCCTGCTCCAATTGC-3′
dhhc-6 Rev	5′-***GGGGACCACTTTGTACAAGAAAGCTGGG***TCTTCAGTAGTAGCCGTATCCTGGG-3′
dhhc-8 Fwd	5′-***GGGGACAAGTTTGTACAAAAAAGCAGGCT***GTGTAAACGGATATCAGCATTATTGCC-3′
dhhc-8 Rev	5′-***GGGGACCACTTTGTACAAGAAAGCTGGG***TGCGGAAGGTGCTGTAAGATAG-3′
dhhc-13 Fwd	5′-***GGGGACAAGTTTGTACAAAAAAGCAGGCT***GATGGCTGCTGATAAGAGTTTCGC-3′
dhhc-13 Rev	5′-***GGGGACCACTTTGTACAAGAAAGCTGGG***TATCTCGATGGTAGAGACATGACGAG-3′
dhhc-14 Fwd	5′-***GGGGACAAGTTTGTACAAAAAAGCAGGCT***AACCTTATTGGTGGCGTCTTGG-3′
dhhc-14 Rev	5′-***GGGGACCACTTTGTACAAGAAAGCTGGG***TCGCATAATGACTTGTAGCCATGCAG-3′
spe-10 Fwd	5′-***GGGGACAAGTTTGTACAAAAAAGCAGGCT***CGTTCAGTCAACAATTCAAGCAACC-3′
spe-10 Rev	5′-***GGGGACCACTTTGTACAAGAAAGCTGGG***TCGAACAGCACCTTCTAGTGAAGTG-3′

TABLE 4.1: Primers used to clone RNAi vectors

The sequences of the oligonucleotides used for cloning RNAi vectors not already available are shown. The attB sites are shown in bold italic and the annealing sequences in normal type.

pG-L4440 vector was verified by transforming into DH5α cells, miniprepping and performing test digests. The vectors were then transformed into HT115 cells for consistency with the Vidal RNAi library.

4.2.2.3.4 TRANSFORMATION OF CHEMICALLY COMPETENT *E. COLI*

For DH5α cells, an aliquot was thawed on ice. 50 µl cells was mixed with 3 µl DNA from the BP or LR reaction in pre-chilled Eppendorf tubes and incubated on ice for 30 minutes, heat shocked at 42 °C for 45 s and put back on ice for two minutes. 450 µl super optimal broth with catabolite repression (SOC) was added and incubated at 37 °C, 220 rpm for one hour. 100 µl was spread on LB agar plates containing an appropriate selection antibiotic and cultured overnight at 37 °C. Discrete colonies were grown in LB with the antibiotic at 37 °C, 250 rpm overnight.

For HT115 strain, some colonies were added to 100 µl 100 mM $CaCl_2$, mixed to homogeneity and left on ice. 5 µl DNA was added and incubated on ice for 30 minutes, heat shocked at 42 °C for 45 s and put back on ice for two minutes. 400 µl SOC was added and incubated at 37 °C, 220 rpm for one hour. The cells were pelleted at 3000 rpm for one minute. Most of the supernatant was discarded and the cells resuspended in a small volume before plating onto LB agar plates containing a selection antibiotic and culturing overnight at 37 °C. Discrete colonies were grown in LB with the antibiotic at 37 °C, 250 rpm overnight.

4.2.2.4 CLONING OF *PPT-1*/*ATH-1* DOUBLE RNAI VECTOR

An RNAi vector containing sequences for both *ppt-1* and *ath-1* was cloned. Vectors containing *ppt-1* and *ath-1* individually were purified from overnight bacterial cultures. 20 µl DNA was digested in a reaction volume of 25 µl. pG-L4440-*ppt-1* was linearised using Acc65I. pG-L4440-*ath-1* was digested with BsrGI to obtain the *ath-1* sequence but retaining complementary 5' overhangs to enable its ligation into the pG-L4440-*ppt-1* vector. Both digestions were incubated at 37 °C overnight to ensure complete digestion. 5'-phosphates were removed from linearised pG-L4440-*ppt-1* by incubating with 2 µl SAP for 15 minutes at 37 °C. The products were subjected to gel electrophoresis and the only pG-L4440-*ppt-1* band and the approximately 700 bp *ath-1* band were excised and purified into 50 µl using a GenElute™ Gel Extraction Kit. The following ligation reactions were set up: 1 µl, 0.5 µl or no pG-L4440-*ppt-1* was added to 3 µl *ath-1*, 2 µl 5X T4 ligase buffer and 1 µl T4 DNA ligase, made up to 10 µl reaction volume and incubated at room temperature for one hour. The

DNA was transformed into DH5α cells and verified by test digest before transforming into HT115 cells.

4.2.3 ASSAYS

4.2.3.1 MORPHOLOGY

Individual worms were placed on a freshly seeded plate and allowed to acclimatise for ten minutes. Plates were placed on a microscope stage controlled by computer through an Optiscan II box (Prior) and adjusted so the worm was in the centre of the image on screen transmitted by a DinoEye Eyepiece Camera (ANMO Electronics Corporation). WormTracker software (http://www.mrc-lmb.cam.ac.uk/wormtracker/; v2.0.3.1) was used to track the worms and collect data over a two minute period. Data were analysed in Worm Analysis Toolbox software (v1.9) and Microsoft® Office Excel® 2007. The morphological parameters are calculated for each frame of the video and any obvious outliers resulting from mis-assignment of the skeleton to the image were removed. The mean values from all frames in the video of each worm were used.

4.2.3.2 LIFESPAN

To synchronise a worm strain, a relatively full plate of gravid adults was washed with 3.5 ml sterile H_2O and collected in a 15 ml Falcon tube. 1.5 ml bleach mixture (two parts commercial bleach to one part 5 M NaOH) was added and the tube vortexed well every two minutes for a total of 10 minutes. The tubes were centrifuged at 1500 rpm for one minute and the supernatant removed. 5 ml sterile H_2O was added and the tubes vortexed before centrifuging again. The supernatant was removed and the pellet of eggs was transferred to the edge of a seeded plate. These worms were picked onto lifespan plates once they reached adulthood, defined as day 0.

For lifespan analysis of mutants, strains of interest were compared with the wild-type N2 strain. NGM agar plates were prepared containing 50 µM fluorodeoxyuridine (FUdR) to prevent development of any eggs laid. Plates were seeded with 50 µl OP50. The number of live and dead worms on these plates was counted every couple of days, and plates were re-seeded or worms transferred to a fresh FUdR plate if necessary.

For RNAi lifespan studies, worms were already synchronised as a result of the replica plating procedure. Once they reached adulthood, these worms were transferred to lifespan plates seeded with RNAi bacteria but containing no FUdR. All worms were only fed their relevant RNAi bacterial strain throughout the assay, and transferred to fresh plates if necessary. All plates were seeded with 50 µl bacteria.

4.2.3.3 LOCOMOTION

4.2.3.3.1 SOLID MEDIA

Worms were synchronised by allowing a gravid adult to lay eggs on a plate overnight before its removal. Worms were assayed once the progeny reached young adult age. Individual worms were transferred to an unseeded or freshly seeded plate and allowed to acclimatise for five minutes. The number of body bends (complete movement of the head from one side to the other and back again) was observed over a period of two minutes (Miller *et al.*, 1999).

4.2.3.3.2 LIQUID MEDIA

To assess locomotory ability in solution, young adult worms were subjected to thrashing assays (Johnson *et al.*, 2009). 100 µl drops of Dent's Ringer solution (DRS; 10 mM D-glucose, 10 mM HEPES, 140 mM NaCl, 6 mM KCl, 3 mM $CaCl_2$, 1 mM $MgCl_2$, pH 7.4) containing 0.1% (w/v) bovine serum albumin (BSA) were put in each well of a 96-well plate. One worm was picked into each well and allowed to equilibrate for at least 5 minutes. The number of thrashes (complete movement of the head from one side to the other and back again) in one minute was recorded.

For age-dependent locomotion, mutants were synchronised as for lifespan experiments. At day 0 of adulthood, 50 worms of each strain were picked onto an FUdR plate. Every couple of days, ten worms of each strain were subjected to thrashing assays in 30 µl drops of DRS on a dish, then returned to their plate. This was continued until a strain had essentially no movement. Plates were re-seeded and worms transferred to a fresh FUdR plate if necessary.

4.2.3.4 MECHANOSENSATION

This method is based on that in (Chalfie and Sulston, 1981). The root end of an eyebrow hair was glued to the end of a toothpick, leaving the tapered end free. Before each assay, this was sterilised by dipping in 70% ethanol and allowed to air dry. The worm to be assayed was transferred to an unseeded plate and allowed five minutes to acclimatise. Anterior touch response was tested by gently stroking the eyebrow hair behind the pharynx, and posterior touch response by stroking just forward of the anus. A positive response was defined as stopping movement in the direction of the touch or reversal of direction of movement, or for posterior touch suddenly quicker forward movement.

4.2.4 STATISTICAL ANALYSIS

All statistical analyses (with the exception of lifespan and age-dependent locomotion) and all graphs were produced using SigmaPlot (Systat Softare, Inc.; v.12.2.0.45). If two data sets were being directly compared, Student's *t*-test was used. For comparison of multiple data sets in one analysis, a one-way analysis of variance (ANOVA) was used.

Lifespan analyses were performed using the Online Application for the Survival Analysis of Lifespan Assays (OASIS; http://sbi.postech.ac.kr/oasis/introduction/) (Yang *et al.*, 2011). Mean lifespans were compared using the log-rank (Mantel-Cox) test, and mortality at more specific time points was compared using Fisher's exact test. Age-dependent thrashing was compared using one-way analysis of covariance (ANCOVA) in Microsoft Office® Excel® 2007.

4.3 RESULTS

4.3.1 PREPARATORY WORK

4.3.1.1 MUTANT STRAINS

Before screens could be conducted for phenotypes associated with DHHC or PPT enzymes, certain preparatory work was necessary. WormBase was used to find which genes had existing strains available containing a mutation only in that gene (Table 4.2). These strains were obtained from the *Caenorhabditis* Genetics Center (CGC; http://www.cbs.umn.edu/cgc). Mutant strains for the remaining genes in the family were requested from the *C. elegans* Knockout Consortium (http://celeganskoconsortium.omrf.org/) in October 2009 but are still pending.

Further information on the strains used in this study can be found in Table 4.3. The only available strain which was not obtained was the *ppt-1* mutant VC183. This strain carries the allele *gk139*, but has not been outcrossed. Outcrossing is a process of mating a strain with wild-type animals in order to reduce any background mutations which have occurred due to the mutagenic approach in creating strains. The MN1 strain was created by taking the VC183 strain and outcrossing it four times (Porter *et al.*, 2005). It is the MN1 strain which was the subject of published studies, where it was confirmed by Northern analysis to be a null allele (Porter *et al.*, 2005). The only other strain which has been outcrossed is the *dhhc-12* mutant VC2244. The vast majority of the strains are deletion mutants, some of which also contain insertions. The *spe-10* mutant BA744 only carries a point mutation but this does cause a premature stop codon well before the DHHC motif, so shouldn't produce an active enzyme. This is the strain that has been used in previous studies and has shown

Gene	Available Mutant(s)	RNAi Clone Source
ath-1	RB1484	Vidal library
dhhc-1	tm4272	Vidal library
dhhc-2	RB1044	Vidal library
dhhc-3		in-house
dhhc-4		in-house
dhhc-5		Vidal library
dhhc-6		in-house
dhhc-7		Vidal library
dhhc-8		in-house
dhhc-9	VC2067	Vidal library
dhhc-10		Vidal library
dhhc-11		none
dhhc-12	VC2039, VC2244	Vidal library
dhhc-13	VC108	in-house
dhhc-14	VC771, VC918	in-house
ppt-1	MN1, VC166, VC168, VC183, VC184	Vidal library
spe-10	BA744	in-house

TABLE 4.2: *C. elegans* strain and RNAi clone availability

The DHHC and PPT genes in *C. elegans* are listed. If a *C. elegans* strain containing a mutation in the gene-of-interest only is available, it is shown here. More detailed information on the strains used in this study can be found in Table 4.3 and Appendix 1. RNAi clones were either obtained from the Vidal *C. elegans* ORF RNAi Library (Rual *et al.*, 2004) or made in-house. *ath*, acyl-protein thioesterase; *ppt*, palmitoyl-protein thioesterase; *spe*, spermatogenesis-deficient.

Strain	Gene	Allele	Mutation	Outcrossed?	Phenotypes
BA744	*spe-10*	*hc104*	point mutation	unclear	defective spermatogenesis; stress resistance
MN1	*ppt-1*	*gk139*	deletion	x4	delay in L4/adult transition; abnormal mitochondrial morphology
RB1044	*dhhc-2*	*ok990*	deletion	no	
RB1484	*ath-1*	*ok1735*	insertion/deletion	no	
RM2754	*dnj-14*	*ok237*	deletion	no	
tm4272	*dhhc-1*	*tm4272*	deletion	no	
VC108	*dhhc-13*	*gk36*	deletion	no	
VC166	*ppt-1*	*gk131*	insertion/deletion	no	
VC168	*ppt-1*	*gk134*	deletion	no	
VC184	*ppt-1*	*gk140*	insertion/deletion	no	
VC771	*dhhc-14*	*gk330*	deletion	no	
VC918	*dhhc-14*	*ok1032*	insertion/deletion	no	
VC2039	*dhhc-12*	*gk1013*	insertion/deletion	no	
VC2067	*dhhc-9*	*gk985*	deletion	no	
VC2244	*dhhc-12*	*gk981*	deletion	x1	

TABLE 4.3: Information about *C. elegans* strains used in this study

Strain information was collated from WormBase (http://www.wormbase.org/). Detailed information on the nature of each mutation may be found in Appendix 1. *dnj*, DnaJ domain-containing protein.

spermatogenesis and stress resistance phenotypes (Cypser and Johnson, 1999; Gleason *et al.*, 2006; Shakes and Ward, 1989). It is unclear whether the strain obtained from the CGC has been outcrossed; the listings on WormBase and the CGC website say "outcrossed: x" and the first study to use it outcrossed four times after obtaining it (Shakes and Ward, 1989). Another study found an increase in survival persisted over a further two outcrosses (Cypser and Johnson, 1999), suggesting phenotypes found with the BA744 strain are due to the mutation in *spe-10*. The majority of the strains in Table 4.3 have no observed phenotypes.

4.3.1.2 RNAi

4.3.1.2.1 Bacterial clones

An alternative to using mutant strains is to knock down expression of proteins through RNAi. This may be achieved simply in *C. elegans* by culturing the animals on plates seeded with bacteria expressing dsRNA against the gene of interest (Fire *et al.*, 1998; Kamath *et al.*, 2001; Timmons and Fire, 1998). Our laboratory has the Vidal *C. elegans* ORF RNAi Library of bacterial RNAi feeding strains (Rual *et al.*, 2004), which covers approximately 55% of *C. elegans* protein-coding genes. A search of the database revealed that ten of the 15 DHHCs and both PPTs are present. Restriction analysis and DNA sequencing showed that the strain labelled for *dhhc-6* contained a different gene and *dhhc-14* actually contained no insert in the vector. Sequencing showed some other vectors contained the correct gene but with truncations which accounted for fragments which were a different size from what was expected in restriction analysis. *dhhc-2* contained the sequence from 242 base pairs (b.p.) onwards with a G975A point mutation; *dhhc-7* contained the sequence from isoform b, which is a truncated version of isoform a; *dhhc-12* contained the sequence from 215 b.p. onwards. As *C. elegans* lacks the interferon response to long dsRNAs which exists in mammals (Fischer, 2010), the minimum sequence length consistently shown to give effective knockdown is around 500 b.p. (Hammell and Hannon, 2012; Kamath *et al.*, 2001). These constructs include more than sufficient sequence.

The genes not present in the Vidal library were cloned into the empty vector to give a complete set of RNAi clones for the DHHC and PPT families (Table 4.2). Unfortunately, the clone which was thought to contain *dhhc-11* was found to contain the same strain as an adjacent well in the Vidal library plates. This strain contained ZK858.2 which encodes a protein of unknown function showing homology only with proteins from other nematode species. Due to time constraints, the experiment including this clone had to be performed before the sequencing results were returned and so *dhhc-11* is not present in this screen.

4.3.1.2.2 RNAi-SENSITIVE *C. ELEGANS* STRAINS

Before RNAi experiments were commenced, tests were performed to find the best *C. elegans* strain to use, as some tissues are refractory to RNAi treatment, notably neurons (Timmons *et al.*, 2001). In the first test, a strain lacking *eri-1* (RB2025) and a strain containing yellow fluorescent protein (*yfp*) and *sid-1* genes expressed under the *unc-119* promoter, which drives expression in the nervous system and the lumbar and preanal ganglia (Calixto *et al.*, 2010) were used. *eri-1* encodes an exonuclease with activity against the 3' overhangs of siRNAs, and its knockout causes an organism-wide increase in sensitivity to RNAi (Kennedy *et al.*, 2004). *sid-1* encodes a transmembrane protein which allows passive uptake of dsRNA by cells (Winston *et al.*, 2002). Its artificial expression in neurons has been shown to increase the effectiveness of RNAi in these cells (Calixto *et al.*, 2010). These strains were tested by feeding RNAi against genes which should severely restrict movement when compromised: *unc-18*, the *C. elegans* orthologue of Munc-18, and *unc-64*, the orthologue of syntaxin. TU3311 was additionally tested against *unc-119*, which causes an Unc phenotype including lack of movement on plates and locomotion in thrashing assays limited to ten thrashes per minute (Maduro and Pilgrim, 1995). Thrashing assays were conducted and compared with wild-type N2 animals treated using the same procedure and a control against *gfp* (Figure 4.2A). All animals were slower moving than expected on the control against *gfp* and none of the treatments against *unc* genes showed a reduction from the *gfp* rate.

A number of *sid-1*-expressing strains have been created. Given the absence of any discernible effect with the strains above, a further test was performed using TU3335. This strain has an integrated transgene expressing *sid-1* and *yfp* under the *unc-119* promoter, *mec-6* under its own promoter and the *lin-15b* allele *n744*, which also enhances RNAi sensitivity (Wang *et al.*, 2005). The strain was tested using RNAi against *unc-14*, a neuronal protein required for axonogenesis (McIntire *et al.*, 1992) and which showed a severe Unc phenotype indistinguishable from the loss-of-function phenotype in most animals tested (Calixto *et al.*, 2010). However, when compared with an empty vector control in a thrashing assay there was only a mild, non-significant reduction in locomotion (Figure 4.2B). Given the failure of these supposedly hypersensitive strains to respond to RNAi against genes which should give clear phenotypes, it was decided instead to use the *rrf-3* mutant strain (NL2099) which is hypersensitive to RNAi in all tissues (Simmer *et al.*, 2002) and has been successfully used both in this laboratory and in large scale screens (Lejeune *et al.*, 2012; Simmer *et al.*, 2003).

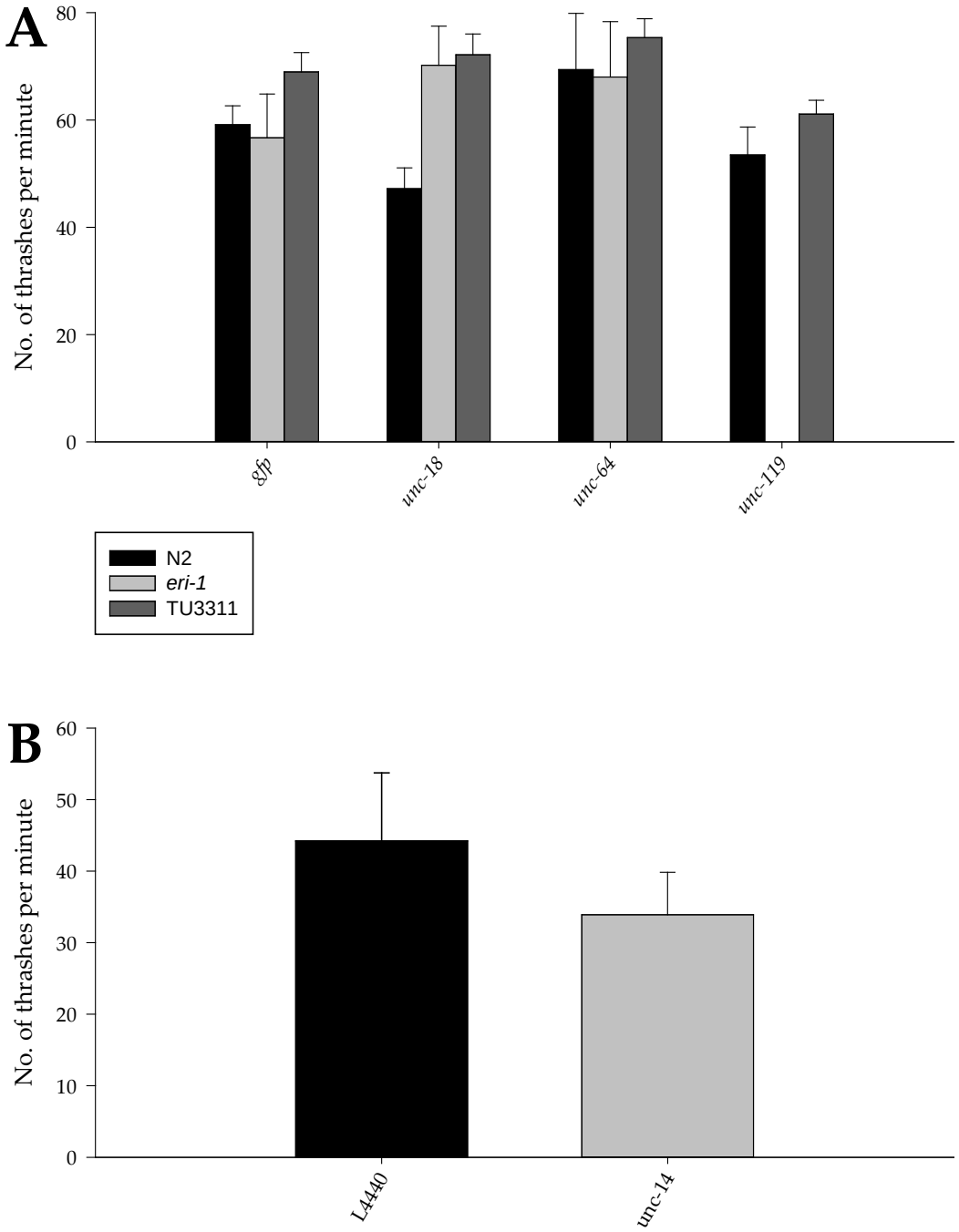

FIGURE 4.2: Locomotion in liquid medium of RNAi-sensitive strains

Thrashing assays were performed on strains treated with RNAi. (A) Strains used were the negative control wild-type N2 and neuronally RNAi-sensitive *eri-1* and TU3311 (*sid-1* overexpressing) strains. RNAi clones were against *gfp* (negative control), the neuronally-expressed gene *unc-18*, and *unc-64* and *unc-119*, both expressed neuronally and elsewhere. *unc-119* was not tested in the *eri-1* strain. *n* = 10-29 over 1-3 experiments. (B) Thrashing assays were performed using the TU3335 strain (*lin-15b* mutant overexpressing *sid-1*). Animals were treated with RNAi against L4440 (control) or *unc-14*, which is required for axonogenesis. *n* = 10 over one experiment. *eri*, enhanced RNAi; *gfp*, green fluorescent protein; *sid*, systemic RNAi defective; *unc*, uncoordinated.

4.3.2 MORPHOLOGY

All strains appeared to have normal morphology, behaviour and fertility during normal culture conditions. To quantify their morphology a few strains were analysed using WormTracker software, which automatically locates an animal on a video feed of a plate, assigns a skeleton of points along the body and uses this to give precise morphological measurements. This is an evolution of previously published methods (Geng *et al.*, 2004). Wild-type N2 animals had an average length of about 1225 µm and width of 83 µm (Figure 4.3). None of the mutant strains tested had a significant difference in length from N2. Mutants for *dhhc-1*, *-2*, *-12* (VC2039) and *-14* (VC918) show a small but significant reduction in width to around 70-75 µm. For RNAi experiments, the *rrf-3* mutant strain was used. When fed the negative control bacteria, which had no insert in the pG-L4440 vector (L4440), *rrf-3* animals were on average about 1450 µm long and 86 µm wide (Figure 4.4). There is no reported figure for the length of *rrf-3* mutants in the literature, although no obvious morphological differences were reported when this strain was first published (Simmer *et al.*, 2002), and on the plates they appear identical to N2 animals by eye. When *rrf-3* animals were treated with RNAi against the same selection of genes as the mutants, no significant differences in length or width were observed.

4.3.3 BEHAVIOUR

4.3.3.1 LOCOMOTION

Locomotion can be assessed in solution (Johnson *et al.*, 2009) or on solid media (Miller *et al.*, 1999). All mutant strains were subjected to thrashing assays in solution along with a strain lacking *dnj-14*, the *C. elegans* orthologue of cysteine string protein (CSP). CSP is the most heavily palmitoylated protein known (Gundersen *et al.*, 1994) and its knockout gives a neurodegenerative phenotype in mice leading to death at about two months of age (Fernandez-Chacon *et al.*, 2004) and a temperature-sensitive reduction in synaptic transmission in *D. melanogaster* leading to paralysis and premature death (Zinsmaier *et al.*, 1994). Mutations in humans lead to the neurodegenerative diseases called neuronal ceroid lipofuscinoses (NCL) (Benitez *et al.*, 2011; Velinov *et al.*, 2012). *dnj-14* mutants have previously been observed in this laboratory to have a slight but significant decrease in thrashing and reduced lifespan (unpublished data). If any mutants showed a similar phenotype to the *dnj-14* strain, the enzyme involved may be responsible for DNJ-14 palmitoylation. In thrashing assays, the *dnj-14* mutants did show a small decrease but it was not significantly different from wild-type N2 animals. One of the *dhhc-12* mutants

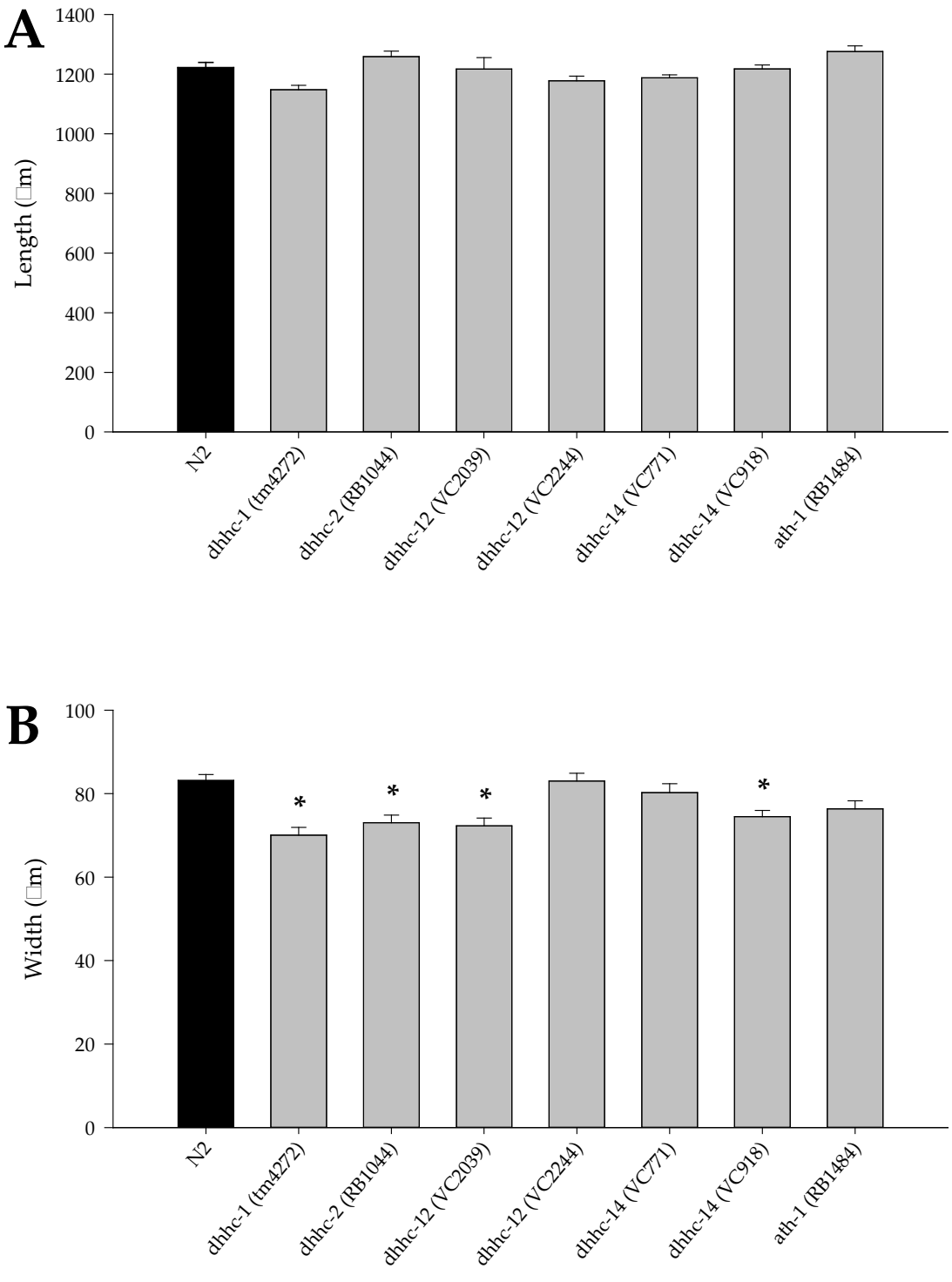

FIGURE 4.3: Morphology of selected mutant strains

Length (A) and width (B) data were collected using WormTracker. *n* = 4-10 animals over one experiment. * $p < 0.05$ by one-way ANOVA. ANOVA, analysis of variance.

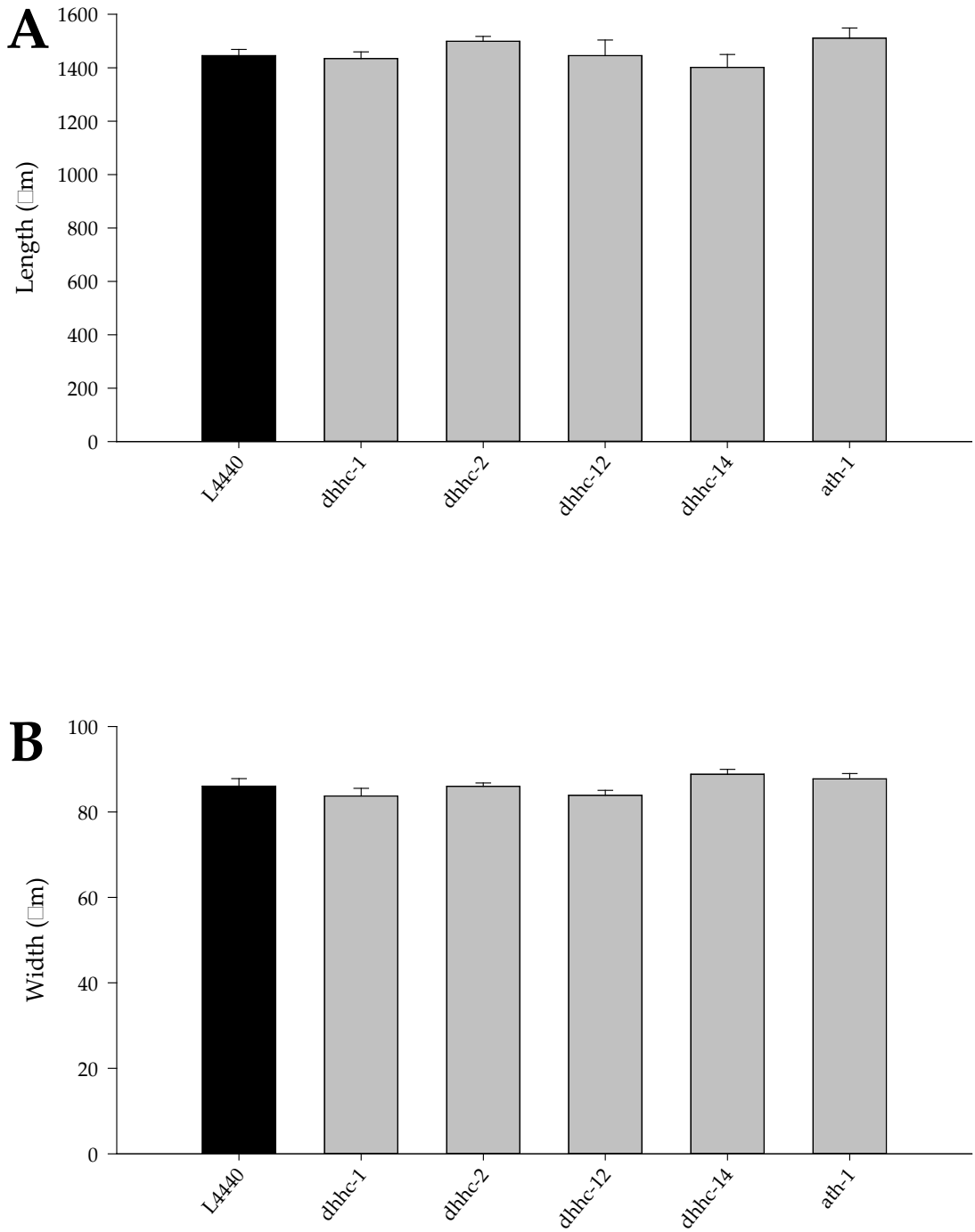

FIGURE 4.4: Morphology of *rrf-3* mutant animals treated with RNAi against selected genes

Length (A) and width (B) data were collected using WormTracker. There were no morphological differences between animals treated with RNAi against the genes shown and the control treatment (L4440). *n* = 4-8 animals over one experiment. *rrf*, RNA-dependent RNA polymerase family.

(VC2039) shows a significant decrease in locomotion, and *dhhc-14* (VC918) shows a significant increase (Figure 4.5A). However, in both cases the other strain available for the gene shows a non-significant difference in the opposite direction. The *dhhc-12* strain VC2039 has a deletion downstream of the DHHC-CRD and strain VC2244 has a deletion including the DHHC-CRD and most of the protein (Appendix 1). It is unknown whether both alleles result in no expression of the DHHC-12 protein as antibodies to use in Western blotting are unavailable. Both *dhhc-14* strains carry deletions which include the DHHC-CRD of DHHC-14, so no enzymatically active protein would be produced. All the *ppt-1* strains have deletions which include most of the PPT-1 protein, yet only VC166 and VC184 show a significant increase in thrashing compared with wild-type animals (Figure 4.5B). In all these cases, the most likely explanation for these differences is the presence of secondary mutations as a result of the mutagenesis process; it seems unlikely that relatively small differences between alleles should produce such disparate effects. Thrashing assays were also carried out on RNAi-treated *rrf-3* mutants covering all the genes of interest except *dhhc-11*, as discussed above. The only gene which gave a significant difference was *dhhc-6*, whose knockdown gave a reduction in thrashing rate (Figure 4.6).

Locomotion of all the DHHC mutant strains was assessed on solid medium (Figure 4.7A). In addition, the published MN1 strain lacking *ppt-1* and the *ath-1* mutant were tested (Figure 4.7B). None of the strains showed a significant difference from wild-type locomotion. Similar results were gained using an RNAi approach (Figure 4.8).

It is possible that this lack of obvious locomotory phenotypes is due to a certain level of redundancy, that is, that other DHHCs can take over the roles of missing enzymes. Feeding RNAi can be used to knockdown expression of multiple genes at the same time, albeit at a reduced efficiency compared with feeding RNAi against only one gene, by culturing the animals on a mixture of bacterial strains (Gouda *et al.*, 2010; Kamath *et al.*, 2001; Min *et al.*, 2010). In order to test whether redundancy may play a part in these locomotion assays, pairs of closely related DHHCs were knocked down based on phylogenetic analysis (Figure 3.3). These thrashing assays only showed a difference with knockdown of *dhhc-1* and *-10*, giving a small but significant increase in speed (Figure 4.9). The rest of the combinations thrashed at the same rate as the negative control.

4.3.3.2 MECHANOSENSATION

One of the phenotypes which can occur due to dysfunction of a subset of neurons is a defect in mechanosensation, whereby animals fail to respond to a mechanical stimulus by

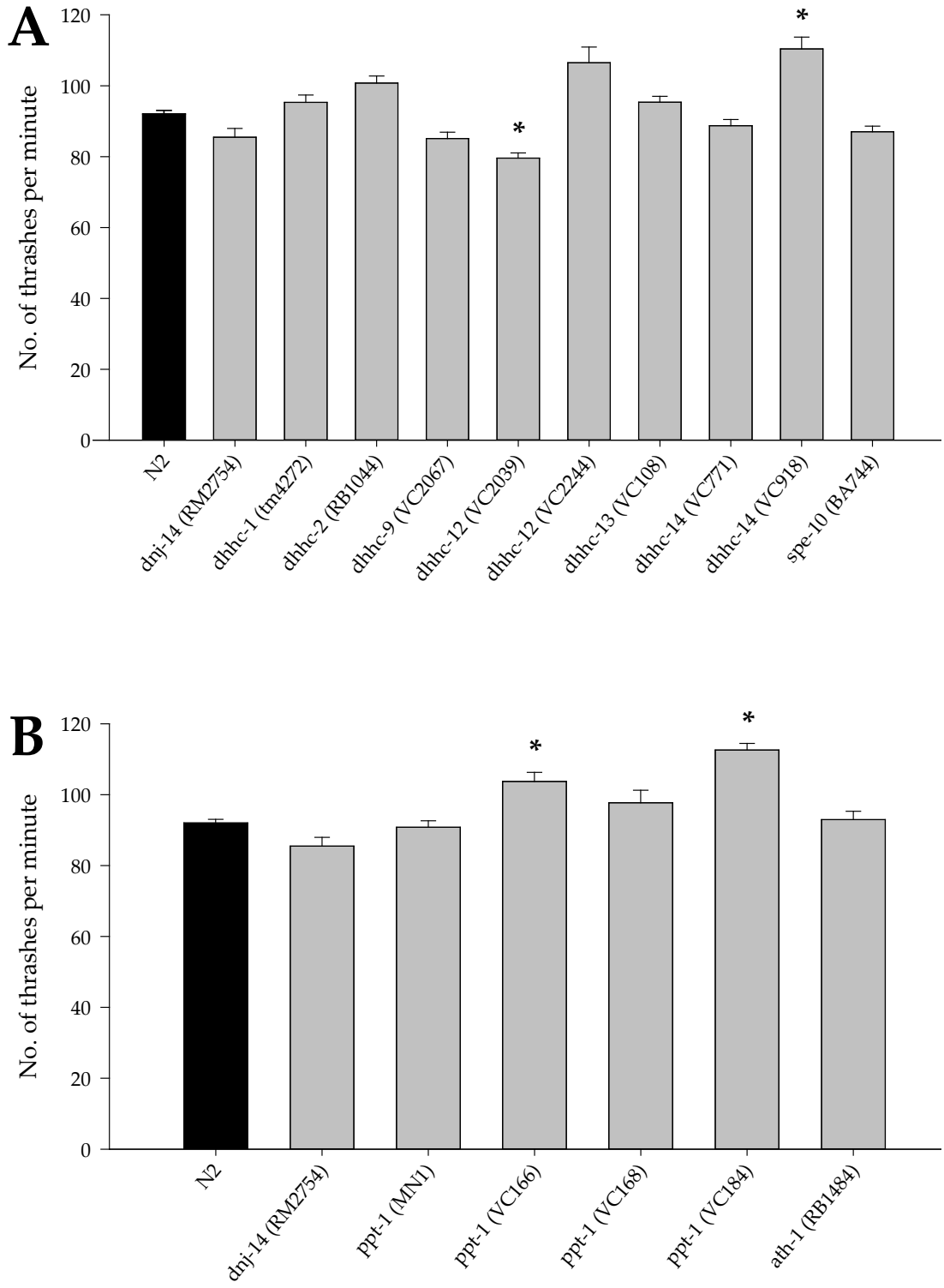

FIGURE 4.5: Locomotion of mutant strains in liquid medium

Thrashing assays were conducted on wild-type N2 animals and mutants for *dnj-14*, DHHC enzymes (A) and PPT enzymes (B). The strain designation is shown in parentheses. Some data were collected by Tim Frost under my supervision. n = 10-268 over 1-10 experiments. * $p < 0.05$ by one-way ANOVA. ANOVA, analysis of variance; *dnj*, DnaJ domain-containing protein.

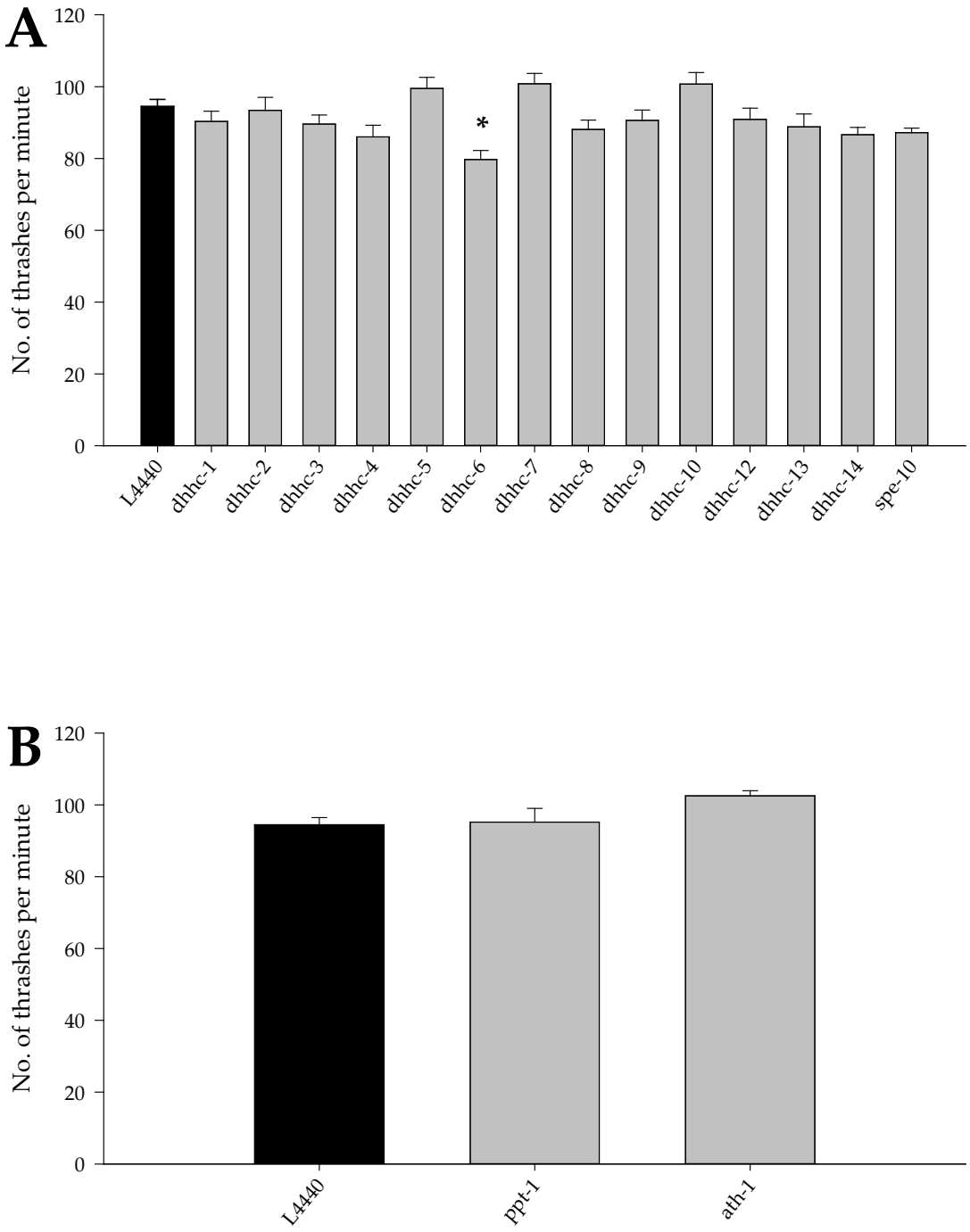

FIGURE 4.6: Locomotion of *rrf-3* mutant animals treated using RNAi in liquid medium

Thrashing assays were conducted on RNAi-sensitive *rrf-3* mutant animals using feeding RNAi against DHHC enzymes (A) and PPT enzymes (B). The negative control was the empty L4440 vector. Data could not be collected for *dhhc-11* as the construct was subsequently found to target a different gene. n = 10-40 over 1-4 experiments. * $p < 0.05$ by one-way ANOVA. ANOVA, analysis of variance.

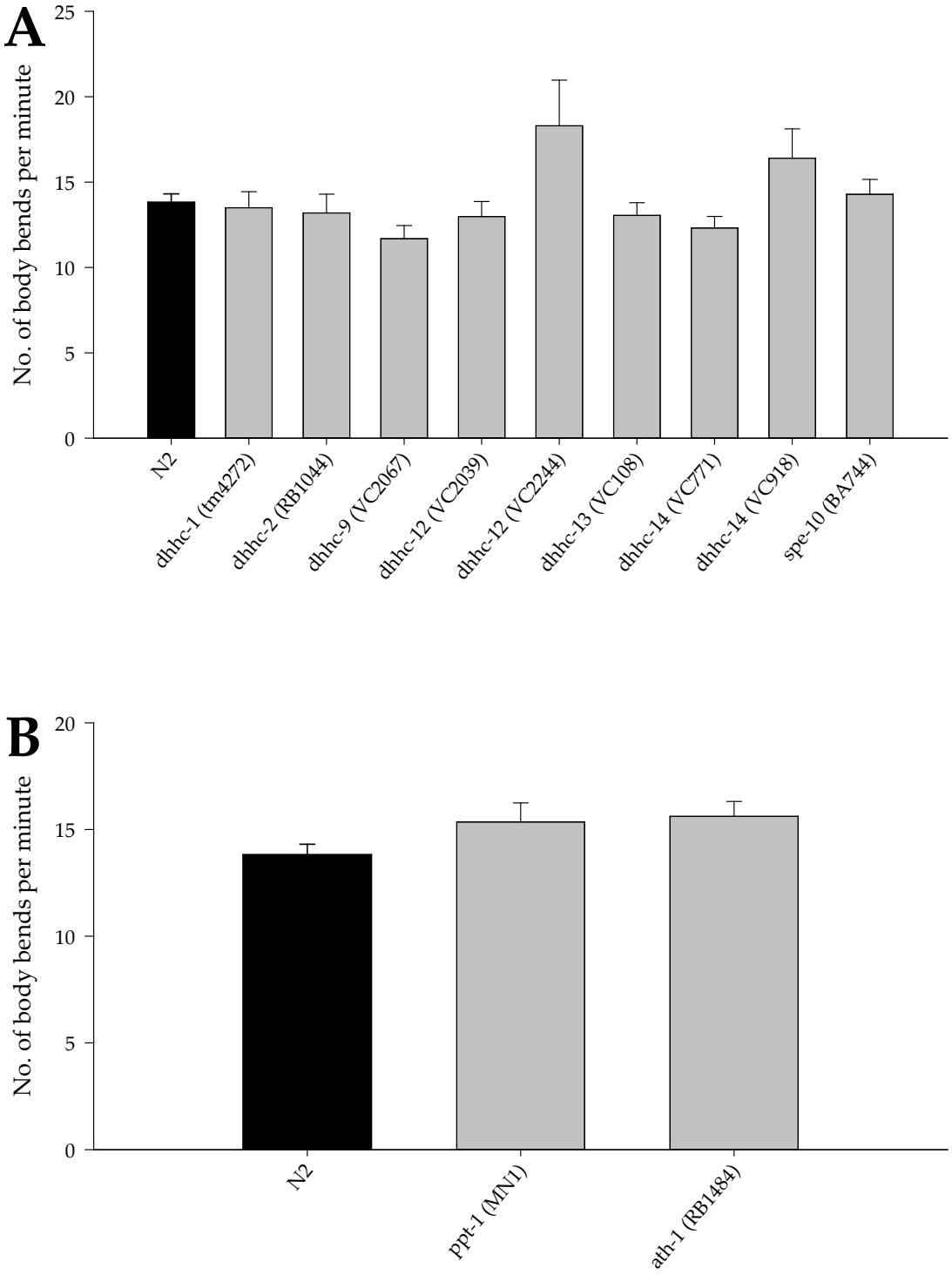

FIGURE 4.7: Locomotion of mutant strains on solid medium

Body bend assays were conducted on wild-type N2 animals and mutants for DHHC enzymes (A) and PPT enzymes (B). The strain designation is shown in parentheses. Some data were collected by Tim Frost under my supervision. *n* = 4-45 over 1-2 experiments.

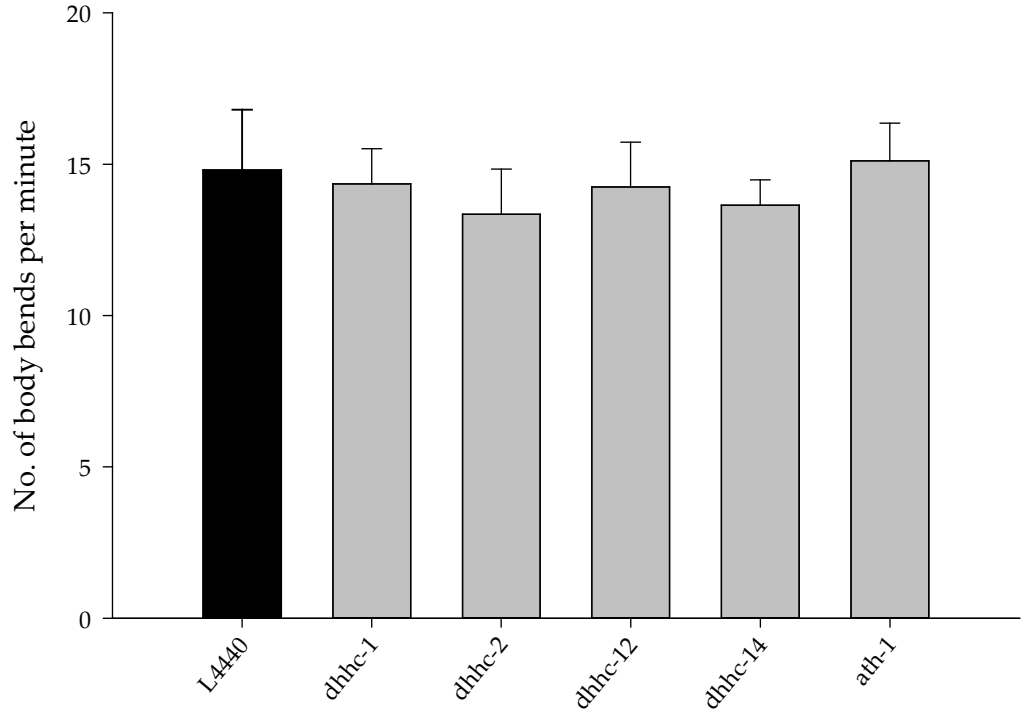

FIGURE 4.8: Locomotion of *rrf-3* mutant animals treated using RNAi on solid medium

Body bend assays were conducted on RNAi-sensitive *rrf-3* mutant animals using feeding RNAi against DHHC and PPT enzymes. The negative control was the empty L4440 vector. *n* = 5-10 over one experiment.

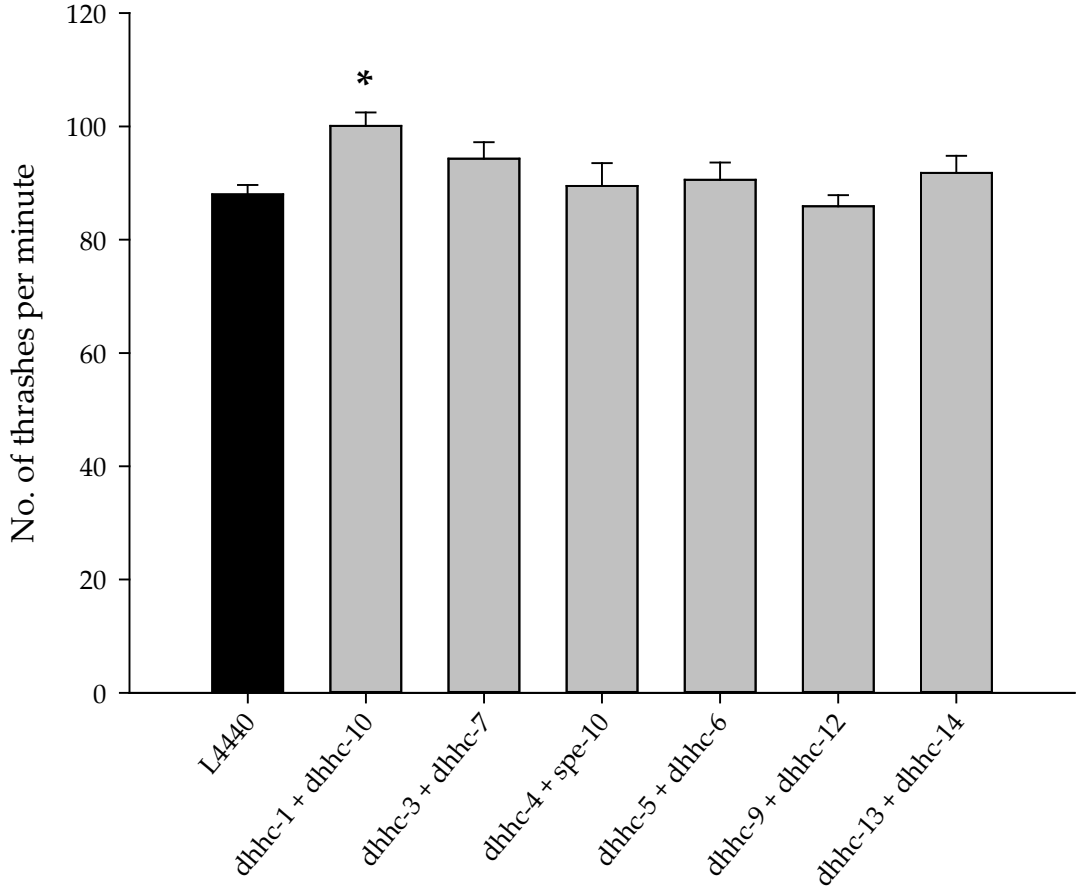

FIGURE 4.9: Locomotion in liquid medium of *rrf-3* animals treated with multiple RNAi clones against *dhhc* genes

Thrashing assays were performed on *rrf-3* animals subjected to feeding RNAi against L4440 (control) or combinations of *dhhc* genes. n = 10-30 over 1-3 experiments. * $p < 0.05$ by one-way ANOVA. ANOVA, analysis of variance.

increasing movement in the opposite direction (Chalfie and Sulston, 1981). Selected mutant strains were tested for the presence of such a phenotype (Table 4.4). All of the strains were found to have normal responses to both anterior and posterior mechanical stimuli.

4.3.4 AGEING PHENOTYPES

4.3.4.1 LIFESPAN

The only DHHC enzyme whose loss has been studied previously is SPE-10. One of the observations which has been made is a small increase in lifespan (Cypser and Johnson, 1999). *dnj-14* mutants have been observed to have a reduced lifespan in this laboratory (unpublished data) and its orthologue CSP shows premature death in *Drosophila* and mouse models (Fernandez-Chacon *et al.*, 2004; Zinsmaier *et al.*, 1994). It was therefore decided to investigate whether any of the other mutant strains obtained also had any differences in lifespan. Survival plots of strains showing a significant difference from wild-type N2 animals are shown in Figure 4.10A, and those with no difference from N2 in Figure 4.10B. Precise values for mean and median lifespan, 90% mortality and maximum lifespan are collated in Table 4.5. As expected, the *dnj-14* mutants showed a significantly reduced mean lifespan, as did mutants for *dhhc-1*, *-9*, *-14* (VC771), and *-14* (VC918). Of these, *dhhc-9* and *-14* (VC771) also showed a reduced median lifespan, and *dnj-14*, *dhhc-1*, *-14* (VC771), and *-14* (VC918) had reduced time to 90% mortality. The *spe-10* mutant did not show an increased mean or median lifespan, although its maximum lifespan was extended considerably compared with wild-type. Strains which did show an increase in mean lifespan were *ppt-1* (VC166) and *ppt-1* (VC184); an increase in median lifespan was seen in *dhhc-12* (VC2244), *-13*, *ppt-1* (VC166) and *ppt-1* (VC184); and an increase in time to 90% mortality was seen in *dhhc-12* (VC2039), *-13* and *ppt-1* (VC166).

Lifespan analysis was also carried out on *rrf-3* mutants treated with RNAi against potential genes of interest identified in the lifespan analysis of mutants above. In addition to *dnj-14* and *spe-10*, *dhhc-1* and *-14*, which were generally shorter-lived, and *ppt-1*, which was longer-lived in two of the four mutant strains, were also tested (Figure 4.11, Table 4.5). Of these, only *dnj-14* showed a difference in mean and median lifespan, coming out much shorter in both measures. *dhhc-1* and *-14* showed a significant decrease in time to 90% mortality, agreeing with analysis of their mutant strains. Neither *spe-10* nor *ppt-1* showed any statistically significant difference in any measure of lifespan when knocked down.

Strain	% Response to anterior touch	% Response to posterior touch
N2	97.5	97.5
dhhc-2 (RB1044)	100	95
dhhc-9 (VC2067)	100	100
dhhc-12 (VC2039)	100	100
dhhc-13 (VC108)	100	100
dhhc-14 (VC771)	100	100
spe-10 (BA744)	100	100
ppt-1 (MN1)	100	95
ath-1 (RB1484)	100	100

TABLE 4.4: Mechanosensation of mutant strains

Mechanosensation was assessed by passing an eyebrow hair over either the anterior or posterior of the animal. A positive response to anterior touch was defined as a change of direction of movement of the animal from forwards to reverse. A positive response to posterior touch was defined as a sudden increase in forward movement. *n* = 20 per strain. Data were collected by Tim Frost.

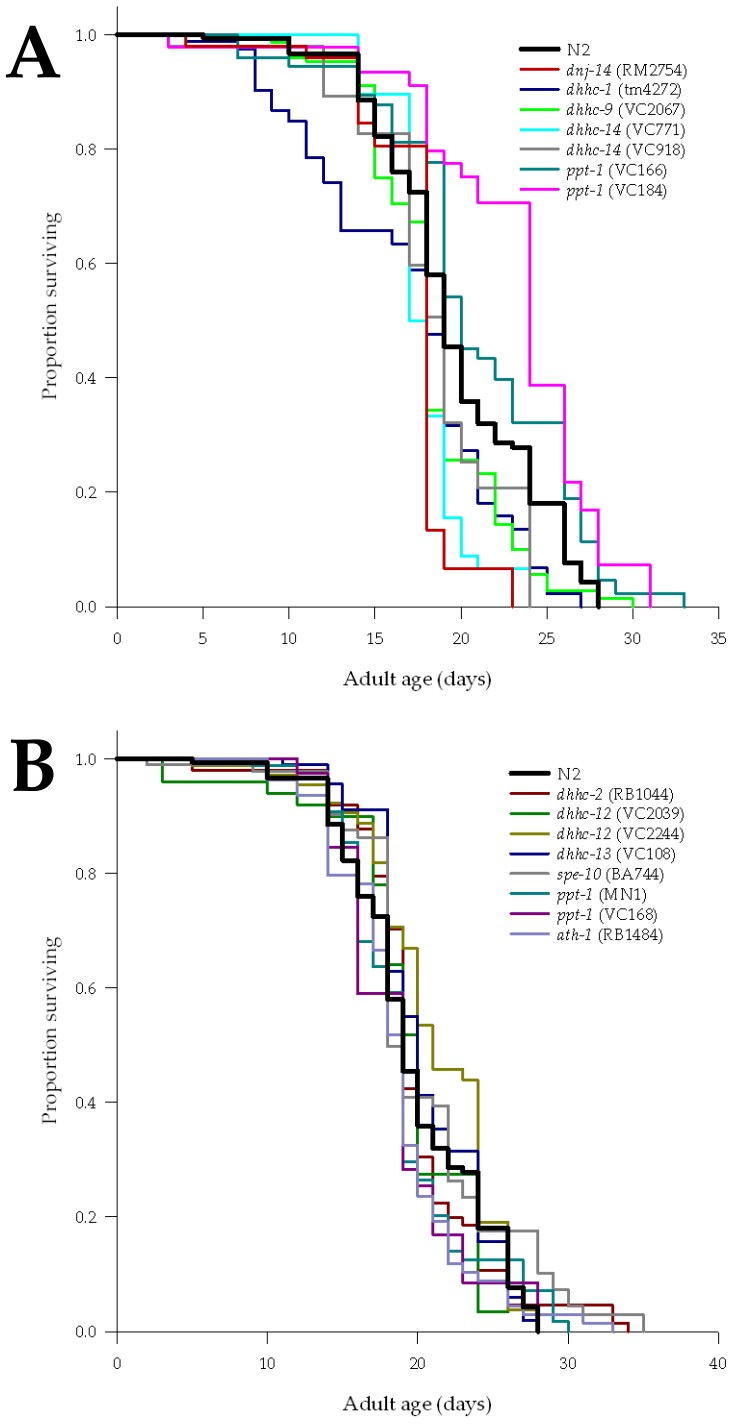

FIGURE 4.10: Survival analysis of mutant strains

The lifespan of populations of synchronised animals was observed and compared with the wild-type N2 strain. The gene affected is shown along with the strain code in parentheses. (A) Strains showing a significantly different lifespan from N2. $p < 0.05$ by log-rank (Mantel-Cox) test. (B) Strains showing no significant difference from N2 lifespan. Statistical analysis was performed using OASIS (Yang *et al.*, 2011). n = 43-165 animals over 1-5 experiments. OASIS, online application for survival analysis.

Strain	*n*	Mean (days)	Median (days)	90% mortality (days)	Maximum (days)
N2	165	20	19	26	28
dnj-14 (RM2754)	50	17*	19	23†	23
dhhc-1 (tm4272)	97	17*	18	24†	27
dhhc-2 (RB1044)	100	20	19	26	34
dhhc-9 (VC2067)	143	19*	19†	24	30
dhhc-12 (VC2039)	50	19	20	26	26
dhhc-12 (VC2244)	93	21	21†	26†	28
dhhc-13 (VC108)	93	21	20†	26†	28
dhhc-14 (VC771)	49	18*	18†	20†	24
dhhc-14 (VC918)	48	18*	19	24†	24
spe-10 (BA744)	95	21	19	29	35
ppt-1 (MN1)	86	19	19	27	30
ppt-1 (VC166)	88	21*	20†	28†	33
ppt-1 (VC168)	43	19	19†	23	28
ppt-1 (VC184)	48	23*	24†	28	31
ath-1 (RB1484)	80	18	19	24	33

RNAi strain	*n*	Mean (days)	Median (days)	90% mortality (days)	Maximum (days)
L4440	164	17	17	25	31
dnj-14	131	14*	13†	23	26
dhhc-1	79	16	16	24†	25
dhhc-14	99	19	19	22†	31
spe-10	79	18	19	24	29
ppt-1	59	15	14	25	30

RNAi strain(s)	*n*	Mean (days)	Median (days)	90% mortality (days)	Maximum (days)
L4440	164	17	17	25	31
dhhc-1 + dhhc-10	50	18	18	24†	29
dhhc-3 + dhhc-7	23	19	20	26	28
dhhc-4 + spe-10	34	21*	21†	27	33
dhhc-5 + dhhc-6	27	17	16	25†	26
dhhc-9 + dhhc-12	44	18	18	24†	26
dhhc-13 + dhhc-14	38	21	21†	24†	30
ppt-1 + ath-1	98	14*	12†	25	30

TABLE 4.5: Parameters measured in survival analysis

Various measures were extracted from the lifespan experiments with mutants (top) and single (middle) and multiple (bottom) RNAi treatments of *rrf-3* mutants. Statistical tests were applied using OASIS (Yang *et al.*, 2011). * $p < 0.05$ by the log-rank (Mantel-Cox) test. † $p < 0.05$ by Fisher's exact test. OASIS, online application for survival analysis.

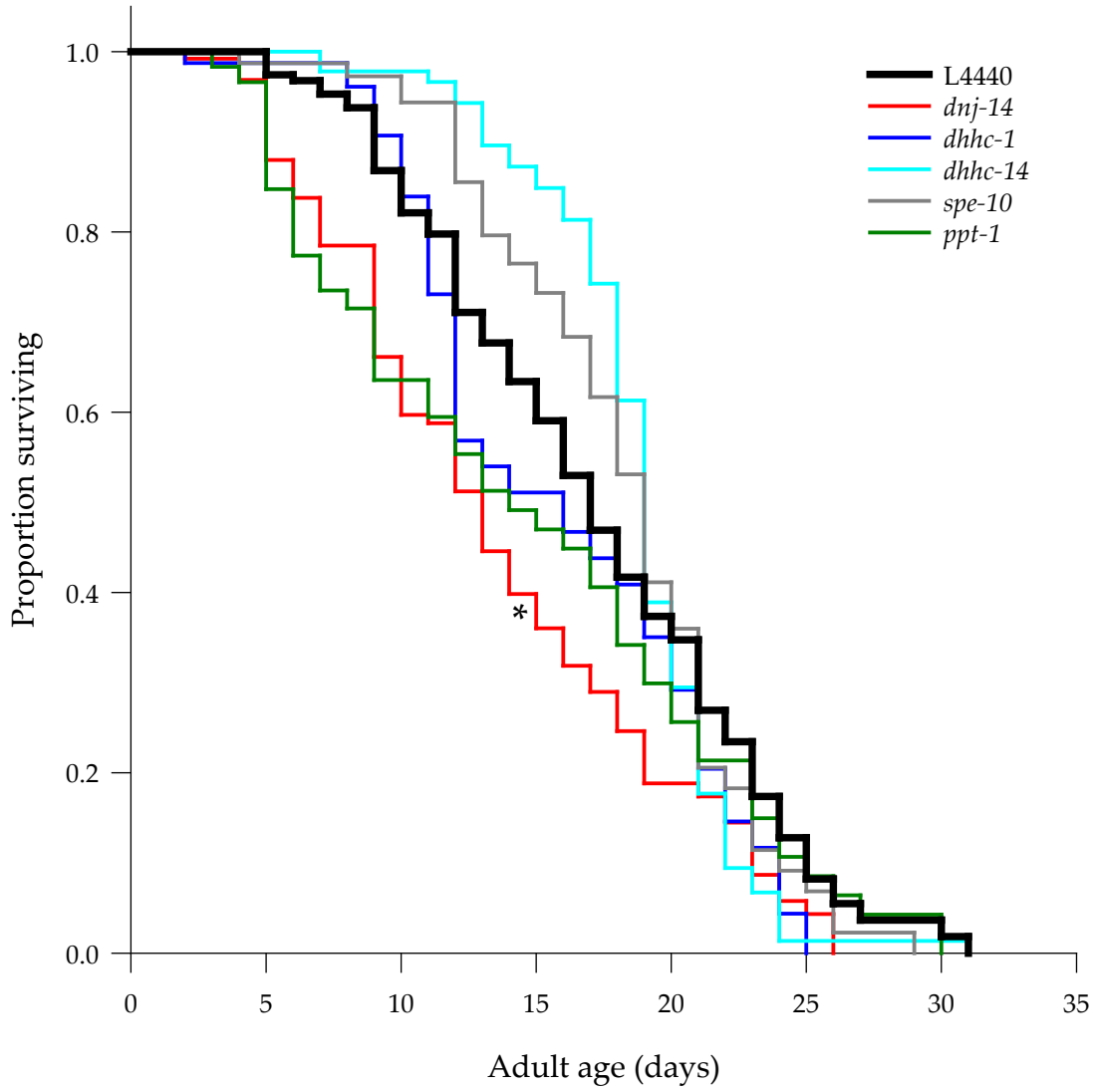

FIGURE 4.11: Survival analysis of *rrf-3* animals treated with RNAi against single genes

The lifespan of populations of synchronised *rrf-3* animals treated with RNAi against single genes was observed and compared with the control treated with the empty L4440 vector. Statistical analysis was performed using OASIS (Yang *et al.*, 2011). * $p < 0.05$ by log-rank (Mantel-Cox) test. n = 59-164 animals over 1-4 experiments. OASIS, online application for survival analysis.

As with the locomotion assays above, RNAi was carried out against the same combinations of genes to test whether this made any difference to the lifespans observed in mutants and single RNAi experiments. A combination of *ppt-1* and *ath-1* showed a much decreased mean and median lifespan, whereas concurrent knockdown of *dhhc-4* and *spe-10* resulted in an increase in mean and median lifespan (Figure 4.12, Table 4.5). The remaining combinations showed no difference in mean lifespan from the negative control. The combination of *dhhc-13* and *-14* showed an increased median lifespan. The combinations of *dhhc-1* and *-10*, *dhhc-5* and *-6*, *dhhc-9* and *-12* and *dhhc-13* and *-14* all showed a significantly quicker time to 90% mortality than the negative controls.

4.3.4.2 LOCOMOTION

As palmitoylation is known to be involved in a number of neurodegenerative processes (Das *et al.*, 2001; Rush *et al.*, 2012; Singaraja *et al.*, 2011; Sutton *et al.*, 2012; Velinov *et al.*, 2012; Vetrivel *et al.*, 2009), a possible readout of this process would be a faster than normal decrease in locomotion rate as *C. elegans* ages. Indeed, *dnj-14* mutants have already shown such an effect (unpublished data). All of the mutant strains except *dhhc-1*, which was not yet available at the time, were synchronised and subjected to thrashing assays as they aged. The results of each of the three experiments performed are shown in Figure 4.13. None of the mutant strains showed a significant difference from the shape of decay in the wild-type N2 rate of thrashing. Given this result and the time-consuming nature of these experiments, it was decided not to repeat this experiment using an RNAi approach.

4.3.5 ALTERNATIVE APPROACH TO KNOCKDOWN OF MULTIPLE GENES USING RNAI

As mentioned above, it has been observed that knockdown of two or more genes by mixing the feeding RNAi bacterial strains gives variable efficacy in an apparently gene-dependent manner (Gouda *et al.*, 2010; Kamath *et al.*, 2001; Min *et al.*, 2010). Recently described is an approach in which the sequences from two or more genes of interest are cloned into the same vector, giving efficient knockdown of all the genes involved (Figure 4.14A) (Gouda *et al.*, 2010; Min *et al.*, 2010). As there are only two known PPTs in *C. elegans*, it is possible that concurrent knockdown of both would produce relatively severe effects compared with those already observed in this chapter. With this in mind, it was decided to test this effect by comparing the thrashing rates of knockdown of *ppt-1* and *ath-1* either by mixing the separate bacterial strains or by feeding a bacterial strain expressing the conjugated sequences from the individual vectors. However, no difference was seen from the negative control in either condition (Figure 4.14B).

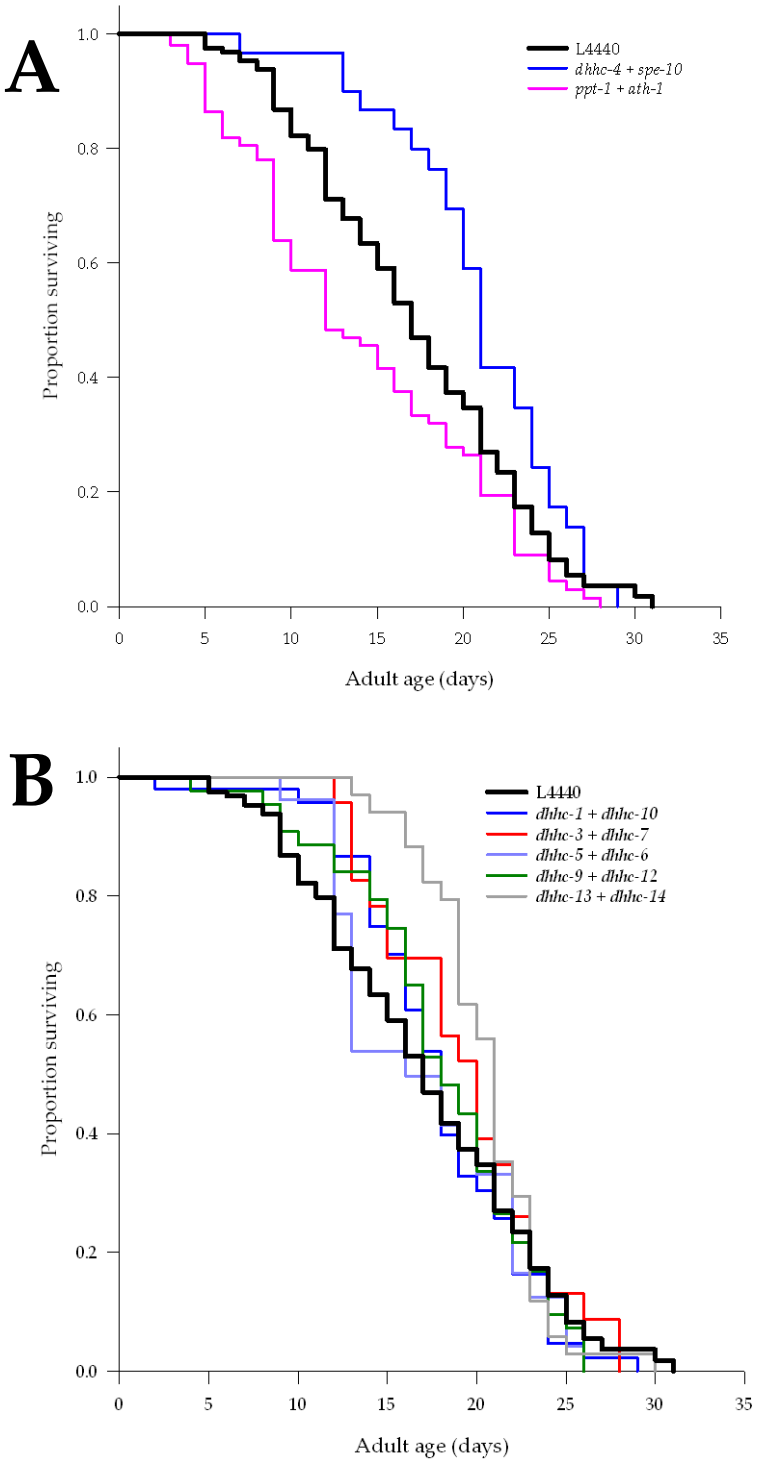

FIGURE 4.12: Survival analysis of *rrf-3* animals treated multiply with RNAi against single genes

The lifespan of populations of synchronised *rrf-3* animals treated with multiple RNAi strains against single genes was observed and compared with the control treated with the empty L4440 vector. (A) Treatments showing a significantly different lifespan from the control. $p < 0.05$ by log-rank (Mantel-Cox) test. (B) Treatments showing no significant difference from control lifespan. n = 23-164 animals over 1-4 experiments. Statistical analysis was performed using OASIS (Yang *et al.*, 2011). OASIS, online application for survival analysis.

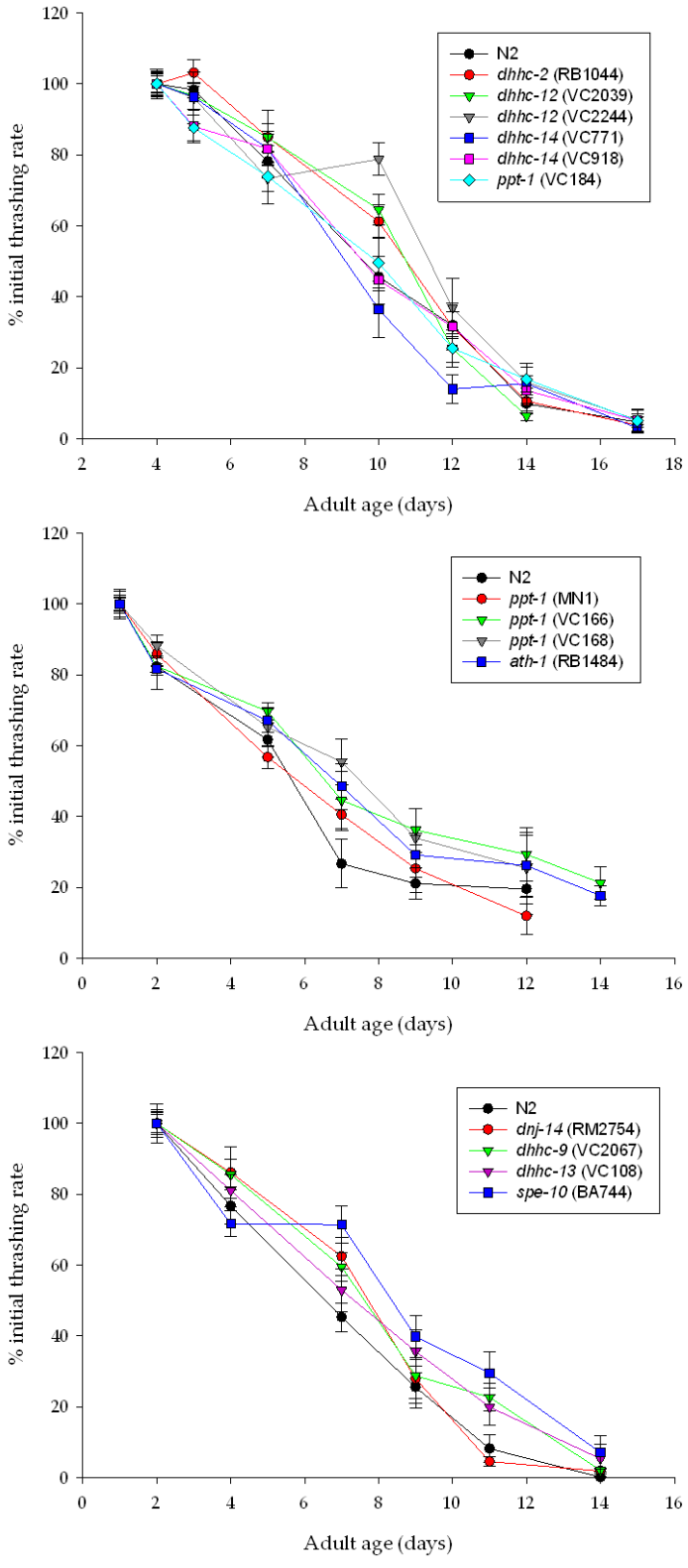

FIGURE 4.13: Age-dependent decline in locomotion of mutant strains

Thrashing assays were performed on synchronised animals at various ages and compared with the wild-type N2 strain. Each individual experiment is shown for ease of viewing. The gene affected is shown along with the strain code in parentheses. No significant difference in decline of locomotion from wild-type was observed in any experiment as assessed by one-way ANCOVA. *n* = 4-10 animals per strain per time point. ANCOVA, analysis of covariance.

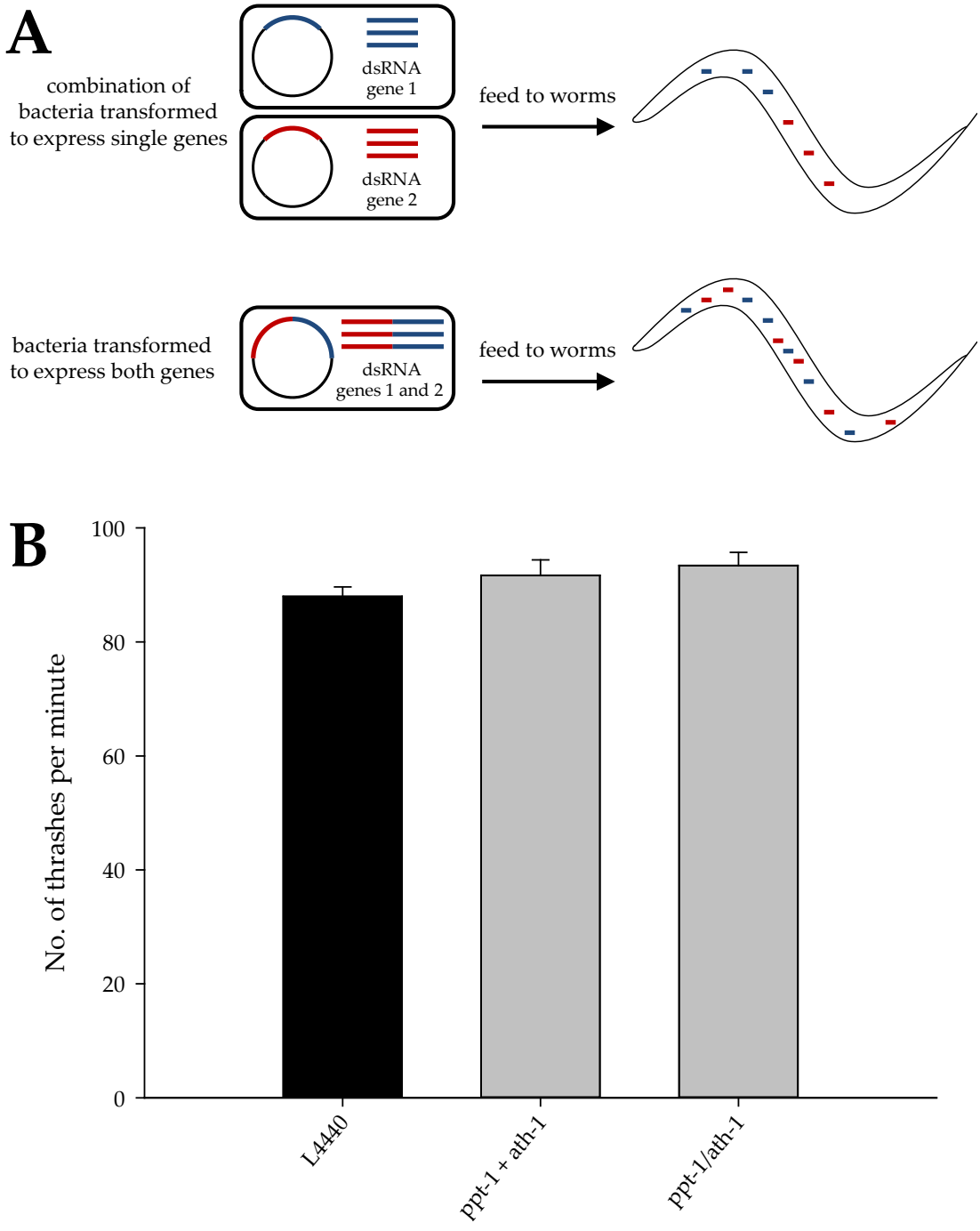

FIGURE 4.14: Comparison of strategies for simultaneous knockdown of two genes using RNAi

(A) Cartoon showing two strategies for feeding RNAi for multiple genes. The upper strategy was used for previous experiments. The lower strategy is thought to increase the effective dose of siRNA to the organism. (B) Locomotion of *rrf-3* mutant animals was assessed after RNAi treatment with control L4440 or against *ppt-1* and *ath-1* by feeding with a mixture of bacteria expressing one or the other (*ppt-1* + *ath-1*) or a single bacterial line expressing both from one plasmid (*ppt-1*/*ath-1*). *n* = 10-30 animals over 1-3 experiments. dsRNA, double-stranded ribonucleic acid.

4.4 DISCUSSION

4.4.1 OVERVIEW OF RESULTS

In this chapter, a combination of mutant strains and feeding RNAi treatment were used to try to tease out phenotypes associated with loss of enzymes involved in palmitoylation, both individually and in combinations. Both of these approaches have advantages and limitations. Mutant strains can result in no expression of a protein at all or in expression of a truncated or functionally inert protein. However, the methods which are classically used to produce these strains are likely to produce mutations elsewhere in the genome. The outcrossing process to remove background mutations is laborious but improves confidence that any effects are specific to the gene of interest. Of the strains used in this study, only *ppt-1* (MN1) has been outcrossed extensively, *dhhc-12* (VC2244) has been outcrossed once and *spe-10* (BA744) may have been outcrossed four times (Table 4.3). Studies using mutants were also hampered by not being able to investigate every gene in the DHHC family. Although mutants for the remaining genes were requested from the *C. elegans* Knockout Consortium at the beginning of the project, funding issues have since severely limited their capabilities and unfortunately these strains have not been generated.

The feeding RNAi method has the advantage that it is easy to perform and a screen of the entire family of DHHC enzymes can be achieved. There is also scope for knockdown of multiple genes simultaneously, although an experiment comparing strategies with both PPTs shows this requires further optimisation (Figure 4.14). There are two main caveats to the use of RNAi. First is the efficiency of the knockdown. When the feeding RNAi technique used here was first optimised, analysis of genes which produce embryonic lethality gave the expected phenotype in around 100% of embryos for most genes tested (Kamath *et al.*, 2001). When the *rrf-3* hypersensitive RNAi strain was first characterised, phenotypes which could not be observed with RNAi in wild-type N2 animals could be seen in 0-82% of *rrf-3* animals (Simmer *et al.*, 2002). Quantitative polymerase chain reaction (PCR) analysis of knockdown of oocyte maturation defective 1 (*oma-1*) and *oma-2* in wild-type N2 animals showed a decrease in expression of 80-90% and also had a dilution to around 40% knockdown when two bacterial strains were mixed which did not occur when a single bacterial strain expressing both constructs was used (Gouda *et al.*, 2010). Second is the differing penetration of RNAi in different tissues in *C. elegans*. Various strains have been created which give increased sensitivity to RNAi in all tissues or specific tissues. These were tested using constructs which were expected to give clear phenotypes (Figure 4.2). However, none of the strains tested appeared to give expected phenotypes in our hands

and so the globally hypersensitive *rrf-3* strain was chosen (Simmer *et al.*, 2002). This strain gave the expected sterile phenotype with the positive control knockdown of *hsp-1* (Simmer *et al.*, 2003) and the reduction in lifespan after *dnj-14* knockdown (Figure 4.11, Table 4.5), giving confidence that feeding RNAi is indeed knocking down expression.

To gain an overview of all the analyses performed in this chapter, a matrix was produced showing which genes were tested in which ways and the results (Figure 4.15). In terms of morphology, a handful of mutants showed a slight reduction in width but this was not seen in any RNAi experiments and are difficult to explain based on current knowledge. It is possible the mutant strains have a mild effect during development which results in a thinner body, or perhaps they contain fewer eggs. It may be that phenotypes which are seen in mutants but not RNAi like this are due to the remaining low level of expression still being enough for the protein to perform its function.

As many of the DHHC enzymes are closely related (Figure 3.3) there may be a compensatory effect which complements the small amount of expression of the protein. In view of this, some combinatorial RNAi was also performed for the locomotion and lifespan assays. Some strains showed no difference from controls in either locomotion or lifespan under any conditions tested. *dhhc-2*, *-3*, *-7*, and *-8* fell into this category. *dhhc-1* showed a reduction in lifespan in mutants and when treated with RNAi on its own and with *dhhc-10*, which did not show a difference on its own. The combined knockdown of *dhhc-1* and *-10* also gave an increase in thrashing rate. The same was true for *dhhc-5* and *-6* and although they were not tested individually for lifespan, *dhhc-6* did also show a decrease in thrashing rate. *dhhc-9* mutants showed a decrease in lifespan and, when knocked down in combination with *dhhc-12*, a reduction in time to 90% mortality. This is interesting given that both *dhhc-12* mutants showed an increase in lifespan, although VC2039 also shows a decrease in locomotion. A similar effect was seen in *dhhc-13* and *-14*. Mutants for *dhhc-13* and *-14* showed an increase and decrease in lifespan, respectively, but when knocked down in combination showed an increase in median lifespan with a decrease in time to 90% mortality. This may indicate that *dhhc-13* acts earlier in life whereas *dhhc-14* acts towards the end of the animals' lifespan to extend it. *spe-10* and *dhhc-4* did not show phenotypes when altered on their own, but knockdown in concert resulted in an increase in lifespan.

Analysis of *ppt-1* produced somewhat challenging data from which to draw conclusions. Two of the four mutant strains available showed an increase in thrashing rate, yet one of these showed an increase in lifespan and the other a decrease. The VC184 strain also

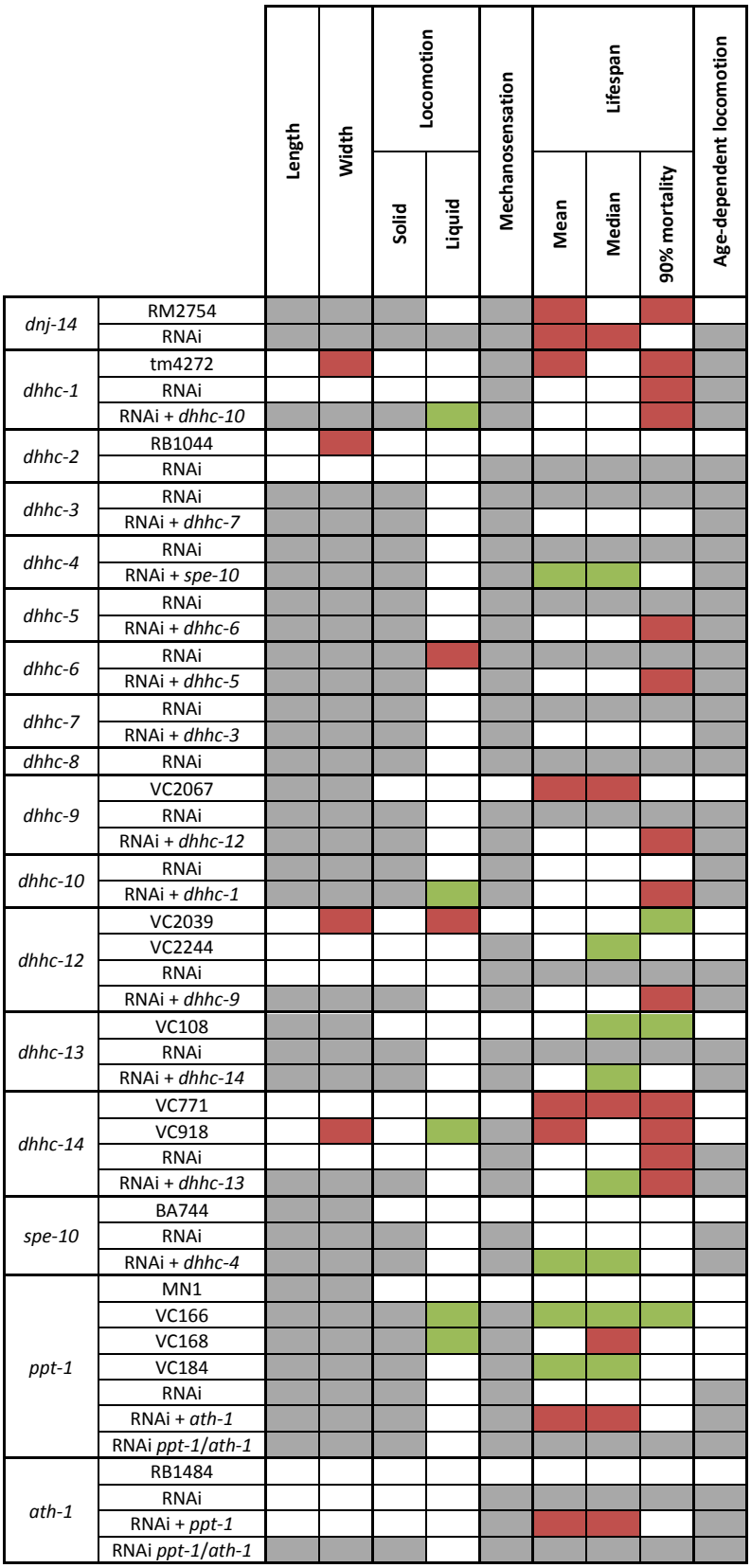

FIGURE 4.15: Summary of observations in this chapter

This matrix summarises the results presented in this chapter. A significant increase in quantity or time is coloured green and a significant decrease is in red. Grey indicates a test was not performed.

showed an increase in lifespan, although the MN1 strain and RNAi treatment against *ppt-1* showed no phenotypes. When combined with *ath-1*, which showed no phenotypes on its own, there was a marked reduction in mean and median lifespan. It would be interesting to investigate whether RNAi using the double *ppt-1*/*ath-1* vector or a double mutant reproduce this finding.

4.4.2 COMPARISON WITH EXISTING KNOWLEDGE AND *IN SILICO* PREDICTIONS

The DHHC family member *spe-10* has already been studied in relation to its spermatogenesis phenotype (Gleason *et al.*, 2006; Shakes and Ward, 1989) and resistance to certain stresses (Cypser and Johnson, 1999). The BA744 strain appeared normal and did not have any obvious reduction in fertility during normal strain maintenance at 20 °C (data not shown). The moderate increase in lifespan previously reported in some experiments (Cypser and Johnson, 1999) was not observed here (Figure 4.10B, Figure 4.11, Table 4.5), although these experiments were performed at 20 °C in contrast to the published observations at 25.5 °C. As *spe-10* mutants also have a resistance to heat stress (Cypser and Johnson, 1999), it is possible this is the main factor determining lifespan at higher temperatures. An increase in maximum lifespan was observed both in that study and here, however. In addition, an increase in mean and median lifespan was seen when RNAi was performed on both *spe-10* and its most closely related gene *dhhc-4* simultaneously (Table 4.5).

The main subject of the published analysis of *ppt-1* was the MN1 strain (Porter *et al.*, 2005). This included an analysis of lifespan at both 20 and 25 °C which showed no difference from wild-type N2 lifespan. It is gratifying that their survival curves for N2 and MN1 show roughly the same shape as those presented here, with MN1 survival slightly below N2 for most of the time followed by a minority which have a longer maximum lifespan (Figure 4.10B). Although the VC184 strain was also used in some assays (Porter *et al.*, 2005), it does not appear to have been tested for lifespan, so the observation of increased lifespan (Figure 4.10, Table 4.5) cannot be corroborated. The observation that MN1 animals seemed to age more quickly on the plates, becoming less motile earlier than N2 animals (Porter *et al.*, 2005), was not backed up by analysis of age-dependent locomotion (Figure 4.13), which showed no differences in any strains. The lack of consistency in phenotypes shown between different alleles of *ppt-1* are puzzling given that each one would be expected to result in lack of *ppt-1* expression (Appendix 1). Strains VC166 and VC168 show an increased thrashing rate; VC168 shows reduced median lifespan, MN1 shows no difference from wild-type and VC166 and VC184 show increased mean and

median lifespan. The allele in MN1 has been confirmed to be a null allele (Porter *et al.*, 2005). Detection of wild-type PPT-1 protein was also attempted in that study but was hampered by not being able to detect PPT-1 in wild-type animals using either immunofluorescence or Western blotting. The antibody used was able to detect PPT-1 overexpressed in bacteria, suggesting wild-type PPT-1 levels are low and/or diffuse. The same study suggested a possible explanation for the relatively mild phenotype of MN1 animals could be as a result of compensation by ATH-1 (Porter *et al.*, 2005). The results of the multiple RNAi presented here suggest this may be the case, as even with the reduced dsRNA dosage from mixing the feeding bacterial strains (Gouda *et al.*, 2010; Kamath *et al.*, 2001; Min *et al.*, 2010) this gave the biggest effect on lifespan of any of the conditions tested, with a decrease in mean and median lifespan (Figure 4.12, Table 4.5). As no difference was seen between the different multiple RNAi strategies in locomotion, perhaps lifespan would be a more suitable condition to test. Animals treated with both dsRNAs expressed from the same vector appeared normal and had no locomotion defects, but a quantitative test of their lifespan could be predicted to show an additional reduction given the increased knockdown expected with this method (Gouda *et al.*, 2010; Min *et al.*, 2010). Unfortunately this could not be performed in this study due to time constraints.

One of the predictions made using the *in silico* analyses from Chapter 3 was that disruption of *dhhc-14* may lead to locomotion or lifespan phenotypes given its orthologues in *S. cerevisiae* and *H. sapiens* are known to palmitoylate important proteins in membrane fusion (Table 3.7). Whilst neither mutant strain nor RNAi treatment against *dhhc-14* gave locomotion phenotypes, VC771 showed reductions in all lifespan parameters tested, VC918 showed reductions in mean lifespan and time to 90% mortality and treatment with RNAi both individually and in combination with *dhhc-13* gave a reduction in time to 90% mortality (Table 4.5). This is one of the most consistent phenotypes observed between several different disruptions of the same gene. Its lack of locomotion phenotype but reduction in most lifespan parameters also mirrors what was seen with disruption of *dnj-14*. The orthologues of DHHC-14 in *D. melanogaster* and *H. sapiens*, Hip14 and DHHC17/HIP14 respectively, have CSP as one of their substrates (Table 3.7). In addition, the *D. melanogaster* knockouts of *hip14* and *csp* show similar phenotypes of a temperature sensitive exocytotic defect (Ohyama *et al.*, 2007; Zinsmaier *et al.*, 1994). These lines of evidence suggest DHHC-14 may be one of the enzymes responsible for palmitoylating DNJ-14 in *C. elegans*. However, other predictions did not play out. For example, it was suggested based on homology that DHHC-3 and -7 may be responsible for palmitoylating

egg-laying defective 30 (EGL-30), the $G\alpha_q$ orthologue, and therefore might offer phenotypes. However, neither gave any phenotypes either individually or in combination (Figure 4.15). It is probable that the predictive power of such *in silico* analyses will increase as more information is gathered on enzyme-substrate interactions in each species. In addition, as more is discovered about palmitoylation in *C. elegans*, this may inform studies in other species. For example, disruption of *dhhc-1* gives a reduction in lifespan but its orthologue in *H. sapiens*, DHHC24, has yet to have any substrates assigned to it (Table 3.7).

4.4.3 EXTENDING PHENOTYPIC ANALYSIS

Although some *C. elegans* phenotypes associated with DHHC and PPT enzymes were uncovered in this chapter, it was by no means a complete analysis. The lack of availability of mutants limited the mutant screen to seven of the DHHCs and there was not enough time in this project to do a complete screen of all assays with all the available strains. There are now more avenues open to obtaining mutants in genes of interest. There is a knockout project underway in the Mitani lab in Japan called the National Bioresource Project for the Experimental Animal "Nematode *C. elegans*" from which the *dhhc-1* mutant tm4272 was obtained. This is presently the only mutant strain for a member of either the DHHC or PPT family in this project, although more will surely come through as time goes on. In addition a more focused and precise approach to generating knockouts in genes of interest is based on use of the *Drosophila Mos1* transposon in methods such as *Mos1*-induced transgene-instructed gene conversion (MosTIC) (Robert, 2012), *Mos1*-mediated single-copy insertion (MosSCI) (Frokjaer-Jensen *et al.*, 2008) and *Mos1*-mediated targeted deletions (MosDEL) (Frokjaer-Jensen *et al.*, 2010). These methods avoid the problem of background mutations when strains are generated by random mutagenesis and might clarify conflicting results such as those seen with the *ppt-1* mutant strains. In order to perform these techniques, *C. elegans* strains containing *Mos1* elements in the relevant positions in the genome are needed. A library of such strains is in the early stages of development by the NemaGENETAG project (http://elegans.imbb.forth.gr/nemagenetag/) (Vallin *et al.*, 2012). A search using the MosLocator tool (http://www.ciml.univ-mrs.fr/applications/MosLocator/) found there are currently strains available with *Mos1* alleles in *dhhc-2*, *-6*, and *-11*. Mutants are currently not available for *dhhc-6* and *-11*, so this is potentially a good source of targeted mutants in the future.

The current strains and reagents available could be used in assays investigating more subtle phenotypes such as chemotaxis, egg-laying, developmental timing, pharyngeal pumping and thermotolerance, and neuronal function could be assayed using the

acetylcholinesterase inhibitor aldicarb. The choice of assay could be better directed if GFP is expressed under the control of endogenous promoters of each of the genes of interest to see in which cell types they are expressed, although this would be expensive and time-consuming to perform for all 15 DHHCs and both PPTs. It would be useful to quantify the knockdown achieved by feeding RNAi using quantitative PCR, both of individual genes and of the different methods of combinatorial RNAi. The best method for knocking down expression from multiple genes could then be used to extend the number of combinations tested in different assays. Given the many substrates which can be palmitoylated by more than one palmitoyltransferase in mammals (Table 3.7) it may be that efficient knockdown of many DHHC enzymes simultaneously is required to uncover more severe phenotypes. This is supported by the relative difficulty of finding phenotypes in *S. cerevisiae* with knockdown of many DHHC family members simultaneously (Roth *et al.*, 2006). However, despite these issues of redundancy, there are still some severe phenotypes which can result from disruption of enzymes involved in palmitoylation. In *D. melanogaster*, *hip14* mutants show a relatively severe exocytotic phenotype (Ohyama *et al.*, 2007). Mouse knockouts of *Hip14* and *Hip14l* show progressive neurodegeneration with features reminiscent of Huntington's disease (HD) (Singaraja *et al.*, 2011; Sutton *et al.*, 2012). In addition, the severe infantile neurodegenerative disorder INCL is caused by mutations in *PPT1* in humans (Vesa *et al.*, 1995). Similar phenotypes may be discovered in the remaining mutants, by crossing existing mutants to obtain multiple knockout strains, or with complete knockdown in *C. elegans*.

This chapter set out to explore the phenotypes associated with disruption of members of the DHHC and PPT families. Mild phenotypes were found for a number of genes, mainly in the lifespan analysis. As only *spe-10* and *ppt-1* had been previously characterised, this information is potentially valuable as a starting point for future studies into specific enzymes. The confirmation of the prediction that *dhhc-14* might have a deleterious phenotype from the information collected in Chapter 3 gives proof of principle that such analyses can be helpful. Of course their usefulness will increase as more knowledge is uncovered. More specific validation can be given to predictions of enzyme substrate interactions by characterising which proteins are palmitoylated in *C. elegans*. This information can be combined with characterising which proteins remain palmitoylated in mutant strains to provide higher confidence enzyme-substrate pairs and complement these phenotypic data.

Chapter 5:

PALMITOYL-PROTEOMICS

5.1 INTRODUCTION

Two main techniques have emerged for purifying palmitoylated proteins from an extract, such as a cell lysate or a tissue homogenate. Both techniques will be used in this chapter and their principles are shown in Figure 5.1. One is acyl-biotin exchange (ABE), which was originally developed in response to the lack of sensitivity in existing methods and their restriction to living cells (Drisdel and Green, 2004; Roth *et al.*, 2006). The main technique of labelling with [^{3}H]-palmitate was particularly cumbersome, with autoradiograph exposure times of weeks or months, purification of the individual protein of interest and often a prior knowledge of the palmitoylated protein required (Bizzozero, 1995). Problems may also arise from metabolic conversion of radiolabelled palmitate to other types of fatty acid. Some proteomic techniques have addressed some of these problems by use of palmitate analogues such as 17-octadecynoic acid (17-ODYA) (Martin and Cravatt, 2009; Martin *et al.*, 2012) or alk-16 (Charron *et al.*, 2009; Yount *et al.*, 2010) which are not radioactive but instead may be purified using cycloaddition reactions, or so-called click chemistry. However, some of the limitations of [^{3}H]-palmitate labelling are retained: the penetration of labelled palmitate into the cells, its ratio to unlabelled palmitate and the previous level of palmitoylation and its turnover must be taken into account. The lack of sensitivity of [^{3}H]-palmitate labelling means that proteins expressed at a low level, such as receptors or ion channels, and proteins with a high palmitate turnover may not be detected (Drisdel and Green, 2004). Despite this, the use of radiolabelled palmitate remains the "gold standard" which is used to verify possibly contentious hits from proteomic scale screens.

The principle of ABE derives from the labile nature of the thioester bond between palmitate and the modified cysteine residue. This can be easily cleaved using neutral hydroxylamine (HA) (Omary and Trowbridge, 1981), revealing a free sulfhydryl group on the cysteine residue which can be labelled with a variety of constructs (Drisdel and Green, 2004). The selectivity of this method for palmitoylation depends on prior blocking of any existing sulfhydryl groups on unmodified cysteine residues, which can be performed using the thioreactive compounds N-ethylmaleimide (NEM) or methyl methanethiosulphonate (MMTS). The negative control is identically treated except with the use of Tris.HCl in place of HA. A proof-of-principle was also performed in the study using a biotin construct to label revealed sulfhydryls. In one case a streptavidin-horseradish peroxidise (HRP) overlay was used to identify palmitoylated chimeras of nicotinic receptor α7 subunits and serotonin (5-hydroxytryptamine; 5-HT) receptor 3A subunits; the other demonstrated selective

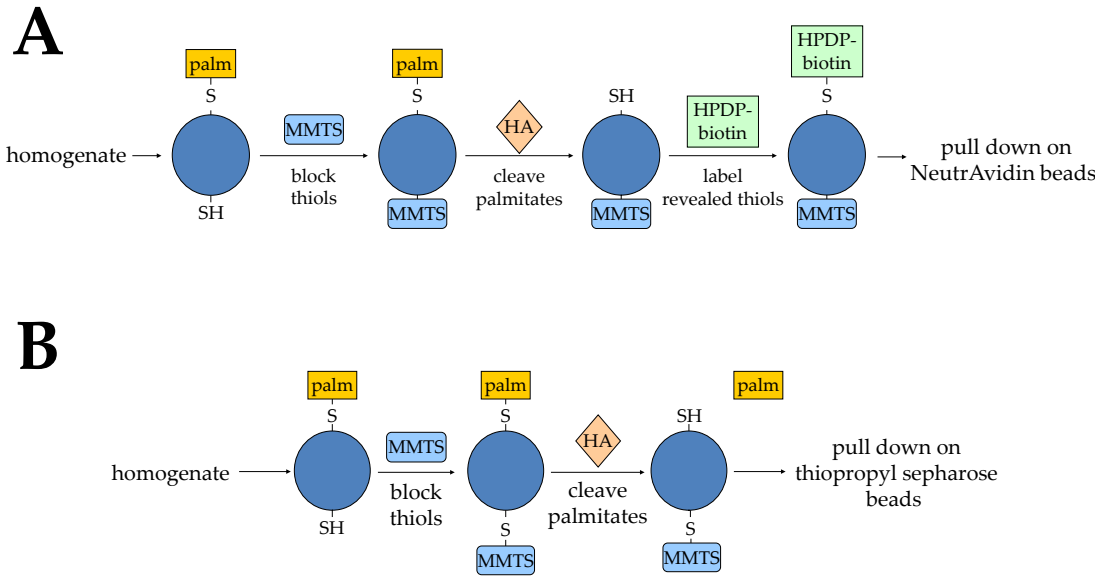

FIGURE 5.1: Proteomics methods used in this chapter

The procedures for (A) acyl-biotin exchange and (B) acyl-resin-assisted capture are shown in cartoon form. biotin-HPDP, N-[6-(biotinamido)hexyl]-3'-(2'-pyridyldithio)propionamide; HA, hydroxylamine; MMTS, methyl methanethiosulphonate; palm, palmitate.

pulldown of the purified palmitoyl-protein using a streptavidin agarose (Drisdel and Green, 2004).

The applicability of ABE to lysates to allow characterisation of *in vivo* palmitoylation was first demonstrated in *Saccharomyces cerevisiae* to characterise its palmitoylated membrane proteins (Roth *et al.*, 2006). This group took the ABE method developed by Drisdel and Green – labelling using a biotin construct and purifying all labelled proteins on streptavidin agarose – and extended it by using multi-dimensional protein identification technology (MudPIT) mass spectrometry to identify them. The power of this method over previous ones was demonstrated by the identification of 12 of the 15 previously known palmitoyl-proteins along with 35 new candidates. Such an analysis would not have been possible using radiolabelling approaches. A similar study soon followed using mammalian tissue, in this case rat cultured embryonic neurons and synaptosomes (Kang *et al.*, 2008). Again the value of the proteomic scale of ABE was shown by the identification of 68 known palmitoyl-proteins along with 113 previously unknown high confidence candidates. ABE has been applied to many mammalian cell types, including endothelial cells (Marin *et al.*, 2012), platelets (Dowal *et al.*, 2011), macrophages (Merrick *et al.*, 2011), and B lymphocytes (Ivaldi *et al.*, 2012). The palmitoyl-proteins present in lipid rafts have been characterised in human prostate cancer cells by ABE (Yang *et al.*, 2010), and the method has recently been used for the first characterisation of palmitoylation in *Arabidopsis thaliana* (Hemsley *et al.*, 2012).

Acyl-resin-assisted capture (acyl-RAC) is a technique which has been described recently (Forrester *et al.*, 2011) which was derived from a modification of the biotin switch assay used to study *S*-nitrosylation (Forrester *et al.*, 2009). It works in a similar way to ABE but shortens the protocol by pulling down the HA-treated proteins directly using a thioreactive sepharose (Figure 5.1). This has the advantage of reducing the number of steps and reactions, which may enable palmitoyl-proteins to be more efficiently purified and therefore increase the sensitivity over ABE. An initial proof-of-principle was performed using bovine brain membrane proteins, showing detection of the palmitoyl-proteins $G\alpha_z$ and growth-associated protein of 43 kDa (GAP43; neuromodulin) by immunoblotting but not synaptophysin, which is known not to be palmitoylated. The characterisation of acyl-RAC was extended by examining H-Ras, which is known to be palmitoylated on cysteine residues 181 and 184 and farnesylated on cysteine-186 (Hancock *et al.*, 1989), in human embryonic kidney 293 (HEK293) cells. Wild-type but not unpalmitoylatable C181/184S mutants were detected, showing specificity of acyl-RAC for palmitoylation over

prenylation. Treatment of cells expressing wild-type H-Ras with varying concentrations of the palmitoylation inhibitor 2-bromopalmitate (2-BP) showed the semi-quantitative nature of acyl-RAC, which is similar to ABE. This study then extended acyl-RAC by labelling experimental and control HEK293 cells with reporter tags of different atomic masses. By performing the trypsin digestion for mass spectrometry whilst the proteins were still bound to the resin, they were able to identify palmitoylation sites on 84 proteins. These included both previously known sites and novel sites, a few of which were validated using cysteine to serine mutants. This illustrates the potential of acyl-RAC not only to provide palmitoyl-proteomes but palmitoyl site identification as well which will be valuable given the present lack of consensus motifs for predicting palmitoylation sites.

None of these methods has been used with *Caenorhabditis elegans*. In this chapter, ABE and acyl-RAC approaches will first be tested on rat brain homogenate and compared with published results to determine an efficient protocol. Both methods will then be applied to wild-type *C. elegans* lysate to identify its palmitoyl-proteome. These methods will also be applied to the acyl-protein thioesterase 1 (*ath-1*) knockout strain RB1484. In the many published accounts of palmitoyl-proteomes in different species and cell types, some have looked at the effects of disrupting one or more palmitoyl acyl-transferase (PAT) enzymes but none have looked at mutation of a palmitoyl-protein thioesterase (PPT). However, an analysis has been done using an inhibitor of PPTs to enrich palmitoyl-proteins undergoing rapid palmitate turnover in the analysis of mouse T cell hybridoma cells (Martin *et al.*, 2012). Of the two PPTs in *C. elegans*, PPT-1 is the orthologue of a PPT localised to lysosomes, synaptic vesicles and synaptosomes (Lehtovirta *et al.*, 2001; Verkruyse and Hofmann, 1996) whereas ATH-1 is the orthologue of a cytoplasmic PPT, acyl-protein thioesterase 1 (APT1), which is not restricted to certain subcellular regions (Duncan and Gilman, 1998). APT1 was recently shown to be palmitoylated itself (Yang *et al.*, 2010) which may provide an element of substrate specificity by regulation of its subcellular localisation. The knockout of *ath-1* was chosen to compare with the wild-type palmitoyl-proteome as it was reasoned that it may be responsible for depalmitoylation of a wider range of substrates and so may have more of an effect. It would be expected that disruption of PPT activity would result in a roadblock effect, with build-up of palmitate on proteins with either a high palmitate turnover or a slow rate of palmitoylation which is no longer counteracted. These proteins would appear only in the *ath-1* mutant palmitoyl-proteome. The wild-type palmitoyl-proteome will be the first achieved in *C. elegans* and

comparative analysis with the *ath-1* mutant palmitoyl-proteome may provide some insights into important substrates of this enzyme.

5.2 METHODS

5.2.1 NEMATODE CULTURE

5.2.1.1 STRAINS

Wild-type N2 *C. elegans* and *ath-1* knockout strain RB1484 were obtained from the *Caenorhabditis* Genetics Center (University of Minnesota, Twin Cities, MN, USA). *Escherichia coli* OP50 strain was obtained from the *Caenorhabditis* Genetics Center.

5.2.1.2 PLATES

C. elegans were cultured in 60 mm plates on nematode growth medium agar (NGM; 2% (w/v) agar, 0.3% (w/v) NaCl, 0.25% (w/v) peptone, 1 mM $CaCl_2$, 5 µg ml^{-1} cholesterol, 25 mM KH_2PO_4, 1 mM $MgSO_4$) at 20 °C, seeded with 30 µl *E. coli* OP50 culture as a food source, using standard methods (Brenner, 1974).

5.2.1.3 LIQUID CULTURE

S medium was first made. 1 ml 5 mg ml^{-1} cholesterol in ethanol was added to 1 l sterile S basal (5.845 g l^{-1} NaCl, 1 g l^{-1} K_2HPO_4, 6 g l^{-1} KH_2PO_4). A trace metals solution (1.86 g l^{-1} disodium EDTA, 0.69 g l^{-1} $FeSO_4 \bullet 7H_2O$, 0.2 g l^{-1} $MnCl_2 \bullet 4H_2O$, 0.29 g l^{-1} $ZnSO_4 \bullet 7H_2O$, 0.025 g l^{-1} $CuSO_4 \bullet 5H_2O$) and 1 M potassium citrate solution (20 g l^{-1} citric acid monohydrate, 293.5 g l^{-1} tri-potassium citrate monohydrate, pH 6.0) were also made and sterilised. The trace metals solution was stored in the dark. To make S medium, 10 ml 1 M potassium citrate pH 6.0, 10 ml trace metals solution, 3 ml 1 M $CaCl_2$ and 3 ml 1 M $MgSO_4$ were added to 1 l S basal.

1 l sterile Luria-Bertani broth (LB; 1% tryptone, 0.5% yeast extract, 1% NaCl) was seeded with 1 ml of an overnight culture of *E. coli* OP50 in LB and grown overnight at 37 °C, 200 rpm. The bacteria were harvested by centrifugation in clean bottles at 4000 rpm, 4 °C for 10 minutes. The supernatant was discarded and the pellets resuspended in 25 ml sterile S medium. Concentrated OP50 was stored at 4 °C.

Four 100 mm NGM plates were seeded with 100 µl OP50 spread into a lawn. The following day a chunk of a full plate of well-fed worms was put on each plate. Once the plates were full but not starved, they were bleached to extract eggs as follows. Each plate was washed with 3.5 ml sterile H_2O and collected in a 15 ml Falcon tube. 1.5 ml bleach mixture (two

parts commercial bleach to one part 5 M NaOH) was added and the tube vortexed well every two minutes for a total of 10 minutes. The tubes were centrifuged at 1500 rpm for one minute and the supernatant removed. 5 ml sterile H_2O was added and the tubes vortexed before centrifuging again. The supernatant was removed to leave the eggs in about 1 ml of H_2O. The eggs were added to 475 ml S medium and 25 ml concentrated OP50 in a two litre flask. The flask was incubated at 20 °C, 160 rpm over several days until the OP50 had been consumed as assessed by viewing a sample under a dissection microscope.

To harvest the worms, the flask was tilted on ice for at least 60 minutes to allow the worms to collect at the bottom before removing most of the liquid. The worms were moved into 50 ml Falcon(s) and washed with 0.1 M NaCl. The tubes were spun at 700 rpm, 4°C for 2 minutes with little or no braking to preserve the worm pellet. The supernatant was removed and the worms resuspended in 0.1 M NaCl added to 20 ml total and mixed with 20 ml ice-cold 60% (w/v) sucrose. The tubes were spun at 700 rpm, 4 °C for 5 minutes to 'float' the worms. The worms were transferred to another tube using a glass Pasteur pipette and washed twice with 0.1 M NaCl, spinning at 700 rpm, 4 °C for 2 minutes between washes. The worms were transferred to pre-weighed Eppendorf tubes in 500 µl aliquots, weighed again to determine the yield of worms and stored at -80 °C.

5.2.2 PROTEIN BIOCHEMISTRY

5.2.2.1 PREPARATION OF LYSATES

5.2.2.1.1 RAT BRAIN

10 ml homogenisation buffer (HB; 0.32 M sucrose, 10 mM HEPES pH 7.4) containing one Complete Mini EDTA-free protease inhibitor (PI) tablet (Roche, Mannheim, Germany) was made up and pre-chilled on ice. An adult female Sprague Dawley rat brain, snap-frozen (SeraLab, Barnet, UK), was thawed on ice in about 5 ml HB. The brain was cut into pieces that were as small as possible using dissection scissors on a glass plate. The brain was transferred to a specialised glass tube, the remaining HB added and processed using an electric homogeniser (Janke & Kunkel K.G., now IKA®-Werke GmbH & Co. K.G., Staufen, Germany) until homogenous. The homogenate was spun at 3500 rcf at 4 °C for five minutes to remove debris. The supernatant was split into 1 ml aliquots in Eppendorf tubes and sodium dodecyl sulphate (SDS) added to 2% final concentration. These were rotated for 10-20 minutes at room temperature and spun at 14000 rpm, 4 °C for five minutes. The supernatant was transferred to a 15 ml Falcon tube for use in the assays.

5.2.2.1.2 NEMATODES

Worm pellets were frozen at -80 °C and thawed on ice before use. Up to 500 µl worms and an equal volume of worm homogenisation buffer (WHB: 140 mM KCl, 1 mM EDTA, 50 mM HEPES pH 7.4, 2% SDS) with PIs were put in a 2 ml round-bottom cryogenic vial (Corning, Amsterdam, the Netherlands). 425-600 µm acid-washed glass beads (Sigma, Dorset, UK) were added up to the meniscus using a tip box lid. Tubes were shaken in a Mikro-Dismembrator S (B. Braun Biotech International, Melsungen, Germany) at 2000 rpm for two minutes. Three holes were made in the base of each tube with a BD Microlance™ 3 25G (Becton Dickinson & Co. Ltd, Ireland). The tube was placed in a 15 ml Falcon and spun at 5000 rpm, 4 °C for five minutes. The lysate was transferred to Eppendorfs and spun at 13000 rpm, 4 °C for 20 minutes. The supernatant was transferred to fresh tubes and used immediately.

5.2.2.2 BICINCHONINIC ACID ASSAY

The concentration of protein in a sample was determined by a BCA assay. The working range of this assay is 0.02-2.0 mg ml^{-1}, so in addition to the neat sample, dilutions of 1:10 and 1:100 were also included. A Pierce® BCA Protein Assay Kit was used in the 96-well plate format. A series of standards of BSA in water ranging from 0 mg ml^{-1} to 2 mg ml^{-1} was prepared. Three replicates of each sample were included. The manufacturer's procedure was followed and the plate read at 595 nm in an Emax Precision Microplate Reader (Molecular Devices) and data analysed using SOFTmax (Molecular Devices, v2.35) and Microsoft® Office Excel® 2007.

5.2.2.3 PRELIMINARY TESTS

To determine the best depalmitoylation agent, 100 µl 2 M methyl methanethiosulphonate (MMTS) in N,N-dimethylformamide (N,N-DMF) (20 mM final concentration) was added to rat brain homogenate and made up to 10 ml with lysis buffer (LB; 150 mM NaCl, 50 mM Tris.HCl, 5 mM EDTA, pH 7.4) and a PI tablet was added. The mixture was incubated at room temperature for two hours. Three 500 µl samples were taken and treated with the following:

- 500 µl 2 M hydroxylamine (HA) pH 7.4 overnight at room temperature
- 500 µl 40 mM dithiothreitol (DTT) for one hour at 37 °C
- 500 µl 200 mM Tris pH 8.9 (high pH sample) for one hour at room temperature

Samples were subjected to Western blotting against cysteine string protein (CSP); its depalmitoylation is indicated by a mass shift from about 29 to 22 kDa.

The time required for complete depalmitoylation of samples was also assessed. 100 µl rat brain homogenate was incubated with an equal volume of 2 M HA pH 7.4 or 2 M Tris.HCl pH 7.4 for 30 minutes, one hour, two hours, four hours or overnight. Samples were subjected to three methanol precipitations (see ABE protocol, Section 5.2.2.4) to remove HA. Western blotting was performed against CSP to determine the extent of depalmitoylation by mass shift.

5.2.2.4 ACYL-BIOTIN EXCHANGE

The protocol presented here represents the optimised method, based on protocols previously published in proteomic analyses (Kang *et al.*, 2008; Roth *et al.*, 2006). Variations used whilst optimising the protocol are highlighted in Table 5.1. A schematic workflow of this method is shown in Figure 5.2.

1. Rat brain homogenate was made up to 10 ml with LB and a PI tablet was added. Worm lysates were transferred to a 15 ml Falcon, 2 ml 20% SDS was added, LB added to 10 ml total volume and a PI tablet added. From this point onwards all samples were treated the same. 500 µl was taken out, split into 100 µl aliquots and frozen at -80 °C to provide "input" for SDS-PAGE. 100 µl 2 M MMTS in N,N-DMF (20 mM final concentration) was added and the samples incubated at room temperature for two hours.
2. The sample was split into three 15 ml Falcon tubes and a methanol precipitation performed three times as follows:
    a. a three-times volume of -20 °C methanol was added and the tubes vortexed and spun at 3500 rcf, 4 °C for two minutes
    b. the supernatant was discarded and the pellet resuspended in 1 ml solubilisation buffer (SB; 4% SDS, 50 mM Tris.HCl, 5 mM EDTA, pH 7.4) and incubated at 37 °C, 220 rpm for 30 minutes
    c. the solution was made up to 4 ml total volume with LB + 0.2% Triton X-100 (LB-T)
3. The combined volume was split into two 15 ml Falcons. 5 ml 2 M HA pH 7.4 was added to one tube and 5 ml 2 M Tris.HCl pH 7.4 to the other (1 M final concentration). For the pH-based protocol, the experimental samples were treated with high pH buffer (200 mM Tris, 0.5% SDS, pH 8.9) and control samples with low pH buffer (200 mM Tris, 0.5% SDS, pH 6.5). 1.25 ml 4 mM EZ-link® N-[6-(biotinamido)hexyl]-3'-(2'-pyridyldithio)propionamide (biotin-HPDP) (Thermo Scientific, Rockford, IL, USA) stock was added to each tube (0.5 mM final

Method	Source material	Output	Test	Result	Notes
ABE	1x rat brain	Western blot	compared NEM and MMTS as blocking agents	MMTS gave consistently stronger and tighter bands	
ABE	1x rat brain	Western blot	HA reaction speed	overnight incubation required	see Figure 5.4B
			compared biotin-BMCC and biotin-HPDP as thioreactive agents	biotin-BMCC shows signal in control lanes; biotin-HPDP shows much more specific signal	
			doubled amount of beads used	improved signal in HA-treated samples	
ABE	2x rat brain	SDS-PAGE stained with ProtoSafe Blue		enrichment in HA-treated sample	
		Western blot		specific signal for CSP, SNAP-25, VAMP-2; no signal for syntaxin-3	
		mass spectrometry		227 hits; many expected but also several suspected non-specific hits	
ABE	10x 100 mm plates N2 strain *C. elegans*	SDS-PAGE stained with ProtoSafe Blue	initial test on *C. elegans* material	apparent slight overall enrichment in HA-treated over control sample	lysis method: One Shot Cell Disrupter
ABE	1x rat brain	SDS-PAGE stained with ProtoSafe Blue; Western blot	comparison of HA, DTT and high pH to cleave palmitates	only HA gave an increase in mobility of CSP and SNAP-25	see Figure 5.4A
			full ABE using pH method	no signal in eluates – all in unbound fraction	see Figure 5.5A
			trial of 1% β-ME elution	moderate improvement in specificity	
ABE	1x rat brain	SDS-PAGE stained with ProtoSafe Blue; Western blot	1% β-ME elution with MeOH precipitation to concentrate eluate	specific signal in HA-treated lane; considerable signal from CSP and syntaxin-1, but not Munc18	see Figure 5.5B, C
ABE	8x 100 mm plates N2 strain *C. elegans*	SDS-PAGE stained with ProtoSafe Blue or silver stained; Western blotting[1]	test using improved elution	no difference between HA-treated and control in β-ME or Laemmli elutions; very little protein visible in final eluates	lysis method: One Shot Cell Disrupter; tested other lysis methods after this experiment (see Section 5.3.1)
ABE	5 ml concentrated N2 strain *C. elegans* from liquid culture (~4 ml homogenate)	SDS-PAGE stained with ProtoSafe Blue or silver stained; Western blotting[1]	much greater protein input (~16 mg)	some specific bands in HA-treated sample but difficult to detect even with silver stain	

Method	Source material	Output	Test	Result	Notes
ABE	10 ml concentrated N2 strain *C. elegans* from liquid culture (~7 ml homogenate)	SDS-PAGE with silver staining	MeOH precipitation of initial homogenate to remove potential non-protein contaminants	BCA assay showed overall input reduced from ~70 mg to~50 mg protein by this step	
			greater protein input	still only trace protein in final eluates	
acyl-RAC (NaCl control)	1x rat brain	SDS-PAGE stained with ProtoSafe Blue	initial acyl-RAC test	enrichment in HA-treated sample, although β-ME elution ran strangely	
		Western blotting		expected HA-specific signal for CSP and SNAP-25	
ABE	concentrated *C. elegans* from liquid culture: 2 ml N2; 3.5 ml *dhhc-14* mutant; 3 ml *ath-1* mutant	SDS-PAGE stained with ProtoSafe Blue		essentially no signal after input	final method
acyl-RAC (NaCl control)	concentrated *C. elegans* from liquid culture: 2 ml N2; 2.5 ml *dhhc-14* mutant; 2.5 ml *ath-1* mutant	SDS-PAGE stained with ProtoSafe Blue		essentially no signal after input	final method
		SDS-PAGE with silver staining		essentially no signal after input	
acyl-RAC (Tris.HCl control)	1x rat brain	SDS-PAGE stained with ProtoSafe Blue	Tris.HCl control	specific signal in HA-treated sample	final method with mass spectrometry; rat and *C. elegans* material processed in parallel; see Figure 5.6B and Figure 5.7B
	concentrated *C. elegans* from liquid culture: 1x 2 ml N2 1x 4 ml N2 1x 2.5 ml *ath-1* mutant 1x 5.5 ml *ath-1* mutant	SDS-PAGE with silver staining		only 4 ml N2 sample gave specific bands in HA-treated sample	
ABE	1x rat brain			specific signal in HA-treated sample	final method with mass spectrometry; rat and *C. elegans* material processed in parallel; BCA assays on inputs showed final signal correlated with input concentration; see Figure 5.6A and Figure 5.7A, C
	concentrated *C. elegans* from liquid culture: 1x 2.5 ml N2 1x 4 ml N2 1x 3 ml *ath-1* mutant 1x 5.5 ml *ath-1* mutant	SDS-PAGE with silver staining		both N2 samples and 5.5 ml *ath-1* sample gave specific bands in HA-treated sample	

[1] Western blotting was attempted with anti-RIC-4 (SNAP-25 orthologue) and anti-DNJ-14 (CSP orthologues) antibodies, but no immunoreactivity was observed even in the input lane.

TABLE 5.1: Optimisation of acyl-biotin exchange and acyl-resin-assisted capture

All ABE and acyl-RAC experiments are listed in chronological order along with the specific aspect of the protocol being tested or altered, if any, and the outcome. The final methods can be found in Sections 5.2.2.4 (ABE) and 5.2.2.5 (acyl-RAC). β-ME, β-mercaptoethanol; ABE, acyl-biotin exchange; acyl-RAC, acyl-resin-assisted capture; *ath*, acyl-protein thioesterase; BCA, bicinchoninic acid; biotin-BMCC, 1-biotinamido-4-[4'-(maleimidomethyl)cyclohexanecarboxamido]butane; biotin-HPDP, N-[6-(biotinamido)hexyl]-3'-(2'-pyridyldithio)propionamide; CSP, cysteine string protein; DTT, dithiothreitol; HA, hydroxylamine; MeOH, methanol; MMTS, methane methylthiosulphonate; Munc18, mammalian UNC-18; NEM, N-ethylmaleimide; SDS-PAGE, sodium dodecylsulphate polyacrylamide gel electrophoresis; SNAP-25, synaptosomal-associated protein of 25 kDa; VAMP, vesicle-associated membrane protein.

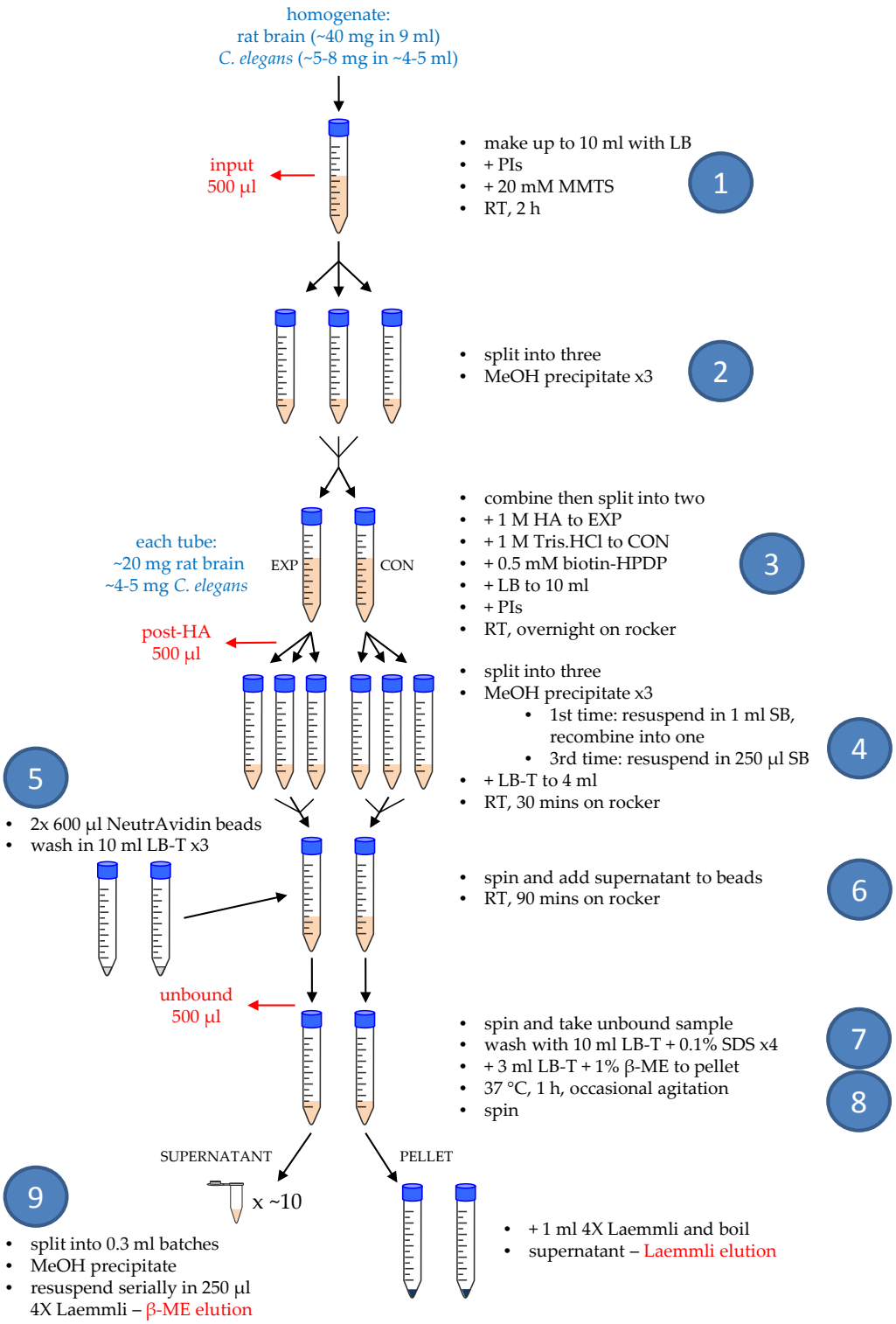

FIGURE 5.2: Flow diagram of acyl-biotin exchange methodology

A summary of the experimental process of acyl-biotin exchange is shown, including approximate quantities of material (blue) and points at which samples are removed for subsequent SDS-PAGE and Western blotting analysis (red). The numbers in blue circles refer to the step numbers in Section 5.2.2.4. β-ME, β-mercaptoethanol; biotin-HPDP, N-[6-(biotinamido)hexyl]-3'-(2'-pyridyldithio)propionamide; CON, control sample; EXP, experimental sample; HA, hydroxylamine; LB, lysis buffer; LB-T, lysis buffer + 0.2% Triton X-100; MMTS, methyl methanethiosulphonate; PI, protease inhibitor; RT, room temperature; SB, solubilisation buffer; SDS-PAGE, sodium dodecyl sulphate polyacrylamide gel electrophoresis.

3. *[continued]* concentration), both were made up to 10 ml with LB and a PI tablet was added. Tubes were incubated at room temperature on a rocker overnight.
4. The next day, 500 µl was taken aside from each tube, split into 100 µl aliquots and frozen at -80 °C to give "post-HA" for SDS-PAGE. Each main sample was divided into three tubes and a methanol precipitation performed. Each treatment was combined back into one tube and made up to 4 ml total with LB-T before methanol precipitating a second time. In the third methanol precipitation, 250 µl SB was used for solubilisation and the solution was then made up to 10 ml with LB-T before incubating on a rocker at room temperature for 30 minutes.
5. Meanwhile, 600 µl NeutrAvidin® UltraLink® Resin (Thermo Scientific, Rockford, IL, USA) was put in a 15 ml Falcon for each sample. These were washed three times in 10 ml LB-T and spun at 3500 rcf, 4 °C for two minutes between washes.
6. The samples (from step 4) were spun at 3500 rcf, 4 °C for two minutes. Their supernatant was added to the washed beads and incubated at room temperature on a rocker for 90 minutes.
7. After spinning at 3500 rcf, 4 °C for two minutes, 500 µl of the supernatant was taken and stored at -80 °C to use as "unbound" in SDS-PAGE. The pellet was washed four times with 10 ml LB-T + 0.1% SDS, spinning at 3500 rcf, 4 °C for two minutes between washes.
8. Proteins were eluted in 3 ml LB-T + 1% β-mercaptoethanol (β-ME) by incubating at 37 °C for one hour with occasional agitation. The samples were spun at 3500 rcf, 4 °C for two minutes. The supernatant was removed and treated as step 9 below. 1 ml 4X Laemmli buffer (8% SDS, 40% glycerol, 20% β-ME, 0.008% bromophenol blue, 0.25 M Tris.HCl, pH 6.8) was added to the bead pellet, which was resuspended and boiled – the supernatant of which ("Laemmli elution") was taken off and stored at -20 °C.
9. The supernatant from above was split into 0.3 ml aliquots in 1.5 ml Eppendorfs. A three-times volume of -20 °C methanol was added, the tubes were vortexed and then spun at 10000 rpm, 4 °C for five minutes. The supernatant was discarded carefully. The pellet from the first tube was resuspended in 250µl 4X Laemmli buffer. The same 250 µl was transferred to the next tube to resuspend that pellet and so on, giving the "β-ME elution".

5.2.2.5 ACYL-RESIN-ASSISTED CAPTURE

The protocol presented here represents the optimised method, based on a protocol previously published in a proteomic analysis (Forrester *et al.*, 2011). Variations used whilst optimising the protocol are highlighted in Table 5.1. A schematic workflow of this method is shown in Figure 5.3.

1. A BCA assay was performed on all homogenates to determine their concentrations. Each sample was diluted to 2 mg ml^{-1} with blocking buffer (100 mM HEPES, 1 mM EDTA, 2.5% SDS, pH 7.4). An aliquot for SDS-PAGE was taken and frozen at -80 °C ("input"). The volume of the aliquot depended on the total volume available.
2. MMTS was added to 0.5% and the samples incubated at 40 °C for one hour with frequent vortexing.
3. The samples were methanol precipitated three times in as few tubes as possible. They were recombined back into one tube after the first solubilisation. The final time, the samples were resuspended in 1 ml binding buffer (100 mM HEPES, 1 mM EDTA, 1% SDS, pH 7.4) instead of SB and incubated at 37 °C, 220 rpm for 30 minutes.
4. Meanwhile, 0.25 g thiopropyl Sepharose® 6B beads (Sigma, Dorset, UK) per sample were washed in 20 ml distilled water for 15 minutes. 1 g thiopropyl Sepharose® 6B will normally swell to 4-5 ml volume. The beads were spun at 3500 rcf, 4 °C for two minutes, the supernatant removed and an equal volume of binding buffer added to the settled slurry.
5. Each sample from step 3 was split into two tubes and 1 ml slurry added to each. An equal volume of 2 M HA pH 7.4 was added to one tube, an equal volume of 2 M Tris.HCl pH 7.4 to the other and a PI tablet added. Samples were incubated on a rocker at room temperature overnight.
6. The following day, samples were spun at 3500 rcf, 4 °C for two minutes. 1 ml was taken from the supernatant of each tube ("unbound") and frozen at -80°C. The remaining supernatant was discarded. The bead pellet was washed five times with 5 ml binding buffer, spinning at 3500 rcf, 4 °C for two minutes between washes.
7. Proteins were eluted in 3 ml LB-T + 1% β-ME by incubating at 37 °C for one hour with occasional agitation. The samples were spun at 3500 rcf, 4 °C for two minutes. The supernatant was removed and treated as step 8 below. 1 ml 4X Laemmli was added to the bead pellet, which was resuspended and boiled. The supernatant was taken off and stored at -20 °C ("Laemmli elution").

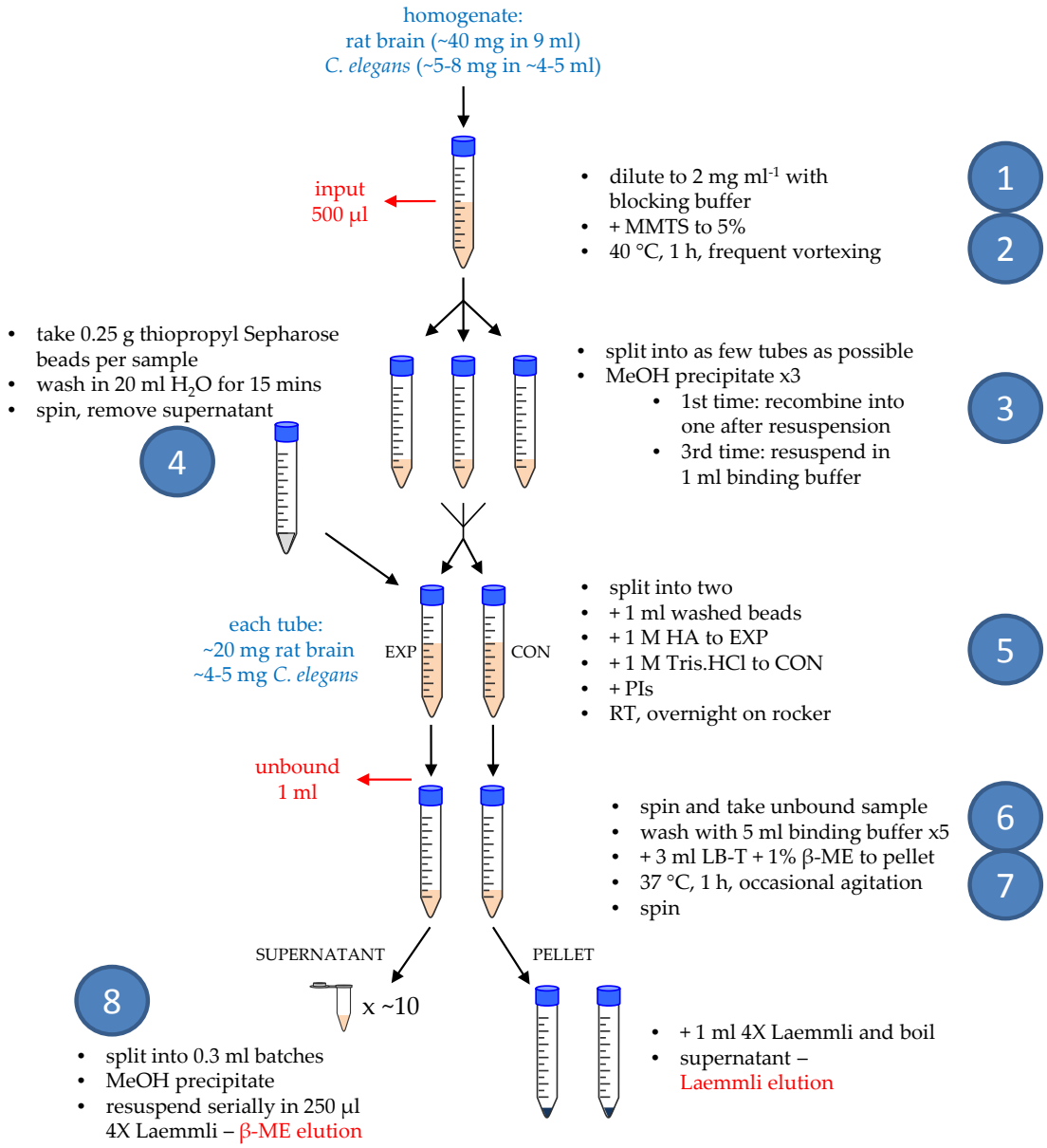

FIGURE 5.3: Flow diagram of acyl-resin-assisted capture methodology

A summary of the experimental process of acyl-resin-assisted capture is shown, including approximate quantities of material (blue) and points at which samples are removed for subsequent SDS-PAGE and Western blotting analysis (red). The numbers in blue circles refer to the step numbers in Section 5.2.2.5. β-ME, β-mercaptoethanol; CON, control sample; EXP, experimental sample; HA, hydroxylamine; LB-T, lysis buffer + 0.2% Triton X-100; MMTS, methyl methanethiosulphonate; PI, protease inhibitor; RT, room temperature; SDS-PAGE, sodium dodecyl sulphate polyacrylamide gel electrophoresis.

8. The supernatant from step 7 was split into 0.3 ml aliquots in Eppendorfs. A three-times volume of -20 °C methanol was added, the tubes were vortexed and then spun at 10000 rpm, 4 °C for five minutes. The supernatant was discarded carefully. The pellet from the first tube was resuspended in 250µl 4X Laemmli buffer. The same 250 µl was transferred to the next tube to resuspend that pellet and so on, giving the "β-ME elution".

5.2.3 SAMPLE ANALYSIS

5.2.3.1 SDS-PAGE

Separation of protein samples was performed using SDS-polyacrylamide gel electrophoresis (SDS-PAGE). Samples were prepared by boiling in Laemmli buffer at 95 °C for five minutes. 15% gels were cast in the Mini PROTEAN 3 system (BioRad, Hemel Hempstead, UK) or pre-cast NuPAGE® 12% Bis-Tris Gels were also used (Life Technologies, Paisley, UK).

Samples were loaded alongside 5 µl pre-stained protein ladder (Geneflow, Fradley, UK). Gels were run at 180-200 V until the dye reached the bottom of the gel. Gels were visualised by staining with Coomassie Blue, ProtoBlue Safe (Geneflow, Fradley, UK) or IRBlue (Licor, Lincoln, NE, USA), or by silver staining. Gels were imaged in a ChemiDoc XRS with Quantity One software (Biorad).

5.2.3.2 SILVER STAINING

Silver staining of polyacrylamide gels is a more sensitive procedure, allowing protein bands at lower concentrations to be detected. The gel is fixed in 50% methanol, 10% acetic acid for 30 minutes, then 5% methanol, 7% acetic acid for 30 minutes, followed by two 15 minute washes in water. 0.2 mg ml^{-1} sodium thiosulphate was added for one minute, followed by two two minute washes in water. 100 ml 0.1% $AgNO_3$ supplemented with 8 µl formaldehyde was added for 30 minutes, followed by a one minute wash in water. The gel was developed in 100 ml 6% Na_2CO_3 supplemented with 48 µl formaldehyde. The reaction was stopped by adding 10 ml 2.3 M citric acid. Gels were imaged in a ChemiDoc XRS with Quantity One software. Gels were stored in 20% ethanol at 4 °C.

5.2.3.3 WESTERN BLOTTING

Proteins were transferred to nitrocellulose submerged in transfer buffer (0.025 M Tris, 0.192 M glycine, 20% methanol) in a BioRad Trans-blot Electrophoresis Transfer Cell, either at 100 V for one hour with an ice pack or 20 V overnight. Nitrocellulose was blocked for one hour in Tris-buffered saline (TBS; 20 mM Tris, 140 mM NaCl, pH 7.4) with 0.1% Tween 20 (TBS-T) and 5% (w/v) dried skimmed milk. The primary antibody was applied at

an appropriate dilution in TBS-T supplemented with 5% (w/v) BSA and incubated on a rocker for either one hour at room temperature or at 4 °C overnight. The nitrocellulose was washed three times in TBS-T for five minutes before incubation in an appropriate HRP-conjugated secondary antibody at 1:2000 dilution for one hour on a rocker. The nitrocellulose was rinsed with TBS-T and visualised using enhanced chemiluminescence (ECL) reagents A (2.5 mM luminol, 400 µM *p*-coumaric acid, 100 mM Tris.HCl pH 8.5) and B (0.018% H_2O_2, 100 mM Tris.HCl pH 8.5) mixed 1:1. Imaging was performed in a ChemiDoc XRS using Quantity One software.

5.2.3.4 MASS SPECTROMETRY

5.2.3.4.1 DATA COLLECTION

The β-ME or Laemmli eluates were sent to Dr Mary Doherty (University of the Highlands and Islands, Inverness, UK) who kindly performed mass spectrometry on them. Briefly, the protein extracts were separated using one dimensional SDS-PAGE. Each gel lane was cut into 24 equal slices and digested with trypsin following reduction of any disulphide bonds with DTT and alkylation of free cysteine residues with iodoacetamide. The samples were then transferred into clean sample tubes and centrifuged to remove any debris. The protein digests were placed into glass vials prior to mass spectrometric analysis.

Peptide analysis by liquid chromatography-tandem mass spectrometry (LC-MS/MS) was performed in positive ion mode using a Thermo LTQ-Orbitrap XL LC-MS^n mass spectrometer equipped with a nanospray source and coupled to a Waters nanoAcquity ultra performance liquid chromatography (UPLC) system. The samples were initially desalted and concentrated on a BEH C18 trapping column (Waters, Milford, MA, USA). The peptides were then separated on a BEH C18 nanocolumn (1.7 µm, 75 µm x 250mm, Waters) at a flow rate of 400 nl min^{-1} using an acetonitrile-water gradient as follows:

Time (minutes)	Flow rate (µl min^{-1})	% Buffer A (0.1% formic acid)	% Buffer B (acetonitrile + 0.1% formic acid)
0	0.4	99.0	1.0
1	0.4	97.0	3.0
21	0.4	37.5	62.5
22.5	0.4	15.0	85.0
24.5	0.4	15.0	85.0
25.5	0.4	99.0	1.0

5 µl samples were injected onto the trapping column and washed with the initial conditions at a flow rate of 15 µl min^{-1} for one minute before starting the gradient. Spectra were collected using data-dependent acquisition in the range m/z 300-2000 following which

individual precursor ions were automatically fragmented using collision induced dissociation (CID).

5.2.3.4.2 DATA ANALYSIS

The data were subsequently analysed using Proteome Discoverer software (Thermo Scientific, Rockford, IL, USA) and MaxQUANT (http://maxquant.org/index.htm). Data were searched against a locally implemented MASCOT server (v2.3.01). The initial search parameters allowed for a single trypsin missed cleavage, carbamidomethyl modification of cysteine residues, oxidation of cysteine residues up to trioxidation, oxidation of methionine, N-terminal *N*-acetylation, a peptide mass tolerance of ± 10 ppm and a fragment mass tolerance of ± 0.8 Da. Peptide charge was +1, +2, +3 and the data were searched against both Swissprot and UniRef, Taxonomy – Rat or *C. elegans*.

After receiving these datasets from Dr Doherty, they were processed by removing trypsin, keratin and actin and discarding identifications which have been removed from official databases. The ratio of experimental:control scores was taken and any with a ratio of less than five were discarded (Martin and Cravatt, 2009). A control value of 0.2 was given to proteins present only in the experimental samples to avoid dividing by zero (Dowal *et al.*, 2011; Roth *et al.*, 2006; Yang *et al.*, 2010). Results were considered higher confidence if identified from multiple unique peptides and lower confidence if identified from a single unique peptide.

Venn diagrams were constructed using eulerAPE (University of Kent, http://www.eulerdiagrams.org/eulerAPE/; v2.0.3) and annotated in Microsoft® Office PowerPoint® 2010. Unfortunately there were insufficient repeats to perform robust statistical analysis of the mass spectrometry output.

5.3 RESULTS

5.3.1 OPTIMISATION AND APPLICATION OF ABE AND ACYL-RAC

Before attempting a proteomic analysis using *C. elegans* lysates, some initial tests were performed using rat brain homogenate to optimise the reactions as best as possible. First of all, various methods of removing the palmitate groups from palmitoyl-proteins were investigated. The classical ABE and acyl-RAC methods described above use HA to cleave the labile thioester bond between cysteine residues and palmitate groups. However, there have also been reports of disruption of this bond using 20 mM dithiothreitol (DTT) (Levental *et al.*, 2010) and high pH (J.R. Burgoyne, personal communication). In light of this, free

thiols on proteins in rat brain homogenate were blocked using MMTS and then treated with HA, DTT or high pH (Figure 5.4A). Samples were immunoblotted for cysteine string protein (CSP) because removal of all of its palmitate groups gives a detectable shift in molecular weight from approximately 29 kDa to 22 kDa (Gundersen *et al.*, 1994). This shift was only seen with treatment with HA (Figure 5.4A). Next it was investigated whether an overnight treatment with HA was truly necessary for complete depalmitoylation of a sample. Rat brain homogenate pre-treated with MMTS was incubated with HA for various lengths of time before removal of HA by methanol precipitation. This was found to be necessary as the HA reaction continued to completion if the samples were simply boiled in Laemmli buffer (data not shown). Samples were again immunoblotted for CSP, as it is the protein with the most known palmitoylated cysteine residues (Figure 5.4B). A gradual downward shift in the molecular weight of CSP with increasing length of HA treatment was seen with complete depalmitoylation only occurring with an overnight incubation, showing this is required.

Having established depalmitoylation conditions, a full scale ABE protocol was carried out on rat brain homogenate. Samples were taken after the HA treatment, from the solution after incubation with NeutrAvidin-conjugated beads (UB; unbound) and after eluting from the beads by boiling in 4X Laemmli (L) and were all immunoblotted for CSP (Figure 5.4C). All the HA-treated samples show the characteristic mass shift of depalmitoylated CSP. If a protein is palmitoylated, it should be present in the final eluate from the HA-treated sample but not the control sample. This is the case with CSP, which is specifically detected in the +HA eluate. There is still quite a lot of CSP retained in the unbound +HA sample however, suggesting incomplete binding to the beads. As a result of this, the quantity of beads used in the final binding was doubled for subsequent experiments. Given the successful detection of CSP, the unbound and eluted samples were also probed for other proteins (Figure 5.4D). Along with CSP, the known palmitoyl-proteins synaptosomal-associated protein of 25 kDa (SNAP-25) (Veit *et al.*, 1996) and vesicle associated membrane protein 2 (VAMP-2; synaptobrevin-2) (Veit *et al.*, 2000) are specifically found in the +HA elution. Syntaxin-1 was found to be palmitoylated in the first proteomic scale screen of mammalian material using this method (Kang *et al.*, 2008) and is also detected here. Syntaxin-3 was also probed as an overall negative control, as it contains no cysteine residues and so cannot be palmitoylated. Consistent with this, it is only detected in the unbound samples. Complexes of soluble NEM-sensitive fusion protein (NSF)-attachment protein (SNAP) receptor (SNARE) proteins have been shown to be resistant to denaturation by SDS even at

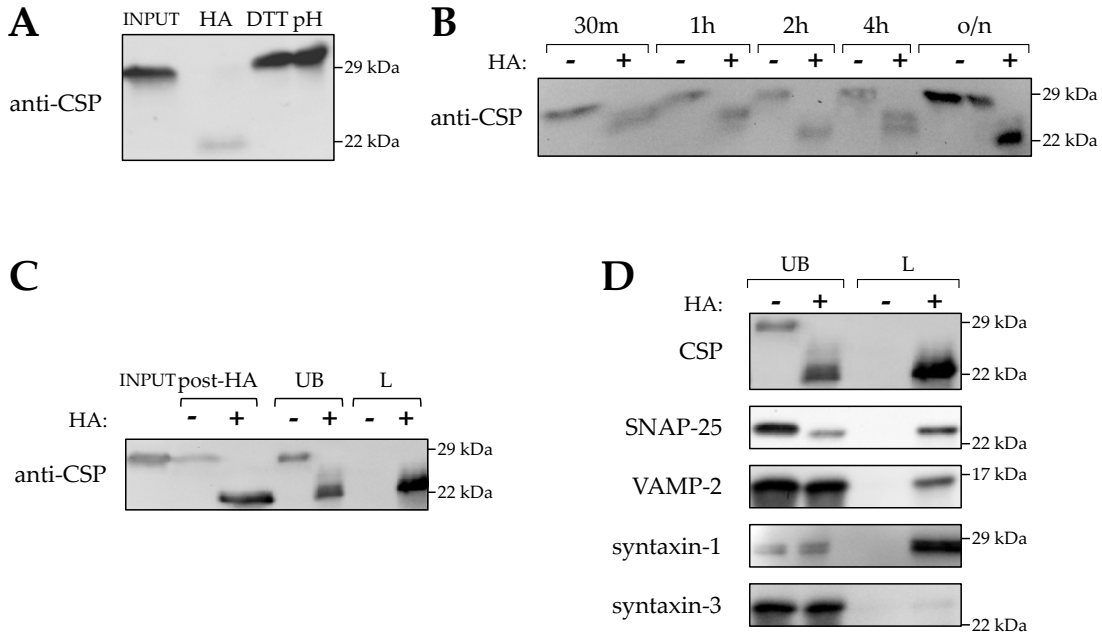

FIGURE 5.4: Initial optimisation tests

(A) Rat brain homogenate was treated with final concentrations of either 1 M HA overnight at room temperature, 20 mM DTT for one hour at 37 °C or 100 mM Tris pH 8.9 for one hour at room temperature. Samples were subjected to Western blotting and probed using anti-CSP. Removal of all palmitates results in a mass shift from 29 to 22 kDa. (B) Rat brain homogenate was treated with HA for the times shown. Protein was recovered by three methanol precipitations before subjecting to Western blotting and probing with anti-CSP. (C) Samples from an ABE experiment were subjected to Western blotting and probed with anti-CSP. Post-HA was taken after the HA treatment; unbound was the fraction that did not bind to NeutrAvidin-coated beads; the elution of proteins from the beads was performed with Laemmli buffer. (D) After ABE, unbound proteins and proteins eluted from the NeutrAvidin beads using Laemmli were subjected to Western blotting. Western blots were probed using antibodies against the proteins shown. ABE, acyl-biotin exchange; CSP, cysteine string protein; DTT, dithiothreitol; h, hours; HA, hydroxylamine; L, Laemmli buffer; m, minutes; o/n, overnight; SNAP-25, synaptosomal protein of 25 kDa; UB, unbound; VAMP, vesicle-associated membrane protein.

temperatures up to 80 °C (Hayashi *et al.*, 1994). As SDS is used in ABE, we were concerned that detection of syntaxin-1 might be a false positive if it was retained in SNARE complexes with SNAP-25. If this was the case then syntaxin-3 would also be detected in this way and so it served as a control for this effect as well.

The eluates from this initial ABE experiment were analysed using mass spectrometry, and after curation of the results there were many hits which seemed likely false positives, such as subunits of haemoglobin and actin at high abundance (data not shown). To try to combat this, a gentler elution condition from the beads was used. Instead of boiling in 4X Laemmli, the beads were incubated in a buffer containing 1% β-mercaptoethanol (β-ME) at 37 °C for an hour with occasional agitation. The beads were also boiled in 4X Laemmli after this elution to get a measure of how much of the genuine palmitoyl-proteins was being eluted with the β-ME. An initial test of this elution was performed using ABE methods with HA or pH as the depalmitoylating agent. Eluates were immunoblotted against SNAP-25 (Figure 5.5A). SNAP-25 was specifically detected in the HA-treated samples after the β-ME elution, and the relatively weak signal from the Laemmli elution suggests the majority of SNAP-25 has been released from the beads by β-ME. The complete lack of signal from the elutions of the pH-based protocol indicates that high pH is not sufficient to disrupt the thioester link to palmitate and this is not just a quirk of CSP (Figure 5.5A). To visualise the overall effect of using a β-ME elution over a Laemmli elution, samples from the HA-based ABE were subjected to sodium dodecyl sulphate polyacrylamide gel electrophoresis (SDS-PAGE) and the gel stained with ProtoBlue Safe (Figure 5.5B). At the post-HA treatment and unbound stages, there are roughly equal amounts of protein in both the experimental and control samples. The β-ME elution shows a clear enrichment of proteins in the HA-treated lane over the control lane. Whilst enrichment can also be seen in the Laemmli elutions, it is to a much lesser degree and there are clearly many non-specific bands which appear strongly in both HA and control treatments. These samples were also subjected to immunoblotting against various proteins (Figure 5.5C). The known palmitoyl-proteins CSP, SNAP-25 and syntaxin-1 show enrichment in the β-ME HA-treated sample in relation to both the control sample and the Laemmli HA-treated elution. The negative control syntaxin-3 continues to show no signal in the final elutions. Munc-18, the mammalian orthologue of *C. elegans* UNC-18, was also probed as it was one of the suspected false positive hits from the mass spectrometric analysis of the Laemmli elutions. Here it shows only the faintest hint of a signal after β-ME elution, and another faint signal after Laemmli elution. The total of these two signals may have been enough to push it over

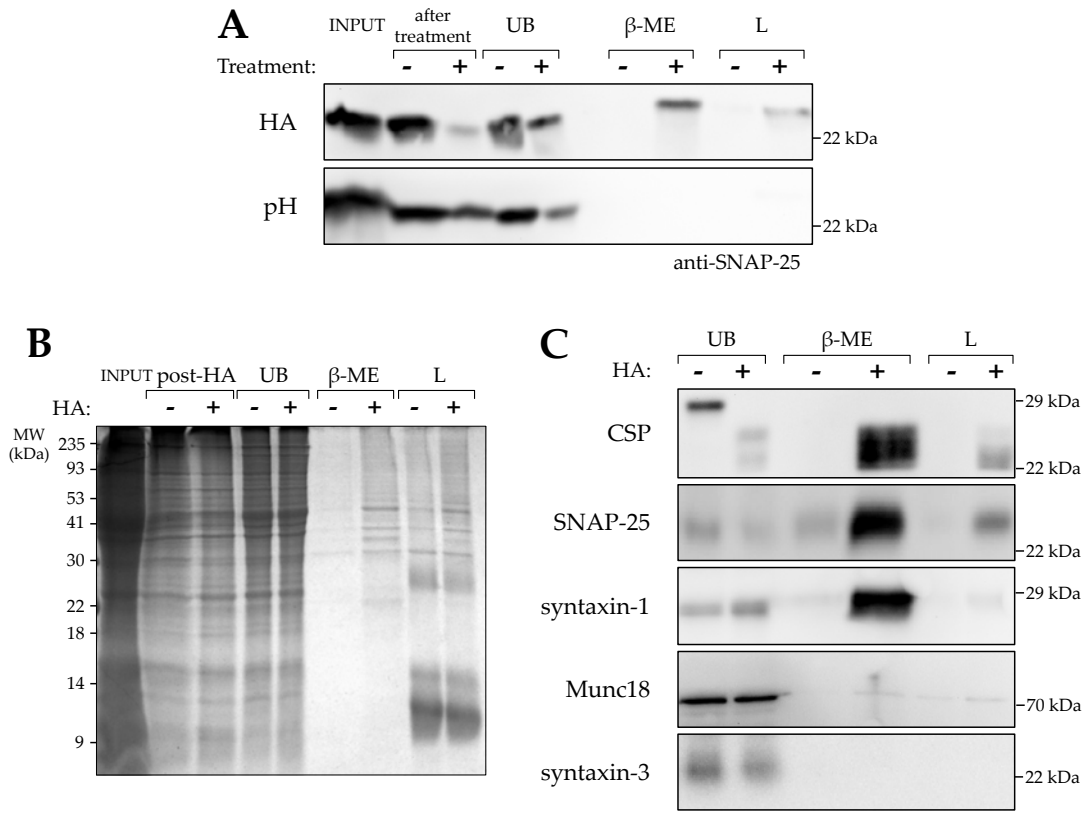

FIGURE 5.5: Comparison of different elution conditions

ABE was performed on rat brain homogenate. (A) The depalmitoylation step was performed using HA or high pH. Elutions were performed with 1% β-ME then Laemmli. Western blots were probed with anti-SNAP-25. (B) Elutions were performed with 1% β-ME then Laemmli. An SDS-PAGE gel stained using ProtoBlue Safe shows specific bands in the HA-treated samples, with less background using the β-ME elution. (C) Western blots were probed using antibodies against the proteins shown. β-ME, β-mercaptoethanol; ABE, acyl-biotin exchange; CSP, cysteine string protein; HA, hydroxylamine; L, Laemmli; Munc18, mammalian orthologue of UNC-18; SDS-PAGE, sodium dodecyl sulphate polyacrylamide gel electrophoresis; SNAP-25, synaptosomal protein of 25 kDa; UB, unbound.

the threshold for a hit with an elution solely in Laemmli. Such statistical flukes have been described previously in ABE and may result from chance underdetection in the control sample (Roth *et al.*, 2006). These data indicate that β-ME specifically elutes genuine palmitoyl-proteins from the beads whilst reducing contamination from non-specific proteins and so will be used from now on.

At this point, the alternative method of acyl-RAC came to our attention. Our initial attempt using rat brain homogenate and the control treatment of 2 M NaCl (Forrester *et al.*, 2011) was unsuccessful. However, changing the control treatment to 2 M Tris.HCl, as in ABE, solved this problem. Stained gels of rat brain homogenate ABE and acyl-RAC show specific bands in the HA-treated β-ME elution (Figure 5.6, asterisks). There is no post-HA sample in the acyl-RAC protocol because the HA treatment and binding to the resin occur in the same step. The improved specificity of the β-ME elution over the Laemmli elution can again be seen, both through better enrichment in HA-treated samples over control samples (Figure 5.6, arrows) and non-specific bands which are present in Laemmli elutions but absent from β-ME elutions (Figure 5.6, dagger). These β-ME elutions were also sent for mass spectrometric analysis as described below.

As both ABE and acyl-RAC were successful on rat brain homogenate, the next step was to apply it to lysates from wild-type *C. elegans*. There are several methods available to extract lysates from *C. elegans*, so these were compared to determine the most efficacious. Lysates from each method were subjected to a bicinchoninic acid (BCA) assay to determine protein concentration and compared with the rat brain homogenate, which was found to contain 4 mg ml^{-1} protein. An existing method in our lab using a One Shot Cell Disruptor (Constant Systems, Daventry UK) gave a protein concentration of 0.6 mg ml^{-1}. Snap freezing in liquid nitrogen, thawing and sonication (Van Raamsdonk and Hekimi, 2012) resulted in a concentration of 3 mg ml^{-1}. Grinding using a pestle and mortar under liquid nitrogen (Eimer *et al.*, 2007) gave a concentration of 1 mg ml^{-1}. An adaptation of a protocol for lysing *S. cerevisiae* by shaking with glass beads was found to give the highest protein concentration of 4 mg ml^{-1} and so was adopted as the lysis method (see Section 5.2.2.1.2).

Initial attempts of these assays on *C. elegans* were made using several large plates of animals but this resulted in an inability to detect more than trace amounts of protein from the final elutions on SDS-PAGE gels after silver staining. Mass spectrometric analysis of these samples turned up only non-specific and uncharacterised proteins and none of the expected putative palmitoyl-proteins discussed in Chapter 3. The observation of a small

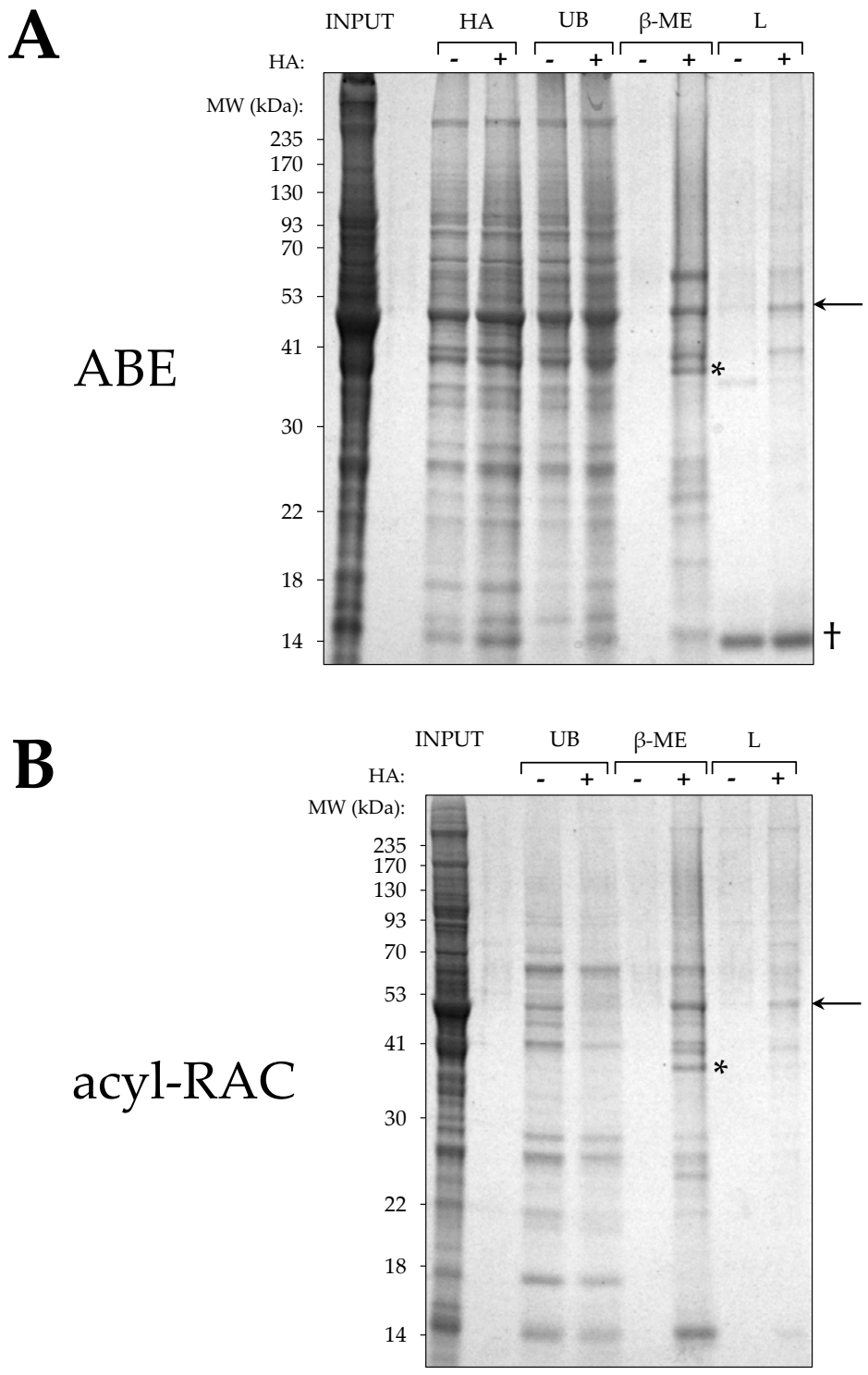

FIGURE 5.6: Selective purification of palmitoyl-proteins from rat brain homogenate

Rat brain homogenate was subjected to ABE (A) or acyl-RAC (B). SDS-PAGE gels were stained using IRBlue. Purification of palmitoyl-proteins is seen by an enrichment in the +HA samples compared with the -HA samples in the β-ME elutions. Examples are shown by symbols: an arrow shows bands enriched in the +HA samples with both β-ME and subsequent Laemmli elution; an asterisk shows bands enriched in the +HA samples only in the β-ME elution; a dagger shows non-specific bands which are present in the Laemmli elutions only. β-ME, β-mercaptoethanol; ABE, acyl-biotin exchange; acyl-RAC, acyl-resin-assisted capture; HA, hydroxylamine; HA (gel lanes), post-HA treatment sample; L, Laemmli; MW, molecular weight; SDS-PAGE, sodium dodecyl sulphate polyacrylamide gel electrophoresis; UB, unbound.

protein pellet in early methanol precipitation steps which quickly diminished and disappeared led us to suspect that then main problem was the starting amount of protein available. As large quantities of *C. elegans* can be grown relatively simply in liquid culture, this method was used to generate several millilitres of concentrated animals. Protein extracts from these were used for both ABE and acyl-RAC. SDS-PAGE gels of samples were silver stained (Figure 5.7A, B), as the final concentrations of protein were still small enough to be unclear at the level of Coomassie staining. Although relatively faint, there is enrichment in the HA-treated sample β-ME elution in the ABE experiment of bands which also appear in the Laemmli elution (Figure 5.7, arrow), whilst non-specific bands appear in the Laemmli elution only (Figure 5.7, dagger). The acyl-RAC protocol seems to result in much better protein recovery, presumably due to having much fewer methanol precipitation steps which probably each result in loss of a small amount of protein. Acyl-RAC also shows a specific β-ME HA-treatment signal, this time with several bands visible in the HA-treated β-ME elution only (Figure 5.7, asterisk). The ABE protocol was simultaneously carried out on an extract from a liquid culture of *ath-1* mutant animals, which again resulted in a specific β-ME signal after HA treatment (Figure 5.7C). Unfortunately, the acyl-RAC protocol was not successful on this strain and there was insufficient time to repeat it. The β-ME eluates from the successful *C. elegans* experiments were also subjected to mass spectrometric analysis.

5.3.2 MASS SPECTROMETRY

Eluates from two ABE and acyl-RAC experiments on rat brain homogenate and one each of wild-type *C. elegans* ABE and acyl-RAC and *ath-1* mutant strain RB1484 acyl-RAC were kindly analysed using mass spectrometry by our collaborator Dr Mary Doherty (University of the Highlands and Islands, Inverness, UK). A list of identified proteins for both the experimental (HA-treated) and control (Tris.HCl-treated) conditions was obtained for each experiment. After removing contaminants the ratio of the label-free quantification (LFQ) intensity for each protein was calculated; proteins which were not detected in the control sample were given a control value of 0.2 to avoid dividing by zero (Dowal *et al.*, 2011; Roth *et al.*, 2006; Yang *et al.*, 2010). Proteins which had an experimental:control ratio of less than 5 were also removed (Martin and Cravatt, 2009). Hits were divided into higher confidence hits, which had identifications from multiple peptides, and lower confidence hits, which were identified from a single peptide.

Analysis of ABE on rat brain homogenate yielded 105 higher confidence hits and 156 lower confidence hits (Appendix 3). All high confidence hits from previous proteomic screens

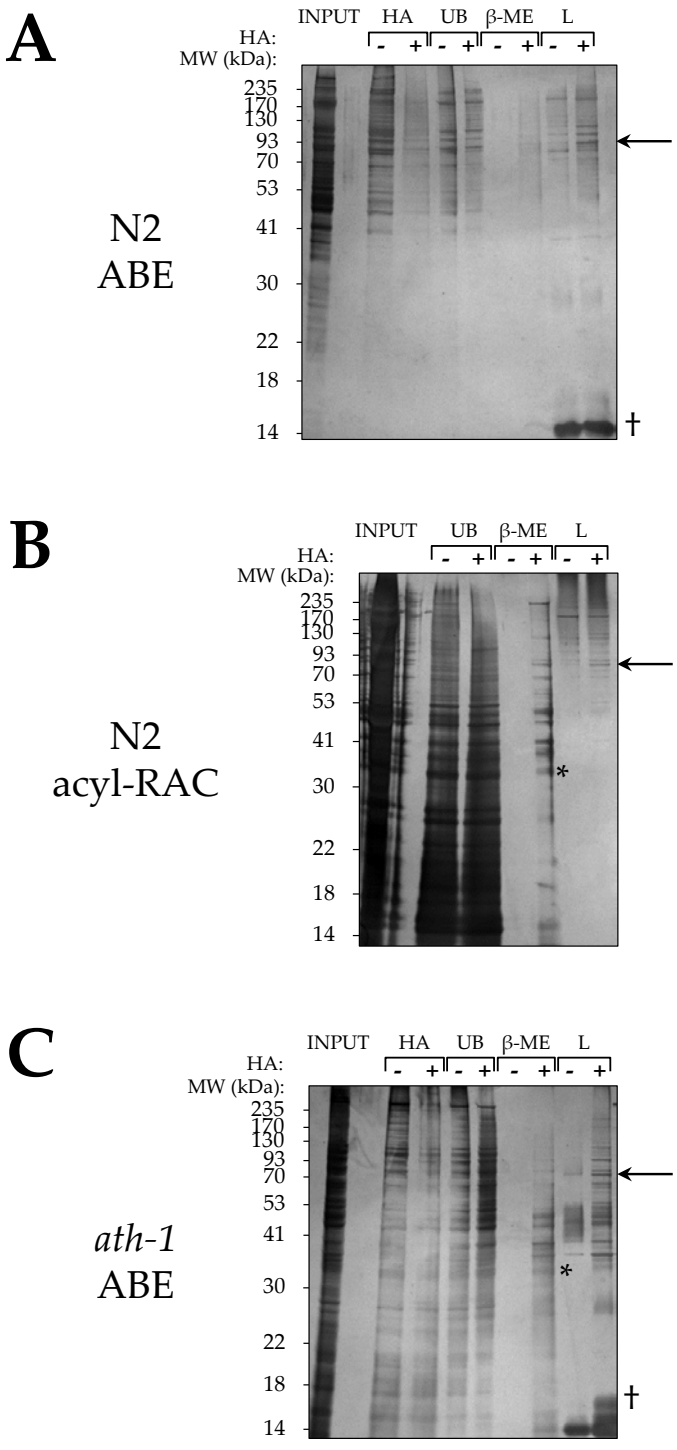

FIGURE 5.7: Selective purification of palmitoyl-proteins from *C. elegans* homogenates

Wild-type *C. elegans* homogenate was subjected to ABE (A) or acyl-RAC (B), and *ath-1* mutant *C. elegans* homogenate was subjected to ABE (C). SDS-PAGE gels were silver stained. Purification of palmitoyl-proteins is seen by an enrichment in the +HA samples compared with the -HA samples in the β-ME elutions. Examples are shown by symbols: an arrow shows bands enriched in the +HA samples with both β-ME and subsequent Laemmli elution; an asterisk shows bands enriched in the +HA samples only in the β-ME elution; a dagger shows non-specific bands which are present in the Laemmli elutions only. β-ME, β-mercaptoethanol; ABE, acyl-biotin exchange; acyl-RAC, acyl-resin-assisted capture; ath, acyl-protein thioesterase; HA, hydroxylamine; HA (gel lanes), post-HA treatment sample; L, Laemmli; MW, molecular weight; SDS-PAGE, sodium dodecyl sulphate polyacrylamide gel electrophoresis; UB, unbound.

using mammalian material were collated (Appendix 2) and compared with the hits presented here. Hits which had been previously found in proteomic studies accounted for 44% (46 of 105) of higher confidence hits and 27% (42 of 156) of lower confidence hits. Hits from rat brain homogenate using acyl-RAC totalled 63 higher confidence and 106 lower confidence hits (Appendix 4). Of these, 56% (35 of 63) of higher confidence hits and 23% (24 of 106) of lower confidence hits were previously found using proteomic methods. In addition a number of proteins which are known palmitoyl-proteins but were found as lower confidence hits in previous screens are present in these hits, notably GAP43/neuromodulin (Skene and Virag, 1989) and cell division control protein 42 (CDC42) (Kang *et al.*, 2008). Among the hits were also some likely false positives which use thioester linkages, such as the ubiquitin-conjugating enzymes UBE2L3 and UBE2D3.

100 proteins were found in common between the ABE and acyl-RAC analyses, which can be considered the highest confidence hits (Table 5.2). This corresponds to 38% (100 of 261) of the ABE hits and 59% (100 of 169) of the acyl-RAC hits. Of these common hits, 48% (48 of 100) were previously found in other proteomic screens and 17% (17 of 100) in a previous study using rat neuronal material (Kang *et al.*, 2008) (Figure 5.8). Both methods have been shown in this analysis to be able to purify known palmitoyl-proteins. The lower number of hits but higher proportion of known hits in the acyl-RAC experiment suggests that it is the better performing of the two methods in terms of selectivity. However in terms of absolute numbers the ABE method found more known hits. As both methods had merits, both were applied to *C. elegans* lysates.

The application of ABE to wild-type *C. elegans* lysate found four higher confidence hits and 33 lower confidence hits (Appendix 5). In contrast, acyl-RAC found 38 higher confidence hits and 24 lower confidence hits (Appendix 6). Any mammalian orthologues of these hits were found using basic local alignment search tool (BLAST) searching on WormBase (www.wormbase.org/) and these were compared with the list of previous hits from mammalian proteomic screens (Appendix 2) and the hits from rat brain homogenate in this study (Appendix 3, Appendix 4). For the ABE hits, 25% (1 of 4) of higher confidence and 22% (5 of 23) of lower confidence hits with mammalian orthologues had also been found elsewhere (Figure 5.9A). For acyl-RAC, all of the hits had mammalian orthologues. 55% (21 of 38) of higher confidence and 38% (9 of 24) of lower confidence hits had mammalian orthologues which had been previously found. Eight proteins were common between the two analyses, accounting for 22% (8 of 37) ABE and 13% (8 of 62) acyl-RAC hits (Table 5.3).

Gene	Protein	Abbreviation
Aco2	aconitate hydratase, mitochondrial	
Ak2	adenylate kinase 2, mitochondrial isoform 1	
Aldoa	fructose-bisphosphate aldolase A	
Aldoc	fructose-bisphosphonate aldolase C	
Amph	amphiphysin	
Atp1a1	sodium/potassium transporting ATPase subunit α1	
Atp1a2	sodium/potassium transporting ATPase subunit α2	
Atp1a3	sodium/potassium transporting ATPase subunit α3	
Atp1b1	sodium/potassium transporting ATPase subunit β1	
Atp1b2	sodium/potassium transporting ATPase subunit β2	
Atp5a1	ATP synthase subunit α, mitochondrial	
Avp	vasopressin-neurophysin 2-copeptin	
Cfl1	cofilin-1	
Ckb	creatine kinase B-type	
Cltc	clathrin heavy chain 1	
Cnp	2,3-cyclic-nucleotide 3-phosphodiesterase	
Crmp1	dihydropyrimidinase-related protein 1	
Dbn1	isoform A of drebrin	
Ddb2	damage specific DNA binding protein 2	
Dnajc5	DnaJ homolog subfamily C member 5; cysteine string protein	CSP
Dnm1	dynamin-1 isoform 1	
Dpysl2	dihydropyrimidinase-related protein 2	
Eno2	γ-enolase	
Fbn1	fibrillin-1	
Fxyd1	phospholemman	
Gap43	neuromodulin	
Gapdh	glyceraldehyde-3-phosphate dehydrogenase	
Gdi1	Rab-GDP dissociation inhibitor α	
Glul	glutamine synthetase	
Gnao1	guanine nucleotide-binding protein G(o) subunit α isoform α2	
Gpm6a	glycoprotein m6a	
Gstm1	glutathione *S*-transferase μ1	
Hk1	hexokinase-1	
Hsp90aa1	heat shock protein HSP90α	
Hsp90ab1	heat shock protein HSP90β	
Hspa1l	heat shock 70 kDa protein 1L	
Hspa8	heat shock cognate 71 kDa protein	
Kcnma1	calcium-activated potassium channel subunit α1 isoform 3	
Kcnq5l	PREDICTED: potassium voltage-gated channel subfamily KQT member 5 isoform 1	
Khsrp	far upstream element binding protein 2	
Kpnb1	importin subunit β1	
Ldha	L-lactate dehydrogenase A chain	
Ldhb	L-lactate dehydrogenase B chain	
Ldhb	L-lactate dehydrogenase B chain	
LOC100361349	hypothetical protein LOC100361349	
LOC682206	PREDICTED: LOW QUALITY PROTEIN: zinc finger protein 91	
Lrrc4b	leucine-rich repeat-containing protein	
Map1a	microtubule-associated protein 1A	
Map1a	microtubule-associated protein 1	
Map2	microtubule-associated protein 2 isoform MAP2x	
Mdh1	malate dehydrogenase, cytoplasmic	
Mdh2	malate dehydrogenase, mitochondrial	
Mt3	metallothionein 3	
Ncam1	neural cell adhesion molecule	
Ncdn	neurochondrin	
Ndrg2	N-Myc downstream regulated gene 2	
Ndrg2	N-Myc downstream regulated gene 2 isoform 1	
Ndufv2	NADH dehydrogenase flavoprotein 2, mitochondrial	
Nfxl1	nuclear transcription factor, X-box binding-like 1	
Pafah1b2	platelet-activating factor acetylhydrolase IB subunit β2	
Palm	paralemmin	
Palm	paralemmin	
Pebp1	phosphatidylethanolamine-binding protein 1	
Pgam1	phosphoglycerate mutase 1	
Pkm2	pyruvate kinase isozymes M1/M2 isoform M1	
Plp1	myelin proteolipid protein	
Ppp2r1a	protein phosphatase 2 regulatory subunit A	

Gene	Protein	Abbreviation
Prdx6	peroxiredoxin-6	
Rap1gds1	RAP1, GTP-GDP dissociation stimulator 1	
Rap2b	Ras-related protein Rap-2B	
Sdhb	succinate dehydrogenase iron-sulphur subunit, mitochondrial	
Sh3gl2	endophilin-A1	
Slc1a2	excitatory amino acid transporter 2 GLT1 subunit	EAAT2
Slc25a3	solute carrier family 25 (mitochondrial carrier, phosphate carrier), member 3	
Snap25	synaptosomal-associated protein of 25 kDa	
Snap91	clathrin coat assembly protein AP180 long isoform	
Stip1	stress-induced phosphoprotein 1	
Stx1a	syntaxin-1A	
Syx1b	syntaxin-1B	
Tomm70a	mitochondrial import receptor subunit TOM70	
Tpi1	triosephosphate isomerase	
Trappc3	trafficking protein particle complex subunit 3	Bet3
Tuba1a	tubulin α1A chain	
Tuba4a	tubulin α4A chain	
Tubb2a	tubulin β2A chain	
Tubb2c	tubulin β2C chain	
Tubb3	tubulin β3 chain	
Tubb4	tubulin β4	
Tubb5	tubulin β5 chain isoform 1	
Tubb5	tubulin β5 chain isoform 1	
Vamp2	vesicle-associated membrane protein 2; synaptobrevin 2	
Vcp	transitional endoplasmic reticulum ATPase	
Wisp1	WNT1-inducible-signaling pathway protein 1	
Ywhae	14-3-3 protein ε	
Ywhag	14-3-3 protein γ	
Ywhah	14-3-3 protein ε	
Ywhaq	14-3-3 protein θ	
Ywhaz	14-3-3 protein ζ/δ	
Zfp438	zinc finger protein 438	

TABLE 5.2: Hits found in both ABE and acyl-RAC using rat brain homogenate

Proteins identified in both ABE and acyl-RAC on rat brain homogenate are listed in alphabetical order of gene name. The abbreviation of the protein name is also given where it is different from the gene name. Hits also identified in previous proteomic studies are highlighted in green. ABE, acyl-biotin exchange; acyl-RAC, acyl-resin-assisted capture.

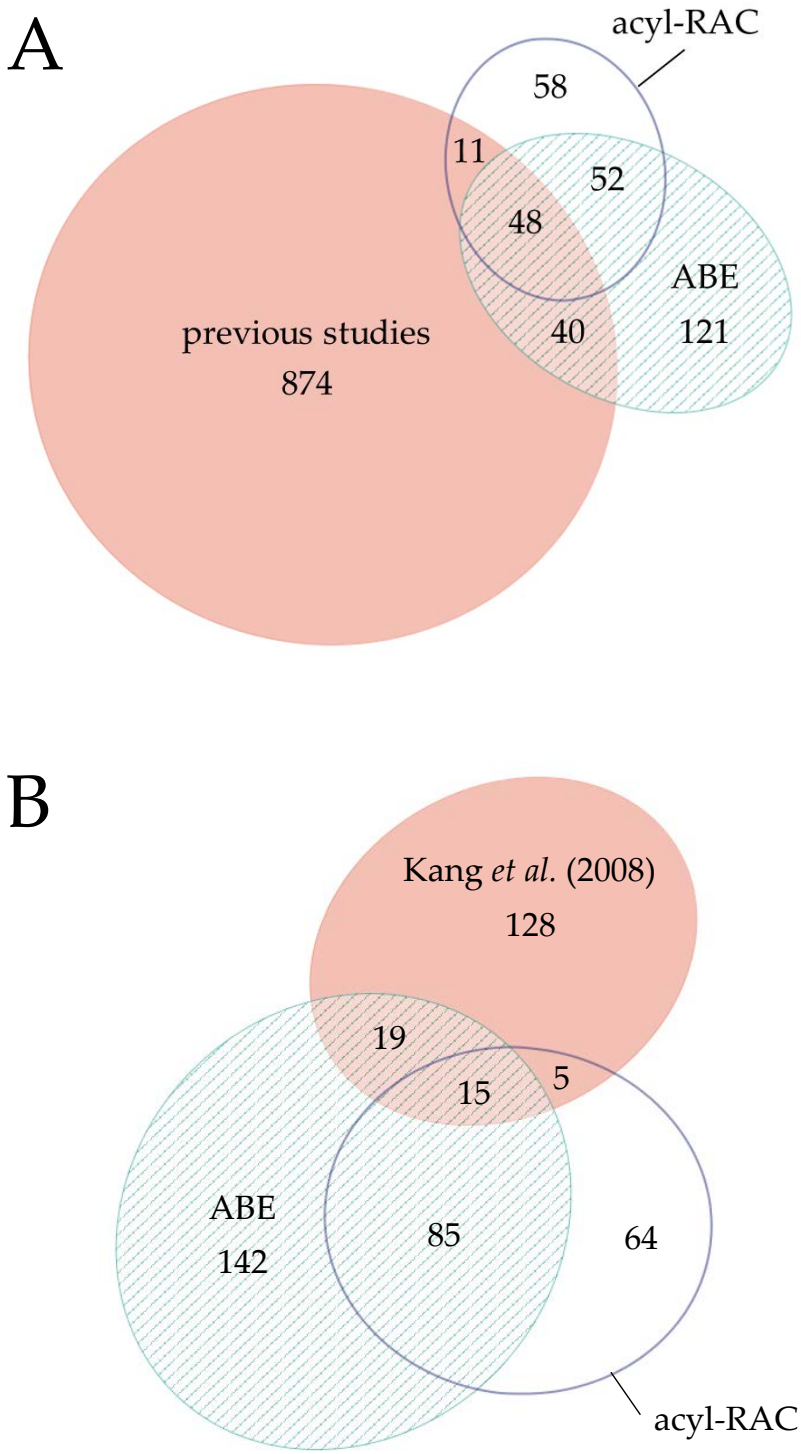

FIGURE 5.8: Overlap of mammalian hits from this and previous studies

Venn diagram showing the crossover of hits from the ABE and acyl-RAC experiments in this study and from (A) all proteomic studies on mammalian material to date or (B) Kang *et al.* (2008) only, which used rat neuronal material. ABE, acyl-biotin exchange; acyl-RAC, acyl-resin-assisted capture.

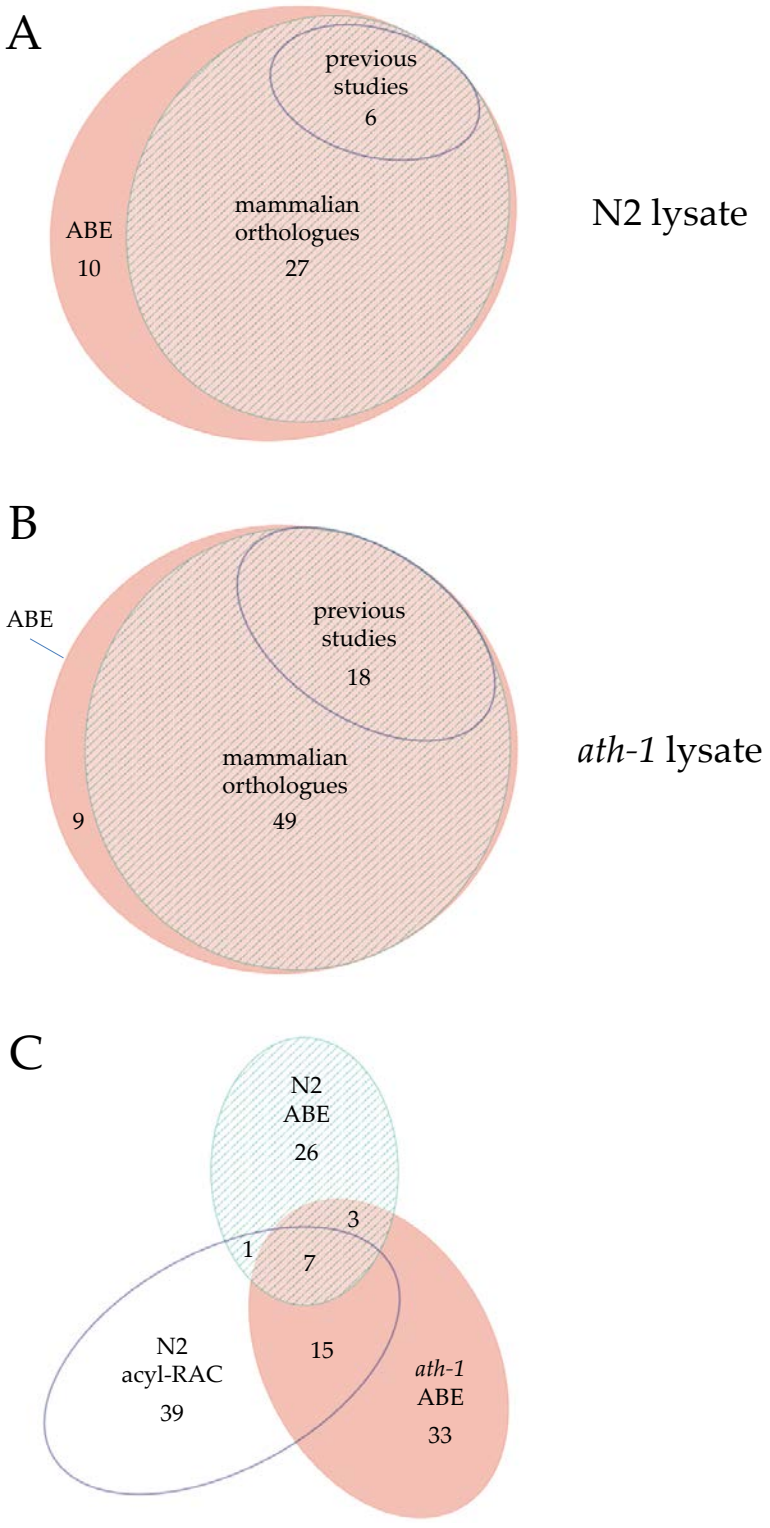

FIGURE 5.9: Distribution of hits from *C. elegans* ABE and acyl-RAC experiments

Venn diagrams showing the proportion of wild-type N2 (A) and *ath-1* mutant (B) ABE hits which have mammalian orthologues, and how many of these orthologues are known palmitoyl-proteins.
(C) Venn diagram showing the overlap in the hits obtained from the two experiments using wild-type N2 lysate and their relationship to the *ath-1* mutant hits. *ath*, acyl-protein thioesterase; ABE, acyl-biotin exchange; acyl-RAC, acyl-resin-assisted capture.

Gene	Protein description	Mammalian orthologue	
		Gene	Name
alh-8	aldehyde dehydrogenase	*Aldh6a1*	methylmalonate-semialdehyde dehydrogenase [acylating], mitochondrial precursor
eef-1A.1	eukaryotic translation elongation factor	*Eef1a2*	elongation factor 1α 2
F46H5.3a.1		*Ckm*	creatine kinase M-type
tbb-2	tubulin β	*Tubb4b*	tubulin β-4B chain
vit-2	vitellogenin	*Wdr87*	WD repeat-containing protein 87
vit-4	vitellogenin	*Apob*	apolipoprotein B-100
vit-5	vitellogenin	*Cenpe*	centromere-associated protein E
vit-6	vitellogenin	*Bmper*	BMP-binding endothelial regulator protein precursor

TABLE 5.3: Hits found in both ABE and acyl-RAC using wild-type *C. elegans* lysate

Proteins identified in both ABE and acyl-RAC on wild-type C. elegans lysate are listed in alphabetical order of gene name. The mammalian orthologue of each protein is shown. Hits are coloured according to their mammalian orthologue: those also identified in previous proteomic studies are highlighted in green; those identified in the proteomic analysis of rat brain homogenate in this study but not in previous studies are highlighted in blue. ABE, acyl-biotin exchange; acyl-RAC, acyl-resin-assisted capture.

From these analyses it seems that acyl-RAC has worked better than ABE on wild-type lysates, although both methods seem to have problems detecting many proteins.

At the same time, *ath-1* mutant strain RB1484 was also subjected to ABE. This gave 17 higher confidence hits and 41 lower confidence hits (Appendix 7). Palmitoylated proteins accounted for 59% (10 of 17) of higher confidence and 25% (8 of 32) of lower confidence hits with mammalian orthologues (Figure 5.9B). 27% (10 of 37) of the wild-type ABE hits and 35% (22 of 62) of acyl-RAC hits were also found in the *ath-1* mutant, including seven of the eight proteins found in both wild-type analyses (Figure 5.9C). This suggests the remaining hits (Table 5.4) may be substrates for the *C. elegans* ATH-1 enzyme.

5.4 DISCUSSION

After initial optimisation tests, the proteomic techniques ABE and acyl-RAC were applied first to rat brain homogenate and then wild-type and *ath-1* mutant *C. elegans* to determine their palmitoyl-proteomes. These methods are appropriate for gaining an appreciation of proteins which are robustly palmitoylated in the context of tissues or whole organisms, as living cells are not required for labelling. In this case they give the first indication of which *C. elegans* proteins may be palmitoylated and potential substrates of the PPT ATH-1. This should provide a valuable resource for future researchers wishing to pursue palmitoylation of specific proteins or by specific enzymes.

Both ABE and acyl-RAC were optimised at the SDS-PAGE and Western blot level using rat brain homogenate. The eluates were analysed using mass spectrometry and compared with similar previous studies. The number of hits found with each method was similar to those found in previous studies (Table 1.1). Both methods gave similar proportions of hits which had been previously found. Although a higher proportion of acyl-RAC hits belonged to this category, they were fewer in absolute number. Whilst these proteomic hits give a good guide as to potential palmitoyl-proteins, they should not be taken as proof. Known palmitoyl-proteins were found here which had not been found in other screens, the stand-out example being GAP43/neuromodulin. Equally, Munc18 appeared as a lower confidence hit in the ABE experiment even though it appeared to have been eliminated as a palmitoyl-protein by Western blot analysis (Figure 5.5C, Appendix 3.2), although it is possible this may be a statistical fluke as already discussed (Roth *et al.*, 2006) as it was detected from only one unique peptide in one of the two ABE experiments. Additionally, some well-known palmitoyl-proteins were not picked up in this study, for example SNAP-23 and H- and N-Ras. Despite these caveats, proteomics approaches do allow a large list of candidate palmitoyl-

Gene	Protein description	Mammalian orthologue	
		Gene	Name
abl-1	oncogene Abl-related	*Abl1*	c-Abl oncogene 1
abtm-1	ABC transporter, mitochondrial	*Abcb7*	ATP-binding cassette sub-family B member 7, mitochondrial
alh-9	aldehyde dehydrogenase	*Aldh7a1*	α-aminoadipic semialdehyde dehydrogenase
ant-1.1	adenine nucleotide translocator	*Slc25a6*	ADP/ATP translocase 3
asp-1	aspartyl protease	*Pgc*	gastricsin
bed-1	BED-type zinc finger putative transcription factor		
C08H9.2a.1		*Hdlbp*	vigilin
C09B9.1			
C33H5.8		*Rpap3*	RNA polymerase II-associated protein 3
C35E7.7			
eef-2	eukaryotic translation elongation factor	*Eef2*	elongation factor 2
F01G4.6b.1		*Slc25a3*	phosphate carrier protein, mitochondrial
F02H6.7		*Bai1*	brain-specific angiogenesis inhibitor 1
F09G2.2		*Cnppd1*	cyclin Pas1/PHO80 domain-containing protein 1
F46B3.15			
F46F11.11			
faah-5	fatty acid amide hydrolase homolog	*Faah1*	fatty-acid amide hydrolase 1
fbxa-16	F box A protein		
hel-1	helicase	*Ddx39a*	ATP-dependent RNA helicase DDX39
lim-7	LIM homeodomain protein	*Isl2*	insulin gene enhancer protein ISL-2
nhr-134	nuclear hormone receptor	*Ppara*	peroxisome proliferator-activated receptor α
nhr-268	nuclear hormone receptor	*Rarg*	retinoic acid receptor γ2
nsf-1	N-ethylmaleimide sensitive factor homolog	*Nsf*	vesicle fusing ATPase
ptr-3	patched-related family	*Npc1*	Niemann-Pick C1 protein
R12E2.8		*Ush2a*	usherin
rps-26	small ribosomal protein subunit S26	*Rps26*	40S ribosomal protein S26
rps-4	small ribosomal protein subunit S4	*Rps4x*	40S ribosomal protein S4, X isoform
rps-5	small ribosomal protein subunit S5	*Rps5*	40S ribosomal protein S5
sdha-1	succinate dehydrogenase complex subunit A	*Shda1*	succinate dehydrogenase (ubiquinone) flavoprotein subunit, mitochondrial
sphk-1	sphingosine kinase	*Sphk1*	sphingosine kinase 1
T04B2.7			
unc-15	paramyosin homolog	*Myh7*	myosin-7
W09D6.1c		*Aasdh*	Acyl-CoA synthetase family member 4
Y47D3A.28		*Mcm10*	minichromosome maintenance deficient 10 (*S. cerevisiae*)

TABLE 5.4: Putative ATH-1 substrates

Hits found using ABE on *ath-1* mutant lysate but not using ABE or acyl-RAC on wild-type *C. elegans* lysate are shown along with their mammalian orthologue, where applicable. Hits are coloured according to their mammalian orthologue: those also identified in previous proteomic studies are highlighted in green; those identified in the proteomic analysis of rat brain homogenate in this study but not in previous studies are highlighted in blue; those identified both in this and previous studies are highlighted in orange. ABE, acyl-biotin exchange; acyl-RAC, acyl-resin-assisted capture.

proteins to be produced which is not possible using classical methods of studying palmitoylation. Indeed, nearly two-thirds of the acyl-RAC hits were also found in ABE experiments, giving additional confidence to the half of these hits which were not found in previous proteomic studies. As there are currently no known palmitoyl-proteins in *C. elegans*, these methods were applied to uncover candidates.

At the level of a silver stained SDS-PAGE gel, the ABE and particularly the acyl-RAC outputs from wild-type *C. elegans* lysates looked promising. It was disappointing therefore to see so few hits from both methods. ABE uncovered just 37 hits, only four of which were higher confidence, whilst acyl-RAC gave 62 hits, though nearly two-thirds of these were of higher confidence. These numbers seem miserly compared with those from rat brain homogenate (261 ABE hits; 169 acyl-RAC hits), especially as the lysates are derived from brain material for rats but the whole organism for *C. elegans*, which might lead to the expectation of many identifications of proteins found away from the brain. There were eight identifications which were found in both the ABE and acyl-RAC analyses. However, when the mammalian homologues are compared with previous studies and the data above, only one had been previously found and a further two identified in rat brain homogenate here. When the hits are compared with the predictions made using *in silico* data (Table 3.8, Table 3.9) only TBA-2, the orthologue of *S. cerevisiae* tubulin TUB1, is found in either experiment. It therefore seems likely that rather than genuine palmitoyl-proteins, many of these eight are abundant proteins which have been purified as false positives. However, it was encouraging that nearly half of the acyl-RAC hits with mammalian orthologues were known palmitoyl-proteins. It remains to be seen whether any of these hits are genuine palmitoyl-proteins.

ABE had also been applied to the *ath-1* mutant strain RB1484 with the objective of identifying possible ATH-1 substrates. As ATH-1 is the orthologue of the only known cytoplasmic PPT, APT1, it was reasoned that it was likely to be the most physiologically relevant enzyme with the largest range of potential substrates. Whilst *ath-1* mutants have no gross phenotypes (Figure 4.15), its substrates would be expected to have reduced or no depalmitoylation which may enrich their palmitoylated form to levels detectable by ABE. Application of the PPT inhibitor hexadecafluorophosphonate (HDFP) to human embryonic kidney 293 (HEK293) cells showed a quantitative increase in palmitoylation of palmitoyl-proteins over a 6 hour period (Martin *et al.*, 2012), so there may be a substantial increase over the lifetime of *ath-1* mutants. Indeed, this was what was seen. ABE on lysate from *ath-1* mutants identified 58 proteins, compared with 37 for wild-type *C. elegans*. The fact

that a quarter of the ABE hits on wild-type lysates, a third of the wild-type acyl-RAC hits and all but one of the identifications found in both wild-type experiments are also found in this analysis suggests that there are ATH-1 substrates enriched in the remaining identifications. Amongst the proteins found only in the *ath-1* analysis are SPHK-1 and UNC-15, which were predicted to be palmitoylated as orthologues of *S. cerevisiae* long chain base 4 (LCB4) and mammalian cytoskeleton-associated protein 4 (CKAP4)/p63 respectively (Table 3.8, Table 3.9). Whilst higher than the wild-type analysis, the overall number of identifications from *ath-1* mutants was still relatively small. This may be explained by evidence that the majority of palmitoyl-proteins are stably palmitoylated, with relatively few undergoing active palmitate turnover (Kang *et al.*, 2008; Martin *et al.*, 2012). Alternatively, the other *C. elegans* PPT PPT-1 may be able to compensate by depalmitoylating some of the substrates of ATH-1 in its absence.

Why are there so few identifications from the *C. elegans* experiments? It proved difficult to apply ABE and acyl-RAC to *C. elegans* lysates and end up with protein in the final eluates. This was partially resolved by growing large liquid cultures to obtain significantly more starting material. Unfortunately the technical difficulties meant there was insufficient time to perform repeat experiments, so the results presented using *C. elegans* lysates must be considered as preliminary. Perhaps palmitoylation is not an important modification in *C. elegans*, which would account for so few apparent palmitoyl-proteins. This seems unlikely given the 15 DHHC enzymes identified, although some mammalian DHHCs have been shown to have functions independent of their palmitoyltransferase activity, such as ion transport (Goytain *et al.*, 2008; Hines *et al.*, 2010) and mediation of c-Jun N-terminal kinase (JNK) activation (Yang and Cynader, 2011), so maybe similar functions are more important in *C. elegans*. There are some caveats associated with the ABE and acyl-RAC methods of determining palmitoyl-proteins. Both methods rely on thioester bond cleavage and labelling of cysteine thiols, which can only give a snapshot of the palmitoylated proteins present in the sample. This can result in underrepresentation of proteins which undergo rapid palmitate turnover or which may only be palmitoylated on a subset of the total protein. *C. elegans* could have a much higher proportion of rapid palmitate turnover than in mammals, leading to a low proportion of palmitoylated proteins at any one time and thus many genuine palmitoyl-proteins failing to reach the detection threshold.

Some of these limitations of ABE and acyl-RAC and the fact that they cannot differentiate between thioester modification with palmitate and other rarer fatty acids can be overcome in cell culture with the use of palmitate analogues such as 17-ODYA (Martin and Cravatt,

2009; Martin *et al.*, 2012) or alk-16 (Yount *et al.*, 2010) to metabolically label proteins undergoing palmitoylation before purifying them using so-called click chemistry. This has been extended recently by combining 17-ODYA labelling with a stable-isotope labelling with amino acids in cell culture (SILAC) approach to improve its sensitivity (Martin *et al.*, 2012). In this approach, one set of mouse T cell hybridoma cells which had been grown in medium containing isotopically heavy arginine and lysine was treated with 17-ODYA and a control set grown in light (i.e. standard) medium was treated with palmitic acid. A repeat experiment was also performed in which the light isotope labelled cells were treated with 17-ODYA and the heavy isotope labelled cells with palmitic acid. This approach identified about 400 palmitoyl-proteins. *C. elegans* has the advantage of being easily manipulated through the bacteria fed to the animals. As a result, a similar approach could be taken in *C. elegans* by culturing wild-type and mutant animals on a diet of bacteria carrying amino acids containing different isotopes of nitrogen or carbon (Fredens *et al.*, 2011; Gouw *et al.*, 2011; Larance *et al.*, 2011). This would allow lysates from animals raised on isotopically heavy or light amino acids to be combined at the start of an ABE or acyl-RAC experiment, controlling for any variability that might occur in the treatment of the samples during the assay. In addition to being a potentially rapid means of determining substrates of DHHC or PPT enzymes by profiling mutants, the accumulation of several sets of wild-type palmitoyl-proteome data would increase the confidence of the list of palmitoyl-proteins in *C. elegans*. The increased sensitivity afforded by this method may also extend the list of candidate palmitoyl-proteins from the initial analysis presented here.

Chapter 6:

DISCUSSION

6.1 PALMITOYLATION IN *C. ELEGANS*

The importance of palmitoylation of individual proteins has been known about since the first discoveries of the modification, first on viral proteins (Schmidt and Schlesinger, 1979) and subsequently on mammalian proteins (Omary and Trowbridge, 1981). The number of proteins shown to be palmitoylated with functional consequences gradually increased, but the extent of palmitoylation as a post-translational modification leapt forwards with two major advances in the past decade. The first was the identification of the enzyme family responsible for catalysing palmitoylation and its characteristic DHHC motif (Lobo *et al.*, 2002; Roth *et al.*, 2002), resolving a debate as to whether the majority of *in vivo* palmitoylation was spontaneous or not. The second was the advent of proteomic methods enabling purification of palmitoyl-proteins to provide large lists of candidates (Drisdel and Green, 2004; Kang *et al.*, 2008; Roth *et al.*, 2006). These steps have enabled the field to move forward with gathering pace and gained palmitoylation recognition as an important regulating post-translational modification analogous to phosphorylation and ubiquitination.

Model organisms have been useful throughout the study of palmitoylation. The identification of the palmitoyl acyl-transferase (PAT) DHHC enzymes took place in *Saccharomyces cerevisiae* in studies which also showed the importance of subcellular localisation of proteins by palmitoylation to enable them to fully perform their functions (Lobo *et al.*, 2002; Roth *et al.*, 2002). The fruit fly *Drosophila melanogaster* has been used to show the importance of palmitoylation of cysteine string protein (CSP) and synaptosomal-associateds protein of 25 kDa (SNAP-25) by Huntingtin-interacting protein 14 (Hip14) in synaptic transmission (Ohyama *et al.*, 2007; Stowers and Isacoff, 2007). The palmitoyl-protein thioesterase 1 (*Ppt1*) gene in *D. melanogaster* has also been mutated to create a model of infantile neuronal ceroid lipofuscinosis (INCL) and shows the progressive neurodegeneration of the human disease (Buff *et al.*, 2007; Chu-LaGraff *et al.*, 2010; Glaser *et al.*, 2003; Hickey *et al.*, 2006; Korey and MacDonald, 2003). Several knockout mice lacking enzymes involved in palmitoylation have been made in recent years. The knockouts of the DHHCs *HIP14* and HIP14-like (*HIP14L*) show pathological features similar to a mouse model of Huntington's disease (HD), for example (Singaraja *et al.*, 2011; Sutton *et al.*, 2012; Young *et al.*, 2012). The mouse knockouts of *PPT1* (Bible *et al.*, 2004; Gupta *et al.*, 2001; Kielar *et al.*, 2009) and *PPT2* (Gupta *et al.*, 2001; Gupta *et al.*, 2003) have replicated the phenotype of INCL and given clues as to the potential mechanisms of neurodegeneration in this disorder. However, the simple eukaryotic model organism *Caenorhabditis elegans* has

been relatively overlooked, with directed studies limited to a model of INCL (Porter *et al.*, 2005).

In order to address this gap in palmitoylation research and characterise palmitoylation in *C. elegans*, the first step was to glean as much information as possible both from published data and *in silico* resources. The DHHC-cysteine rich domain (CRD) was used to identify 15 PAT enzymes in the *C. elegans* genome. This number fits in well with an expansion in the number of PATs over evolutionary time, intermediate between *S. cerevisiae* and *D. melanogaster*. The two *C. elegans* PPTs had previously been identified by homology to known PPTs (Porter *et al.*, 2005). The homology of these enzyme families to *S. cerevisiae*, *D. melanogaster* and *Homo sapiens* counterparts was used to make predictions about possible phenotypes to be found in *C. elegans* knockouts. Known palmitoyl-proteins in other organisms were also used to predict possible substrates of these enzymes in *C. elegans*. Whilst some of the enzymes showed relatively high homology to those in other organisms, there were several which appeared to be specific to nematodes. Similar issues occurred with some known palmitoyl-proteins which did not have close orthologues in *C. elegans*. In addition, there is scant information available on many of the PATs simply due to the relatively early stage at which research is in this field. These factors limited the ability to make predictions using current knowledge to a few enzymes with well-studied counterparts.

With the information gathered from *in silico* sources in mind, a screen of *C. elegans* PATs and PPTs was performed using both mutant and RNA interference (RNAi) approaches. The initial intention was to be able to characterise mutants for each individual enzyme and complement these results with RNAi data. However, the expected source of mutants for enzymes which were not yet available was unable to provide strains due to unforeseen circumstances, restricting the number of mutants which could be assayed. Whilst a complete RNAi screen was undertaken, there is always the caveat with RNAi data that even a very efficient knockdown may still leave enough residual protein available for there to be no effect on its normal function. The highest chance of detecting a phenotype would occur in mutants which lack the protein entirely. Nonetheless, there was a reasonable degree of agreement between results obtained from mutants and RNAi-treated animals, where both were available.

The majority of strains and RNAi-treated animals tested showed no difference from controls in many experimental conditions. The assay which showed the most differences

from controls was lifespan. One example is the case of *dhhc-14*, disruption of which was predicted to give a reduction in locomotion and lifespan. Whilst there was no difference in locomotion, both *dhhc-14* mutant strains and RNAi against *dhhc-14* showed decreases in various parameters of lifespan. Despite this example, few of the predictions made came to fruition, illustrating the limitations of computer-only approaches and the confounding factors introduced when applying data across different organisms. In addition, all of the *ppt-1* mutants showed slightly different phenotypes, suggesting these may be partly caused or at least influenced by background mutations as all the alleles should result in nulls. These strains could be outcrossed back to the wild-type N2 strain multiple times. The same assays could then be repeated to determine whether any difference is made to the phenotypes observed and hopefully produce more unified results.

There are a number of ways in which the analysis of these strains could be extended. Obtaining a complete set of mutant strains to cover every gene in the PAT family would be a priority. Although the *C. elegans* Knockout Consortium no longer appears able to generate requested strains within six months, there are some other routes opening up for obtaining mutants. Leading amongst these are the set of methods based on use of the *Mos1* transposon (Frokjaer-Jensen *et al.*, 2010; Frokjaer-Jensen *et al.*, 2008; Robert, 2012). These have the advantage of being clean knockouts of the gene-of-interest without the potentially confounding background mutations generated by random mutagenesis methods.

Unfortunately, confusion over whether requested mutant strains would be forthcoming delayed some assays to the extent that many could not be performed on all strains. Therefore, to obtain a truly complete screen the assays presented here should be extended to include all the available RNAi and mutant strains. There are more subtle assays available to dissect phenotypes which may result from dysfunction of specific tissues or subsets of neurons. These range from relatively simple tests, such as egg-laying and food race assays, to various thermo-, osmo- and chemosensation assays, to more complex tests which can assess learning and mating behaviours and circadian rhythm. All of these have protocols which are collated in WormBook (Hart (ed.)). These assays could also be applied to all the mutants and RNAi-treated animals to search for more robust phenotypes. Once such phenotypes are found, their dependence on the enzyme in question can be confirmed by rescuing the phenotype back to wild-type by injecting a plasmid allowing the gene to be expressed in the mutant.

As palmitoyl-proteomics is being applied to an ever-increasing number of cell types and tissues from different organisms and there are no confirmed palmitoyl-proteins in *C. elegans*, it seemed a natural step to attempt to use the power of such methods to come up with a list of candidate palmitoyl-proteins. Before applying the methods of acyl-biotin exchange (ABE) and acyl-resin-assisted capture (acyl-RAC) to *C. elegans* lysates, preliminary experiments were conducted to confirm they were working in our hands. To this end, both ABE and acyl-RAC were applied to rat brain homogenate and optimised. Nearly a thousand high confidence mammalian hits obtained from all the palmitoyl-proteomic studies performed to date were collated and compared with the hits obtained in this study. The overlap of 111 hits between the ABE and acyl-RAC assays performed here and the previous studies along with a handful of known palmitoyl-proteins not previously detected shows that these methods can reliably detect known palmitoyl-proteins. However approximately two thirds of the hits had not been previously found, at least at high confidence. This underlines the importance of using such lists as a guide only and confirming palmitoylation of individual proteins on a case-by-case basis using classical methods such as [^{3}H]-palmitate labelling.

ABE and acyl-RAC were both applied to wild-type *C. elegans* lysates, but the results were disappointing. Initial experiments showed no protein in the final pulldowns, suggesting an issue with protein abundance in the input. The use of animals derived from liquid cultures, which yield much higher numbers of animals, appeared to resolve this issue by producing enrichment of protein in experimental eluates which was clearly detectable by silver staining of polyacrylamide gels. However, mass spectrometric analysis of these same eluates produced very low levels of protein identifications. Many of these look suspiciously like contaminating abundant proteins, as could be seen by the small proportion of those with mammalian orthologues which are known to be palmitoylated. The time taken to modify the techniques to get detectable protein output unfortunately left only enough time for one run of each experiment. Therefore the first thing to do when extending these experiments would be to repeat these experiments at least twice more, which would give enough runs to perform a proper statistical analysis on the mass spectrometry data. If the results continue to be poor, aspects of the protocol such as the lysis conditions and input quantity can be looked at. Alternative techniques to improve sensitivity such as click chemistry (Martin and Cravatt, 2009; Martin *et al.*, 2012; Yount *et al.*, 2010) and use of different amino acid isotopes in control and experimental samples (Fredens *et al.*, 2011; Gouw *et al.*, 2011; Larance *et al.*, 2011) could also be explored. Although it would be

extremely difficult to isolate individual *C. elegans* tissues in sufficient quantity to perform ABE or acyl-RAC on them, techniques exist to culture *C. elegans* embryonic cells and differentiate them into, for example, muscle or neuronal tissue (Christensen *et al.*, 2002; Strange *et al.*, 2007). Culture can also be performed using cells from different larval stages (Zhang *et al.*, 2011). As palmitoyl-proteomic methods have been previously used on cell lines, this may be more productive in terms of reducing potential contaminating factors from whole animal lysates.

6.2 THE PPT QUESTION

A central question in the palmitoylation field at present is whether the low number of known PPT enzymes represents the entire family. This is especially relevant as only one human PPT is both cytoplasmic and has known depalmitoylating activity: acyl-protein thioesterase 1 (APT1). Although the reversible nature of palmitoylation allows scope for regulation, it is interesting to consider whether removal of the modification is as important for palmitoylation as it is for other post-translational modifications. There are some proteins whose depalmitoylation is essential for their function, the most well known being the role of palmitoylation in the cycling of Ras between different membrane systems (Dekker *et al.*, 2010; Rocks *et al.*, 2005). Assessment of palmitate turnover on a subset of proteins (Kang *et al.*, 2008) and at a proteomic scale (Martin *et al.*, 2012) showed that the majority of palmitoyl-proteins are stably palmitoylated, suggesting that under normal conditions depalmitoylation is not necessarily required for many proteins. The finding that APT1 is itself palmitoylated (Yang *et al.*, 2010) suggests that regulation of depalmitoylation may in fact be the important process. This view is supported by the observation of changes in palmitoylation dynamics in response to physiological and pathophysiological stimuli (Kang *et al.*, 2008).

C. elegans has one representative from each branch of the PPT family: PPT-1 and ATH-1. Phenotypic analysis of mutants lacking each enzyme only showed phenotypes for *ppt-1* knockouts, which is somewhat surprising given ATH-1 is the orthologue of APT1. RNAi treatment against each PPT showed no phenotypes whatsoever in the assays used. There are four possible explanations for these observations: 1) there is a functional redundancy allowing the unaffected PPT enzyme to perform the function of the disrupted PPT; 2) there are other PPT enzymes which can perform the role of the disrupted PPT; 3) there is insufficient knockdown by RNAi to replicate mild mutant phenotypes; 4) depalmitoylation is a relatively unimportant process in *C. elegans*. A concomitant knockdown of both PPTs by

RNAi gave a reduction in lifespan but the animals appeared otherwise normal. This would be consistent with any of explanations 2-4, and the problems with mixing RNAi bacterial strains which were discussed earlier should be borne in mind. A double mutant strain which lacks both *ppt-1* and *ath-1* would be interesting to study and would give higher confidence results than the RNAi studies.

The *ath-1* mutant strain was also subjected to ABE analysis to see whether any proteins which were not present in the wild-type study appeared as potential substrates. Whilst the overall recovery of hits from the *C. elegans* analyses was poor, there was an increase in the number of hits compared with the same technique on wild-type lysates, suggesting the principle is sound. If the assay can be improved upon as discussed above, analysis of *ppt-1* knockout strains would also be interesting and also a double mutant once it has been created. A lack of any major changes in the double mutant hits compared with wild-type would strongly suggest that other PPT enzymes exist in *C. elegans* to compensate, and presumably therefore also in other organisms.

If other PPTs do exist, how can they be found? As there is no obvious unifying motif in the same way as there is for the PATs, genome data searching is not currently an option. One way would be to perform depalmitoylation assays on a panel of representative palmitoyl-proteins. Whole cell extracts could be fractionated and tested for depalmitoylation activity. Through repeated fractionation, this depalmitoylation activity could be honed down to a fraction containing a few hundred proteins. These could be analysed by mass spectrometry and any potential candidates cloned and tested individually – for example any which share structural homology to the published structures of the PPTs. This type of analysis would be particularly effective if a cell line lacking the known PPTs could be established, thus eliminating them as potential hits. The published structures could also be used to search for structural homologues if a method for producing predicted structures from only the primary sequence of proteins on a large scale can be established. An alternative approach could use the fact that *S. cerevisiae* only has one known PPT, APT1, and the availability of whole genome screening techniques. For example, a synthetic genetic array analysis could be performed using an *APT1* knockout strain. This enables the entire library of *S. cerevisiae* non-essential genes to be screened for synthetic sick and synthetic lethal genetic interactions (Boone *et al.*, 2007). If the lack of a severe phenotype in *APT1* knockouts is due to compensation by other PPT(s), this type of analysis could uncover novel PPT candidates.

6.3 FUTURE PERSPECTIVES

The field of palmitoylation is still young, with the main surge of interest coming only in the past decade or so. As such there are still many gaps in the knowledge, such as several enzymes with completely unknown function or substrates, as outlined in the *in silico* analysis. Even where palmitoyl-proteins are known, the function of the palmitate moiety is often not clear. That includes several proteins identified in this study, such as syntaxin isoforms and heat shock proteins. In this respect, simple model organisms such as *C. elegans* can provide useful pointers, as their short lifespan and relatively easy genetic manipulation allow screens of whole enzyme families to be performed. Such an analysis has been started through the phenotypic assays presented in this study. However, there are still several avenues which could be explored. For example, plasmids containing green fluorescent protein under the promoter of each PAT and PPT could be injected to allow examination of the tissue specificity of their expression, and potentially even the subcellular localisation. This information can be used to complement expression studies performed in other organisms (Ohno *et al.*, 2006). In order to add confidence to potential functional orthologues in *C. elegans* based on sequence homology, *S. cerevisiae* could be used as an expression system to see which DHHCs palmitoylate model substrates from each type of palmitoyl-protein, similar to the analysis already performed with *H. sapiens* and *S. cerevisiae* enzymes (Ohno *et al.*, 2012). It would be interesting to see how this experiment tallies with the *in silico* data collected in Chapter 3.

Whilst unexpected problems arose while conducting proteomic analyses of *C. elegans* lysates, if these can be resolved then the systematic analysis of the palmitoyl-proteome of mutants lacking each individual PAT becomes very achievable. This promises to be a way of rapidly profiling potential substrates for each enzyme in a way which, whilst achievable using knockout mice, for example, would be much quicker and more cost effective in *C. elegans*. In addition the function of palmitoylation on individual cysteine residues can be probed using this information along with predictions of likely palmitoylated residues. The ease of genetic manipulation means that, for example, a knockout for a palmitoyl-protein could be rescued with a construct containing an unpalmitoylatable cysteine-to-serine mutation at a putative modified residue. This would allow examination of the effects of disrupted palmitoylation on individual residues on the function of a protein. The information gained can then be used as a resource for directing studies in the mammalian context. Along with the other data which could be produced using *C. elegans* as a model, this will provide insight into the true extent of this interesting post-translational

modification, its importance in cell biology and its potential role in the progression of certain diseases.

APPENDICES

APPENDIX 1: MUTATIONS IN *C. ELEGANS* STRAINS

Key:
exon
exon of adjacent gene
insertion
deletion
point mutation
frame shift
DHHC motif

ath-1: strain RB1484, allele *ok1735*

before exon 1 ->
TAGAGAactgtccacccttctcgtcaaattccacattttcttcttcaccaaaaacttttctagcttcaataatag
gttcgttgaaactattttgtgttttgtgtgtcgttgctttcttttaatgttttcatactaatcgcggacattgaca
atcagagcgctacgtttcgaaagatcctcacttctttattctttatctaaaattcatgaaaaaaaccacagaaaac
ttcagggtcatcactttcttcccgtcttctctgttcacttggtggaccgccatccgacgaagaagattcgacaaga
atgtctgcagtctccaacggaaatccttcgattgtgtcgccacgtggcgagcataaaggaacattaatcttccttc
atggactcggtgatcaagggcatggttgggcagatgctttcaagacagaagccaaacacgataatatcaagtttat
ctgtccacacaggtacttttgaatgcagaattattaattatagcagaaaagtacatttataatagaattaaacaaa
agtatcgaaaaactaagagaaaattaacaaaaaaaattttttaataaaatttcggttatatattgatgagataaaa
cataattttcttcttaaaagaggaaaaatatagaaaatttcaagctatttttcaaatcgatcttttaaatatcgg
taaaaacaaaaaatcgaaaaaccgacaccctccattatccactgaaacagattcacttttttcagctctgaacgtc
cagtaaccctcaatatgggaatgcgaatgccagcttggttcgacttatttggcctcgatccaaatgctcaggaaga
tgagcaaggaattaatcgagctacccaatatgttcatcaattgattgatgcggaagttgcagctggaattccagct
tctcgaattgctgtcggtggattttcaatgggtggagctctcgctatttacgctggtctcacatatccacagaaac
ttggaggaattgttggactcagttcattcttttgcagagaaccaaattcccaggggtgattattcaaattattta
aaaaaaaattttttttgatttttatagagcttcactgcgaacaatgctacaccaatcttcctcggacatggaacag
acgacttttggttcctcttcaattcggacaaatgtccgagcagtatattaaaaaattcaatccgaaagttgagct
tcacacctacaggggaatgcagcattcgagctgtggagaggtatttttatttttaaaaaacgatttcggaacatga
gtgtcggttttccttttttaaaaatcgaaaacgatatttttttttttaatataaaaaaaaggaaaaaaattgtcgac
tttagattcctcgaattctggaaaaaaaacgttttaaaataatttccagatttcgaattttcgaaaaagttataaa
aatgaaaatgccctgaaatttaaataaaaaactttttttttttcaaaaatcgagaaatctaatttttcactgttttt
taatcaaaaaatcataaattgagaaactgggaaacatgttagaaaaattgtacggaaaaaacgaggaagccattga
tttttcaaaattatgtaaaatttttttgtgaaaaagaaaaatattaaaaaggattaaaacaaaaaaataaaataataa
catttcttctattcccaaaaaatctacatatttttgatatatctataaatagtttcctcgtctttttccgtatttt
tctaaaatttttccaagtttaaatttttcgaattttcgacgtcctcgtttcgggtaaagaattacaaagaattaaa
caaaatgaaaacttcaaactattagatcaaactacacatcatattatgcataatcaaaattatattaatcatatta
atgtattttcaggagatgcgtgatgtgaagaccttcttgagcgcccacattgcccactaa
<- exon 4

ATH-1 protein:
MSAVSNGNPSIVSPRGEHKGTLIFLHGLGDQGHGWADAFKTEAKHDNIKFICPHSSERPVTLNMGMRMPAWFDLFG
LDPNAQEDEQGINRATQYVHQLIDAEVAAGIPASRIAVGGFSMGGALAIYAGLTYPQKLGGIVGLSSFFLQRTKFP
GSFTANNATPIFLGHGTDDFLVPLQFGQMSEQYIKKFNPKVELHTYRGMQHSSCGEEMRDVKTFLSAHIAH

dhhc-1*: strain tm4272, allele *tm4272

exon 5 ->
atactttgtcgccgcagtcatcaacctcttcattatgactctgccactagtctcctactcatggagccttctcaat
atcaaaatgacgaacgaaatcggcttcggaaacatttggcaagtggtcattccccatcttgcctggatcgccggat
acatctcaatctaccaattcctccacgtccttctatttgtcttcaccttcaccgtttcgctgttcacttttacct
gctgactgctcaagttttctgcatttatcagggacagacaagaatcgagttttgatggtgagctatatgtacaat
tgaaaataatttttaaatgttttaaattattatagcagaaaataatagatcaaatggtgacgatttttgtaatact
gtttcactttatggggttattcaagtaatgtcggaaaattaaaaagtgtagaacaattacgtcacaactgtattca
agtatacacctttacctttttaaaaacatgtatttagatacatttgtgacgtcacaaatgtatttaaatacatt
ttgatacattacttgaataaccccattagctcgaatgtatcgaatctagattttactgcttttaatattttgctca
aacatcaaattcggccggcatctcgaatgtcgcataacatttttctttcttccaatacaaaaatttttcgatat
ctttctgcctagaagacttccgtttggtctgtgaggaagtcaccttaactgcaacataaaatctcaaacaaatata
aatccaattttcaggacgttcacgcataccagctcggactccttgaaaacctccaccaatcgctcggctcccggtg
gccattcattgccatttcttgcttcatcccaagtcctctgccaactgatggactcggctttgtcactcgcgagatg
ttcaatcttcataccaaagatctctaa
<- exon 6

DHHC-1 protein:
MQMLYDDGENVDFNKKLQRMMPTQIQDIIATFIFLILLPCGILLHLLYVLPTWYPVMGEAWVIRATCFGVLVFNLY
SNWVYMIKTGPNGHHSALPNVIKPGYKHCHSCHSMSPLRAHHCPVCDVCILRRDHHCSFGAVCVGHFNQRYFVAAV
INLFIMTLPLVSYSWSLLNIKMTNEIGFGNIWQVVIPHLAWIAGYISIYQFLHVLLFVFTFTVSLFTFYLLTAQVF
CIYQGQTRIEFLMGRSRIPARTP-KPPPIARLPVAIHCHFLLHPKSSAN-WTRLCHSRDVQSSYQRSL

dhhc-2: strain RB1044, allele *ok990*

exon 5 ->
atgacgttgctcatttgaggcctcgttttcaagatgtcgttgtgaatggggagcatgtaaaaatgaaatattgtac
gacgtgtcggttatatcggccaccgagatgctcacattgtgcaatttgtgataattgtgttcttatgttcgatcat
catt gtaagttattttagttttaattagttagctttgacggcccatatagtaggtaatttatgagatatcaaaaaa
tgttcaaatacaaatatagagaaaaatatttatgcaatatttcgtcagtaaacagttttgaataaaaccgaagac
aactgactagggaaccgtcagaaggtgcccatcggacttgcatatgagacctatgccattcaatagtccatgtctt
aaaatgattactcgtgaatttttagcggtaaaactccagaatcaagctcacggcgggctctcaaatatcctaaaat
atcactttaacaaagaatttaagggccaattctcctatttcactatgacagctcatatctccgcgggtaaatttttt
tgcagaaaagtcgccaactaaaaagttgttggtattgctgtaaagaacaagtttgtagttgaaagtttttacaaa
aaaatttttgtttgagataaaagcgctgaagtgcggcactgctgctgttattttatgctgttattgatattctaat
gcttatatctcaaactaaattgttttggtaaaaactttcaactacaaacttgttctttacaacgatatcaacaact
ttttagttgatgacttttctgtaaaaaatttatctacggagatatgagttaccaaaatgaaattggaaaattgctt
cgttagatcgttaaattgcttccttacagtgctattttaggatatttgaaagcccgccgtgagcttggttctggag
ttttgccgctaaaaattcacgagtaaccattttaagacatgcactatcatggcataggtctcatatgcaagtccaa
tgggcaccttctgacggttccctagtgagatataagccatgaaatttcggcaagacatggtgtatcgaccaagatt
acttggtttagctttggcagcttatatcttggaggacttttctaaaaataagttttgatgatcccctgacgttta
aaataataaattatcatttactatatataaagcgcttattctgtgtgtccatagtttgtagtctatgtagtctttg
tagtctgtgaagttttggcttctggagggatagtgacttggggttagtgtagggatatagtcggggtactgtagtg
gtacaatagtggtacggtaggaatactgtagggttacggtagttttataaaaaaattaattttcagccccagaagt
caggggccgcgccgaaggtgcggtccacggctggtccctatatattctatttcaggcccgtgggtcggcaactgta
tcggactccgaaattacacgtatttctatcgattcgtattttgtctttcaattcttgtgatctacctatttgccag
tgcagtcacacatatcagtttatgtgagttccatgtgatttttcaaatcaatttaccgtatttgctctattagtct
tgcatgcaagactaattttcaattgacctgtaggagtgcaagactaatagagaaaatacggtatattcttgtcatc
ttttaatacatagatacataaaattgggaaatttgaaaaaaaaataaaggataaaacaaaaagtttgaatgtttcc
agtagctcaagagatgccattcggagatgtcatgcgaaaaactcccgggtctgcagtcgtcattgtcatatgcttt
ttcacaacgtggttagttattataagaatttttgcgttttgaagttcaaaaagttcaaaaaaatttccaggtcaat
tattggtttggcatgcttccatacttatcttctgtgcgcggatcttacgacaaatgaagatgtaagtagattttga
aatttttattggtaaacttctacagctttaattttcaatttaaaagccaataataatgttctactatcattttaaa
agttttttttttttgaattaattctcagtttccaagctttttttatagtgtatgtttcagctaaaaggcctgtacc
gccggaagcatcgtccaacacctccatcatctacaccatcaacatctgcagctaccaattcttctgtaggacattc
gacaaaaaatccattttacgctggatgcttcaagagttttttttggaagactgttcaagtccagatttccaaggtaa
ggaactttacttttttatatacaaaactataacaaaaagaaaacaaatacattgtagttagaaatttgaaaataaat
gcaaaaaaaagtgagagtaacatggtgcatcgactgaaactaccacatataactttgacagcatatatcttggttt
acagttgggatggaagaaacattcaactgaaagattatagaacaaataacgacaaatattttgccagtttatgatt
tttcgattaaacacaagacagcggagatatacgctaccgaattagtaaggagagtttatccgccatgtttctttga
cagctcatatctcggttagtagtttgattagcaaaatatgtttcactacaaaattatagaagtgtacattttaaat
attttgtcaatttacaattctaagataaaacaaaagacaacggagatataagccgtcaaagattcatggagctttt
ttggtcgatgcaccatgtttctaaactttgaaagcctatatctcggtttaaataaattgtatcaaaaatctttcaa
ctggaaatatatatttattacatgttttactataaattttctctggaaataaactgataaattcaaaatgaactga
gatataagcagcgaaagttatatggagtaatttcgatcgatgcaccatgttttcaaattttaacagctttcatctc
gcttggcttttgttttatcaaaaaactgtcaactaacaaaatattgttcaattatttcttattattttgtaattac
aattatgttaataactagaaagttaaccgatatataagcaaccgaaattatataatgcaatttcggtcgatgcccc
atgtttcaaaaatttaacagctcatttttttagatttatcaaaaagttgtcaactaacaaaatattgctcaggtgt
ttttctacaactttgcagtagaacaattattgatagctgcaaagtgaacgcccgtttaggatccgcccatttttta
cctcactccaaatttccttcgaaatttttttaaagtttgctattaaattgtctaaaaaacacaataaattaaaat
ccttgggaaagaaaaaatcaataatttaaatttccgagaggagtacaccacgaacatttatcgctagagcgcgtt
tgctctcaaaaaaaccaataatatttcagcttactcgacgcccgcggctacctggacccacatccgacaatcgaaa
tccgagttccgaaaaaatcggaaaaatcgatcgaaaatcattaa
<- exon 10

DHHC-2 protein:
MALMTQRLLDEEIAIDEETERSRDTERHETHVNQCEMSSSFSATSPSTSSAYQLEEHISAPRATPELPPSDPKRRK
WQSHPGRNRFGCGGRLVCSRSHGAFVVTVILMIATLTVYFVFDAPFLWGYSPAIPIVAAVLSLIVITNFFATSFTD
PGILPRVDNIEIIEMDRQQANGNGINDVAHLRPRFQDVVVNGEHVKMKYCTTCRLYRPPRCSHCAICDNCVLMFDH
HCPWVGNCIGLRNYTYFYRFVFCLSILVIYLFASAVTHISLLAQEMPFGDVMRKTPGSAVVIVICFFTTWSIIGLA
CFHTYLLCADLTTNEDLKGLYRRKHRPTPPSSTPSTSAATNSSVGHSTKNPFYAGCFKSFFGRLFKSRFPSYSTPA
ATWTHIRQSKSEFRKNRKNRSKII

dhhc-9*: strain VC2067, allele *gk985

exon 3 ->
tttctggtgttcttcgtatacttcatctccacatttctagccttcacatccttttttcataatcattccatatgaac
aactgtgagtttttttgttgaaaaactattattaataaaaagtcaaacacaccacgctgtttttatgaaacttttc
ttcgattgtcaattttgtgcatatgcaattaaaaaaaaaacatatatataaactgtcccgtttagtttctggtaat
tttgagaacactgtagtaattacgaaaaagatgtacaaaccaagggtgggcgacaattgccgttcgtcgacaagtt
cggcaaatcggcagattgtcggtttgccgatttgccggatatcagttttgccaaaaatatttttagggatttttt
caaagacggtaacagttaaactgtgcctctttgtaggaacattcataggatgcgtacaatttcgcagattgaaatt
taaattctgaaatttccaaataaaaatgcaaaaacacaattcgacgtaaaattttggcaattgccgtcttaccggc
aaattcgacaaatcggcaatttgtcggcttaccaatttgctgaacattttgaaatttttactcaaccttcacact
taacagttctcgaaaaacttgtattattttagatacaaacctgcctggctactcttgctgctcggcacttgcggcc
tgtatttcttattcaacatccaatatcattactacaaagccaggacaataccaccagttgcaaatcctgga
                                                                <- exon 4

DHHC-9 protein:
MCHDKMNHFCDFIDRKIDDGTFIPMVKAANSSMRQIGKFLVFFVYFISTFLAFTSFFIIIPYEQLYKPAWLLLLLG
TCGLYFLFNIQYHYYKARTIPPVANPGEEGDSFCSKCNYWKSDNAHHCSVCEKCVLGMDHHCIWINQCVGLHNHRH
FFLFIANLTLAAATIIIAGYQSFSDHLFLESSQTTYCTTILEHAPLQDIICDYDGFARTSVVFCYLLSGILLVMVG
GLTSWNIYLISIGCTYIDYLKLTGSKKNTSARKRLNKGFKANWRNFLGLRRNRTFFKCVIMPTALPPVKYEDISPK
SDAYDIV

dhhc-12*: strain VC2039, allele *gk1013

exon 6 ->
actcgtaaagaactaactgcaatcccggatgatcaatgctggcctccatattgttttaatagatattactacttga
ttacacgttctcaaggaagtatgtctgatgcatttgaacctttctaacttctcaaaGAGCACCACCTTCCGCTACT
GTAGACAACGTGTACTACTTCttccagccgaagacactatggttaaattcgcatttttccttttcgtaacacttca
ttggattatgtggggatttgttggtgtctacgtaggaatcatttcatttggattaactatggcgatgaaaatggta
atcaaattggcaacatctgaaccaattcagaatttccagtttcaaaagtcggacgctgaatctcgtaaacctttca
cttggttcacaatcaaagctcgttggagaaaatacatgaactgtcaagatgagccactttggaagatatttttat
tccgaaaacccgcaaaattgtgtcgtataacgattataaggagttaattatgtagaattattgtagaattgtctaa
ttttctctttttaat
 <- after exon 8

DHHC-12 protein:
MDVCRIFNRIVYFLVEKSLGDISKFDPFDVLKLVALWGGRLCLLIFVGTLCNVTYVVIFKMIPVEWNECQNMSFFV
FRFVLLIYIYYSVVFHYYKARTLTPVVNPGTPSDSFCIKCNNWKGPSTSHCKACDKCIYRMDHHCPHIGQCVGAHN
QSHFFLFLFYLQIATGLFFLMATTFWMKWIETRKELTAIPDDQCWPPYCFNRYYYLITRSQGTEDTMVKFAFFLFV
TLHWIMWGFVGVYVGIISFGLTMAMKMFQKSDAESRKPFTWFTIKARWRKYMNCQDEPLWKIFFIPKTRKIVSYND
YKELIM

dhhc-12*: strain VC2244, allele *gk981

exon 4 ->
cgaatgccaaaatatgtcgttcttcgtgttccgttttgtgctccttatctacatttactacagtgtcgtttttcac
tactacaaggcccggactctgacacctgttgtgaatccaggggtaagcctccaaaaacaaagatatgacgtcataa
gcataaacggtcgtccgaaatcaagcatttgagacaaatactgtaatacacatttctccacgaggagtacacacaa
agaacgtaaatcgacacgttctttgttttacagtcatttctcaataagctagaaattgtagagccttttgagatt
ttttttcttaaaatttcaaatcaaacttttcagactcccagtgactcattttgtatcaaatgcaacaattggaaagg
tccatcaacatctcattgtaaagcttgtgacaaatgtatctaccgtatggatcatcattgccctcatattggacaa
tgtgttggagcacacaatcagagccacttcttccttttttcttttctatcttcaaattgcaacgggcctctttttct
tgatggctacaacgttttggatgaaatggatagaggttggtttggtgcctgccttgtgcctgcctatccttaaact
agtaaattattagtccttcagactcgtaaagaactaactgcaatcccggatgatcaatgctggcctccatattgtt
ttaatagatattactacttgattacacgttctcaaggaa
<- exon 6

DHHC-12 protein
MDVCRIFNRIVYFLVEKSLGDISKFDPFDVLKLVALWGGRLCLLIFVGTLCNVTYVVIFKMIPVEWNECQNMSFFV
FRFVLLIYIYYSVVFHYYKARTLTPVVNPGTPSDSFCIKCNNWKGPSTSHCKACDKCIYRMDHHCPHIGQCVGAHN
QSHFFLFLFYLQIATGLFFLMATTFWMKWIETRKELTAIPDDQAGLHIVLIDITT-LHVLKEPKTLWLNSHFSFS-
HFIGLCGDLLVST-ESFHLD-LWR-KCFKSRTLNLVNLSLGSQSKLVGENT-TVKMSHFGRYFLFRKPAKLCRITI
IRS-LC

dhhc-13*: VC108 strain, allele *gk36

exon 1 ->
atggccatggaaaaaatcaaaaaatttccgatttttcagtttttttttaattgttttgatgtttttcagaaaaa
ctcgaatattgaaaaagggaaaatcgaaaagggatttcggagtttttttcgatgattcgtttttgtatgtattta
tcaaaaatatgtcgatttattctcctgttatttttcttttaaagatttccttagcatggcgaccactaaataaaaag
atcctacaatcttcaaagcacaagatgagtctaatctttcgccagcaaatcggaagatgtctatcgacactgaaag
atctccatgaagaagcacaagacgacattgaaaatgttgtggaaatccggaaaggaccgatcgatgctctattcgg
aacaatcttcgatattgtcgacctcgcagagagaacaatcactgaatcaaatcgcattgagcaacactcgacaaaa
tggaaactccg
<- exon 2

DHHC-13 protein
MAMEKIKKFPIFSVFFLIVLMFFRKTRILKKGKSKRDFRSFFSMIRFISLAWRPLNKKILQSSKHKMSLIFRQQIG
RCLSTLKDLHEEAQDDIENVVEIRKGPIDALFGTIFDIVDLAERTITESNRIEQLDKMETPWRRNGFKNASSGTCL
PNRRNSNRSISVEWTCFG--IRSRRMWTSSLGCN---IGYYSTAAFTSR-H-FNWRKYEIDTSSLGLL-FTIWSSH
GSCQEWRRSNN-KYKRRDSSSLGCLHWKLYYNCLFARKI--YQRYER-FRSFGTYDGC--EFRTISYSYIHKS-CI
S-LH---EGEYCSSYFSCSSEFERSC-ADLFWSR-HENR-QWGFST-FDGQQIPKSS-QASDSSKYL-TGYNL-KG
YLSLVPWPIFYCNHFRLFSFLFHH-RLCNDWCSNWSIFSHKLLGGLGWTCFDSFIAFYFGTKKTNGSIWMSSSHLY
LLDGNC-ICIVNFQFKWIGSLVGSDFCLLNLGYFSIVLLDNVYNNFKN-LH-FQLDPNKSRCPSSFYNSVQRFHQR
SGRETNR-ILFYLLDSKDFILSSLLSM-QMCRWI-SSLSMDSQMCLSEESSSFRVFLSYNLHVSRVLRSIVVVHDW
CLHECIRIR-VSFRTSYCQK-RRRQVVEFG-LLSVNF-GIK-LFPTRLFFDAHFQKS-FRKPAKTNPKRPWFDGNQ
SHPRNPSCFRSRSHHLYSILTNFSSCLYHRDYSETKTPEKF--KDHNIART-SMGIQTKCED-NSKCV-SIGI-QV
WRWRRN—RTWIIFIRNIVFIFL

dhhc-14: strain VC771, allele *gk330*

exon 6 ->
ggaacttctcgaaggaaacgctaatgtgaacattcggaataaacaatcagaaacaccactggatatggctaggacg
atcaaaagtccacaaatcctaggtaacgcgctacactctaaagcgaccaaaattcaattgttcaactgcagatttg
atggaagacgctgctcgtcgccagggagtcagtcgaacaagttgtttccgacgatctttcgtgccgccaatcagca
catacttttcttcctggtcccaatgtttggatttttcatgacctatctccttttcaagtacttgccattgattat
tgccactttctccacactgatctcctgcatctttcttatggttcttattcggtttgactatcatgatcctacttac
aagctgcttccttatggagttacaattgcagaagccatcttaatggtcttatcgtggtaggtattcaagtttgaaa
atcttgccgttacactcttcacttttaatttcacttttgtcgtcaaacaaaagccaaaggataaaacggaccagat
aacgaacaggtgccgttggaaagagaaaggaagggcagattgatatctcgagtaaactagacgggtttataatgcc
atacgtatgattttatctcaatccacgtaaaaaaattattttcgaaaagtcgatcgtggggaaatagacttcaaaa
ataaaaatttaagaattttctagaacgcaaaaaagtttgctcaaattatttacaaaaatactttgaaatgactatt
tgaaattcttcaggtcagcatatgctcattggtacgtgccatggtgggctcaaatgctctttgttctttctgttct
tgctcttgcattcacattgttcaggtgagaaacagtattgtggcacttgaataacatagtgaataatttagaata
gggacactggatccgggggtcgtaagagctgccaagaactgtcatcagctatttgtgaatgaagctgaagcgggta
tccaacatcagcaaaaatactgcttcacttgcttcattcgcaaaatggatcatacaaagcactgcgccgtttgcgg
att
<- exon 9

DHHC-14 protein:
MNGDTEVLTHNLLKPAVVVDSFNLHAVISATQHGHVESVEAALKQGLSPNTTDDDGCSLLHWAAINNRLEVARLLI
SYNADANLIGGVLASSPIHWAARNGLVAMCAVLVKGGAVCNVRDIQGYTPIHLAIQGNHVPLVAYFLLKFEYAKDI
SDNSGMTPAMMCAKRSFTMFPLRLIVRAGADLSLKEHFSGNTALHLAAQDRNSSAVMELLEGNANVNIRNKQSETP
LDMARTIKSPQILDLMEDAARRQGVSRTSCFRRSFVPPISTYFFFLVPMFGFFMTYLLFKYLPLIIATFSTLISCI
FLMVLIRFDYHDPTYKLLPYGVTIAEAILMVLSWSAYAHWYVPWWAQMLFVLSVLALAFTLFRIGTLDPGVVRAAK
NCHQLFVNEAEAGIQHQQKYCFTCFIRKMDHTKHCAVCGFCVNNFDHHCPWLNSCVTRRNMREFIMFVISVSVSSA
IYCMATSHYALLQIEDHGLEEFLETDAFLMITIILSAMHALMLAVLFCVQMNQISQGVTTNDRIKARRAGHAHSHS
GSTDYNVIHHKPSISKRCHNLLEFFSSNGDPNW

dhhc-14: strain VC918, allele *ok1032*

exon 7 ->
atttgatggaagacgctgctcgtcgccagggagtcagtcgaacaagttgtttccgacgatctttcgtgccgccaat
cagcacatacttttcttcctggtcccaatgtttggatttttcatgacctatctccttttcaagtacttgccattg
attattgccactttctccacactgatctcctgcatctttcttatggttcttattcggtttgactatcatgatccta
cttacaagctgcttccttatggagttacaattgcagaagccatcttaatggtcttatcgtggtaggtattcaagtt
tgaaaatcttgccgttacactcttcacttttaatttcacttttgtcgtcaaacaaaagccaaaggataaaacggac
cagataacgaacaggtgccgttggaaagagaaaggaagggcagattgatatctcgagtaaactagacgggtttata
atgccatacgtatgattttatctcaatccacgtaaaaaaattattttcgaaaagtcgatcgtggggaaatagactt
caaaaataaaaatttaagaattttctagaacgcaaaaaagtttgctcaaattatttacaaaaatactttgaaatga
ctatttgaaattcttcaggtcagcatatgctcattggtacgtgccatggtgggctcaaatgctctttgttctttct
gttcttgctcttgcattcacattgttcaggtgagaaacagtattgtggcacttgaataacatagtgaataatttta
gaatagggacactggatccgggggtcgtaagagctgccaagaactgtcatcagctatttgtgaatgaagctgaagc
gggtatccaacatcagcaaaaatactgcttcacttgcttcattcgcaaaatggatcatacaaagcactgcgccgtt
tgcggattgtaagttttcatttctttgtatacaaaaataaactttataaatttgagttgcgtgaacaattttgat
catcattgcccatggctgaacagttgtgtgactcgccgaaacatgagggaattcatcatgtttgtcatttcggtgt
cagtgtcatcagcaatttactgcatggctacaagtcattatgcgctgctccaaattgaagatcatggtttgggtga
gtcgtttttacagtacctctaactagtaagaggttaatctgagaggttgaccactaagaggttaatcggattaaga
aaaaaaaattcaataaatgcgacttgggaaactccccaaacatgtttttttatgtcatgggaaattggttgtaaaac
taaactggtaaaatgttaactgcgactaactatgcatacattccttactcaggagtttatccgaaaaatatatgaa
tatttatttttacagaagaattcctggaaactgacgcgttcttgatgatcaccatcattctctcggcgatgcaGCA
GAAGCCATCTTAATGcgcactcatgcttgccgtgctgttctgtgttcaaatgaaccag
<- exon 11

DHHC-14 protein:
MNGDTEVLTHNLLKPAVVVDSFNLHAVISATQHGHVESVEAALKQGLSPNTTDDDGCSLLHWAAINNRLEVARLLI
SYNADANLIGGVLASSPIHWAARNGLVAMCAVLVKGGAVCNVRDIQGYTPIHLAIQGNHVPLVAYFLLKFEYAKDI
SDNSGMTPAMMCAKRSFTMFPLRLIVRAGADLSLKEHFSGNTALHLAAQDRNSSAVMELLEGNANVNIRNKQSETP
LDMARTIKSPQILDLMEDAARRQGVSRTSCFRRSFVPPISTYFFFLVPMFGFFMTYLLFKYLPLIIATFSTLISCI
FLMVLIRFDYHDPTYKLLPYGVTIAEAILMVLSWSAYAHWYVPWWAQMLFVLSVLALAFTLFRIGTLDPGVVRAAK
NCHQLFVNEAEAGIQHQQKYCFTCFIRKMDHTKHCAVCGFCVNNFDHHCPWLNSCVTRRNMREFIMFVISVSVSSA
IYCMATSHYALLQIEDHGLEEFLETDAFLMITIILSAMGRSHLNNAHSCLPCCSVFK-TR-IFHESGKYFSY-YCM
QYYF--FKFSSRLPIFK-NSYCVR-RFKKSC-K-INY-RFFC-LVVRSFIIHRRQLNCK--KSLKLAFPTKLGLLE
T-TQIFVDTFKCVIDSNSHITNREHSVIQF-KLFILVTKN-IQ-LL-ISQGVTTNDRIKARRAGHAHSHSGSTDYN
VIHHKPSISKRCHNLLEFFSSNGDPNW-KYKFGFYLHRT-KTCPAPRIFQT-ESKLFYGITNLSIKNKILVNVNQK
PKFKFHPRPFPHSQSTLFHFLSVLHEILHLYNLVVKRF-MLSISLFPSFISFFVKLFVHSG-NQVLGDI-SFPSVF
LLCSSLLRISEISFSLLFS-M-INFLEIK

dnj-14: RM2754 strain, allele *ok237*

between exons 1 and 2 of *glit-1* ->
aataatcaattcagtttctttaaaataatcttacatcattattttataacattctattttctatcattttgataat
aactactagaaaagtttaaatttctaggtaaacatagtttaaaaaattcaaaatacttacttggtttactccgcca
tggggaaatggtgttgtcgttgttttaaacggatcccatagatctactggacgcgttggtggtggaacaaattgtg
aaatgaccagcggtaatgtgaataagctattgaaaattgtgccggtgaacattccatgtgacgcgatctctgaaaa
atttaattttaaaaaagaaaaataaaatatctcttcgaaaaatttcattgaaaattgaaaattgataaaagccacg
caaaaaaaagcgaaaaatttttaggcaacgagtgatcatcaggttgatgacctacggtaacacacatttcgagctg
tgtcaatatgggaaacaacgcgctgcgggaccgcatgcgaggccggcggagcgcatttacgaccctcttcctctcc
cccactatgtgtcaccactgccgtatgggaatggttgcgtctatttacactctcatttttcgccgttgtctctccc
aattttcgcgctctccgtcaaggctcataagtgttttacatattgattttgacttgtgatctgaactgttcggcga
atatttcgctaaactgtttcccctcgacactctctctagttttttttctattggcattttaatgtgataggttta
gttttcaatttccgttgttttaaataaattcctccttgtttcctttctttttaaatgcaaatctaatttcaggga
aatgaactcagacggattacgggaagcggaggaagggagaacaagtggaggagcatctccccgtgaagaatctcca
gccgctgatcattcgcacgatccgaaaaagggacttcatttgtacaatgttctcggcattcagaaaaatgccacag
atgacgaaatcaaaaagtgagtctttgagttgaaaatacattttctaaattcctattcttgctataaagaagtatt
gttatcagtgtaacgcagttatttttattataatcgttaaatttaatcaattgtggtttcttctgacttgaaaatt
gtacaaattgggtgtgtccattccgaacgaaatcgagtaaattttgtgaaaagtgaaaattgttggaacaatttga
cgaatgtacccaaatgaccaaatttcgtaatgtgacttctcgaaatttttaatgaggcttcaaagtttcgaaaaa
atgtttcatttttgataatttctccaatttttggtccattttccgtgttgcagcggtcaaaaattagcgtttatca
gccttctttacatattttggttgcttgtcttaccttatgtcgtcgatagaagtacatttaaagcctaggtaaccaa
ttttgatcattcatggttgactaatggcttgatttgtactttagctattaaaaaacgcgatataaactatcaaatc
acgcaaaaaatattatttaaggcattggagactggagatattggcgaaaattgagccatttttttcaagactttg
aagccccataaatgtttttgagaaattctcgtgaactgtcattacaaaattctttaatttcgccacctttattgaa
tctatactaatcttttaaaaagttcgataacttggtacgataactagatattgaaaactgacagttcagggagaga
ccaatagttttttttgaaacaattaaatttttttcagagcgtatcgcaaactagccctccgctatcatcccgacaa
aaacctagatggagatccggaaaaaacggaaatgttcaaagaaatcaactacgcaaatgcagtgctctcaaatcca
aataaacgtcgtgtctatgacgagatgggagagaccgggctgaaactgatggagcagtttggagaggatgagaaga
ttctgcagtggatgttgaagccttggttcaaatggacatttttcgcgttcggacttctcacgggtggcttcttctg
ctgctgttgtggttgtatgtgttgttgtcaatgctgttgcaatttctgttgtggaaagtacaagccgaagcacgat
gatgagtttgccgatgagacgtcggacggagatgtgattgttgatcaaccgacagcttccgagccaatgccagata
cgaataacagacaggtgccgattgtgattgccatgcctccaccgccttctcaaaa
<- exon 2

DNJ-14 protein
MNSDGLREAEEGRTSGGASPREESPAADHSHDPKKGLHLYNVLGIQKNATDDEIKKAYRKLALRYHPDKNLDGDPE
KTEMFKEINYANAVLSNPNKRRVYDEMGETGLKLMEQFGEDEKILQWMLKPWFKWTFFAFGLLTGGFFCCCCGCMC
CCQCCCNFCCGKYKPKHDDEFADETSDGDVIVDQPTASEPMPDTNNRQVPIDCHASTAFSKRL

ppt-1: strain MN1, allele *gk139*

```
exon 2 ->
gtgactgttgttgcaatccgttgtctatgggatctgtgaaaaaactattcgaggagcaaattcctggagtttacgt
tcacagtcttcaattgggatctagtattacaaaagacattgagcatggattttatgcaaataccaatgaacttgtc
tatatggcatgtatcaaaattaagaacgatcctgaactaaagaatggatataatgcgatcggattctcacaaggag
cacagttttgtaaatcgcgtttattgaatttaaattttaaaaaattttgtagaacggcaatttttcaggagagcg
gttgcccaaagatgcccaaatccaccaatgaagaatttggtgtcagtcggtggtcaacatcaaggagttttggag
ccccgtactgcattggtgacaatattatgtgcaatggcgtgagacgtctcattgacttgggagcttatcttccatt
tgtacaaaaacggtacgagtatttttgtctttcatttcattatttttaacagttttctagagttgttcaagccca
gtactggcacgacccaaatcaagtcgaagagtataaaaaaacgttctattttcttggctgatatcaataacgaaaac
gtaaggatttttaaaacatttttttgaagtattaattaataatttctgtacattttggtccttttttgttttgaaa
aaactgtttttggtgattgaaaattataactttttctgtaaaaagatgcgccgggattagtttaatgaacggtggt
gctttatttttctttttctaaaaattattcctgccggttgacatttgaatttcaaaatcgttagaaaatcgtaatcat
taaaataattgaaaaaaaaagtatttttgtttcagaataacaacccgacttacaaacgcaacttattgagtctcaa
aaacctggttctggtgaaattcaatcaagatcatatggttgtaccaaaggattcatct
                                                    <- exon 5

PPT-1 protein
MRYFPLLLCLLAITTAEFRNATKQVPVVMWHGMGDCCCNPLSMGSVKKLFEEQIPGVYVHSLQLGSSITKDIEHGF
YANTNELVYMACIKIKNDPELKNGYNAIGFSQGAQFLRAVAQRCPNPPMKNLVSVGGQHQGVFGAPYCIGDNIMCN
GVRRLIDLGAYLPFVQKRVVQAQYWHDPNQVEEYKKRSIFLADINNENE-QPDLQTQLIESQKPGSGEIQSRSYGC
TKGFILVRVLQRR-Y-HNSPNERNRPVQRGSYWIEEAS-EWTNPFYGRGWRSLANSKKCACQRYYQKIFYVNLFDF
QKETTRIVKLVRKNEL-NYH
```

ppt-1: strain VC166, allele *gk131*

```
exon 1 ->
atgagatattttccccttctactttgcctactggccataactacagcagaattccggaatgTTTctacaaagcagg
ttccagtggtcatgtggcatggaatgggttagttgtaacttaattactgaaaaagtgcgaacattatgatttttag
gtgactgttgttgcaatccgttgtctatgggatctgtgaaaaaactattcgaggagcaaattcctggagtttacgt
tcacagtcttcaattgggatctagtattacaaaagacattgagcatggattttatgcaaataccaatgaacttgtc
tatatggcatgtatcaaaattaagaacgatcctgaactaaagaatggatataatgcgatcggattctcacaaggag
cacagttttt
 <- exon 2

PPT-1 protein
MRYFPLLLCLLAITTAEFRNVATKQVPVVMWHGMGDCCCNPLSMGSVKKLFEEQIPGVYVHSLQLGSSITKDIEHG
FYANTNELVYMACIKIKNDPELKNGYNAIGFSQGAQFLRAVAQRCPNPPMKNLVSVGGQHQGVFGAPYCIGDNIMC
NGVRRLIDLGAYLPFVQKRVVQAQYWHDPNQVEEYKKRSIFLADINNENNNNPTYKRNLLSLKNLVLVKFNQDHMV
VPKDSSWFGFYKDGDIDTILPMNETDLYKEDRIGLKKLHESGRIHFMDVDGDHLQIPRSVLVNDIIKKYFM
```

ppt-1: strain VC168, allele *gk134*

```
before exon 1 ->
aactgtttttggtgattgaaaattataacttttttctgtaaaaagatgcgccgggattagtttaatgaacggacccc
actctaatcatttcttcgttttcttgaagaatgagatattttccccttctactttgcctactggccataactacag
cagaattccggaatgctacaaagcaggttccagtggtcatgtggcatggaatgggttagttgtaacttaattactg
aaaaagtgcgaacattatgattttaggtgactgttgttgcaatccgttgtctatgggatctgtgaaaaaactatt
cgaggagcaaattcctggagtttacgttcacagtcttcaattgggatctagtattacaaaagacattgagcatgga
ttttatgcaaataccaatgaacttgtctatatggcatgtatcaaaattaagaacgatcctgaactaaagaatggat
ataatgcgatcggattctcacaaggagcacagttttgtaaatcgcgtttattgaatttaaattttaaaaaatttt
gtagaacggcaatttttcaggagagcggttgcccaaagatgcccaaatccaccaatgaagaatttggtgtcagtcg
gtggtcaacatcaaggagtttttggagccccgtactgcattggtgacaatattatgtgcaatggcgtgagacgtct
cattgacttgggagcttatcttccatttgtacaaaaacggtacgagtatttttgtctttcatttcattatttttta
acagttttctagagttgttcaagcccagtactggcacgacccaaatcaagtcgaagagtataaaaaacgttctatt
ttcttggctgatatcaataacgaaaacgtaaggatttttaaaacatttttttgaagtattaattaataatttctgt
acattttggtccttttttgttttgaaaaaactgtttttggtgattgaaaattataacttttctgtaaaaagatgc
gccgggattagtttaatgaacggtggtgctttattttcttttctaaaaattattcctgccggttgacatttgaatt
tcaaaatcgttagaaaatcgtaatcattaaaataattgaaaaaaaaagtatttttgtttcagaataacaacccgac
ttacaaacgcaacttattgagtctcaaaaacctggttctggtgaaattcaatcaagatcatatggttgtaccaaag
gattcatct
 <-exon 5

PPT-1 protein
MRYFPLLLCLLAITTAEFRNATKQVPVVMWHGMGDCCCNPLSMGSVKKLFEEQIPGVYVHSLQLGSSITKDIEHGF
YANTNELVYMACIKIKNDPELKNGYNAIGFSQGAQFLRAVAQRCPNPPMKNLVSVGGQHQGVFGAPYCIGDNIMCN
GVRRLIDLGAYLPFVQKRVVQAQYWHDPNQVEEYKKRSIFLADINNENNNNPTYKRNLLSLKNLVLVKFNQDHMVV
PKDSSWFGFYKDGDIDTILPMNETDLYKEDRIGLKKLHESGRIHFMDVDGDHLQIPRSVLVNDIIKKYFM
```

ppt-1: strain VC184, allele *gk140*

```
exon 1 ->
atgagatattttccccttctactttgcctactggccataactacagcagaattccggaatgctacaaagcaggttc
cagtggtcatgtggcatggaatggttagttgtaacttaattactgaaaaagtgcgaacattatgatttttTAagg
tgactgttgttgcaatccgttgtctatgggatctgtgaaaaaactattcgaggagcaaattcctggagtttacgtt
cacagtcttcaattgggatctagtattacaaaagacattgagcatggattttatgcaaataccaatgaacttgtct
atatggcatgtatcaaaattaagaacgatcctgaactaaagaatggatataatgcgatcggattctcacaaggagc
acagttttgtaaatcgcgtttattgaatttaaattttaaaaaattttgtagaacggcaatttttcaggagagcgg
ttgcccaaagatgcccaaatccaccaatgaagaatttggtgtcagtcggtggtcaacatcaaggagtttttggagc
cccgtactgcattggtgacaatattatgtgcaatggcgtgagacgtctcattgacttgggagcttatcttccattt
gtacaaaaacggtacgagtatttttgtctttcatttcattatttttaacagttttctagagttgttcaagcccag
tactggcacgacccaaatcaagtcgaagagtataaaaaacgttctattttcttggctgatatcaataacgaaaac
                                                                  <- exon 4

PPT-1 protein
MRYFPLLLCLLAITTAEFRNATKQVPVVMWHGMGDCCCNPLSMGSVKKLFEEQIPGVYVHSLQLGSSITKDIEHGF
YANTNELVYMACIKIKNDPELKNGYNAIGFSQGAQFLRAVAQRCPNPPMKNLVSVGGQHQGVFGAPYCIGDNIMCN
GVRRLIDLGAYLPFVQKMELFKPSTGTTQIKSKSIKNVLFSWLISITKTITTRLTNATY-VSKTWFW-NSIKIIWL
YQRIHLGSGSTKTVILTQFSQ-TKPTCTKRIVLD-RSFMRVDESILWTWMEITCKFQEVCLSTILSKNILC
```

spe-10: strain BA744, allele *hc104*

```
exon 3 ->
actttatatgtacgtgacagtgacaattggttattacgttcagtcaacaattcaagcaaccatttatttgattgtt
ggatcatttctgtttgttatgtcaatgtggagtcttgcaaaaacgttgttcacgagagttggcagagttccagaaa
gatatcgacctagtaaagaacttgaagatagattgaaagcagtcacaccgatggagaaaaatTgatacgtggtaga
gaaatcgacacctgaacag
```

SPE-10 sequence

MSWYSKIYVAVREYRAKHKITGWILTRCLNVLLFIQLILLWWSLYMYVTVTIGYYVQSTIQATIYLIVGSFLFVMS
MWSLAKTLFTRVGRVPERYRPSKELEDRLKAVTPMEKN*YVVEKSTPEQLAQQNTILEEMCTYCKVVVAECDQVGR
LKYCYECGHIKPDRARHCSSCGKCCIKYDHHCPWINMCVTHVNYKYFLLYIIYTSFLVYWYLLTSLEGAVRYFINQ
QWTDELGKFLFYLFSFIVGGVFGYYPLGELIIFHYQLISLNETTVEQTKPALLRFDNAADYNMGKYNNFQSVFGWG
LWLCPIDSSTQDGLHFDIRYVNTQQRNRFVRIEEEPSSTQSSQSSIQ

APPENDIX 2: HITS FROM PREVIOUS MAMMALIAN PROTEOMIC SCREENS

High confidence hits from previous studies using palmitoyl-proteomics on mammalian material are shown. The studies are numbered as follows:

1. (Kang *et al.*, 2008)
2. (Zhang *et al.*, 2008)
3. (Martin and Cravatt, 2009)
4. (Yang *et al.*, 2010)
5. (Yount *et al.*, 2010)
6. (Dowal *et al.*, 2011)
7. (Merrick *et al.*, 2011)
8. (Forrester *et al.*, 2011)
9. (Martin *et al.*, 2012)
10. (Ivaldi *et al.*, 2012)
11. (Marin *et al.*, 2012)

Abbr., abbreviation of protein (if different from gene name).

Gene	Protein name	Abbr.	1	2	3	4	5	6	7	8	9	10	11
0610007 P14Rik	probable ergosterol biosynthetic protein 28										✓		
1110007 C09Rik	bcl10-interacting caspase-associated recruitment domain (CARD) protein										✓		
1810026 J23Rik	uncharacterized protein C19orf52 homologue										✓		
2510039 O18Rik	uncharacterized protein KIAA2013 precursor								✓				
Abat	4-aminobutyrate aminotransferase							✓					
Abcb6	ATP-binding cassette subfamily B member 6					✓		✓					
Abcc4	multidrug resistance-associated protein 4					✓		✓					
Abce1	ATP-binding cassette subfamily E member 1												✓
Acaa1b	3-ketoacyl-CoA thiolase B, peroxisomal										✓		
Acaa2	3-ketoacyl-CoA thiolase, mitochondrial										✓		
Acadl	long-chain specific acyl-CoA dehydrogenase, mitochondrial precursor									✓			
Acat1	acetyl-CoA acetyltransferase, mitochondrial						✓						
Aco2	aconitate hydratase, mitochondrial						✓						
Acsl3	acyl-CoA synthetase long-chain family member 3										✓		
Acsl5	long-chain fatty-acid-CoA ligase 5										✓		
Acta1	actin, α skeletal muscle				✓								
Acta2	actin, aortic smooth muscle				✓								
Actb	actin, cytoplasmic 1												✓
Actbl	β-actin-like protein 2									✓			
Actc1	actin, α cardiac muscle 1				✓								
Actg1	actin, cytoplasmic 2			✓									✓
Actg2	actin, γ enteric smooth muscle				✓								
Actn1	α-actinin 1												✓
Actn4	α-actinin 4												✓
Adam10	a disintegrin and metalloproteinase 10 precursor										✓	✓	
Adam17	a disintegrin and metalloproteinase 17 precursor isoform B					✓			✓				
Adcy6	adenylate cyclase type 6							✓					
Adfp	adipose differentiation-related protein										✓		
Adpgk	ADP-dependent glucokinase								✓		✓		
Afg3l2	AFG3-like protein 2							✓					
Agpat1	lysophosphatidic acid acyltransferase α	LPAATα	✓		✓				✓				
Ahcy	adenosylhomocysteinase												✓
Ahnak	neuroblast differentiation-associated protein AHNAK												✓
AI462493	UPF0723 protein C11orf83 homologue precursor										✓		
Ak1	adenylate kinase isoenzyme 1 isoform 2										✓		
Akap1	A-kinase anchor protein 1, mitochondrial									✓			
Alb	serum albumin											✓	
Aldh1b1	aldehyde dehydrogenase X, mitochondrial precursor					✓							

Gene	Protein name	Abbr.	1	2	3	4	5	6	7	8	9	10	11
Aldh2	aldehyde dehydrogenase, mitochondrial						✓						
Aldh3a2	fatty aldehyde dehydrogenase									✓			
Aldh3b1	aldehyde dehydrogenase 3B1 isoform 1					✓			✓				
Aldh6a1	methylmalonate-semialdehyde dehydrogenase		✓										
Aldoa	fructose bisphosphonate aldolase A isoform 1			✓						✓			
Alpl	alkaline phosphatase 2, liver precursor										✓		
Amy1a	α-amylase 1							✓					
Antxr1	anthrax toxin receptor 1					✓							
Antxr2	anthrax toxin receptor 2												✓
Anxa2	annexin A2 isoform 1			✓							✓		
Anxa6	annexin A6 isoform a										✓		
Apmap	adipocyte plasma membrane associated protein										✓		
Apoo	apolipoprotein O										✓		
Apool	apolipoprotein O-like										✓		
Arcn1	coatomer subunit δ												✓
Arf1	ADP-ribosylation factor 1				✓						✓		
Arf2	ADP-ribosylation factor 2										✓		
Arf3	ADP-ribosylation factor 3				✓						✓		
Arf4	ADP-ribosylation factor 4												✓
Arf5	ADP-ribosylation factor 5							✓					
Arhgdia	Rho-GDP dissociation inhibitor α		✓								✓		
Arhgdib	Rho-GDP dissociation inhibitor β												✓
Arl15	ADP-ribosylation factor-like protein 15					✓		✓	✓		✓		
Arl6ip1	ADP-ribosylation factor-like protein 6 interaction protein 1										✓		
Arl6ip6	ADP-ribosylation factor-like protein 6 interaction protein 6				✓						✓		
Armc10	armadillo repeat-containing protein 10										✓		
Arpc1a	actin-related protein 2/3 complex subunit 1A		✓										
Art2b	T-cell ecto-ADP-ribosyltransferase 2 precursor										✓		
Asah1	acid ceramidase							✓					
Astn1	astroactin 1		✓										
Atad3a	ATPase family ATPase associated with diverse cellular activities (AAA) domain-containing protein 3A							✓					
Atl1	atlastin-1							✓					
Atp11a	probable phospholipid-transporting ATPase IH					✓							
Atp11b	probable phospholipid-transporting ATPase IF					✓		✓					
Atp1a1	α1 subunit of sodium/potassium ATPase isoform long				✓			✓		✓	✓		
Atp1a3	cation transporting ATPase				✓								
Atp1b1	β1 subunit of sodium/potassium-ATPase		✓										
Atp1b2	β2 subunit of sodium/potassium-ATPase		✓										
Atp1b3	β3 subunit of sodium/potassium-ATPase										✓		
Atp2a1	sarcoplasmic/endoplasmic reticulum calcium ATPase 1										✓		
Atp2a2	sarcoplasmic/endoplasmic reticulum calcium ATPase 2										✓		
Atp2a3	sarcoplasmic/endoplasmic reticulum calcium ATPase 3										✓		
Atp2b3	plasma membrane Ca^{2+} transporting ATPase 3		✓										
Atp2c1	ATPase Ca^{2+}-sequestering		✓										
Atp5a1	ATP synthase subunit α, mitochondrial						✓						✓
Atp5l	ATP synthase subunit γ							✓					
Atp5o	ATP synthase subunit O, mitochondrial						✓						
Atp6v0a2	V-type proton ATPase 116 kDa subunit α isoform 2							✓					
Atp6v1b2	vacuolar ATP synthase subunit B, brain isoform										✓		
Atp9a	probable phospholipid-transporting ATPase IIa		✓										
Atrn	attractin		✓										
AU040320	dyslexia-associated protein KIAA0319-like protein isoform 1												
Aup1	ancient ubiquitous protein 1 isoform long				✓	✓						✓	
B4galt1	β-1,4-galactosyltransferase 1, long isoform										✓	✓	
B4galt3	β-1,4-galactosyltransferase 3										✓		
Bak	BCL2 antagonist/killer 1								✓				
Bat5	B-associated transcript 5				✓	✓							
BC002199	BC002199 protein										✓		
BC031181	UPF0729 protein C18orf32 homologue										✓		
Bcam	Lutheran blood group glycoprotein precursor					✓							
Bckdk	[3-methyl-2-oxobutanoate [lipoamide]] kinase							✓					
Bet1	BET1 homologue							✓			✓	✓	
Bet1l	BET1-like protein							✓			✓		
Bk	brain-kidney protein		✓										
Bri3bp	brain protein I3 (BRI3)-binding protein								✓		✓		
Bsg	basigin precursor isoform 1										✓		
Bst2	bone marrow stromal antigen 2 precursor										✓	✓	

Gene	Protein name	Abbr.	1	2	3	4	5	6	7	8	9	10	11
C12orf10	protein melanocyte proliferating gene 1, mitochondrial	MYG1											✓
C14orf166	protein C14orf166				✓	✓							
C14orf24	protein C14orf24					✓							
C1orf75	transmembrane protein 206					✓							
C1orf95	protein C1orf95							✓					
C1qbp	complement component 1 Q subcomponent-binding protein, mitochondrial							✓					✓
C21orf33	ES1 protein homologue, mitochondrial									✓			
C22orf25	protein C22orf25							✓					
C2orf18	protein C2orf18												✓
C2orf88	protein C2orf88							✓					
C6orf125	uncharacterised protein C6orf125												✓
C8orf82	protein C8orf82							✓				✓	
C9orf169	protein C9orf169					✓							
Cacfd1	calcium channel flower homologue isoform 1										✓		
Cacng	voltage-gated calcium channel γ8 subunit		✓										
Cacybp	calcyclin-binding protein										✓		
Cad	carbamoyl-phosphate synthetase 2, aspartate transcarbamylase, and dihydroorotase									✓			
Cadm4	cell adhesion molecule 4	SynCAM4	✓										
Calhm2	calcium homeostasis modulator protein 2										✓		
Calr	calreticulin precursor			✓									
Canx	calnexin		✓		✓	✓	✓	✓	✓		✓	✓	✓
Cap1	adenylyl cyclase-associated protein 1						✓						
Capg	capping protein (actin filament), gelsolin-like						✓						
Capn5	calpain 5		✓										✓
Carns1	carnitine synthase 1									✓			
Cars2	probable cysteinyl-tRNA synthetase							✓					
Cask	calcium/calmodulin-dependent serine protein kinase					✓							
Cav1	caveolin-1					✓							✓
Ccdc109a	coiled-coil domain-containing protein 109A							✓				✓	
Ccdc69	coiled-coil domain-containing protein 69										✓		
Ccny	cyclin Y		✓		✓	✓		✓	✓				
Ccnyl1	cyclin Y-like 1										✓		
Ccs	copper chaperone for superoxide dismutase							✓					
Cct2	T-complex protein 1 subunit β				✓								
Cct5	T-complex protein 1 subunit ε				✓								✓
Cct6a	T-complex protein 1 subunit ζ												✓
Cct8	T-complex protein 1 subunit θ												✓
Cd151	CD151 antigen					✓		✓		✓	✓		
Cd1d1	antigen-presenting glycoprotein CD1d1 precursor										✓		
Cd1d2	antigen-presenting glycoprotein CD1d2 precursor										✓		
Cd247	CD247 antigen										✓		
Cd28	CD28 antigen										✓		
Cd36	platelet glycoprotein 4							✓	✓				
Cd37	leukocyte antigen CD37										✓		
Cd38	ADP-ribosyl cyclase 1 isoform 1				✓			✓					
Cd3d	T-cell surface glycoprotein CD3 δ chain precursor				✓						✓		
Cd44	CD44 antigen					✓	✓		✓		✓	✓	✓
Cd47	leukocyte surface antigen CD47 precursor										✓		
Cd48	CD48 antigen										✓		
Cd5	T-cell surface glycoprotein CD5 precursor				✓								
Cd53	leukocyte surface antigen CD53											✓	
Cd63	CD63 antigen					✓		✓				✓	✓
Cd69	early activation antigen CD69							✓					
Cd70	tumour necrosis factor ligand superfamily member 7					✓						✓	
Cd74	CD74 molecule, major histocompatibility complex, class II invariant chain								✓			✓	
Cd81	CD81 antigen		✓			✓					✓	✓	
Cd82	CD82 antigen							✓			✓	✓	✓
Cd9	CD9 antigen					✓						✓	✓
Cd99	CD99 antigen									✓			✓
Cd99l2	CD99 antigen-like protein 2							✓					
Cdc42	cell division cycle 42		✓					✓					
Cdc42se1	cell division cycle 42 small effector protein 1							✓			✓		
Cdc42se2	cell division cycle 42 small effector protein 2							✓			✓		
Cdcp1	complement C1r/C1s, Uegf, Bmp1 (CUB) domain-containing protein 1 precursor					✓							
Cdip	liposaccharide induced tumour necrosis factor (TNF) factor (LITAF)-like protein							✓					
Cdipt	CDP-diacylglycerol--inositol 3-phosphatidyltransferase										✓		
Cept	choline/ethanolaminephosphotransferase 1									✓	✓		

Gene	Protein name	Abbr.	1	2	3	4	5	6	7	8	9	10	11
Cetp	cholesteryl ester transfer protein							✓					
Cfl1	cofilin-1			✓									✓
Cfl2	cofilin-2												✓
Chchd3	coiled-coil-helix-coiled-coil-helix domain-containing protein 3, mitochondrial precursor										✓		
Chd5	chromodomain helicase DNA binding protein 5										✓		
Chdh	choline dehydrogenase, mitochondrial precursor										✓		
Chrna5	neuronal acetylcholine receptor subunit α5										✓		
Chst11	carbohydrate sulfotransferase 11 isoform 1				✓								
Cisd1	CDGSH iron sulphur domain 1		✓								✓		
Cisd2	CDGSH iron sulphur domain 2										✓		
Ckap4	cytoskeleton-associated protein 4		✓	✓		✓	✓		✓			✓	✓
Cldn3	claudin-3					✓		✓					
Cldn5	claudin-5							✓					
Cldnd1	claudin domain-containing protein 1 isoform 1					✓							
Clec2d	C-type lectin domain family 2 member D										✓		
Clic1	chloride intracellular channel 1			✓									
Clld6	chronic lymphocytic leukaemia deletion region gene 6 protein							✓					
Cln6	ceroid lipofuscinosis, neuronal 6										✓		
Clptm1	cleft lip and palate transmembrane protein 1										✓		
Cltc	clathrin heavy chain 1 isoform 1				✓								
Cmtm3	chemokine-like factor (CKLF)-like myelin and lymphocyte (MAL) and related proteins for vesicle trafficking and membrane link (MARVEL) transmembrane domain-containing protein 3							✓					
Cmtm5	chemokine-like factor (CKLF)-like myelin and lymphocyte (MAL) and related proteins for vesicle trafficking and membrane link (MARVEL) transmembrane domain-containing protein 5							✓					
Cmtm7	chemokine-like factor (CKLF)-like myelin and lymphocyte (MAL) and related proteins for vesicle trafficking and membrane link (MARVEL) transmembrane domain-containing protein 7							✓					
Cnpy2	protein canopy homologue 2 precursor										✓		
Col4a1	collagen α-1(IV) chain									✓			
Col4a2	collagen α-2(IV) chain									✓			
Commd9	copper metabolism mouse u2af1-rs1 region 1 (MURR1) (COMM) domain-containing protein 9							✓					
Comt	catechol *O*-methyltransferase membrane-bound isoform					✓		✓					
Comtd1	catechol *O*-methyltransferase domain-containing protein 1							✓					
Cox16	cytochrome c oxidase assembly protein COX16 homologue, mitochondrial										✓		
Cox20	cytochrome c oxidase protein 20 homologue										✓		
Cox4nb	endoplasmic reticulum membrane protein complex subunit 8										✓		
Cox6c	cytochrome c oxidase subunit VIc		✓										
Cpd	carboxypeptidase D precursor				✓						✓		
Csnk1g1	casein kinase I isoform γ1							✓			✓		
Csnk1g2	casein kinase I isoform γ2										✓		
Csnk1g3	casein kinase I isoform γ3					✓		✓					
Cst4	cystatin-S							✓					
Ctdsp1	carboxy-terminal domain RNA polymerase II polypeptide A small phosphatase 1					✓					✓		
Ctdspl	carboxy-terminal domain phosphatase-like protein							✓			✓		
Ctl1	choline transporter-like protein 1							✓					
Ctl2	choline transporter-like protein 2							✓					
Ctnnd1	catenin δ1 isoform 1AB					✓							
Ctnnd2	catenin δ2; neural plakophilin-related ARM repeat protein	NPRAP	✓										
Ctse	cathepsin E preproprotein										✓		
Cxadr	coxsackievirus and adenovirus receptor		✓			✓							
Cxcr4	chemokine (C-X-C motif) receptor 4										✓		
Cyb5b	cytochrome b5 type B						✓	✓			✓		✓
Cyb5d2	neuferricin precursor										✓		
Cyb5r3	NADH-dependent cytochrome c reductase		✓		✓						✓		
Cyba	cytochrome b-245 α polypeptide								✓				
Cybb	cytochrome b-245 β polypeptide								✓				
Cycs	cytochrome c									✓			
Cyp51	cytochrome P450, family 51										✓		
Daam1	dishevelled associated activator of morphogenesis 1		✓					✓					
Dag1	dystroglycan							✓			✓		✓
Daglb	Sn1-specific diacylglycerol lipase β				✓	✓		✓	✓				
Dbt2	dihydrolipoamide branched chain transacylase E2							✓					

Gene	Protein name	Abbr.	1	2	3	4	5	6	7	8	9	10	11
Dcun1d3	defective in cullin neddylation 1 (DCN1) domain-containing 3					✓							
Ddx39a	nuclear RNA helicase			✓									
Ddx39b	spliceosome RNA helicase DDX39B			✓									
Degs1	sphingolipid δ4-desaturase DES1										✓		
Derl1	derlin-1										✓		
Desi2/ Pppde1	desumoylating isopeptidase 2	DESI2							✓		✓		
Dhcr24	24-dehydrocholesterol reductase precursor										✓		
Dhrs4	dehydrogenase/reductase SDR family member 4 isoform 1										✓		
Dhrs7b	dehydrogenase/reductase SDR family member 7B isoform 1										✓		
Dlg2	postsynaptic density protein 93	PSD-93	✓										
Dlg4	postsynaptic density protein 95	PSD-95	✓										
Dlgap	discs large-associated protein 4							✓					
Dnah1	dynein heavy chain 1							✓					
Dnajb6	DnaJ homologue subfamily B member 6										✓		
Dnajc11	DnaJ homologue subfamily C member 11										✓		
Dnajc5	cysteine string protein	CSP	✓			✓		✓	✓				
Dolpp1	dolichyldiphosphatase 1							✓					
Dpysl2	dihydropyrimidinase-related protein 2												✓
Dsg1	desmoglein-1												✓
Dsg2	desmoglein-2					✓							
Dsg4	desmoglein-4												✓
Dsp	desmoplakin							✓					
Dync1h1	cytoplasmic dynein heavy chain				✓								
Ebag9	estrogen receptor binding site associated antigen 9	RCAS1	✓		✓						✓		
Ece1	endothelin-converting enzyme 1					✓		✓					✓
Ecgf1	platelet-derived endothelial cell growth factor							✓					
Eef1a1	elongation factor 1α 1			✓									
Eef1b	elongation factor 1β						✓						
Eef1e1	eukaryotic translation elongation factor 1 ε-1							✓					
Eef1g	elongation factor 1γ									✓			
Eef2	elongation factor 2			✓									✓
Efcab14	EF-hand calcium-binding domain-containing protein 14										✓		
Efnb3	ephrin-B3		✓										
Efr3a	*S. cerevisiae* EFR3 homolog A					✓		✓	✓				
Efr3b	*S. cerevisiae* EFR3 homolog B		✓										
Eif3a	eukaryotic translation initiation factor 3 subunit 10				✓								
Eif3g	eukaryotic translation initiation factor 3 subunit G								✓				
Eif3k	eukaryotic translation initiation factor 3 subunit 12					✓							
Eif4a1	eukaryotic translation initiation factor 4A-1						✓						
Eif5a	eukaryotic translation initiation factor 5A-1							✓		✓			
Elovl1	elongation of very long fatty acids protein 1					✓					✓		
Emb	embigin precursor										✓		
Emc1	endoplasmic reticulum membrane protein complex subunit 1 isoform 2 precursor										✓		
Eno1	α-enolase												✓
Eno3	β-enolase isoform 1			✓									
Entpd1	ectonucleoside triphosphate diphosphohydrolase 1											✓	
Epha5	Eph receptor A5		✓										
Ephb2	Eph receptor B2		✓										
Eprs	glutamyl-prolyl-tRNA synthetase		✓		✓								
Erbb2ip	lamina-associated polypeptides 2 isoform 1	LAP2			✓	✓		✓			✓		
Ergic1	endoplasmic reticulum-Golgi intermediate compartment protein 1								✓		✓		
Ergic2	endoplasmic reticulum-Golgi intermediate compartment protein 2				✓						✓		
Ergic3	endoplasmic reticulum-Golgi intermediate compartment protein 3		✓		✓				✓		✓	✓	✓
Ero1l	endoplasmic reticulum oxidoreductase 1 (ERO1)-like										✓		
Esd	*S*-formylglutathione hydrolase									✓			
Esyt1	extended synaptotagmin 1									✓			
Ethe1	ethylmalonic encephalopathy 1								✓				
Exoc3l2	exocyst complex component 3-like protein 2							✓					
Exoc3l4	exocyst complex component 3-like protein 4							✓					
F3	tissue factor precursor					✓							
Fabp4	fatty acid-binding protein, adipocyte												✓
Fam108a1	abhydrolase domain-containing protein FAM108A1							✓			✓		
Fam108b	family with sequence similarity 108, member B								✓		✓		

Gene	Protein name	Abbr.	1	2	3	4	5	6	7	8	9	10	11
Fam108b1	family with sequence similarity 108, member B1		✓		✓	✓		✓					
Fam108c1	family with sequence similarity 108, member C1		✓								✓		
Fam131b	family with sequence similarity 131, member B		✓										
Fam162a	family with sequence similarity 162, member A							✓				✓	
Fam171a2	family with sequence similarity 171, member A2		✓										
Fam171b	family with sequence similarity 171, member B		✓										
Fam219b	family with sequence similarity 219, member B										✓		
Fam49b	family with sequence similarity 49, member B				✓	✓		✓			✓		
Fam62b	family with sequence similarity 62, member B				✓								
Fam78a	family with sequence similarity 78, member A							✓			✓		
Fas	tumour necrosis factor receptor superfamily member 6											✓	
Fasn	fatty acid synthase									✓			✓
Fbxl20	F-box/leucine-rich repeat (LRR)-repeat protein 20							✓					
Fcer2	low affinity immunoglobulin ε Fc receptor											✓	
Fgr	Gardner-Rasheed feline sarcoma viral										✓		
Fkbp8	FK506 binding protein 8 isoform a										✓		
Flg	filaggrin							✓					
Flna	filamin-A isoform 1			✓									
Flnb	filamin-B												✓
Flot1	flotillin 1		✓		✓	✓		✓			✓	✓	✓
Flot2	flotillin 2		✓		✓	✓		✓	✓		✓	✓	✓
Frs2	fibroblast growth factor receptor substrate 2										✓		
Fscn1	fascin			✓									✓
Ftl	ferritin light chain												✓
Fut7	α-1,3-fucosyltransferase isoform 1										✓		
Fxyd5	FXYD domain-containing ion transport regulator 5										✓		
Fxyd6	FXYD domain-containing ion transport regulator 6		✓										
Fyn	Fyn non-receptor tyrosine kinase		✓		✓			✓			✓	✓	✓
Gabarapl2	γ-aminobutyric acid receptor-associated protein-like 2										✓		
Gabrg2	γ-amino butyric acid A receptor subunit γ2		✓										
Galnt1	polypeptide *N*-acetylgalactosaminyltransferase 1										✓		
Galnt12	polypeptide *N*-acetylgalactosaminyltransferase 12										✓		
Galnt2	polypeptide *N*-acetylgalactosaminyltransferase 2										✓		
Gapdh	glyceraldehyde-3-phosphate dehydrogenase			✓									
Gcs1	mannosyl-oligosaccharide glucosidase										✓		
Gcsaml	germinal centre-associated signaling and motility-like protein							✓					
Gfpt1	glucosamine-fructose-6-phosphate aminotransferase [isomerising] 1					✓							
Ggt7	γ-glutamyltranspeptidase		✓										
Glg1	Golgi apparatus protein 1		✓								✓		
Glipr2	Golgi-associated plant pathogenesis-related protein 1										✓		
Gls	glutaminase kidney isoform							✓					
Gm10273	predicted pseudogene 10273										✓		
Gm10366	predicted gene 10366										✓		
Gm10499	predicted gene 10499										✓		
Gm614	interleukin 2 receptor γ chain										✓		
Gna11	Gα11 G protein subunit		✓		✓	✓		✓		✓	✓		✓
Gna12	Gα12 G protein subunit					✓							
Gna13	Gα13 G protein subunit		✓		✓	✓		✓			✓	✓	✓
Gna14	Gα14 G protein subunit		✓										
Gna15	Gα15 G protein subunit				✓			✓					
Gnai1	Gαi1 G protein subunit		✓			✓		✓			✓		
Gnai2	Gαi2 G protein subunit		✓		✓	✓	✓	✓	✓		✓	✓	✓
Gnai3	Gαi3 G protein subunit		✓		✓	✓	✓	✓			✓	✓	✓
Gnao	Gαo G protein subunit		✓		✓								
Gnaq	Gαq G protein subunit		✓		✓	✓		✓	✓		✓		✓
Gnas	Gαs G protein subunit short		✓		✓	✓	✓	✓		✓	✓		✓
Gnas	Gαs G protein subunit XLαs isoform											✓	✓
Gnaz	Gαz G protein subunit		✓										
Gnb2	guanine nucleotide-binding protein G(I)/G(S)/G(T) subunit β2										✓		
Gnb2l1	guanine nucleotide-binding protein subunit β2-like 1												✓
Golga7	golgin subfamily A member 7				✓	✓		✓	✓		✓	✓	
Golgb1	Golgi autoantigen, golgin subfamily b, macrogolgin 1										✓		
Golim4	Golgi integral membrane protein 4					✓					✓		✓
Got2	aspartate aminotransferase, mitochondrial						✓						
Gpi	glucose-6-phosphate isomerase					✓	✓						
Gpm6a	glycoprotein m6a		✓										
Gpm6b	glycoprotein m6b		✓										

Gene	Protein name	Abbr.	1	2	3	4	5	6	7	8	9	10	11
Gpr126	developmentally regulated G protein-coupled receptor β1					✓							
Gprc5a	retinoic acid induced protein 3					✓							✓
Gprc5c	G protein-coupled receptor family 5 member C precursor					✓							
Gprin1	G protein-regulated inducer of neurite outgrowth 1	GRIN1	✓										
Gpsn2	very long chain enoyl-CoA reductase										✓		
Gria1	glutamate receptor subunit α1	GluR1	✓										
Gria2	glutamate receptor subunit α2	GluR2	✓										
Gria3	glutamate receptor subunit α3	GluR3	✓										
Grid1	glutamate receptor subunit δ1	δ1-GluR	✓										
Grk6	G protein-coupled receptor kinase 6							✓					
Grpel1	GrpE protein homologue 1							✓					
Gstp1	glutathione-*S*-transferase P			✓									
H2-Q1	histocompatibility 2, Q region locus 1, precursor										✓		
H2afx	histone H2A							✓					
H2afy	core histone macro-H2A.1 isoform 2				✓								
Hadha	trifunctional enzyme subunit α, mitochondrial precursor				✓								
Hadhb	trifunctional enzyme subunit β, mitochondrial precursor				✓						✓		
Hccs	cytochrome c-type haem lyase									✓			
Hic2	hypermethylated in cancer 2 protein										✓		
Hist1h2bn	histone H2B type 1-N							✓					
Hist1h4a	histone H4												✓
Hla-a	HLA class I histocompatibility antigen				✓								
Hla-b	HLA class I histocompatibility antigen				✓			✓				✓	
Hla-c	HLA class I histocompatibility antigen				✓							✓	✓
Hla-e	major histocompatibility complex class 1, E				✓								
Hla-g	human leukocyte antigen (HLA) class I histocompatibility antigen, α chain G											✓	
Hmgcs1	hydroxymethylglutaryl-CoA synthase, cytoplasmic					✓							
Hmha1	minor histocompatibility protein HA-1							✓					
Hmox2	haem oxygenase 2				✓						✓		
Hnrnpa1	heterogeneous nuclear ribonucleoprotein A1												✓
Hnrnpa1l2	heterogeneous nuclear ribonucleoprotein A1-like 2												✓
Hnrnpa1l3	heterogeneous nuclear ribonucleoprotein A1-like 3												✓
Hnrnpa2b1	heterogeneous nuclear ribonucleoproteins A2/B1												✓
Hnrnpa3	heterogeneous nuclear ribonucleoprotein A3				✓								
Hnrnpk	heterogeneous nuclear ribonucleoprotein K						✓						✓
Hnrnpr	heterogeneous nuclear ribonucleoprotein R			✓									
Hnrnpul1	heterogeneous nuclear ribonucleoprotein U-like protein 1									✓			
Hp1bp3	heterochromatin protein 1-binding protein 3				✓								
Hras	H-Ras		✓		✓	✓		✓		✓	✓	✓	✓
Hsd17b10	hydroxyacyl-CoA dehydrogenase type II isoform 1					✓							
Hsd17b11	estradiol 17β-dehydrogenase 11 precursor										✓		
Hsd17b12	hydroxysteroid (17-β) dehydrogenase 12								✓		✓		
Hsp90aa1	heat shock protein 90 α2			✓									
Hsp90b1	endoplasmin precursor										✓		
Hspa1a	heat shock 70 kDa protein 1A				✓								
Hspa1b	heat shock 70 kDa protein 1B				✓								
Hspa8	heat shock cognate 71 kDa protein isoform 1			✓									
Hspa9	heat shock 70 kDa protein 9									✓			
Hspb1	heat shock protein β1												✓
Hspd1	chaperonin	HSP60		✓			✓						✓
Htatip2	oxidoreductase HIV-1 Tat interactive protein 2							✓					
Hyal2	hyaluronidase 2 precursor										✓		
Icam2	intercellular adhesion molecule 2										✓		✓
Icoslg	ICOS ligand												✓
Ifitm1	interferon-induced transmembrane protein 1											✓	✓
Ifitm2	interferon-induced transmembrane protein 2								✓		✓		✓
Ifitm3	interferon-induced transmembrane protein 3						✓	✓	✓		✓		✓
Igf2r	cation independent mannose-6-phosphate receptor precursor				✓						✓		
Igkc	immunoglobulin κ chain C region												✓
Igsf8	immunoglobulin superfamily member 8		✓		✓						✓		
Il27ra	interleukin 27 receptor subunit α precursor										✓		
Il2rg	cytokine receptor common γ chain precursor										✓		
Ildr2	immunoglobulin-like domain containing receptor 2		✓										
Imp3	U3 small nucleolar ribonucleoprotein protein IMP3										✓		
Inpp5a	inositol polyphosphate-5-phosphatase 40 kDa		✓					✓					

Gene	Protein name	Abbr.	1	2	3	4	5	6	7	8	9	10	11
Irgm	immunity-related GTPase family M protein isoform 1						✓						
Itga3	integrin α3												✓
Itga6	integrin α6										✓		✓
Itgal	integrin αL precursor										✓		
Itgb1	integrin β1 precursor										✓		
Itgb2	integrin β2 precursor										✓		
Itgb4	integrin β4 isoform β4C precursor					✓							
Itm2a	integral membrane protein 2A										✓		
Itm2b	integral membrane protein 2B										✓		
Itm2c	integral membrane protein 2C isoform 1					✓					✓		
Jam3	junctional adhesion molecule C							✓					
Jup	junction plakoglobin												✓
Kalrn	kalirin							✓					
Khdrbs1	KH domain-containing RNA-binding signal transduction-associated protein 1												✓
Khsrp	far upstream element-binding protein 2												✓
Kiaa0152	protein KIAA0152					✓							
Kiaa2013	protein KIAA2013							✓				✓	
Kpnb1	importin subunit β1				✓						✓		
Kras	KRas GTPase isoform 1 precursor				✓	✓					✓		
Krt17	keratin, type I cytoskeletal 17			✓									
L1cam	neural cell adhesion molecule L1		✓										
Lamp2	lysosome-associated membrane glycoprotein 2										✓		
Lamtor1	late endosomal/lysosomal adaptor, MAPK and MTOR activator 1		✓				✓	✓	✓		✓	✓	
Laptm4a	lysosomal-associated transmembrane protein 4A					✓							
Lars	leucyl-tRNA synthetase, cytoplasmic				✓	✓							
Lass2	LAG1 longevity assurance homologue 2										✓		
Lass5	LAG1 longevity assurance homologue 5										✓		
Lat	linker for activation of T cells				✓			✓			✓		
Lat2	linker for activation of T cells family member 2							✓	✓		✓	✓	
Lbr	lamin-B receptor										✓		
Lck	proto-oncogene tyrosine-protein kinase Lck isoform 3				✓						✓	✓	✓
Ldha	L-lactate dehydrogenase A chain isoform 1			✓									
Ldhb	L-lactate dehydrogenase B chain												✓
Ldlr	low density lipoprotein receptor precursor										✓		
Leprot	leptin receptor gene-related protein							✓					
Lgals1	galectin-1			✓									✓
Lgals9	galectin-9 long isoform										✓		
Lhfp	lipoma high mobility group isoform I-C (HMGIC) fusion partner							✓					
Lhfpl2	lipoma high mobility group isoform I-C (HMGIC) fusion partner-like 2							✓					
Lman1	endoplasmic reticulum-Golgi intermediate compartment protein 53 precursor	ERGIC53									✓		
Lman2	vesicular integral membrane protein VIP36 precursor										✓		
Lmbrd2	limb receptor 1 (LMBR) domain-containing protein 2										✓		
Lnp	protein lunapark										✓		
Lnpep	leucyl-cysteinyl aminopeptidase isoform 1				✓	✓		✓	✓		✓	✓	
LOC 665506	T-cell receptor β2 chain C region-like										✓		
Lpcat1	lysophosphatidylcholine acyltransferase 1							✓					
Lphn1	latrophilin 1		✓										
Lrrc1	leucine rich repeat containing 1 isoform 1					✓							
Lrrc32	leucine rich repeat containing 32							✓					
Lrrc7	leucine rich repeat containing 7; densin-180		✓										
Lrrfip1	leucine rich repeat flightless-interacting protein 1												✓
Lsr	lipolysis-stimulated lipoprotein receptor					✓							
Ly6a	lymphocyte antigen 6A-2/6E-1 precursor										✓		
Ly6c1	lymphocyte antigen 6 complex, locus C1										✓		
Ly6c2	lymphocyte antigen 6 complex, locus C2										✓		
Ly6e	lymphocyte antigen 6 complex, locus E										✓		
Ly9	lymphocyte antigen 9								✓		✓		
Lyn	v-yes-1 Yamaguchi sarcoma viral related oncogene homologue					✓		✓					
M6pr	cation-dependent mannose-6-phosphate receptor						✓	✓	✓		✓	✓	
Magt	magnesium transporter protein 1										✓		
Man1b1	mannosidase α class 1B member 1										✓		
Map1lc3b	microtubule-associated proteins 1A/1B light chain 3B										✓		
March	E3 ubiquitin-protein ligase membrane-associated ring finger (C3HC4) (MARCH)							✓					

Gene	Protein name	Abbr.	1	2	3	4	5	6	7	8	9	10	11
Marcks	myristoylated alanine rich C-kinase substrate												✓
Marcksl1	myristoylated alanine rich C-kinase substrate (MARCKS)-related protein										✓		
Mbc2	extended synaptotagmin 1 isoform 1										✓		
Mblac2	metallo-β-lactamase domain containing 2		✓					✓		✓		✓	
Mbp	myelin basic protein		✓										
Mcam	melanoma cell adhesion molecule; cell surface glycoprotein MUC18		✓			✓							✓
Mcoln1	mucolipin-1 isoform 2										✓		
Mdga1	meprin/A5 protein/PTPμ (MAM) domain-containing glycophosphatidylinositol anchor protein 1 precursor										✓		
Mdh2	malate dehydrogenase, mitochondrial												✓
Me1	NADP-dependent malic enzyme												✓
Metap2	methionine aminopeptidase 2												✓
Mfap3	microfibril-associated glycoprotein 3 precursor										✓		
Mfap3l	microfibril-associated glycoprotein 3-like precursor										✓		
Mfsd6	major facilitator superfamily domain-containing protein 2							✓					
Mgst2	microsomal glutathione *S*-transferase 2										✓		
Mgst3	microsomal glutathione *S*-transferase 3									✓			
Mki67	antigen KI-67									✓			
Mlec	malectin		✓		✓			✓	✓		✓	✓	
Mlstd2	fatty acyl-CoA reductase 1										✓		
Mmp14	matrix metalloproteinase 14					✓							✓
Mnf1	mitochondrial nucleoid factor 1		✓						✓				
Mobkl3	MPS one binder kinase activator-like 3							✓					
Mobp	myelin-associated oligodendrocyte basic protein		✓										
Mpdu1	suppressor of Lec15							✓					
Mpp1	55 kDa erythrocyte membrane protein							✓			✓		
Mpp2	membrane protein palmitoylated 2		✓										
Mpp5	membrane-associated guanylate kinase (MAGUK) p55 subfamily member 5 isoform 1					✓							
Mpp6	membrane-associated guanylate kinase (MAGUK) p55 subfamily member 6					✓				✓	✓		
Mpst	mercaptopyruvate sulfotransferase		✓					✓					
Mreg	melanoregulin											✓	
Mrpl12	39S ribosomal protein L12							✓	✓			✓	
Mrps18a	28S ribosomal protein S18a, mitochondrial									✓			
Mrps18b	28S ribosomal protein S18b, mitochondrial											✓	
Ms4a1	B-lymphocyte antigen CD20											✓	
Mtap6	microtubule-associated protein 6	STOP	✓										
Mtch1	mitochondrial carrier homologue 1 isoform 1										✓		
Mtch2	mitochondrial carrier homologue 2										✓		
Mtdh	lysine-rich Ceacam1 co-isolated	Lyric	✓		✓	✓	✓	✓	✓		✓	✓	✓
Mthfd1l	monofunctional C1-tetrahydrofolate synthase, mitochondrial									✓			
Muc1	mucin 1, transmembrane					✓							
Myct1	Myc target protein 1							✓					
Myo1d	unconventional myosin Id									✓			
Myo1g	myosin IG				✓								
Myof	myoferlin								✓				✓
Napa	α-soluble N-ethylmaleimide-sensitive fusion factor (NSF) attachment protein										✓		
Nasp	nuclear autoantigenic sperm protein												✓
Ncam1	neural cell adhesion molecule 1		✓										
Ncam2	neural cell adhesion molecule 2		✓										
Ncl	nucleolin						✓						
Ncstn	nicastrin precursor										✓		
Ndfip1	neural precursor cell expressed developmentally downregulated protein 4 (NEDD4) family-interacting protein 1										✓		
Ndfip2	neural precursor cell expressed developmentally downregulated protein 4 (NEDD4) family-interacting protein 2										✓		
Nfxl1	NF-X1-type zinc finger protein									✓			
Nipsnap1	Nipsnap homolog 1		✓										
Nme1	nucleoside diphosphate kinase A isoform a			✓									
Nme2	nucleoside diphosphate kinase B						✓						
Nnt	NAD(P) transhydrogenase							✓					
Nos3	nitric oxide synthase, endothelial												✓
Npc1	Niemann-Pick C1 protein precursor										✓		
Nqo1	NAD(P)H dehydrogenase [quinone] 1					✓							
Nr4a2	nuclear receptor subfamily 4 group A member 2							✓					
Nras	N-ras		✓			✓	✓	✓	✓		✓	✓	✓
Nrm	nurim										✓		

Gene	Protein name	Abbr.	1	2	3	4	5	6	7	8	9	10	11
Nrp1	neuropilin-1 isoform 1 precursor					✓							
Nrsn2	neurensin 2					✓							
Nsddr	neural stem cell-derived dendrite regulator		✓										
Nucb1	nucleobindin-1 precursor										✓		
Nup210	nuclear pore membrane glycoprotein 210 precursor										✓		
Ociad1	ovarian carcinoma immunoreactive antigen (OCIA) domain-containing protein 1 isoform 1										✓		
Orai1	calcium release-activated calcium channel protein 1							✓					
Osmr	oncostatin M receptor					✓							
Ostc	oligosaccharyltransferase complex subunit OSTC							✓					
Oxa1l	inner membrane protein oxidase (cytochrome c) assembly 1-like (OXA1L), mitochondrial										✓		
Oxsm	3-ocoacyl-[acyl carrier protein] synthase, mitochondrial							✓					✓
P2rx4	purinergic receptor P2X, ligand gated ion channel 4										✓		
P4hb	protein disulphide-isomerase	PDI								✓			
Pacsin3	protein kinase C and casein kinase substrate in neurons 3					✓							
Pag1	phosphoprotein associated with glycosphingolipid-enriched microdomains 1										✓		
Palm	paralemmin-1		✓			✓					✓		
Palm2	paralemmin-2		✓			✓							
Park7	protein DJ-1									✓			
Parp1	poly [ADP ribose] polymerase 1												✓
Pcdh1	protocadherin 1		✓										
Pcdh7	brain-heart protocadherin		✓										
Pdaf	placenta-derived apoptotic factor							✓					
Pdcd1	programmed cell death protein 1 precursor										✓		
Pde10a	phosphodiesterase 10A		✓										
Pdgfra	α-type platelet-derived growth factor receptor						✓						
Pdha1	pyruvate dehydrogenase E1 component subunit α, somatic form, mitochondrial									✓			
Pdia3	protein disulphide-isomerase A3										✓		
Pdia4	protein disulphide-isomerase A4										✓		
Pdia6	protein disulphide-isomerase A6										✓		
Pdro	ragulator complex protein PDRO												✓
Pdzk1ip1	PDZ domain-containing 1 (PDZK1)-interacting protein 1							✓					
Pecam1	platelet endothelial cell adhesion molecule										✓	✓	✓
Per1	period circadian homologue 1										✓		
Pfdn5	prefoldin subunit 5										✓		
Pfn1	profilin-1			✓			✓						✓
Pgam1	phosphoglycerate mutase 1			✓									
Pgam5	phosphoglycerate mutase 5									✓			
Pgd	6-phosphogluconate dehydrogenase, decarboxylating			✓			✓						
Pgrmc1	membrane-associated progesterone receptor component 1										✓		
Pgrmc2	membrane-associated progesterone receptor component 2										✓		
Phb	prohibitin						✓						
Phf8	plant homeo domain (PHD) finger protein 8						✓						
Phgdh	D-3-phosphoglycerate dehydrogenase						✓						
Pi4k2a	phosphatidylinositol 4-kinase type IIα		✓		✓	✓		✓	✓		✓	✓	✓
Pi4k2b	phosphatidylinositol 4-kinase type IIβ				✓	✓		✓			✓		
Pigk	phosphatidylinositol glycan anchor biosynthesis, class K								✓		✓		
Pign	glycophosphatidylinositol (GPI) ethanolamine phosphate transferase 1							✓					
Pigt	phosphatidylinositol glycan anchor biosynthesis, class T								✓				
Pik3r1	phosphatidylinositol 3-kinase regulatory subunit α isoform 2										✓		
Pip	prolactin-inducable protein							✓					
Pkm	pyruvate kinase 3 isoform 2			✓									
Pkm2	pyruvate kinase isozymes M1/M2												✓
Pknox1	homeobox protein PBX/knotted 1 homeobox 1 (PKNOX1)									✓			
Pkp1	plakophilin 1												✓
Pkp4	plakophilin 4		✓										
Plp2	proteolipid protein 2							✓					
Plscr1	phospholipid scramblase 1					✓		✓	✓		✓	✓	
Plscr3	phospholipid scramblase 3		✓			✓		✓	✓		✓	✓	✓
Plscr4	phospholipid scramblase 4							✓					

Gene	Protein name	Abbr.	1	2	3	4	5	6	7	8	9	10	11
Plxnb2	plexin B2		✓										
Pmp2	myelin P2 protein												✓
Podxl	podocalyxin												✓
Pon3	serum paraoxonase/lactonase 3										✓		
Por	NADPH--cytochrome P450 reductase										✓		
Ppia	peptidylprolyl cis-trans isomerase A			✓									
Ppib	peptidylprolyl cis-trans isomerase B		✓										
Ppif	peptidylprolyl cis-trans isomerase, mitochondrial											✓	
Ppp2r1a	serine/threonine protein phosphatase 2A 65 kDa regulatory subunit A α isoform										✓		✓
Praf2	prenylated Rab acceptor 1 family protein 2				✓			✓	✓		✓	✓	
Prdx6	peroxiredoxin 6		✓										✓
Preb	prolactin regulatory element-binding protein										✓		
Prg1	plasticity-related gene 1		✓										
Prg2	plasticity-related gene 2		✓										
Prkcsh	glucosidase 2 subunit β precursor				✓						✓		
Prkdc	DNA-dependent protein kinase catalytic subunit isoform 1				✓								
Prnd	prion-like protein doppel precursor										✓		
Prnp	major prion protein precursor										✓		
Procr	endothelial protein C receptor					✓	✓						✓
Psen1	presenilin-1 isoform 1					✓					✓	✓	
Psip1	PC4 and splicing factor arginine/serine-rich 1 (SFRS1)-interacting protein									✓			
Psmb8	proteasome subunit β type 8 precursor										✓		
Psmc1	26S proteasome regulatory subunit 4				✓								
Psmd11	26S proteasome non-ATPase regulatory subunit 11							✓					
Ptbp1	polypyrimidine tract-binding protein 1 isoform a				✓								
Ptgfrn	prostaglandin F2 receptor negative regulator		✓			✓							
Ptgir	prostacyclin receptor							✓					
Ptk7	protein tyrosine kinase 7 isoform D precursor					✓							
Ptplad1	3-hydroxyacyl-CoA dehydratase 3										✓		
Ptprc	receptor-type protein phosphatase C isoform 2 precursor										✓		
Ptprcap	protein tyrosine phosphatase receptor type C-associated protein precursor										✓		
Ptprf	receptor-type protein tyrosine kinase F precursor					✓							
Ptprn2	protein tyrosine phosphatase receptor type N2		✓										
Ptrh2	peptidyl-tRNA hydrolase 2				✓	✓					✓		
Pttg1ip	pituitary tumour-transforming gene 1 protein-interacting protein precursor				✓	✓		✓			✓		
Pus1	tRNA pseudouridine synthase A											✓	
Pvr	poliovirus receptor					✓					✓		✓
Pycr	pyrroline-5-carboxylate reductase 1										✓		
Rab10	Ras-related GTP-binding protein 10		✓										✓
Rab11a	Ras-related protein Rab-11A										✓		
Rab18	Ras-related protein Rab-18										✓		
Rab1a	Ras-related protein Rab-1A					✓							✓
Rab1b	Ras-related protein Rab-1B				✓								✓
Rab1c	Ras-related protein Rab-1C												✓
Rab2a	Ras-related GTP-binding protein 2A												✓
Rab3a	Ras-related GTP-binding protein 3A		✓										
Rab4a	Ras-related protein Rab-4A										✓		
Rab5b	Ras-related protein Rab-5B										✓		
Rab5c	Ras-related protein Rab-5C					✓					✓		
Rab7	Ras-related protein Rab-7A										✓		
Rac1	Ras-related C3 botulinum toxin substrate 1		✓								✓		
Rac2	Ras-related C3 botulinum toxin substrate 2										✓		
Rala	RalA		✓			✓			✓		✓	✓	✓
Ralb	RalB		✓			✓					✓	✓	✓
Ran	GTP-binding nuclear protein Ran												✓
Ranbp2	E3 SUMO-protein ligase RanBP2									✓			
Rap1a	Ras-related protein Rap-1a										✓		
Rap1b	Ras-related protein Rap-1b										✓		
Rap2a	Ras-related protein Rap-2a		✓		✓	✓		✓			✓	✓	
Rap2b	Ras-related protein Rap-2b		✓		✓	✓		✓	✓		✓	✓	✓
Rap2c	Ras-related protein Rap-2c				✓	✓	✓	✓			✓	✓	✓
Rbm13	maintenance of killer 16 (MAK16)-like protein RBM13 isoform 1										✓		
Rdh11	retinol dehydrogenase 11										✓		
Reep5	receptor accessory protein 5; deleted in polyposis 1		✓								✓		✓
Rell1	receptor expressed in lymphoid tissues (RELT)-like 1					✓				✓	✓		
Rer1	retention in endoplasmic reticulum 1 (RER1) homologue										✓		

Gene	Protein name	Abbr.	1	2	3	4	5	6	7	8	9	10	11
Rfc2	replication factor C subunit 2										✓		
Rftn1	raftilin							✓			✓	✓	
Rfx1	MHC class II regulatory factor RFX1										✓		✓
Rfx3	regulatory factor X3		✓										
RGD 1306271	similar to KIAA1549 protein		✓										
RGD 1563986	similar to RIKEN cDNA E330009J07 gene		✓										
Rgs19	regulator of G protein signaling 19							✓	✓		✓		
Rgs20	regulator of G protein signaling 20 isoform 6					✓							
Rhbdd2	rhomboid domain-containing protein 2				✓						✓		
Rheb	GTP-binding protein RheB							✓					
Rhoa	transforming protein RhoA					✓					✓		
Rhob	Rho-related GTP-binding protein RhoB		✓			✓							
Rhoq	Rho-related GTP-binding protein RhoQ							✓					
Rnasek	ribonuclease κ										✓		
Rnf11	RING finger protein 11							✓					
Rnh1	ribonuclease inhibitor												✓
Rnm1	ribonucleoside diphosphate reductase large subunit												✓
Rp2h	retinitis pigmentosa 2 homologue								✓		✓		
Rpl1	60S ribosomal protein L1						✓						
Rpl10	60S ribosomal protein L10				✓					✓			
Rpl10a	60S ribosomal protein L10a									✓			
Rpl11	60S ribosomal protein L11									✓			
Rpl12	60S ribosomal protein L12			✓									✓
Rpl13	60S ribosomal protein L13				✓								
Rpl15	60S ribosomal protein L15									✓			
Rpl17	60S ribosomal protein L17						✓						
Rpl18a	60S ribosomal protein L18a			✓									
Rpl19	60S ribosomal protein L19						✓						
Rpl29	60S ribosomal protein L29						✓						
Rpl3	60S ribosomal protein L3		✓		✓	✓	✓					✓	
Rpl30	60S ribosomal protein L30					✓							
Rpl3l	60S ribosomal protein L3-like									✓			
Rpl4	60S ribosomal protein L4						✓					✓	
Rpl5	60S ribosomal protein L5						✓						
Rpl6	60S ribosomal protein L6						✓						
Rpl7	60S ribosomal protein L7						✓						✓
Rpl7a	60S ribosomal protein L7a						✓			✓			
Rpl9	60S ribosomal protein L9								✓				✓
Rplp0	ribosomal protein, large P0			✓									
Rpn1	dolichyl-diphosphooligosaccharide--protein glycosyltransferase subunit 1 precursor										✓		
Rpn2	ribophorin II								✓		✓		
Rps11	40S ribosomal protein S11			✓						✓			
Rps15	40S ribosomal protein S15			✓									
Rps15a	40S ribosomal protein S15a			✓									
Rps16	40S ribosomal protein S16									✓			
Rps17	40S ribosomal protein S17				✓		✓						
Rps19	40S ribosomal protein S19		✓										
Rps2	40S ribosomal protein S2			✓									
Rps20	40S ribosomal protein S20 isoform 2			✓						✓			
Rps23	40S ribosomal protein S23				✓								
Rps27a	40S ribosomal protein S27a										✓		
Rps2-ps6	ribosomal protein S2, pseudogene 6						✓						
Rps3	40S ribosomal protein S3						✓						
Rps3a	40S ribosomal protein S3a isoform 1			✓									
Rps5	40S ribosomal protein S5				✓					✓			
Rps6	40S ribosomal protein S6				✓								✓
Rps8	40S ribosomal protein S8						✓						
Rras	R-Ras		✓		✓	✓		✓	✓		✓	✓	✓
Rras2	R-Ras2		✓			✓					✓	✓	✓
Rrs1	ribosome biogenesis regulatory protein homologue										✓		
Rspry1	ring finger and SPIa and ryanodine receptor (SPRY) domain containing 1					✓							
Rtn	reticulon 1		✓										
Rtn3	reticulon 3										✓		
Rtn4	reticulon 4 isoform C			✓	✓								✓
S100a14	protain S100-A14							✓					
S100a9	protein S100-A9												✓
Sacm1l	phosphatidylinositide phosphatase SAC1										✓		
Scamp1	secretory carrier membrane protein 1		✓		✓	✓		✓	✓		✓	✓	
Scamp2	secretory carrier membrane protein 2				✓	✓		✓	✓		✓	✓	
Scamp3	secretory carrier membrane protein 3		✓		✓	✓	✓	✓	✓		✓	✓	

Gene	Protein name	Abbr.	1	2	3	4	5	6	7	8	9	10	11
Scamp4	secretory carrier membrane protein 4					✓		✓			✓		
Scamp5	secretory carrier membrane protein 5		✓										
Scarb1	scavanger receptor class B member 1					✓					✓	✓	
Scarb2	scavanger receptor class B member 2; CD36 antigen-like 2; lysosomal integral membrane protein II	LIMP-II	✓			✓					✓	✓	✓
Scarf1	endothelial cells scavenger receptor							✓					
Scn2a1	sodium channel voltage-gated type 2α1		✓										
Scp2	nonspecific lipid transfer protein							✓					
Scrib	scribble isoform 3	LAP4			✓	✓					✓		
Sdhd	succinate dehydrogenase [ubiquinone] cytochrome b small subunit, mitochondrial										✓		
Sec11a	signal peptidase complex catalytic subunit SEC11A										✓		
Sec22b	vesicle trafficking protein Sec22b precursor										✓		
Sec61b	Protein transport protein Sec61 subunit β									✓			
Selenbp1	selenium-binding protein 1												✓
Selplg	selectin P ligand										✓		
Sema4d	semaphorin 4D		✓					✓			✓		
Sep15	15 kDa selenoprotein precursor										✓		
Sept6	septin 6		✓										
Sept8	septin 8		✓										
Serbp1	plasminogen activator inhibitor 1 RNA-binding protein isoform 1				✓								
Serpinb4	serpin B4												✓
Sf1	splicing factor 1									✓	✓		
Sft2d1	vesicle transport protein SFT2-domain 1				✓						✓		
Sft2d3	vesicle transport protein SFT2-domain 3							✓			✓		
Sidt1	SID1 transmembrane family member 1							✓					
Sidt2	SID1 transmembrane family member 2										✓		
Sil1	endoplasmic reticulum chaperone SIL1 homologue (*S. cerevisiae*)								✓				
Slc11a2	solute carrier family 11 (proton-coupled divalent metal ion transporters), member 2										✓		
Slc15a3	solute carrier family 15 member A3						✓						
Slc16a3	monocarboxylate transporter 4					✓							
Slc19a1	folate transporter 1					✓							
Slc1a1	excitatory amino acid transporter 1	EAAC1	✓										
Slc1a2	glutamate transporter 1; excitatory amino acid transporter 2	EAAC2; GLT1	✓										
Slc1a3	glutamate and aspartate-sodium transporter	GLAST	✓										
Slc1a4	neutral amino acid transporter A											✓	
Slc1a5	neutral amino acid transporter B				✓	✓	✓		✓		✓	✓	✓
Slc25a10	mitochondrial dicarboxylate carrier										✓		
Slc25a13	solute carrier family 25 (mitochondrial carrier, adenine nucleotide translocator), member 13										✓		
Slc25a32	solute carrier family 25 member 32										✓		
Slc25a33	solute carrier family 25 member 33										✓		
Slc25a36	solute carrier family 25 member 36										✓		
Slc25a3	phosphate carrier protein, mitochondrial precursor isoform A				✓								
Slc25a5	ADP/ATP carrier protein; adenine nucleotide translocator 2	ANT2		✓			✓				✓		
Slc25a6	ADP/ATP translocase 3				✓								
Slc26a2	sulphate transporter					✓							
Slc2a1	solute carrier family 2 (facilitated glucose transporter), member 1										✓		
Slc30a1	zinc transporter 1										✓		
Slc32a1	vesicular inhibitory amino acid transporter		✓										
Slc35b2	adenosine 3'-phospho 5'-phosphosulphate transporter 1					✓							
Slc35e2	solute carrier family 35 member E2				✓								
Slc38a2	solute carrier family 38 member A2				✓	✓				✓	✓		
Slc39a4	solute carrier family 39 (zinc transporter), member 4										✓		
Slc3a2	solute carrier family 3 member A2		✓								✓		
Slc43a3	solute carrier family 43 member A3							✓					
Slc44a1	choline transporter-like 1 isoform 1					✓			✓			✓	
Slc44a2	choline transporter-like 2		✓								✓		
Slc5a6	sodium-dependent multivitamin transporter					✓							
Slc7a1	high affinity cationic amino acid transporter 1					✓					✓		
Slc7a5	solute carrier family 7 (cationic amino acid transporter, y+ system), member 5										✓		
Slc8a1	sodium/calcium exchanger 1		✓										
Slc8a2	sodium/calcium exchanger 2		✓										
Slc9a6	sodium/hydrogen exchanger 6 isoform c				✓								
Slc9a9	sodium/hydrogen exchanger 9							✓					

Gene	Protein name	Abbr.	1	2	3	4	5	6	7	8	9	10	11
Smpd3	sphingomyelin phosphodiesterase 3		✓										
Snap23	synaptosomal-associated protein of 23 kDa				✓	✓	✓	✓	✓	✓	✓	✓	✓
Snap25	synaptosomal-associated protein of 25 kDa		✓										
Snd1	Staphylococcal nuclease domain-containing protein 1									✓			
Soat1	sterol *O*-acyltransferase 1										✓		
Sod1	superoxide dismutase [Cu-Zn]			✓									✓
Sod2	superoxide dismutase [Mn], mitochondrial												✓
Sort1	sortilin 1		✓					✓					
Spcs2	signal peptidase complex subunit 2										✓		
Spcs3	signal peptidase complex subunit 3										✓		
Spint2	serine protease inhibitor, Kunitz type 2										✓		
Spred1	sprouty protein with EVH-1 domain 1-related sequence		✓						✓				
Spred2	sprouty protein with EVH-1 domain 2-related sequence										✓		
Spryd7	SPIa and ryanodine receptor (SPRY) domain-containing protein 7										✓		
Src	proto-oncogene tyrosine-protein kinase Src												✓
Srprb	signal recognition particle receptor, B subunit										✓		
St6gal1	β galactoside α 2,6 sialyltransferase 1										✓		
Stard3nl	metastatic lymph node protein 64 (MLN64) N-terminal domain homologue					✓		✓				✓	
Steap3	metalloreductase six-transmembrane epithelial antigen of prostate 3							✓	✓				
Stip1	stress-induced phosphoprotein 1												✓
Stmn3	stathmin-like 3		✓										
Stmn4	stathmin-like 4		✓										
Stom	stomatin; erythrocyte band 7 integral membrane protein		✓		✓	✓		✓	✓		✓	✓	✓
Stt3a	STT3, subunit of the oligosaccharyltransferase complex, homolog A (*S. cerevisiae*)										✓		
Stt3b	STT3, subunit of the oligosaccharyltransferase complex, homolog B (*S. cerevisiae*)										✓		
Stx10	syntaxin 10				✓			✓					
Stx11	syntaxin 11							✓			✓	✓	✓
Stx12	syntaxin 12		✓		✓			✓	✓		✓	✓	✓
Stx1a	syntaxin 1a		✓										
Stx1b2	syntaxin 1b2		✓										
Stx2	syntaxin 2							✓					
Stx4a	syntaxin 4A (placental)										✓		
Stx5a	syntaxin 5 isoform 1										✓		
Stx6	syntaxin 6		✓		✓	✓			✓		✓	✓	✓
Stx7	syntaxin 7		✓						✓		✓	✓	
Stx8	syntaxin 8				✓	✓		✓	✓		✓	✓	
Surf4	surfeit locus protein 4 isoform 1				✓	✓					✓		
Susd3	sushi domain containing 3										✓		
Svip	small VCP/p97-interacting protein							✓					✓
Sybl1	synaptobrevin-like protein 1 isoform 2				✓								
Syne3	nesprin-3										✓		
Syt1	synaptotagmin 1		✓										
Syt11	synaptotagmin 11		✓										
Syt13	synaptotagmin 13										✓		
Syt2	synaptotagmin 2		✓										
Syt3	synaptotagmin 3		✓										
Syt5	synaptotagmin 5		✓										
Syt7	synaptotagmin 7		✓										
Taf15	TATA-binding protein-associated factor 2N												✓
Tap1	transporter 1, ATP-binding cassette, subfamily B				✓						✓		
Tbl2	transducin β-like protein 2									✓			
Tbxa2r	thromboxane A2 receptor							✓					
Tc2n	tandem C2 domains nuclear protein							✓					
Tesc	tescalcin							✓					
Tfrc	transferrin receptor		✓		✓	✓	✓	✓			✓	✓	✓
Them6	UPF0670 protein thioesterase superfamily member 6 (THEM6) homolog precursor										✓		
Thy1	Thy-1 membrane glycoprotein precursor										✓		
Timm22	translocase of inner mitochondrial membrane 22										✓		
Timm50	mitochondrial import inner membrane translocase subunit TIM50							✓		✓			
Timp1	metalloproteinase inhibitor 1							✓					
Tlcd1	TRAM/LAG1/CLN8 (TLC) domain-containing protein 1									✓			
Tloc1	translocation protein SEC62										✓		
Tm2d2	two transmembrane domain (TM2) domain-containing protein 2 precursor										✓		

Gene	Protein name	Abbr.	1	2	3	4	5	6	7	8	9	10	11
Tm4sf19	transmembrane 4 L six family member 19										✓		
Tm9sf2	transmembrane 9 superfamily member 2		✓							✓			
Tmbim1	transmembrane BAX inhibitor motif-containing protein 1							✓					
Tmco1	transmembrane and coiled-coil domains 1										✓		
Tmed10	transmembrane emp24-like trafficking protein 10 (yeast)										✓		
Tmed1	transmembrane emp24 domain-containing protein 1 precursor					✓							
Tmem11	transmembrane protein 11							✓					
Tmem115	transmembrane protein 115										✓		
Tmem134	transmembrane protein 134 isoform 1										✓		
Tmem168	transmembrane protein 168										✓		
Tmem16f	transmembrane protein 16F isoform 1										✓		
Tmem173	transmembrane protein 173										✓		
Tmem184c	transmembrane protein 184C											✓	
Tmem222	transmembrane protein 222							✓				✓	
Tmem33	transmembrane protein 33										✓		
Tmem43	transmembrane protein 43										✓		
Tmem50a	transmembrane protein 50A					✓		✓					
Tmem50b	transmembrane protein 50B							✓					
Tmem55a	transmembrane protein 55A							✓			✓		
Tmem55b	transmembrane protein 55B							✓	✓			✓	
Tmem59	transmembrane protein 59					✓					✓		
Tmem63a	transmembrane protein 63A							✓			✓	✓	
Tmem63b	transmembrane protein 63B					✓		✓					
Tmem97	transmembrane protein 97							✓					
Tmp3l	tropomyosin α3 chain-like protein				✓								
Tmppe	transmembrane protein with metallophosphoesterase domain							✓					
Tmx1	thioredoxin-related transmembrane protein 1											✓	
Tmx3	protein disulphide-isomerase TMX3							✓					
Tmx4	thioredoxin-related transmembrane protein 4							✓					
Tnfaip2	tumour necrosis factor α-induced protein 2					✓							
Tnfrsf10a	tumour necrosis factor superfamily member 10A precursor					✓							
Tnfrsf10b	tumour necrosis factor superfamily member 10B long isoform precursor					✓							
Tnfrsf8	tumour necrosis factor superfamily member 8											✓	
Tomm40	probable mitochondrial import receptor subunit TOM40 homolog isoform 1				✓						✓		
Tomm70a	translocase of outer mitochondrial membrane 70 homolog A (yeast)										✓		
Tpbg	trophoblast glycoprotein precursor					✓							
Tpi1	triosephosphate isomerase			✓									
Tpm3	tropomyosin α3 chain												✓
Traf3ip3	tumour necrosis factor (TNF) receptor-associated factor 3 (TRAF3)-interacting Jun N-terminal kinase-activating modulator				✓							✓	
Trap1	heat shock protein 75 kDa, mitochondrial precursor				✓								
Trappc3	trafficking protein particle complex 3	Bet3	✓			✓		✓	✓		✓	✓	✓
Trav4n-4	T cell receptor alpha variable 4N-4										✓		
Tspan13	tetraspanin-13										✓		
Tspan14	tetraspanin-14							✓		✓	✓		
Tspan15	tetraspanin-15							✓					
Tspan3	tetraspanin-3										✓		
Tspan33	tetraspanin-33							✓					
Tspan9	tetraspanin-9							✓					
Ttyh1	tweety homolog 1		✓										
Ttyh3	tweety homolog 3		✓			✓		✓			✓		
Tuba1a	tubulin α-1A chain										✓		
Tuba1b	tubulin α-1B chain										✓		
Tuba1c	tubulin α-1C chain										✓		
Tubb	tubulin β			✓									
Tubb2c	tubulin β-2C chain										✓		
Tufm	elongation factor Tu, mitochondrial									✓			
Txndc1/ Tmx1	thioredoxin-related transmembrane protein 1		✓	✓	✓	✓		✓	✓				✓
Txndc1	protein disulphide-isomerase thioredoxin domain-containing 1										✓		
Txndc10	protein disulphide-isomerase thioredoxin domain-containing 10					✓					✓		
Txndc12	protein disulphide-isomerase thioredoxin domain-containing 12										✓		
Txndc13	protein disulphide-isomerase thioredoxin domain-containing 13										✓		

Gene	Protein name	Abbr.	1	2	3	4	5	6	7	8	9	10	11
Txndc14	protein disulphide-isomerase thioredoxin domain-containing 14										✓		
Txndc4	protein disulphide-isomerase thioredoxin domain-containing 4										✓		
Uba1	ubiquitin-like modifier-activating enzyme 1									✓			
Uba52	ubiquitin A-52 residue ribosomal protein fusion product 1										✓		
Ubl3	ubiquitin-like protein 3 precursor										✓		
Ubtd1	ubiquitin domain-containing 10					✓							
Ubxd2	ubiquitin regulatory x (UBX) domain-containing protein 2										✓		
Ugt1a7c	UDP glucuronosyltransferase 1 family, polypeptide A7C								✓				
Upf1	regulator of nonsense transcripts 1 isoform 1					✓							
Uqcrfs1	cytochrome b-c1 complex subunit Rieske							✓					
Vamp1	vesicle-associated membrane protein 1; synaptobrevin 1		✓										✓
Vamp2	vesicle-associated membrane protein 2; synaptobrevin 2		✓								✓		✓
Vamp3	vesicle-associated membrane protein 3; synaptobrevin 3				✓	✓		✓	✓		✓	✓	✓
Vamp4	vesicle-associated membrane protein 4; synaptobrevin 4		✓		✓			✓	✓		✓		
Vamp5	vesicle-associated membrane protein 5; synaptobrevin 5							✓	✓				
Vamp7	vesicle-associated membrane protein 7; synaptobrevin 7					✓		✓	✓		✓	✓	
Vangl1	vang-like protein 1 isoform 1					✓							
Vcp	transitional endoplasmic reticulum ATPase						✓						
Vdac1	voltage-dependent anion-selective channel protein 1										✓		
Vdac2	voltage-dependent anion-selective channel protein 2						✓				✓		✓
Vdac3	voltage-dependent anion-selective channel protein 3										✓		✓
Vim	vimentin			✓	✓								
Vsig8	V-set and immunoglobulin domain-containing protein 8												✓
Vsnl1	visinin-like protein 1	VILIP-1	✓										
Vti1b	vesicle transport through interaction with t-SNAREs 1B										✓		
Wdr46	WD repeat-containing protein 46										✓		
Xpo1	exportin-1				✓								
Xrcc6	X-ray repair cross-complementing protein 6			✓									
Yes1	Yes non-receptor tyrosine kinase		✓			✓		✓					✓
Ywhag	14-3-3 protein γ					✓							
Ywhaq	14-3-3 protein θ			✓									
Ywhaz	14-3-3 protein ζ/δ												✓
Zdhhc17	zinc finger, DHHC-type containing 17; huntingtin-interacting protein 14	DHHC17/ HIP14	✓										
Zdhhc20	zinc finger, DHHC-type containing 20	DHHC20			✓	✓					✓		
Zdhhc5	zinc finger, DHHC-type containing 5	DHHC5				✓					✓		
Zdhhc6	zinc finger, DHHC-type containing 6	DHHC6			✓								
Zfyve28	zinc finger FYVE domain-containing protein 28		✓										
Zgpat	zinc finger, CCCH-type with G patch domain										✓		
Zmpste24	CAAX prenyl protease 1 homologue							✓			✓		
Znf330	zinc finger protein 330									✓			
Znf44	zinc finger protein 44 isoform 2			✓									

APPENDIX 3: RAT BRAIN ACYL-BIOTIN EXCHANGE (ABE) HITS

APPENDIX 3.1 HITS WITH MULTIPLE UNIQUE PEPTIDES IN THE EXPERIMENTAL SAMPLE

Proteins identified in previous mammalian proteomic studies are highlighted in green. Proteins which were not present in the control sample were given an arbitrary value of 0.2 to avoid dividing by zero, similar to previous proteomic studies (Dowal *et al.*, 2011; Roth *et al.*, 2006; Yang *et al.*, 2010). Proteins with a ratio of less than 5 were discarded (Martin and Cravatt, 2009). Abbr., abbreviation (if different from gene name); LFQ, label-free quantification.

Gene	Protein	Abbr.	Experiment 1			Experiment 2		
			LFQ intensity ABE	LFQ intensity Control	Ratio LFQ ABE: Control	LFQ intensity ABE	LFQ intensity Control	Ratio LFQ ABE: Control
Abat	4-aminobutyrate aminotransferase, mitochondrial		482100	0.2	2410500	5595900	0.2	27979500
Aco2	aconitate hydratase, mitochondrial		7894300	0.2	39471500	51073000	0.2	2.55E+08
Adamts3	A disintegrin and metalloproteinase with thrombospondin motifs 3 precursor		725400	0.2	3627000			
Ak2	adenylate kinase 2, mitochondrial isoform 1		42217	0.2	211085			
Aldoa	fructose-bisphosphonate aldolase A		2847400	0.2	14237000	1E+08	0.2	5.02E+08
Aldoc	fructose-bisphosphonate aldolase C		3773300	0.2	18866500	42040000	0.2	2.1E+08
Arf3	ADP-ribosylation factor 3		545520	0.2	2727600			
Atp1a1	sodium/potassium-transporting ATPase subunit α1					9444100	0.2	47220500
Atp1a3	sodium/potassium-transporting ATPase subunit α3		2066500	412570	5.008847	2.17E+08	0.2	1.08E+09
Atp5a1	ATP synthase subunit α, mitochondrial		1496700	0.2	7483500			
Atp6v1b2	V-type proton ATPase subunit B, brain isoform		322540	0.2	1612700			
Camk2a	calcium/calmodulin-dependent protein kinase type II α chain		537040	0.2	2685200			
Camk2b	calmodulin-dependent protein kinase II isoform βM					7248700	0.2	36243500
Cfl1	cofilin-1		1023800	0.2	5119000	49261000	0.2	2.46E+08
Ckb	creatine kinase B-type		22954000	0.2	1.15E+08	1.66E+08	0.2	8.28E+08
Ckmt1	creatine kinase U-type, mitochondrial					1346400	0.2	6732000
Cltc	clathrin heavy chain 1					10668000	0.2	53340000
Cnp	2,3-cyclic nucleotide phosphodiesterase		2106800	0.2	10534000			
Crmp1	dihydropyrimidinase-related protein 1		78921	0.2	394605			
Cs	citrate synthase, mitochondrial					11948000	0.2	59740000
Dbn1	drebrin isoform A					11220000	0.2	56100000
Dlg4	disks large homolog 4; post-synaptic density protein of 95 kDa	PSD-95	493370	0.2	2466850			
Dnajc5	DnaJ homolog subfamily C member 5; cysteine string protein	CSP				38940000	0.2	1.95E+08
Dnm1	dynamin-1 isoform 5		751820	0.2	3759100			
Dpysl2	dihydropyrimidinase-related protein 2		1254700	0.2	6273500	3.4E+08	0.2	1.7E+09
Eef1a2	elongation factor 1α2		1508600	0.2	7543000			

Gene	Protein	Abbr.	Experiment 1			Experiment 2		
			LFQ intensity ABE	LFQ intensity Control	Ratio LFQ ABE: Control	LFQ intensity ABE	LFQ intensity Control	Ratio LFQ ABE: Control
Eno2	γ-enolase		8781700	0.2	43908500	1.08E+08	0.2	5.39E+08
Gap43	neuromodulin		7199700	0.2	35998500	59052000	0.2	2.95E+08
Gapdh	glyceraldehyde-3-phosphate dehydrogenase					2.99E+08	0.2	1.49E+09
Gda	guanine deaminase		4129500	0.2	20647500			
Gdi1	Rab-GDP dissociation inhibitor α		3899300	0.2	19496500	17001000	0.2	85005000
Glul	glutamine synthetase					35828000	0.2	1.79E+08
Gnao1	guanine nucleotide-binding protein Gαo isoform α2		10887000	0.2	54435000	47540000	0.2	2.38E+08
Gnaq	guanine nucleotide-binding protein Gαq isoform α		3197800	0.2	15989000			
Gnb1	guanine nucleotide-binding protein G(I)/G(S)/G(T) subunit β1		463150	0.2	2315750			
Got1	aspartate aminotransferase, cytoplasmic; glutamate oxaloacetate transaminase		452090	0.2	2260450			
Gpm6a	glycoprotein m6a		3522000	0.2	17610000	85690000	0.2	4.28E+08
Gprin1	G protein-regulated inducer of neurite outgrowth 1					20692000	0.2	1.03E+08
Gstm5	glutathione-*S*-transferase μ5		145380	0.2	726900	14215000	0.2	71075000
Hsp90aa1	heat shock protein HSP90α					16453000	0.2	82265000
Kcnk12	potassium channel subfamily K member 12		39928	0.2	199640			
Khsrp	far upstream element-binding protein 2					30141000	0.2	1.51E+08
Kpnb1	importin subunit β1					1695000	0.2	8475000
Ldha	L-lactate dehydrogenase A-chain		2311700	0.2	11558500	17208000	0.2	86040000
Ldhb	L-lactate dehydrogenase B chain		10237000	0.2	51185000			
Ldhc	L-lactate dehydrogenase B chain					23133000	0.2	1.16E+08
Map1a	microtubule-associated protein 1A					2.73E+08	0.2	1.36E+09
Map2	microtubule-associated protein 2 isoform MAP2x					9511500	0.2	47557500
Mdh1	malate dehydrogenase, cytoplasmic		1080800	0.2	5404000	19940000	0.2	99700000
Mdh2	malate dehydrogenase, mitochondrial		3508000	0.2	17540000	12105000	0.2	60525000
Mt1a	metallothionein-1					584640	0.2	2923200
Mt3	metallothionein-3					454700	0.2	2273500
Ncdn	neurochondrin		948540	0.2	4742700	17582000	0.2	87910000
Ndrg2	N-Myc downstream regulated gene 2					12000000	0.2	60000000
Ndufs1	NADH-ubiquinone oxidoreductase 75 kDa subunit, mitochondrial		1038100	0.2	5190500	4677500	0.2	23387500
Ndufv2	NADH dehydrogenase flavoprotein 2, mitochondrial					7148700	0.2	35743500
Nsf	vesicle-fusing ATPase; N-ethylmaleimide-sensitive fusion protein		717510	0.2	3587550			
Nyw1	ischaemia related factor NYW-1		1029300	0.2	5146500			
Ola1	Obg-like ATPase 1					1901100	0.2	9505500
Palm	paralemmin isoform CRA_a					9222200	0.2	46111000
Park7	protein DJ-1		1400300	0.2	7001500			
Pebp1	phosphatidyl-ethanolamine-binding protein 1		5347600	0.2	26738000	23406000	0.2	1.17E+08

Gene	Protein	Abbr.	Experiment 1			Experiment 2		
			LFQ intensity ABE	LFQ intensity Control	Ratio LFQ ABE: Control	LFQ intensity ABE	LFQ intensity Control	Ratio LFQ ABE: Control
Pgk1	phosphoglycerate kinase 1		2498200	0.2	12491000	22283000	0.2	1.11E+08
Pkm2	pyruvate kinase isozymes M1/M2 isoform M1		2891100	437250	6.612007	2.75E+08	0.2	1.38E+09
Plp1	myelin proteolipid protein		3315000	0.2	16575000	3.34E+08	0.2	1.67E+09
Ppid	peptidyl-prolyl cis-trans isomerase					9235800	0.2	46179000
Ppp1cc	serine/threonine protein phosphatase PP1γ catalytic subunit isoform γ2		396150	0.2	1980750			
Ppp2r1a	protein phosphatase regulatory subunit 2A					7728500	0.2	38642500
Ppp3ca	serine/threonine protein phosphatase 2B catalytic subunit α isoform isoform 1		90627	0.2	453135			
Prdx2	peroxiredoxin-2		899260	0.2	4496300			
Prdx6	peroxiredoxin-6		154320	0.2	771600	47680000	0.2	2.38E+08
Pygb	phosphoglycerase		265320	0.2	1326600			
Rab1	Ras-related protein Rab-1A		309210	0.2	1546050			
Rhob	Rho-related GTP-binding protein RhoB					8172400	0.2	40862000
Rtn1	reticulon-1		431750	0.2	2158750			
Scrn1	secernin-1		455160	0.2	2275800	7791400	0.2	38957000
Sdhb	succinate dehydrogenase iron-sulphur subunit, mitochondrial		108470	0.2	542350			
Sfrs3	splicing factor, arginine/serine-rich 3					46575000	0.2	2.33E+08
Slc1a2	excitatory amino acid transporter 2 isoform Glt1	EAAT2				46687000	0.2	2.33E+08
Slc25a4	ADP/ATP translocase 1		126470	0.2	632350			
Snap25	synaptosomal-associated protein of 25 kDa		1092200	0.2	5461000	57362000	0.2	2.87E+08
Snap91	clathrin coat assembly protein AP180 long isoform					4719700	0.2	23598500
Stip1	stress-induced phosphoprotein 1					3140800	0.2	15704000
Stx1a	syntaxin-1A		1577000	0.2	7885000	23372000	0.2	1.17E+08
Stx1b	syntaxin-1B		5869800	0.2	29349000	1.33E+08	0.2	6.63E+08
Suv39h1	histone lysine *N*-methyltransferase SUV39H1		368700	0.2	1843500			
Syt1	synaptotagmin 1		1108500	0.2	5542500	27543000	0.2	1.38E+08
Tpi1	triosephosphate isomerase		1961300	0.2	9806500	72368000	0.2	3.62E+08
Trappc3	trafficking protein particle complex subunit C3	Bet3				28084000	0.2	1.4E+08
Ttyh1	tweety homolog 1		775360	0.2	3876800			
Tuba4a	tubulin α4A chain					51013000	0.2	2.55E+08
Tubb2a	tubulin β2A chain					1.14E+09	0.2	5.7E+09
Tubb3	tubulin β3 chain		1249300	0.2	6246500	22050000	0.2	1.1E+08
Tubb4	tubulin β4					13458000	0.2	67290000
Tubb5	tubulin β5 chain isoform 1		5631900	0.2	28159500	59683000	0.2	2.98E+08
Ubqln2	ubiquilin 2					1420100	0.2	7100500
Uchl1	ubiquitin carboxy-terminal hydrolase enzyme L1		259250	0.2	1296250	47077000	0.2	2.35E+08
Vamp2	vesicle-associated membrane protein 2; synaptobrevin 2					73143000	0.2	3.66E+08
Vcp	transitional endoplasmic reticulum ATPase		451070	0.2	2255350	12268000	0.2	61340000

Gene	Protein	Abbr.	Experiment 1			Experiment 2		
			LFQ intensity ABE	LFQ intensity Control	Ratio LFQ ABE: Control	LFQ intensity ABE	LFQ intensity Control	Ratio LFQ ABE: Control
Wisp1	WNT1-inducible signaling pathway protein 1		34670000	0.2	1.73E+08			
Ywhae	14-3-3 protein ε		343230	0.2	1716150	2045000	0.2	10225000
Ywhag	14-3-3 protein γ					6116700	0.2	30583500
Ywhah	14-3-3 protein ε					18347000	0.2	91735000
Ywhaq	14-3-3 protein θ		188190	0.2	940950	1.31E+08	0.2	6.54E+08
Ywhaz	14-3-3 protein ζ/δ		1284800	0.2	6424000	2E+08	0.2	9.99E+08

APPENDIX 3.2 HITS WITH A SINGLE UNIQUE PEPTIDE IN THE EXPERIMENTAL SAMPLE

Proteins identified in previous mammalian proteomic studies are highlighted in green. Proteins which were not present in the control sample were given an arbitrary value of 0.2 to avoid dividing by zero, similar to previous proteomic studies (Dowal *et al.*, 2011; Roth *et al.*, 2006; Yang *et al.*, 2010). Proteins with a ratio of less than 5 were discarded (Martin and Cravatt, 2009). Abbr., abbreviation (if different from gene name); LFQ, label-free quantification.

Gene	Protein	Abbr.	Experiment 1			Experiment 2		
			LFQ intensity ABE	LFQ intensity Control	Ratio LFQ ABE: Control	LFQ intensity ABE	LFQ intensity Control	Ratio LFQ ABE: Control
Actbl2	actin β-like 2					2.8E+08	0.2	1.4E+09
Actg2	actin, α skeletal muscle		1168700	0.2	5843500			
Akt2	RACβ serine/threonine protein kinase		1248400	0.2	6242000			
Amph	amphiphysin					1711500	0.2	8557500
Ap2b1	AP-2 complex subunit β isoform 2		98662	0.2	493310			
Apoa5	apolipoprotein A-V					62751000	0.2	3.14E+08
Arghdia	Rho GDP-dissociation inhibitor 1		60284	0.2	301420			
Atp1a2	sodium/potassium transporting ATPase subunit α2					3328000	0.2	16640000
Atp1b1	sodium/potassium-transporting ATPase subunit β1		1003000	0.2	5015000	8045600	0.2	40228000
Atp1b2	sodium/potassium-transporting ATPase subunit β2		687110	0.2	3435550			
Avp	vasopressin-neurophysin 2-copeptin		313260	0.2	1566300			
B3galt2	UDP-GlcNAc:βGal β-1,3,-N-acetylglucos-aminyl-transferase polypeptide 2					540510	0.2	2702550
B3gnt6	UDP-GlcNAc:βGal β-1,3,-N-acetylglucos-aminyl-transferase 6					2226100	0.2	11130500
Bcat1	branched-chain-amino-acid transferase, cytosolic		228670	0.2	1143350			
Bhlhb9	basic helix-loop-helix b9		7886700	0.2	39433500			
Bub1b	PREDICTED: mitotic checkpoint serine/threonine-protein kinase BUB1β		9368100	0.2	46840500			
Camkv	calmodulin kinase-like vesicle-associated protein					3359200	0.2	16796000
Car2	carbonic anhydrase 2					942210	0.2	4711050

Gene	Protein	Abbr.	Experiment 1			Experiment 2		
			LFQ intensity ABE	LFQ intensity Control	Ratio LFQ ABE: Control	LFQ intensity ABE	LFQ intensity Control	Ratio LFQ ABE: Control
Cc2d2b	PREDICTED: coiled-coil and C2 domain-containing protein 2A-like		466000	0.2	2330000			
Cct2	T-complex protein 1 subunit β		60698	0.2	303490			
Cdc42	cell division control protein 42 isoform 1					477850	0.2	2389250
Cetn4	centrin 4		456830	0.2	2284150			
Chd2	chromodomain helicase DNA-binding protein 2		58531	0.2	292655			
Crmp1	dihydropyrimidinase-related protein 1					3242400	0.2	16212000
Cs	citrate synthase, mitochondrial		75932	0.2	379660			
Csrp2	cysteine- and glycine-rich protein 2		29752	0.2	148760			
Cttnbp2	cortactin-binding protein 2					3545700	0.2	17728500
Dbn1	drebrin isoform A		41923	0.2	209615			
Ddb2	damage specific DNA binding protein 2		685390	0.2	3426950	18981000	0.2	94905000
Defb11	β-defensin 11		4049300	0.2	20246500			
Dgkb	diacylglycerol kinase β		1623600	0.2	8118000			
Dnajc5	DnaJ homolog subfamily C member 5; cysteine string protein	CSP	231860	0.2	1159300			
Dot1l	histone-lysine *N*-methyltransferase, H3 lysine-79 specific		458560	0.2	2292800			
Dync1h1	cytoplasmic dynein 1 heavy chain 1		348530	0.2	1742650			
Eef1a2	elongation factor 1α2					24199000	0.2	1.21E+08
Elmo1	engulfment and cell motility 1					999450	0.2	4997250
Erbb4	receptor tyrosine-protein kinase erb-B4 isoform 1		549400	0.2	2747000			
Fabp7	fatty acid-binding protein, brain		419510	0.2	2097550			
Fam187a	Ig-like V-type domain-containing protein FAM187A precursor		1588100	0.2	7940500			
Fam78a	PREDICTED: protein FAM78A-like		67041	0.2	335205			
Fbn1	fibrillin-1		475350	0.2	2376750	43778000	0.2	2.19E+08
Fcgbp	Fc fragment of IgG binding protein		1636200	0.2	8181000			
Frmd6	FERM domain containing 6					567230	0.2	2836150
Fxyd1	phospholemman					2746400	0.2	13732000
Gdi2	Rab-GDP dissociation inhibitor β		348470	0.2	1742350			
Glo1	lactoylglutathione lyase		142800	0.2	714000			
Glul	glutamine synthetase		516980	0.2	2584900			
Gmfb	glia maturation factor β		37686	0.2	188430			
Got2	aspartate aminotransferase, mitochondrial		864330	0.2	4321650			
Gpm6b	neuronal membrane glycoprotein M6-b					3147000	0.2	15735000
Gpr135	probable G-protein coupled receptor 135		8776.8	0.2	43884			
Gstm1	glutathione *S*-transferase μ1					11094000	0.2	55470000
Henmt1	small RNA 2'-O-methyltransferase					12169000	0.2	60845000
Hhip	hedgehog-interacting protein precursor					14104000	0.2	70520000
Hist1h1b	histone cluster 1, h1b		1376200	0.2	6881000			
Hk1	hexokinase 1		132280	0.2	661400	10276000	0.2	51380000

Gene	Protein	Abbr.	Experiment 1			Experiment 2		
			LFQ intensity ABE	LFQ intensity Control	Ratio LFQ ABE: Control	LFQ intensity ABE	LFQ intensity Control	Ratio LFQ ABE: Control
Hsp90aa1	heat shock protein HSP90α		136080	0.2	680400			
Hsp90ab1	heat shock protein HSP90β		1072300	0.2	5361500			
Hspa1l	heat shock 70 kDa protein 1L					1845500	0.2	9227500
Hspa4	heat shock 70 kDa protein 4		69975	0.2	349875			
Hspa8	heat shock cognate 71 kDa protein		78262	0.2	391310	7078200	0.2	35391000
Il18rap	interleukin 18 receptor accessory protein		70379	0.2	351895			
Inpp1	inositol polyphosphate-1-phosphatase		53260	0.2	266300			
Kcnh2	potassium voltage-gated channel subfamily H member 2					1688000	0.2	8440000
Kcnma1	calcium-activated potassium channel subunit α1 isoform 3		43096000	0.2	2.15E+08			
Kcnq5l	PREDICTED: potassium voltage-gated channel subfamily KQT member 5 isoform 1		40533000	0.2	2.03E+08			
Kcp	PREDICTED: kielin/chordin-like protein-like		44652000	0.2	2.23E+08			
Kif24	PREDICTED: kinesin family member 24		55480	0.2	277400			
Kpnb1	importin subunit β1		31994	0.2	159970			
Kras	KRas isoform 2A		161670	0.2	808350			
Krit1	Krev interaction trapped protein 1		9605600	0.2	48028000	45837000	0.2	2.29E+08
Krtap31-1	keratin associated protein 31-1		23053	0.2	115265			
Limk1	LIM domain kinase 1					374810	0.2	1874050
LOC 100361349	hypothetical protein LOC100361349		302090	0.2	1510450			
LOC 682206	PREDICTED: LOW QUALITY PROTEIN: zinc finger protein 91		2213400	0.2	11067000			
LOC 683430	PREDICTED: BTB/POZ domain-containing protein KCTD8-like					3966600	0.2	19833000
LOC 683788	fascin					546030	0.2	2730150
Lrit3	PREDICTED: leucine-rich repeat, immunoglobulin-like domain and transmembrane domain-containing protein 3-like		478750	0.2	2393750			
Lrrc4b	leucine-rich repeat-containing protein 4B		59693000	0.2	2.98E+08			
Map1a	microtubule-associated protein 1A		19597	0.2	97985			
Map2	microtubule-associated protein 2 isoform MAP2x		35219	0.2	176095			
Mog	myelin oligodendrocyte glycoprotein		53076	0.2	265380			
Mreg	melanoregulin					347000	0.2	1735000
Mrpl47	mitochondrial ribosomal protein L47		2238000	0.2	11190000			
Mt-co2	cytochrome c oxidase subunit 2		193660	0.2	968300			
Muc5b	PREDICTED: mucin-5B		46493	0.2	232465			
Mug1	murinoglobulin-1 isoform 1		19117	0.2	95585			
Napg	N-ethylmaleimide-sensitive factor attachment protein γ					2119600	0.2	10598000

Gene	Protein	Abbr.	Experiment 1			Experiment 2		
			LFQ intensity ABE	LFQ intensity Control	Ratio LFQ ABE: Control	LFQ intensity ABE	LFQ intensity Control	Ratio LFQ ABE: Control
Ncam1	neural cell adhesion molecule		8305.3	0.2	41526.5			
Ndrg2	N-Myc downstream regulated gene 2		767790	0.2	3838950			
Ndufv2	NADH dehydrogenase flavoprotein 2, mitochondrial		26271	0.2	131355			
Nell1	protein kinase C-binding protein NELL1		226090	0.2	1130450			
Nfxl1	nuclear transcription factor, X-box binding-like 1		922770	0.2	4613850			
Nrg1	neuregulin β1a		97871	0.2	489355			
Nsf	vesicle-fusing ATPase; N-ethylmaleimide sensitive factor					4773900	0.2	23869500
Nup160	nucleoporin 160		64025	0.2	320125			
Pafah1b2	platelet-activating factor acetylhydrolase IB subunit β2		25989	0.2	129945	2223900	0.2	11119500
Pdcd6ip	programmed cell death 6-interacting protein					800850	0.2	4004250
Pde4dip	phosphodiesterase 4D interacting protein					383080	0.2	1915400
Pdia3	protein disulphide isomerase A3					1550900	0.2	7754500
Pdia6	protein disulphide isomerase A6					816050	0.2	4080250
Pgam1	phosphoglycerate mutase 1					7134900	0.2	35674500
Pgd	6-phosphogluconate dehydrogenase, decarboxylating		4142800	0.2	20714000			
Phgdh	D-3-phosphglycerate dehydrogenase					2051200	0.2	10256000
Pof1b	premature ovarian failure 1B					170410	0.2	852050
Ppia	peptidyl-prolyl cis-trans isomerase A		1925100	0.2	9625500			
Ppid	40 kDa peptidyl-prolyl cis-trans isomerase		312450	0.2	1562250			
Ppm1e	protein phosphatase 1E		127230	0.2	636150	887270	0.2	4436350
Prdx4	peroxiredoxin 4		126070	0.2	630350			
Prl3a1	prolactin-like protein H		66941	0.2	334705			
Pygb	brain glycogen phosphorylase					866730	0.2	4333650
Rab39	Ras oncogene family member RAB39		261740	0.2	1308700			
Rab3d	GTP-binding protein Rab-3D		43974	0.2	219870			
Rac1	ras-related C3 botulinum toxin substrate 1		118040	0.2	590200			
Rap1gds1	RAP1 GDP-GTP dissociation stimulator 1		23536	0.2	117680			
Rap2a	RAP2A-like protein		98560	0.2	492800			
Rap2b	Ras-related protein 2B		718920	0.2	3594600			
Rasgrp4	Ras guanyl-releasing protein 4		16621	0.2	83105			
RGD 1565117	PREDICTED: 40S ribosomal protein S26-like		113730	0.2	568650			
Rhob	Rho-related GTP-binding protein RhoB		435630	0.2	2178150			
Rps5	40S ribosomal protein S5					2901600	0.2	14508000
Sept10	septin-10		29590	0.2	147950			
Sept9	septin 9 isoform 1					25157000	0.2	1.26E+08
Sh3gl2	endophilin-A1					67760000	0.2	3.39E+08
Slc1a2	excitatory amino acid transporter 2 isoform GLT-1A	EAAT2	959390	0.2	4796950			

Gene	Protein	Abbr.	Experiment 1			Experiment 2		
			LFQ intensity ABE	LFQ intensity Control	Ratio LFQ ABE: Control	LFQ intensity ABE	LFQ intensity Control	Ratio LFQ ABE: Control
Slc1a3	excitatory amino acid transporter 1 isoform GLAST-1	EAAT1	82804	0.2	414020			
Slc25a3	phosphate carrier protein, mitochondrial isoform 2 precursor					6941200	0.2	34706000
Slc25a31	PREDICTED: ADP/ATP translocase 4-like					3116600	0.2	15583000
Slc44a4	choline transporter-like protein 4		99061	0.2	495305			
Spy	synaptophysin		1050900	0.2	5254500			
Sri	sorcin		30451	0.2	152255			
Srprb	signal recognition particle receptor, B subunit		177960	0.2	889800			
Stx12	syntaxin 12		174410	0.2	872050			
Stxbp1	syntaxin-binding protein 1 isoform 2; Munc18		35641	0.2	178205			
Syp	synaptophysin					3448900	0.2	17244500
Syt2	synaptotagmin-2		22717	0.2	113585			
Tecr	trans-2,3,-enoyl-CoA reductase					3250400	0.2	16252000
Tmco5b	PREDICTED: transmembrane and coiled-coil domain-containing protein 5B		116670	0.2	583350			
Tom3	tropomyosin α3 chain isoform 2		13697	0.2	68485			
Tomm70a	mitochondrial import receptor subunit TOM70					659410	0.2	3297050
Tpm3	tropomyosin α3 chain isoform 1					4468000	0.2	22340000
Tppp	tubulin polymerisation promoting protein		35743	0.2	178715			
Tuba1a	tubulin α1A chain					14442000	0.2	72210000
Tubb2a	tubulin β2A chain		45802000	0.2	2.29E+08			
Tubb2b	tubulin β2B chain		202440	0.2	1012200	4040600	0.2	20203000
Tubb2c	tubulin β2C chain		1461700	0.2	7308500	1.52E+08	0.2	7.58E+08
Tubb4	tubulin β4		307200	0.2	1536000			
Tubb6	tubulin β6					3071900	0.2	15359500
Txn1	thioredoxin		886420	0.2	4432100			
Usp5	ubiquitin-specific peptidase 5		105840	0.2	529200			
Vamp1	vesicle-associated membrane protein 1; synaptobrevin 1		471800	0.2	2359000			
Vamp2	vesicle-associated membrane protein 2; synaptobrevin 2		1518900	0.2	7594500			
Ywhag	14-3-3 protein γ		59213	0.2	296065			
Zfp438	zinc finger protein 438					29177000	0.2	1.46E+08
Zfp790	zinc finger protein 790		58494	0.2	292470			
Zmym6	zinc finger, MYM-type 6		75237	0.2	376185			

APPENDIX 4: RAT BRAIN ACYL-RESIN-ASSISTED CAPTURE (ACYL-RAC) HITS

APPENDIX 4.1 HITS WITH MULTIPLE UNIQUE PEPTIDES IN THE EXPERIMENTAL SAMPLE

Proteins identified in previous mammalian proteomic studies are highlighted in green. Proteins which were not present in the control sample were given an arbitrary value of 0.2 to avoid dividing by zero, similar to previous proteomic studies (Dowal *et al.*, 2011; Roth *et al.*, 2006; Yang *et al.*, 2010). Proteins with a ratio of less than 5 were discarded (Martin and Cravatt, 2009). Abbr., abbreviation (if different from gene name); LFQ, label-free quantification.

Gene	Protein	Abbr.	Experiment 1			Experiment 2		
			LFQ intensity ABE	LFQ intensity Control	Ratio LFQ ABE: Control	LFQ intensity ABE	LFQ intensity Control	Ratio LFQ ABE: Control
Aco2	aconitate hydratase, mitochondrial					9477000	0.2	47385000
Aldoa	fructose-bisphosphate aldolase A		11648000	0.2	58240000			
Aldoc	fructose-bisphosphonate aldolase C					9539900	0.2	47699500
Amph	amphiphysin					5547700	0.2	27738500
Arpc3	actin related protein 2/3 complex subunit 3		228730	0.2	1143650			
Atp1a1	sodium/potassium transporting ATPase subunit α1					8810300	0.2	44051500
Atp1a2	sodium/potassium transporting ATPase subunit α2					11684000	0.2	58420000
Atp1a3	sodium/potassium transporting ATPase subunit α3					1.98E+08	0.2	9.9E+08
Atp1b2	sodium/potassium transporting ATPase subunit β2		2246900	0.2	11234500			
Atp5a1	ATP synthase subunit α, mitochondrial					11487000	0.2	57435000
Atp5b	ATP synthase subunit β, mitochondrial					2137300	0.2	10686500
Ccdc84	PREDICTED: coiled-coil domain-containing protein 84-like					1708700	0.2	8543500
Cfl1	cofilin-1					60346000	0.2	3.02E+08
Ckb	creatine kinase B-type					4.59E+08	39747000	11.54251
Cltc	clathrin heavy chain 1					28208000	0.2	1.41E+08
Dnm1	dynamin-1 isoform 1					689720	0.2	3448600
Dpysl2	dihydropyrimidinase-related protein 2					2.03E+08	0.2	1.02E+09
Eef1a1	elongation factor 1α 1					7635000	0.2	38175000
Eno2	γ-enolase					3.2E+08	0.2	1.6E+09
Gap43	neuromodulin		29902000	0.2	1.5E+08	87821000	0.2	4.39E+08
Gapdh	glyceraldehyde-3-phosphate dehydrogenase					2.53E+08	0.2	1.26E+09
Gdi1	Rab-GDP dissociation inhibitor α					5482600	0.2	27413000
Gnao1	guanine nucleotide-binding protein G(o) subunit α isoform α2					27569000	0.2	1.38E+08
Gpm6a	glycoprotein m6a					69799000	0.2	3.49E+08
Hsp90aa1	heat shock protein HSP90α					76342000	3223500	23.68295
Hsp90ab1	heat shock protein HSP90β					13789000	0.2	68945000
Hspa8	heat shock cognate 71 kDa protein					46962000	0.2	2.35E+08
Khsrp	far upstream element binding protein 2					23951000	0.2	1.2E+08
Kpnb1	importin subunit β1					5954100	0.2	29770500

Gene	Protein	Abbr.	Experiment 1			Experiment 2		
			LFQ intensity ABE	LFQ intensity Control	Ratio LFQ ABE: Control	LFQ intensity ABE	LFQ intensity Control	Ratio LFQ ABE: Control
Ldha	L-lactate dehydrogenase A chain					11049000	0.2	55245000
Ldhb	L-lactate dehydrogenase B chain					16062000	0.2	80310000
LOC 685110	hypothetical protein LOC685110		39522	0.2	197610			
Map1a	microtubule-associated protein 1A					49814000	0.2	2.49E+08
Map2	microtubule-associated protein 2 isoform MAP2x					2242900	0.2	11214500
Mbp	myelin basic protein isoform 1		6542300	0.2	32711500			
Mdh1	malate dehydrogenase, cytoplasmic					16848000	0.2	84240000
Ncam1	neural cell adhesion molecule					9478900	0.2	47394500
Ndrg2	N-Myc downstream regulated gene 2		4581300	0.2	22906500			
Palm	paralemmin		11171000	0.2	55855000			
Pkm2	pyruvate kinase isozymes M1/M2 isoform M1					1.2E+08	0.2	6.01E+08
Plp1	myelin proteolipid protein					1.84E+08	0.2	9.22E+08
Ppp2r1a	protein phosphatase 2 regulatory subunit A					53305000	0.2	2.67E+08
Prdx6	peroxiredoxin-6		5977100	0.2	29885500			
Sh3gl2	endophilin-A1					21838000	0.2	1.09E+08
Slc1a2	excitatory amino acid transporter 2 GLT1 subunit	EAAT2				79536000	0.2	3.98E+08
Slc25a5	ADP/ATP translocase 2					9167600	0.2	45838000
Slc34a2	sodium-dependent phosphate transport protein 2B					112260	0.2	561300
Snap25	synaptosomal-associated protein of 25 kDa					35541000	0.2	1.78E+08
Snap91	clathrin coat assembly protein AP180 long isoform					1920600	0.2	9603000
Spna2	αII spectrin					82291000	1723200	47.75476
Stip1	stress-induced phosphoprotein 1					28265000	0.2	1.41E+08
Stx1a	syntaxin-1A					6144500	0.2	30722500
Syx1b	syntaxin-1B					82513000	0.2	4.13E+08
Tpi1	triosephosphate isomerase					31995000	0.2	1.6E+08
Tuba4a	tubulin α4A chain					1.07E+08	0.2	5.35E+08
Tubb2a	tubulin β2A chain					6.91E+08	0.2	3.46E+09
Tubb5	tubulin β5 chain isoform 1					1.61E+08	0.2	8.03E+08
Uba1	ubiquitin-like modifier activating enzyme 1					1036600	0.2	5183000
Ube2d3	ubiquitin-conjugating enzyme E2 D3		1204200	0.2	6021000			
Vamp2	vesicle-associated membrane protein 2; synaptobrevin 2		3591900	0.2	17959500	28661000	0.2	1.43E+08
Ywhae	14-3-3 protein ε					23302000	0.2	1.17E+08
Ywhah	14-3-3 protein ε					10310000	0.2	51550000
Ywhaz	14-3-3 protein ζ/δ					1.1E+08	0.2	5.49E+08

APPENDIX 4.2 HITS WITH A SINGLE UNIQUE PEPTIDE IN THE EXPERIMENTAL SAMPLE

Proteins identified in previous mammalian proteomic studies are highlighted in green. Proteins which were not present in the control sample were given an arbitrary value of 0.2 to avoid dividing by zero, similar to previous proteomic studies (Dowal *et al.*, 2011; Roth *et al.*, 2006; Yang *et al.*, 2010). Proteins with a ratio of less than 5 were discarded (Martin and Cravatt, 2009). Abbr., abbreviation (if different from gene name); LFQ, label-free quantification.

Gene	Protein	Abbr.	Experiment 1			Experiment 2		
			LFQ intensity ABE	LFQ intensity Control	Ratio LFQ ABE: Control	LFQ intensity ABE	LFQ intensity Control	Ratio LFQ ABE: Control
Ak2	adenylate kinase 2, mitochondrial isoform 1		30414	0.2	152070			
Atp13a1	ATPase type 13A1		1876500	0.2	9382500			
Atp1b1	sodium/potassium transporting ATPase subunit β1		701720	0.2	3508600	14385000	0.2	71925000
Atp6v1a	ATPase, H^+ transporting, lysosmal V1 subunit A					485240	0.2	2426200
Avp	vasopressin-neurophysin 2-copeptin		543660	0.2	2718300			
Basp1	brain acid soluble protein 1					3442100	0.2	17210500
Chchd5	coiled-coil-helix coiled-coil-helix domain containing 5		378840	0.2	1894200			
Cnp	2,3-cyclic-nucleotide 3-phosphodiesterase					3015600	0.2	15078000
Crip2	cysteine-rich protein 2		298240	0.2	1491200			
Crmp1	dihydropyrimidinase-related protein 1					5177600	0.2	25888000
Dbn1	isoform A of drebrin					387740	0.2	1938700
Ddb2	damage specific DNA binding protein 2		51037000	0.2	2.55E+08			
Diaph3	PREDICTED: protein diaphanous homolog 3		2184200	0.2	10921000			
Dnajc5	DnaJ homolog subfamily C member 5; cysteine string protein	CSP	164160	0.2	820800			
Eif2b1	translation initiation factor eIF-2B subunit α					22621000	0.2	1.13E+08
Exoc3l	exocyst complex component 3-like		923690	0.2	4618450			
Fam72a	protein FAM72A		39188	0.2	195940			
Fbn1	fibrillin-1		1200800	0.2	6004000			
Fkbp1a	peptidyl-prolyl cis-trans isomerase FKBP1A					3521400	0.2	17607000
Fxyd1	phospholemman		2550900	0.2	12754500			
Fxyd7	FXYD domain-containing ion transport regulator 7		1148600	0.2	5743000			
Glul	glutamine synthetase		2456300	0.2	12281500	20639000	0.2	1.03E+08
Gnao1	guanine nucleotide-binding protein G(o) subunit α isoform α2		846670	0.2	4233350			
Grn	granulin isoform a					2966300	0.2	14831500
Gstm1	glutathione *S*-transferase μ1		331910	0.2	1659550	4770900	0.2	23854500
Gstp1	glutathione *S*-transferase P		214500	0.2	1072500			
Hk1	hexokinase-1					3521600	0.2	17608000
Hmha1	histocompatibility (minor) HA-1					1.23E+08	0.2	6.16E+08
Hspa1l	heat shock 70 kDa protein 1L					5278700	0.2	26393500

Gene	Protein	Abbr.	Experiment 1			Experiment 2		
			LFQ intensity ABE	LFQ intensity Control	Ratio LFQ ABE: Control	LFQ intensity ABE	LFQ intensity Control	Ratio LFQ ABE: Control
Ildr2	immunoglobulin-like domain containing receptor 2		159030	0.2	795150			
Ilkap	integrin-linked kinase-associated serine/threonine phosphatase		109980	0.2	549900			
Isg20	interferon-stimulated protein		23658	0.2	118290			
Itpr1	inositol 1,4,5-trisphosphate receptor type 1 isoform 1		5541900	0.2	27709500			
Kcnma1	calcium-activated potassium channel subunit α1 isoform 3		5.77E+08	0.2	2.89E+09			
Kcnq5l	PREDICTED: potassium voltage-gated channel subfamily KQT member 5 isoform 1		70216000	0.2	3.51E+08	2.85E+09	0.2	1.42E+10
Lamtor1	ragulator complex protein LAMTOR1		658130	0.2	3290650			
Ldhb	L-lactate dehydrogenase B chain		181770	0.2	908850			
Lepr	leptin receptor isoform B					497060	0.2	2485300
LOC 100361349	hypothetical protein LOC100361349		557390	0.2	2786950			
LOC 494539	spectrin β-like		200880	0.2	1004400			
LOC 498122	uncharacterized protein LOC498122		138750	0.2	693750			
LOC 500183	similar to NGF-binding Ig light chain		231800	0.2	1159000			
LOC 680396	hypothetical protein LOC680396		22957	0.2	114785			
LOC 682206	PREDICTED: LOW QUALITY PROTEIN: zinc finger protein 91		1.51E+08	0.2	7.57E+08			
LOC 682914	similar to zinc finger protein 326		18151	0.2	90755			
LOC 686961	similar to discs large homolog 5					1.33E+08	0.2	6.67E+08
LOC 687873	similar to kallikrein 5 preproprotein					3.08E+08	0.2	1.54E+09
LOC 688272	PREDICTED: RING finger protein 157-like		2087400	0.2	10437000			
Lrrc4b	leucine-rich repeat-containing protein		1.2E+08	0.2	6.02E+08			
Lrsam1	leucine-rich repeat and sterile α motif containing 1		380630	0.2	1903150			
Ltbp1	latent-transforming growth factor β-binding protein 1 precursor		149870	0.2	749350			
Map1a	microtubule-associated protein 1		65730	0.2	328650			
Mdh2	malate dehydrogenase, mitochondrial		431680	0.2	2158400	2728000	0.2	13640000
Med24	mediator complex subunit 24		514170	0.2	2570850			
Mt3	metallothionein 3		369010	0.2	1845050			
Ncdn	neurochondrin					3363200	0.2	16816000
Ndrg2	N-Myc downstream regulated gene 2 isoform 1					18938000	0.2	94690000
Ndufv2	NADH dehydrogenase flavoprotein 2, mitochondrial		206430	0.2	1032150			
Neu4	sialidase 4		301330	0.2	1506650			
Nfxl1	nuclear transcription factor, X-box binding-like 1		272930	0.2	1364650			
Nlk	similar to nemo-like kinase					13692000	0.2	68460000

Gene	Protein	Abbr.	Experiment 1			Experiment 2		
			LFQ intensity ABE	LFQ intensity Control	Ratio LFQ ABE: Control	LFQ intensity ABE	LFQ intensity Control	Ratio LFQ ABE: Control
Nsd1	nuclear receptor binding SET domain protein 1		442990	0.2	2214950			
P2rx7	P2X purinoceptor 7					1189200	0.2	5946000
Pacsin1	protein kinase C and casein kinase substrate in neurons protein 1					17918000	0.2	89590000
Pafah1b2	platelet-activating factor acetylhydrolase IB subunit β2					4591100	0.2	22955500
Palm	paralemmin					12971000	0.2	64855000
Pebp1	phosphatidyl-ethanolamine-binding protein 1					7370500	0.2	36852500
Pgam1	phosphoglycerate mutase 1					7212000	0.2	36060000
Plscr4	phospholipid scramblase 4		17587	0.2	87935			
Prdx1	peroxiredoxin-1		142310	0.2	711550			
Prss7	protease, serine, 7		46090	0.2	230450			
Ptgs1	putative cyclooxygenase 3		29083	0.2	145415			
Rap1gds1	RAP1, GTP-GDP dissociation stimulator 1					4499200	0.2	22496000
Rap2b	Ras-related protein Rap-2B		193690	0.2	968450			
RGD 1559921	PREDICTED: macrophage migration inhibitory factor-like		2479000	0.2	12395000			
RGD 1560880	similar to RIKEN cDNA 2310002J15					96002	0.2	480010
RGD 1561197	PREDICTED: uncharacterized protein LOC290392		3387800	0.2	16939000			
Rplp1	60S acidic ribosomal protein P1		284330	0.2	1421650			
Sdhb	succinate dehydrogenase iron-sulphur subunit, mitochondrial		89003	0.2	445015			
Slc13a1	solute carrier family 13 member 1					336970	0.2	1684850
Slc25a3	solute carrier family 25 (mitochondrial carrier, phosphate carrier), member 3					6428500	0.2	32142500
Slc38a8	putative sodium-coupled neutral amino acid transporter 8		30935000	0.2	1.55E+08			
Spire1	spiro homolog 1		125580	0.2	627900			
Sptbn1	non-erythroid spectrin β					877530	0.2	4387650
Stx19	syntaxin 19		585400	0.2	2927000			
Tgm1	protein-glutamine γ-glutamyltransferase K					649390	0.2	3246950
Tmeff2	transmembrane protein with EGF-like and two follistatin-like domains 2					1083900	0.2	5419500
Tmem55b	transmembrane protein 55B		20441	0.2	102205			
Tomm70a	mitochondrial import receptor subunit TOM70					4972700	0.2	24863500
Trappc3	trafficking protein particle complex subunit 3	Bet3	1821400	0.2	9107000			
Ttc39b	tetratricopeptide repeat domain 39B		389120	0.2	1945600			
Tuba1a	tubulin α1A chain					34861000	0.2	1.74E+08
Tubb2c	tubulin β2C chain					1.5E+09	0.2	7.52E+09
Tubb3	tubulin β3 chain					59551000	0.2	2.98E+08
Tubb4	tubulin β4					13823000	0.2	69115000

Gene	Protein	Abbr.	Experiment 1			Experiment 2		
			LFQ intensity ABE	LFQ intensity Control	Ratio LFQ ABE: Control	LFQ intensity ABE	LFQ intensity Control	Ratio LFQ ABE: Control
Tubb5	tubulin β5 chain isoform 1		261100	0.2	1305500			
Ube2l3	ubiquitin-conjugating enzyme E2L 3		693320	0.2	3466600			
Uchl1	ubiquitin carboxyl-terminal hydrolase L1		438910	0.2	2194550			
Usp3	ubiquitin-specific protease 3		53450	0.2	267250			
Vcp	transitional endoplasmic reticulum ATPase					1549100	0.2	7745500
Vom2r53	vomeronasal 2 receptor, 53					149530	0.2	747650
Wisp1	WNT1-inducible-signaling pathway protein 1		4.18E+08	0.2	2.09E+09	5.14E+08	0.2	2.57E+09
Ywhag	14-3-3 protein γ					7400200	0.2	37001000
Ywhaq	14-3-3 protein θ					30465000	0.2	1.52E+08
Zfp438	zinc finger protein 438		1658700	0.2	8293500			
Znf574	zinc finger protein 574					1091700	0.2	5458500

APPENDIX 5: WILD-TYPE *C. ELEGANS* ACYL-BIOTIN EXCHANGE (ABE) HITS

APPENDIX 5.1 HITS WITH MULTIPLE UNIQUE PEPTIDES IN THE EXPERIMENTAL SAMPLE

Hits are coloured according to their mammalian orthologue: those identified in the proteomic analysis of rat brain homogenate in this study but not in previous studies are highlighted in blue. Proteins which were not present in the control sample were given an arbitrary value of 0.2 to avoid dividing by zero, similar to previous proteomic studies (Dowal *et al.*, 2011; Roth *et al.*, 2006; Yang *et al.*, 2010). Proteins with a ratio of less than 5 were discarded (Martin and Cravatt, 2009). LFQ, label-free quantification.

Gene	Protein description	LFQ intensity ABE	LFQ intensity Control	Ratio LFQ ABE:Control	Mammalian orthologue	
					Gene	Name
tbb-2	tubulin β	10213000	0.2	51065000	Tubb4b	tubulin β-4B chain
vit-4	vitellogenin	1.7E+08	0.2	8.52E+08	Apob	apolipoprotein B-100
vit-5	vitellogenin	21978000	0.2	1.1E+08	Cenpe	centromere-associated protein E
vit-6	vitellogenin	93227000	0.2	4.66E+08	Bmper	BMP-binding endothelial regulator protein precursor

APPENDIX 5.2 HITS WITH A SINGLE UNIQUE PEPTIDE IN THE EXPERIMENTAL SAMPLE

Hits are coloured according to their mammalian orthologue: those also identified in previous proteomic studies are highlighted in green; those identified in the proteomic analysis of rat brain homogenate in this study but not in previous studies are highlighted in blue; those identified both in this and previous studies are highlighted in orange. Proteins which were not present in the control sample were given an arbitrary value of 0.2 to avoid dividing by zero, similar to previous proteomic studies (Dowal *et al.*, 2011; Roth *et al.*, 2006; Yang *et al.*, 2010). Proteins with a ratio of less than 5 were discarded (Martin and Cravatt, 2009). LFQ, label-free quantification.

Gene	Protein description	LFQ intensity ABE	LFQ intensity Control	Ratio LFQ ABE:Control	Mammalian orthologue	
					Gene	Name
alh-8	aldehyde dehydrogenase	1320300	0.2	6601500	Aldh6a1	methylmalonate-semialdehyde dehydrogenase [acylating], mitochondrial precursor
arrd-6	arrestin domain protein	2302700	0.2	11513500	Arrdc3	arrestin domain-containing protein 3
C06C3.4		2046600	0.2	10233000		
C50F7.3		59495000	0.2	2.97E+08		
cdr-2	cadmium responsive	3.19E+09	0.2	1.59E+10	Faxc	failed axon connections homologue
ckr-2	cholecystokinin receptor homolog	377720	0.2	1888600	Cckbr	gastrin/cholecystokinin type B receptor
eef-1A.1	eukaryotic translation elongation factor	7778300	0.2	38891500	Eef1a2	elongation factor 1α 2
F07G11.3		164880	0.2	824400		
F14F9.3		22427000	0.2	1.12E+08		
F29D10.1		2059000	0.2	10295000		
F43G6.8		724560	0.2	3622800	Trim23	E3 ubiquitin-protein ligase TRIM23
F46H5.3a.1		32744000	0.2	1.64E+08	Ckm	creatine kinase M-type
fbxc-55	F-box C protein	2504600	0.2	12523000		
grl-6	ground-like; hedgehog-like protein	118690	0.2	593450		
lin-54	abnormal cell lineage	124470	0.2	622350	Lin54	protein lin-54 homologue
nhr-254	nuclear hormone receptor family	502320	0.2	2511600	Nr1hr	bile acid receptor isoform 3

Gene	Protein description	LFQ intensity ABE	LFQ intensity Control	Ratio LFQ ABE:Control	Mammalian orthologue	
					Gene	Name
nhr-98	nuclear hormone receptor family	11677000	0.2	58385000	Nr2e3	photoreceptor-specific nuclear receptor
npr-33	neuropeptide receptor family	23477000	0.2	1.17E+08	Galr2	galanin receptor type 2
rap-3	RAP homolog	285890	0.2	1429450	Rap1a	Ras-related protein Rap1A
sun-1	SUN (S. pombe sad1/Ce-UNC-84) domain protein	2.14E+08	0.2	1.07E+09		
T05C3.2	may be involved in apoptosis	2370700	0.2	11853500	Kiaa1239	leucine-rich repeat and WD repeat-containing protein KIAA1239
T06E6.10		3178700	0.2	15893500	Krtap9-1	keratin-associated protein 9-1
T22F7.3		62633000	0.2	3.13E+08	Tfpi	tissue factor pathway inhibitor
tba-1	tubulin α	4430100	0.2	22150500	Tuba1a	tubulin α-1A chain
tbc-3	TBC (Tre-2/Bub2/Cdc16) domain family	16198000	0.2	80990000	Tbc1d22b	TBC1 domain family member 22B
tsp-9	tetraspanin family	788320	0.2	3941600	Cd9	CD9 antigen
vit-2	vitellogenin	5840800	0.2	29204000	Wdr87	WD repeat-containing protein 87
W02F12.8		175290	0.2	876450		
W09D6.1c		69287000	0.2	3.46E+08	Aasdh	Acyl-CoA synthetase family member 4
Y45G12B.2a		1.06E+08	0.2	5.32E+08	Zfpl1	zinc finger-like protein 1
Y49G5A.1		6239400	0.2	31197000	Eppin	eppin
Y71F9AL.6		2582600	0.2	12913000	HIT 000048221	conserved hypothetical protein
ZC13.2		395600	0.2	1978000		

APPENDIX 6: WILD-TYPE *C. ELEGANS* ACYL-RESIN-ASSISTED CAPTURE (ACYL-RAC) HITS

APPENDIX 6.1 HITS WITH MULTIPLE UNIQUE PEPTIDES IN THE EXPERIMENTAL SAMPLE

Hits are coloured according to their mammalian orthologue: those also identified in previous proteomic studies are highlighted in green; those identified in the proteomic analysis of rat brain homogenate in this study but not in previous studies are highlighted in blue; those identified both in this and previous studies are highlighted in orange. Proteins which were not present in the control sample were given an arbitrary value of 0.2 to avoid dividing by zero, similar to previous proteomic studies (Dowal *et al.*, 2011; Roth *et al.*, 2006; Yang *et al.*, 2010). Proteins with a ratio of less than 5 were discarded (Martin and Cravatt, 2009). LFQ, label-free quantification.

Gene	Protein description	LFQ intensity ABE	LFQ intensity Control	Ratio LFQ ABE:Control	Mammalian orthologue	
					Gene	Name
aco-2	aconitase	29247000	0.2	1.46E+08	Aco2	aconitate hydratase, mitochondrial
ahcy-1	*S*-adenosyl-homocysteine hydrolase	55061000	0.2	2.75E+08	Ahcy	adenosylhomocysteinase
aldo-2	fructose-biphosphate aldolase	22058000	0.2	1.1E+08	Aldoa	fructose-bisphosphate aldolase A
alh-8	methylmalonate-semialdehyde dehydrogenase	53161000	0.2	2.66E+08	Aldh6a1	methylmalonate-semialdehyde dehydrogenase [acylating], mitochondrial precursor
anc-1	abnormal nuclear anchorage	2.74E+08	0.2	1.37E+09	Syne1	nesprin-1
atp-2	ATP synthase β chain	3878800	0.2	19394000	Atp5b	ATP synthase β subunit, mitochondrial
C39D10.7		6699300	0.2	33496500	Muc2	mucin-2
cdc-48.2	P97 protein	8357600	0.2	41788000	Vcp	transitional endoplasmic reticulum ATPase
cpg-2	chondroitin proteoglycan	8083300	0.2	40416500	HIT 000056302	conserved hypothetical protein
daf-21	heat shock protein HSP90	2.75E+08	0.2	1.37E+09	Hsp90ab1	heat shock protein 90β
eef-1A.1	elongation factor 1α	2.99E+08	0.2	1.5E+09	Eef1a2	elongation factor 1α 2
eft-2	elongation factor Tu family	32941000	0.2	1.65E+08	Eef2	elongation factor 2
enol-1	enolase	33173000	0.2	1.66E+08	Eno1	α-enolase
F09B12.3		61215000	0.2	3.06E+08	Plbd2	putative phospholipase B-like 2
F46H5.3a		6.05E+08	61143000	9.891239	Ckm	creatine kinase M-type
gdh-1	glutamate dehydrogenase	22755000	0.2	1.14E+08	Glud1	glutamate dehydrogenase, mitochondrial
gpd-3	glyceraldehyde-3-phosphate dehydrogenase	12634000	0.2	63170000	Gapdh	glyceraldehyde-3-phosphate dehydrogenase
hsp-1	heat shock 70 kDa protein A	26086000	0.2	1.3E+08	Hspa8	heat shock cognate 71 kDa protein
hsp-60	heat shock protein	22092000	0.2	1.1E+08	Hspd1	60 kDa heat shock protein, mitochondrial
imb-3	importin β nuclear transport factor	9716400	0.2	48582000	Ipo5	importin 5
inf-1	initiation factor	5995500	0.2	29977500	Eif4a2	eukaryotic initiation factor 4A-II
paa-1	protein phosphatase 2A	29583000	0.2	1.48E+08	Ppp2r1a	serine/threonine-protein phosphatase 2A 65 kDa regulatory subunit A α isoform
pck-1	phosphoenoylpyruvate kinase	26218000	0.2	1.31E+08	Pck2	phosphoenolpyruvate carboxykinase [GTP], mitochondrial
pck-2	phosphoenoylpyruvate kinase	64737000	0.2	3.24E+08	Pck2	phosphoenolpyruvate carboxykinase [GTP], mitochondrial
pdi-1	protein disulphide isomerase	5402000	0.2	27010000	P4hb	protein disulphide-isomerase
pdi-2	protein disulphide isomerase	33680000	0.2	1.68E+08	P4hb	protein disulphide-isomerase
rla-0	deoxyribonuclease	34886000	0.2	1.74E+08	Rplp0	60S acidic ribosomal protein P0

Gene	Protein description	LFQ intensity ABE	LFQ intensity Control	Ratio LFQ ABE:Control	Mammalian orthologue	
					Gene	Name
rps-0	40S ribosomal protein	20489000	0.2	1.02E+08	Rpsa	40S ribosomal protein SA
spc-1	spectrin	51761000	0.2	2.59E+08	Sptan1	spectrin alpha chain, non-erythrocytic 1 isoform 3
tba-2	tubulin α	43641000	0.2	2.18E+08	Tuba1a	tubulin α-1A chain
tbb-2	tubulin β	68335000	0.2	3.42E+08	Tubb4b	tubulin β-4B chain
uba-1	ubiquitin-activating enzyme	54829000	0.2	2.74E+08	Uba1	ubiquitin-like modifier-activating enzyme 1
unc-54	myosin heavy chain	19660000	0.2	98300000	Myh3	myosin 3
vha-13	ATP synthase α and β subunits	6488300	0.2	32441500	Atp6v1a	V-type proton ATPase catalytic subunit A
vit-2	vitellogenin	1.84E+08	0.2	9.22E+08	Wdr87	WD repeat-containing protein 87
vit-4	vitellogenin	2.51E+08	0.2	1.26E+09	Apob	apolipoprotein B-100
vit-5	vitellogenin	28088000	0.2	1.4E+08	Cenpe	centromere-associated protein E
vit-6	vitellogenin	5.79E+08	0.2	2.9E+09	Bmper	BMP-binding endothelial regulator protein precursor

APPENDIX 6.2 HITS WITH A SINGLE UNIQUE PEPTIDE IN THE EXPERIMENTAL SAMPLE

Hits are coloured according to their mammalian orthologue: those also identified in previous proteomic studies are highlighted in green; those identified in the proteomic analysis of rat brain homogenate in this study but not in previous studies are highlighted in blue; those identified both in this and previous studies are highlighted in orange. Proteins which were not present in the control sample were given an arbitrary value of 0.2 to avoid dividing by zero, similar to previous proteomic studies (Dowal *et al.*, 2011; Roth *et al.*, 2006; Yang *et al.*, 2010). Proteins with a ratio of less than 5 were discarded (Martin and Cravatt, 2009). LFQ, label-free quantification.

Gene	Protein description	LFQ intensity ABE	LFQ intensity Control	Ratio LFQ ABE:Control	Mammalian orthologue	
					Gene	Name
aco-1	iron-responsive element-binding like protein; aconitase	1555600	0.2	7778000	Aco1	cytoplasmic aconitate hydratase
ant-1.3	adenine nucleotide	1250800	0.2	6254000	Slc25a4	ADP/ATP translocase 1
cct-2	t-complex protein 1	1884500	0.2	9422500	Cct2	T-complex protein 1 subunit β
cct-5	TCP-1 like chaperonin	1879400	0.2	9397000	Cct5	T-complex protein 1 subunit ε
clec-122	C-type lectin	5164100	0.2	25820500	Muc21	mucin-21
csk-1	C-terminal Src kinase	584400	0.2	2922000	Csk	tyrosine-protein kinase CSK
cts-1	citrate synthase	4919500	0.2	24597500	Cs	citrate synthase, mitochondrial
cyc-2.1	cytochrome c	2229900	0.2	11149500	Cycs	cytochrome c
eef-1B.2	eukaryotic translation elongation factor	946520	0.2	4732600	Fdxacb1	ferredoxin-fold anticodon-binding domain-containing protein 1
har-2	hemiasterlin resistent	2.3E+08	0.2	1.15E+09	Dspp	dentin sialophosphoprotein
hrp-2	hetergeneous nuclear ribonucleoprotein homologue	2233700	0.2	11168500	Hnrnpr	heterogeneous nuclear ribonucleoprotein R
hsp-6	heat shock protein 70 kDa family protein	3898300	0.2	19491500	Hspa9	stress-70 protein, mitochondrial
kars-1	lysyl(K) amino-acyl tRNA synthetase	547560	0.2	2737800	Kars	lysine--tRNA ligase 1
mdh-1	malate dehydrogenase	8413900	0.2	42069500	Mdh1	malate dehydrogenase, cytoplasmic
mig-6	protease inhibitor	3777700	0.2	18888500	Papln	papilin
mtr-4	RNA helicase	32798000	0.2	1.64E+08	Skiv2l2	superkiller viralicidic activity 2-like 2
nuc-1	DNase II homolog	2.32E+09	0.2	1.16E+10	Dnase2b	deoxyribonuclease-2β
prdx-2	peroxiredoxin	3443100	0.2	17215500	Prdx2	peroxiredoxin-2
prmt-1	protein arginine methyltransferase	3743400	0.2	18717000	Hrmt1l2	protein arginine *N*-methyltransferase 1
R08D7.2		7007400	0.2	35037000	Rpap2	putative RNA polymerase II subunit B1 CTD phosphatase RPAP2
rme-4	receptor mediated endocytosis	81060000	0.2	4.05E+08	Dennd1a	DENN domain-containing protein 1A
wars-1	tryptophanyl-tRNA synthetase	2506800	0.2	12534000	Wars	tryptophanyl-tRNA synthetase

Gene	Protein description	LFQ intensity ABE	LFQ intensity Control	Ratio LFQ ABE:Control	Mammalian orthologue	
					Gene	Name
Y22D7AL.9		7E+08	0.2	3.5E+09	Ttc28	tetratricopeptide repeat protein 28
Y64G10A.7	fibrillin-1 homolog	17415	0.2	87075	Megf6	multiple epidermal growth factor-like domains protein 6

APPENDIX 7: *ath-1* MUTANT *C. ELEGANS* ACYL-BIOTIN EXCHANGE (ABE) HITS

APPENDIX 7.1 HITS WITH MULTIPLE UNIQUE PEPTIDES IN THE EXPERIMENTAL SAMPLE

Hits are coloured according to their mammalian orthologue: those also identified in previous proteomic studies are highlighted in green; those identified in the proteomic analysis of rat brain homogenate in this study but not in previous studies are highlighted in blue; those identified both in this and previous studies are highlighted in orange. Proteins which were not present in the control sample were given an arbitrary value of 0.2 to avoid dividing by zero, similar to previous proteomic studies (Dowal *et al.*, 2011; Roth *et al.*, 2006; Yang *et al.*, 2010). Proteins with a ratio of less than 5 were discarded (Martin and Cravatt, 2009). LFQ, label-free quantification.

Gene	Protein description	LFQ intensity ABE	LFQ intensity Control	Ratio LFQ ABE:Control	Mammalian orthologue	
					Gene	Name
aco-1	aconitase	2444500	0.2	12222500	Aco1	cytoplasmic aconitate hydratase
alh-8	aldehyde dehydrogenase	8700500	0.2	43502500	Aldh6a1	methylmalonate-semialdehyde dehydrogenase [acylating], mitochondrial precursor
ant-1.1	adenine nucleotide translocator	11436000	0.2	57180000	Slc25a6	ADP/ATP translocase 3
cts-1	citrate synthase	1519500	0.2	7597500	Cs	citrate synthase, mitochondrial
daf-21	heat shock protein HSP90	1024500	0.2	5122500	Hsp90ab1	heat shock protein 90β
eef-1A.1	eukaryotic translation elongation factor	98082000	0.2	4.9E+08	Eef1a2	elongation factor 1α 2
eef-2	eukaryotic translation elongation factor	15635000	0.2	78175000	Eef2	elongation factor 2
F09B12.3		5765800	0.2	28829000	Plbd2	putative phospholipase B-like 2
F46H5.3		32668000	0.2	1.63E+08	Ckm	creatine kinase M-type
gpd-3	glyceraldehyde-3-phosphate dehydrogenase	40323000	0.2	2.02E+08	Gapdh	glyceraldehyde-3-phosphate dehydrogenase
pck-2	phosphoenoylpyruvate kinase	1344200	0.2	6721000	Pck2	phosphoenolpyruvate carboxykinase [GTP], mitochondrial
tba-1	tubulin α	7149900	0.2	35749500	Tuba1a	tubulin α-1A chain
tbb-2	tubulin β	10503000	0.2	52515000	Tubb4b	tubulin β-4B chain
uba-1	ubiquitin activating enzyme	1617400	0.2	8087000	Uba1	ubiquitin-like modifier-activating enzyme 1
vit-2	vitellogenin	2173100	0.2	10865500	Wdr87	WD repeat-containing protein 87
vit-5	vitellogenin	16044000	0.2	80220000	Cenpe	centromere-associated protein E
vit-6	vitellogenin	2603900	0.2	13019500	Bmper	BMP-binding endothelial regulator protein precursor

APPENDIX 7.2 HITS WITH A SINGLE UNIQUE PEPTIDE IN THE EXPERIMENTAL SAMPLE

Hits are coloured according to their mammalian orthologue: those also identified in previous proteomic studies are highlighted in green; those identified in the proteomic analysis of rat brain homogenate in this study but not in previous studies are highlighted in blue; those identified both in this and previous studies are highlighted in orange. Proteins which were not present in the control sample were given an arbitrary value of 0.2 to avoid dividing by zero, similar to previous proteomic studies (Dowal *et al.*, 2011; Roth *et al.*, 2006; Yang *et al.*, 2010). Proteins with a ratio of less than 5 were discarded (Martin and Cravatt, 2009). LFQ, label-free quantification.

Gene	Protein description	LFQ intensity ABE	LFQ intensity Control	Ratio LFQ ABE:Control	Mammalian orthologue	
					Gene	Name
abl-1	oncogene Abl-related	72603	0.2	363015	Abl1	c-Abl oncogene 1
abtm-1	ABC transporter, mitochondrial	43351000	0.2	2.17E+08	Abcb7	ATP-binding cassette sub-family B member 7, mitochondrial
aco-2	aconitase	120460	0.2	602300	Aco2	aconitate hydratase, mitochondrial
ahcy-1	*S*-adenosylhomocysteine hydrolase homolog	2846200	0.2	14231000	Ahcy	adenosylhomocysteinase
alh-9	aldehyde dehydrogenase	932600	0.2	4663000	Aldh7a1	α-aminoadipic semialdehyde dehydrogenase
asp-1	aspartyl protease	1161300	0.2	5806500	Pgc	gastricsin
bed-1	BED-type zinc finger putative transcription factor	3.66E+08	0.2	1.83E+09		
C08H9.2a.1		686890	0.2	3434450	Hdlbp	vigilin
C09B9.1		8454000	0.2	42270000		
C33H5.8		862690	0.2	4313450	Rpap3	RNA polymerase II-associated protein 3
C35E7.7		717150	0.2	3585750		
F01G4.6b.1		1459800	0.2	7299000	Slc25a3	phosphate carrier protein, mitochondrial
F02H6.7		1174800	0.2	5874000	Bai1	brain-specific angiogenesis inhibitor 1
F09G2.2		173810	0.2	869050	Cnppd1	cyclin Pas1/PHO80 domain-containing protein 1
F46B3.15		100820	0.2	504100		
F46F11.11		1349900	0.2	6749500		
faah-5	fatty acid amide hydrolase homolog	29982000	0.2	1.5E+08	Faah1	fatty-acid amide hydrolase 1
fbxa-16	F box A protein	238240	0.2	1191200		
gdh-1	glutamate dehydrogenase	1021200	0.2	5106000	Glud1	glutamate dehydrogenase, mitochondrial
har-2	hemiasterlin resistant	15270000	0.2	76350000	Dspp	dentin sialophosphoprotein
hel-1	helicase	2872900	0.2	14364500	Ddx39a	ATP-dependent RNA helicase DDX39
imb-3	importin β family	422820	0.2	2114100	Ipo5	importin 5
lim-7	LIM homeodomain protein	3838400	0.2	19192000	Isl2	insulin gene enhancer protein ISL-2
nhr-134	nuclear hormone receptor	2289900	0.2	11449500	Ppara	peroxisome proliferator-activated receptor α
nhr-268	nuclear hormone receptor	667360	0.2	3336800	Rarg	retinoic acid receptor γ2
nsf-1	N-ethylmaleimide sensitive factor homolog	906140	0.2	4530700	Nsf	vesicle fusing ATPase
pck-1	phosphoenoylpyruvate carboxykinase	655470	0.2	3277350	Pck2	phosphoenolpyruvate carboxykinase [GTP], mitochondrial
pdi-2	protein disulphide isomerase	1720400	0.2	8602000	P4hb	protein disulphide-isomerase
ptr-3	patched-related family	3513600	0.2	17568000	Npc1	Niemann-Pick C1 protein
R12E2.8		1497700	0.2	7488500	Ush2a	usherin
rps-26	small ribosomal protein subunit S26	893520	0.2	4467600	Rps26	40S ribosomal protein S26
rps-4	small ribosomal protein subunit S4	892020	0.2	4460100	Rps4x	40S ribosomal protein S4, X isoform
rps-5	small ribosomal protein subunit S5	1517700	0.2	7588500	Rps5	40S ribosomal protein S5
sdha-1	succinate dehydrogenase complex subunit A	220670	0.2	1103350	Shda1	succinate dehydrogenase (ubiquinone) flavoprotein subunit, mitochondrial
sphk-1	sphingosine kinase	259010	0.2	1295050	Sphk1	sphingosine kinase 1
sun-1	SUN (*S. pombe* sad1/Ce-UNC-84) domain protein	18057000	0.2	90285000		
T04B2.7		314640	0.2	1573200		

Gene	Protein description	LFQ intensity ABE	LFQ intensity Control	Ratio LFQ ABE:Control	Mammalian orthologue	
					Gene	Name
unc-15	paramyosin homolog	916140	0.2	4580700	Myh7	myosin-7
W02F12.8		538170	0.2	2690850		
W09D6.1c		55055000	0.2	2.75E+08	Aasdh	Acyl-CoA synthetase family member 4
Y47D3A.28		19882	0.2	99410	Mcm10	minichromosome maintenance deficient 10 (*S. cerevisiae*)

REFERENCES

Abrami, L., Kunz, B., Iacovache, I., and van der Goot, F.G. (2008). Palmitoylation and ubiquitination regulate exit of the Wnt signaling protein LRP6 from the endoplasmic reticulum. *Proc Natl Acad Sci U S A*. **105**:5384-5389.

Ames, J.B., Tanaka, T., Stryer, L., and Ikura, M. (1996). Portrait of a myristoyl switch protein. *Curr Opin Struct Biol*. **6**:432-438.

Asikainen, S., Vartiainen, S., Lakso, M., Nass, R., and Wong, G. (2005). Selective sensitivity of Caenorhabditis elegans neurons to RNA interference. *Neuroreport*. **16**:1995-1999.

Bannan, B.A., Van Etten, J., Kohler, J.A., Tsoi, Y., Hansen, N.M., Sigmon, S., Fowler, E., Buff, H., Williams, T.S., Ault, J.G., Glaser, R.L., and Korey, C.A. (2008). The Drosophila protein palmitoylome: characterizing palmitoyl-thioesterases and DHHC palmitoyl-transferases. *Fly (Austin)*. **2**:198-214.

Barstead, R.J., and Moerman, D.G. (2006). C. elegans deletion mutant screening. *Methods Mol Biol*. **351**:51-58.

Bartels, D.J., Mitchell, D.A., Dong, X., and Deschenes, R.J. (1999). Erf2, a novel gene product that affects the localization and palmitoylation of Ras2 in Saccharomyces cerevisiae. *Mol Cell Biol*. **19**:6775-6787.

Baumgart, F., Corral-Escariz, M., Perez-Gil, J., and Rodriguez-Crespo, I. (2010). Palmitoylation of R-Ras by human DHHC19, a palmitoyl transferase with a CaaX box. *Biochim Biophys Acta*. **1798**:592-604.

Bellizzi, J.J., 3rd, Widom, J., Kemp, C., Lu, J.Y., Das, A.K., Hofmann, S.L., and Clardy, J. (2000). The crystal structure of palmitoyl protein thioesterase 1 and the molecular basis of infantile neuronal ceroid lipofuscinosis. *Proc Natl Acad Sci U S A*. **97**:4573-4578.

Benitez, B.A., Alvarado, D., Cai, Y., Mayo, K., Chakraverty, S., Norton, J., Morris, J.C., Sands, M.S., Goate, A., and Cruchaga, C. (2011). Exome-sequencing confirms DNAJC5 mutations as cause of adult neuronal ceroid-lipofuscinosis. *PLoS One*. **6**:e26741.

Bessereau, J.L., Wright, A., Williams, D.C., Schuske, K., Davis, M.W., and Jorgensen, E.M. (2001). Mobilization of a Drosophila transposon in the Caenorhabditis elegans germ line. *Nature*. **413**:70-74.

Bible, E., Gupta, P., Hofmann, S.L., and Cooper, J.D. (2004). Regional and cellular neuropathology in the palmitoyl protein thioesterase-1 null mutant mouse model of infantile neuronal ceroid lipofuscinosis. *Neurobiol Dis*. **16**:346-359.

Bizzozero, O.A. (1995). Chemical analysis of acylation sites and species. *Methods Enzymol*. **250**:361-379.

Bohm, S., Frishman, D., and Mewes, H.W. (1997). Variations of the C2H2 zinc finger motif in the yeast genome and classification of yeast zinc finger proteins. *Nucleic Acids Res*. **25**:2464-2469.

Boone, C., Bussey, H., and Andrews, B.J. (2007). Exploring genetic interactions and networks with yeast. *Nat Rev Genet*. **8**:437-449.

Brandes, R., Zohar, Y., Arad, R., and Shapiro, B. (1973). Two forms of microsomal palmitoyl-coenzyme A synthetase. *Eur J Biochem*. **34**:329-332.

Braun, T., and Fenaux, P. (2008). Farnesyltransferase inhibitors and their potential role in therapy for myelodysplastic syndromes and acute myeloid leukaemia. *Br J Haematol*. **141**:576-586.

Brenner, S. (1974). The genetics of Caenorhabditis elegans. *Genetics*. **77**:71-94.

Brundage, L., Avery, L., Katz, A., Kim, U.J., Mendel, J.E., Sternberg, P.W., and Simon, M.I. (1996). Mutations in a C. elegans Gqalpha gene disrupt movement, egg laying, and viability. *Neuron*. **16**:999-1009.

Buff, H., Smith, A.C., and Korey, C.A. (2007). Genetic modifiers of Drosophila palmitoyl-protein thioesterase 1-induced degeneration. *Genetics*. **176**:209-220.

Bursten, S.L., Locksley, R.M., Ryan, J.L., and Lovett, D.H. (1988). Acylation of monocyte and glomerular mesangial cell proteins. Myristyl acylation of the interleukin 1 precursors. *The Journal of clinical investigation*. **82**:1479-1488.

C. elegans Sequencing Consortium. (1998). Genome sequence of the nematode C. elegans: a platform for investigating biology. *Science*. **282**:2012-2018.

Calero, G., Gupta, P., Nonato, M.C., Tandel, S., Biehl, E.R., Hofmann, S.L., and Clardy, J. (2003). The crystal structure of palmitoyl protein thioesterase-2 (PPT2) reveals the basis for divergent substrate specificities of the two lysosomal thioesterases, PPT1 and PPT2. *J Biol Chem*. **278**:37957-37964.

Calixto, A., Chelur, D., Topalidou, I., Chen, X., and Chalfie, M. (2010). Enhanced neuronal RNAi in C. elegans using SID-1. *Nat. Methods*. **7**:554-559.

Callejo, A., Torroja, C., Quijada, L., and Guerrero, I. (2006). Hedgehog lipid modifications are required for Hedgehog stabilization in the extracellular matrix. *Development*. **133**:471-483.

Camp, L.A., and Hofmann, S.L. (1993). Purification and properties of a palmitoyl-protein thioesterase that cleaves palmitate from H-Ras. *J Biol Chem*. **268**:22566-22574.

Camp, L.A., Verkruyse, L.A., Afendis, S.J., Slaughter, C.A., and Hofmann, S.L. (1994). Molecular cloning and expression of palmitoyl-protein thioesterase. *J Biol Chem*. **269**:23212-23219.

Carr, S.A., Biemann, K., Shoji, S., Parmelee, D.C., and Titani, K. (1982). n-Tetradecanoyl is the NH2-terminal blocking group of the catalytic subunit of cyclic AMP-dependent protein kinase from bovine cardiac muscle. *Proc Natl Acad Sci U S A*. **79**:6128-6131.

Chalfie, M., and Sulston, J. (1981). Developmental genetics of the mechanosensory neurons of Caenorhabditis elegans. *Dev Biol*. **82**:358-370.

Chamberlain, L.H., and Burgoyne, R.D. (1996). Identification of a novel cysteine string protein variant and expression of cysteine string proteins in non-neuronal cells. *J Biol Chem*. **271**:7320-7323.

Chamoun, Z., Mann, R.K., Nellen, D., von Kessler, D.P., Bellotto, M., Beachy, P.A., and Basler, K. (2001). Skinny hedgehog, an acyltransferase required for palmitoylation and activity of the hedgehog signal. *Science*. **293**:2080-2084.

Charollais, J., and Van Der Goot, F.G. (2009). Palmitoylation of membrane proteins (Review). *Mol Membr Biol*. **26**:55-66.

Charron, G., Zhang, M.M., Yount, J.S., Wilson, J., Raghavan, A.S., Shamir, E., and Hang, H.C. (2009). Robust fluorescent detection of protein fatty-acylation with chemical reporters. *J Am Chem Soc*. **131**:4967-4975.

Charych, E.I., Jiang, L.X., Lo, F., Sullivan, K., and Brandon, N.J. (2010). Interplay of palmitoylation and phosphorylation in the trafficking and localization of phosphodiesterase 10A: implications for the treatment of schizophrenia. *J Neurosci*. **30**:9027-9037.

Chen, W.Y., Shi, Y.Y., Zheng, Y.L., Zhao, X.Z., Zhang, G.J., Chen, S.Q., Yang, P.D., and He, L. (2004). Case-control study and transmission disequilibrium test provide consistent evidence for association between schizophrenia and genetic variation in the 22q11 gene ZDHHC8. *Hum Mol Genet*. **13**:2991-2995.

Chintapalli, V.R., Wang, J., and Dow, J.A. (2007). Using FlyAtlas to identify better Drosophila melanogaster models of human disease. *Nat Genet*. **39**:715-720.

Cho, S.K., and Hofmann, S.L. (2004). pdf1, a palmitoyl protein thioesterase 1 Ortholog in Schizosaccharomyces pombe: a yeast model of infantile Batten disease. *Eukaryot Cell*. **3**:302-310.

Christensen, M., Estevez, A., Yin, X., Fox, R., Morrison, R., McDonnell, M., Gleason, C., Miller, D.M., 3rd, and Strange, K. (2002). A primary culture system for functional analysis of C. elegans neurons and muscle cells. *Neuron*. **33**:503-514.

Chu-LaGraff, Q., Blanchette, C., O'Hern, P., and Denefrio, C. (2010). The Batten disease Palmitoyl Protein Thioesterase 1 gene regulates neural specification and axon connectivity during Drosophila embryonic development. *PLoS One*. **5**:e14402.

Clague, M.J., Coulson, J.M., and Urbe, S. (2012). Cellular functions of the DUBs. *J Cell Sci*. **125**:277-286.

Cooper, J.D. (2010). The neuronal ceroid lipofuscinoses: the same, but different? *Biochem Soc Trans*. **38**:1448-1452.

Cypser, J.R., and Johnson, T.E. (1999). The spe-10 mutant has longer life and increased stress resistance. *Neurobiol Aging*. **20**:503-512.

Das, A.K., Lu, J.Y., and Hofmann, S.L. (2001). Biochemical analysis of mutations in palmitoyl-protein thioesterase causing infantile and late-onset forms of neuronal ceroid lipofuscinosis. *Hum Mol Genet*. **10**:1431-1439.

Dekker, F.J., Rocks, O., Vartak, N., Menninger, S., Hedberg, C., Balamurugan, R., Wetzel, S., Renner, S., Gerauer, M., Scholermann, B., Rusch, M., Kramer, J.W., Rauh, D., Coates, G.W., Brunsveld, L., Bastiaens, P.I., and Waldmann, H. (2010). Small-molecule inhibition of APT1 affects Ras localization and signaling. *Nat Chem Biol*. **6**:449-456.

Devedjiev, Y., Dauter, Z., Kuznetsov, S.R., Jones, T.L., and Derewenda, Z.S. (2000). Crystal structure of the human acyl protein thioesterase I from a single X-ray data set to 1.5 A. *Structure*. **8**:1137-1146.

Dighe, S.A., and Kozminski, K.G. (2008). Swf1p, a member of the DHHC-CRD family of palmitoyltransferases, regulates the actin cytoskeleton and polarized secretion independently of its DHHC motif. *Mol Biol Cell*. **19**:4454-4468.

Dowal, L., Yang, W., Freeman, M.R., Steen, H., and Flaumenhaft, R. (2011). Proteomic analysis of palmitoylated platelet proteins. *Blood*. **118**:e62-73.

Draper, J.M., and Smith, C.D. (2010). DHHC20: a human palmitoyl acyltransferase that causes cellular transformation. *Mol Membr Biol*. **27**:123-136.

Drisdel, R.C., and Green, W.N. (2004). Labeling and quantifying sites of protein palmitoylation. *Biotechniques*. **36**:276-285.

Ducker, C.E., Stettler, E.M., French, K.J., Upson, J.J., and Smith, C.D. (2004). Huntingtin interacting protein 14 is an oncogenic human protein: palmitoyl acyltransferase. *Oncogene*. **23**:9230-9237.

Duncan, J.A., and Gilman, A.G. (1996). Autoacylation of G protein alpha subunits. *J Biol Chem*. **271**:23594-23600.

Duncan, J.A., and Gilman, A.G. (1998). A cytoplasmic acyl-protein thioesterase that removes palmitate from G protein alpha subunits and p21(RAS). *J Biol Chem*. **273**:15830-15837.

Duncan, J.A., and Gilman, A.G. (2002). Characterization of Saccharomyces cerevisiae acyl-protein thioesterase 1, the enzyme responsible for G protein alpha subunit deacylation in vivo. *J Biol Chem*. **277**:31740-31752.

Eimer, S., Gottschalk, A., Hengartner, M., Horvitz, H.R., Richmond, J., Schafer, W.R., and Bessereau, J.L. (2007). Regulation of nicotinic receptor trafficking by the transmembrane Golgi protein UNC-50. *EMBO J*. **26**:4313-4323.

El-Husseini Ael, D., Schnell, E., Dakoji, S., Sweeney, N., Zhou, Q., Prange, O., Gauthier-Campbell, C., Aguilera-Moreno, A., Nicoll, R.A., and Bredt, D.S. (2002). Synaptic strength regulated by palmitate cycling on PSD-95. *Cell*. **108**:849-863.

Esposito, G., Di Schiavi, E., Bergamasco, C., and Bazzicalupo, P. (2007). Efficient and cell specific knock-down of gene function in targeted C. elegans neurons. *Gene*. **395**:170-176.

Fang, C., Deng, L., Keller, C.A., Fukata, M., Fukata, Y., Chen, G., and Luscher, B. (2006). GODZ-mediated palmitoylation of GABA(A) receptors is required for normal assembly and function of GABAergic inhibitory synapses. *J Neurosci*. **26**:12758-12768.

Faul, T., Gawlik, M., Bauer, M., Jung, S., Pfuhlmann, B., Jabs, B., Knapp, M., and Stober, G. (2005). ZDHHC8 as a candidate gene for schizophrenia: analysis of a putative functional intronic marker in case-control and family-based association studies. *BMC Psychiatry*. **5**:35.

Fay, D. Genetic mapping and manipulation: Chapter 1-Introduction and basics. *In* WormBook. T.C.e.R. Community, editor. WormBook.

Fernandez-Chacon, R., Wolfel, M., Nishimune, H., Tabares, L., Schmitz, F., Castellano-Munoz, M., Rosenmund, C., Montesinos, M.L., Sanes, J.R., Schneggenburger, R., and Sudhof, T.C. (2004). The synaptic vesicle protein CSP alpha prevents presynaptic degeneration. *Neuron*. **42**:237-251.

Fernandez-Hernando, C., Fukata, M., Bernatchez, P.N., Fukata, Y., Lin, M.I., Bredt, D.S., and Sessa, W.C. (2006). Identification of Golgi-localized acyl transferases that palmitoylate and regulate endothelial nitric oxide synthase. *J Cell Biol*. **174**:369-377.

Fire, A., Albertson, D., Harrison, S.W., and Moerman, D.G. (1991). Production of antisense RNA leads to effective and specific inhibition of gene expression in C. elegans muscle. *Development*. **113**:503-514.

Fire, A., Xu, S., Montgomery, M.K., Kostas, S.A., Driver, S.E., and Mello, C.C. (1998). Potent and specific genetic interference by double-stranded RNA in Caenorhabditis elegans. *Nature*. **391**:806-811.

Fischer, S.E. (2010). Small RNA-mediated gene silencing pathways in C. elegans. *Int J Biochem Cell Biol*. **42**:1306-1315.

Folch-Pi, J., and Stoffyn, P.J. (1972). Proteolipids from membrane systems. *Ann N Y Acad Sci*. **195**:86-107.

Folch, J., and Lees, M. (1951). Proteolipids, a new type of tissue lipoproteins; their isolation from brain. *J Biol Chem*. **191**:807-817.

Forrester, M.T., Hess, D.T., Thompson, J.W., Hultman, R., Moseley, M.A., Stamler, J.S., and Casey, P.J. (2011). Site-specific analysis of protein S-acylation by resin-assisted capture. *J Lipid Res*. **52**:393-398.

Forrester, M.T., Thompson, J.W., Foster, M.W., Nogueira, L., Moseley, M.A., and Stamler, J.S. (2009). Proteomic analysis of S-nitrosylation and denitrosylation by resin-assisted capture. *Nat Biotechnol*. **27**:557-559.

Franch-Marro, X., Wendler, F., Griffith, J., Maurice, M.M., and Vincent, J.P. (2008). In vivo role of lipid adducts on Wingless. *J Cell Sci*. **121**:1587-1592.

Fredens, J., Engholm-Keller, K., Giessing, A., Pultz, D., Larsen, M.R., Hojrup, P., Moller-Jensen, J., and Faergeman, N.J. (2011). Quantitative proteomics by amino acid labeling in C. elegans. *Nat Methods*.

Frokjaer-Jensen, C., Davis, M.W., Hollopeter, G., Taylor, J., Harris, T.W., Nix, P., Lofgren, R., Prestgard-Duke, M., Bastiani, M., Moerman, D.G., and Jorgensen, E.M. (2010). Targeted gene deletions in C. elegans using transposon excision. *Nat Methods*. **7**:451-453.

Frokjaer-Jensen, C., Davis, M.W., Hopkins, C.E., Newman, B.J., Thummel, J.M., Olesen, S.P., Grunnet, M., and Jorgensen, E.M. (2008). Single-copy insertion of transgenes in Caenorhabditis elegans. *Nat Genet*. **40**:1375-1383.

Fukata, M., Fukata, Y., Adesnik, H., Nicoll, R.A., and Bredt, D.S. (2004). Identification of PSD-95 palmitoylating enzymes. *Neuron*. **44**:987-996.

Fukata, Y., and Fukata, M. (2010). Protein palmitoylation in neuronal development and synaptic plasticity. *Nat Rev Neurosci*. **11**:161-175.

Geng, W., Cosman, P., Berry, C.C., Feng, Z., and Schafer, W.R. (2004). Automatic tracking, feature extraction and classification of C elegans phenotypes. *IEEE Trans Biomed Eng*. **51**:1811-1820.

Gengyo-Ando, K., and Mitani, S. (2000). Characterization of mutations induced by ethyl methanesulfonate, UV, and trimethylpsoralen in the nematode Caenorhabditis elegans. *Biochem Biophys Res Commun*. **269**:64-69.

Givan, S.A., and Sprague, G.F., Jr. (1997). The ankyrin repeat-containing protein Akr1p is required for the endocytosis of yeast pheromone receptors. *Mol Biol Cell*. **8**:1317-1327.

Glaser, B., Schumacher, J., Williams, H.J., Jamra, R.A., Ianakiev, N., Milev, R., Ohlraun, S., Schulze, T.G., Czerski, P.M., Hauser, J., Jonsson, E.G., Sedvall, G.C., Klopp, N., Illig, T., Becker, T., Propping, P., Williams, N.M., Cichon, S., Kirov, G., Rietschel, M., Murphy, K.C., O'Donovan, M.C., Nothen, M.M., and Owen, M.J. (2005). No association between the putative functional ZDHHC8 single nucleotide polymorphism rs175174 and schizophrenia in large European samples. *Biol Psychiatry*. **58**:78-80.

Glaser, R.L., Hickey, A.J., Chotkowski, H.L., and Chu-LaGraff, Q. (2003). Characterization of Drosophila palmitoyl-protein thioesterase 1. *Gene*. **312**:271-279.

Gleason, E.J., Lindsey, W.C., Kroft, T.L., Singson, A.W., and L'Hernault S, W. (2006). spe-10 encodes a DHHC-CRD zinc-finger membrane protein required for endoplasmic reticulum/Golgi membrane morphogenesis during Caenorhabditis elegans spermatogenesis. *Genetics*. **172**:145-158.

Gonzalez Montoro, A., Quiroga, R., Maccioni, H.J., and Valdez Taubas, J. (2009). A novel motif at the C-terminus of palmitoyltransferases is essential for Swf1 and Pfa3 function in vivo. *Biochem J*. **419**:301-308.

Gouda, K., Matsunaga, Y., Iwasaki, T., and Kawano, T. (2010). An altered method of feeding RNAi that knocks down multiple genes simultaneously in the nematode Caenorhabditis elegans. *Biosci Biotechnol Biochem*. **74**:2361-2365.

Gouw, J.W., Tops, B.B., and Krijgsveld, J. (2011). Metabolic labeling of model organisms using heavy nitrogen (15N). *Methods Mol Biol*. **753**:29-42.

Goytain, A., Hines, R.M., and Quamme, G.A. (2008). Huntingtin-interacting proteins, HIP14 and HIP14L, mediate dual functions, palmitoyl acyltransferase and Mg2+ transport. *J Biol Chem*. **283**:33365-33374.

Greaves, J., Gorleku, O.A., Salaun, C., and Chamberlain, L.H. (2010). Palmitoylation of the SNAP25 protein family: specificity and regulation by DHHC palmitoyl transferases. *J Biol Chem*. **285**:24629-24638.

Greaves, J., Prescott, G.R., Gorleku, O.A., and Chamberlain, L.H. (2009). The fat controller: roles of palmitoylation in intracellular protein trafficking and targeting to membrane microdomains (Review). *Mol Membr Biol*. **26**:67-79.

Greaves, J., Salaun, C., Fukata, Y., Fukata, M., and Chamberlain, L.H. (2008). Palmitoylation and membrane interactions of the neuroprotective chaperone cysteine-string protein. *J Biol Chem*. **283**:25014-25026.

Guang, S., Bochner, A.F., Pavelec, D.M., Burkhart, K.B., Harding, S., Lachowiec, J., and Kennedy, S. (2008). An Argonaute transports siRNAs from the cytoplasm to the nucleus. *Science*. **321**:537-541.

Gundersen, C.B., Mastrogiacomo, A., Faull, K., and Umbach, J.A. (1994). Extensive lipidation of a Torpedo cysteine string protein. *J Biol Chem*. **269**:19197-19199.

Gupta, P., Soyombo, A.A., Atashband, A., Wisniewski, K.E., Shelton, J.M., Richardson, J.A., Hammer, R.E., and Hofmann, S.L. (2001). Disruption of PPT1 or PPT2 causes neuronal ceroid lipofuscinosis in knockout mice. *Proc Natl Acad Sci U S A*. **98**:13566-13571.

Gupta, P., Soyombo, A.A., Shelton, J.M., Wilkofsky, I.G., Wisniewski, K.E., Richardson, J.A., and Hofmann, S.L. (2003). Disruption of PPT2 in mice causes an unusual lysosomal storage disorder with neurovisceral features. *Proc Natl Acad Sci U S A*. **100**:12325-12330.

Hammell, C.M., and Hannon, G.J. (2012). Inducing RNAi in C. elegans by Feeding with dsRNA-expressing E. coli. *Cold Spring Harb Protoc*. **2012**.

Hancock, J.F., Magee, A.I., Childs, J.E., and Marshall, C.J. (1989). All ras proteins are polyisoprenylated but only some are palmitoylated. *Cell*. **57**:1167-1177.

Hancock, J.F., Paterson, H., and Marshall, C.J. (1990). A polybasic domain or palmitoylation is required in addition to the CAAX motif to localize p21ras to the plasma membrane. *Cell*. **63**:133-139.

Hantschel, O., Nagar, B., Guettler, S., Kretzschmar, J., Dorey, K., Kuriyan, J., and Superti-Furga, G. (2003). A myristoyl/phosphotyrosine switch regulates c-Abl. *Cell*. **112**:845-857.

Harashima, T., and Heitman, J. (2005). Galpha subunit Gpa2 recruits kelch repeat subunits that inhibit receptor-G protein coupling during cAMP-induced dimorphic transitions in Saccharomyces cerevisiae. *Mol Biol Cell*. **16**:4557-4571.

Hart (ed.), A.C. Behavior. *In* WormBook. T.C.e.R. Community, editor. WormBook.

Hayashi, T., McMahon, H., Yamasaki, S., Binz, T., Hata, Y., Sudhof, T.C., and Niemann, H. (1994). Synaptic vesicle membrane fusion complex: action of clostridial neurotoxins on assembly. *EMBO J*. **13**:5051-5061.

Hayashi, T., Thomas, G.M., and Huganir, R.L. (2009). Dual palmitoylation of NR2 subunits regulates NMDA receptor trafficking. *Neuron*. **64**:213-226.

Hedo, J.A., Collier, E., and Watkinson, A. (1987). Myristyl and palmityl acylation of the insulin receptor. *J Biol Chem*. **262**:954-957.

Hellsten, E., Vesa, J., Olkkonen, V.M., Jalanko, A., and Peltonen, L. (1996). Human palmitoyl protein thioesterase: evidence for lysosomal targeting of the enzyme and disturbed cellular routing in infantile neuronal ceroid lipofuscinosis. *EMBO J*. **15**:5240-5245.

Hemsley, P.A., and Grierson, C.S. (2011). The ankyrin repeats and DHHC S-acyl transferase domain of AKR1 act independently to regulate switching from vegetative to mating states in yeast. *PLoS One*. **6**:e28799.

Hemsley, P.A., Weimar, T., Lilley, K.S., Dupree, P., and Grierson, C.S. (2012). A proteomic approach identifies many novel palmitoylated proteins in Arabidopsis. *New Phytol*.

Hickey, A.J., Chotkowski, H.L., Singh, N., Ault, J.G., Korey, C.A., MacDonald, M.E., and Glaser, R.L. (2006). Palmitoyl-protein thioesterase 1 deficiency in Drosophila melanogaster causes accumulation of abnormal storage material and reduced life span. *Genetics*. **172**:2379-2390.

Hines, R.M., Kang, R., Goytain, A., and Quamme, G.A. (2010). Golgi-specific DHHC zinc finger protein GODZ mediates membrane Ca2+ transport. *J Biol Chem*. **285**:4621-4628.

Ho, G.P., Selvakumar, B., Mukai, J., Hester, L.D., Wang, Y., Gogos, J.A., and Snyder, S.H. (2011). S-nitrosylation and S-palmitoylation reciprocally regulate synaptic targeting of PSD-95. *Neuron*. **71**:131-141.

Hoffman, G.R., Nassar, N., and Cerione, R.A. (2000). Structure of the Rho family GTP-binding protein Cdc42 in complex with the multifunctional regulator RhoGDI. *Cell*. **100**:345-356.

Hou, H., John Peter, A.T., Meiringer, C., Subramanian, K., and Ungermann, C. (2009). Analysis of DHHC acyltransferases implies overlapping substrate specificity and a two-step reaction mechanism. *Traffic*. **10**:1061-1073.

Hou, H., Subramanian, K., LaGrassa, T.J., Markgraf, D., Dietrich, L.E., Urban, J., Decker, N., and Ungermann, C. (2005). The DHHC protein Pfa3 affects vacuole-associated palmitoylation of the fusion factor Vac8. *Proc Natl Acad Sci U S A*. **102**:17366-17371.

Huang, K., Sanders, S., Singaraja, R., Orban, P., Cijsouw, T., Arstikaitis, P., Yanai, A., Hayden, M.R., and El-Husseini, A. (2009). Neuronal palmitoyl acyl transferases exhibit distinct substrate specificity. *FASEB J*. **23**:2605-2615.

Huang, K., Yanai, A., Kang, R., Arstikaitis, P., Singaraja, R.R., Metzler, M., Mullard, A., Haigh, B., Gauthier-Campbell, C., Gutekunst, C.A., Hayden, M.R., and El-Husseini, A. (2004). Huntingtin-interacting protein HIP14 is a palmitoyl transferase involved in palmitoylation and trafficking of multiple neuronal proteins. *Neuron*. **44**:977-986.

Huh, W.K., Falvo, J.V., Gerke, L.C., Carroll, A.S., Howson, R.W., Weissman, J.S., and O'Shea, E.K. (2003). Global analysis of protein localization in budding yeast. *Nature*. **425**:686-691.

Ingham, P.W. (2001). Hedgehog signaling: a tale of two lipids. *Science*. **294**:1879-1881.

Ivaldi, C., Martin, B.R., Kieffer-Jaquinod, S., Chapel, A., Levade, T., Garin, J., and Journet, A. (2012). Proteomic analysis of S-acylated proteins in human B cells reveals palmitoylation of the immune regulators CD20 and CD23. *PLoS One*. **7**:e37187.

Izant, J.G., and Weintraub, H. (1984). Inhibition of thymidine kinase gene expression by anti-sense RNA: a molecular approach to genetic analysis. *Cell*. **36**:1007-1015.

Jennings, B.C., Nadolski, M.J., Ling, Y., Baker, M.B., Harrison, M.L., Deschenes, R.J., and Linder, M.E. (2009). 2-Bromopalmitate and 2-(2-hydroxy-5-nitro-benzylidene)-benzo[b]thiophen-3-one inhibit DHHC-mediated palmitoylation in vitro. *J Lipid Res*. **50**:233-242.

Jia, L., Linder, M.E., and Blumer, K.J. (2011). Gi/o signaling and the palmitoyltransferase DHHC2 regulate palmitate cycling and shuttling of RGS7 family-binding protein. *J Biol Chem*. **286**:13695-13703.

Johnson, J.R., Ferdek, P., Lian, L.Y., Barclay, J.W., Burgoyne, R.D., and Morgan, A. (2009). Binding of UNC-18 to the N-terminus of syntaxin is essential for neurotransmission in Caenorhabditis elegans. *Biochem J*. **418**:73-80.

Johswich, A., Kraft, B., Wuhrer, M., Berger, M., Deelder, A.M., Hokke, C.H., Gerardy-Schahn, R., and Bakker, H. (2009). Golgi targeting of Drosophila melanogaster beta4GalNAcTB requires a DHHC protein family-related protein as a pilot. *J Cell Biol*. **184**:173-183.

Joseph, M., and Nagaraj, R. (1995). Interaction of peptides corresponding to fatty acylation sites in proteins with model membranes. *J Biol Chem*. **270**:16749-16755.

Jung, V., Chen, L., Hofmann, S.L., Wigler, M., and Powers, S. (1995). Mutations in the SHR5 gene of Saccharomyces cerevisiae suppress Ras function and block membrane attachment and palmitoylation of Ras proteins. *Mol Cell Biol*. **15**:1333-1342.

Kamath, R.S., Martinez-Campos, M., Zipperlen, P., Fraser, A.G., and Ahringer, J. (2001). Effectiveness of specific RNA-mediated interference through ingested double-stranded RNA in Caenorhabditis elegans. *Genome Biol*. **2**:RESEARCH0002.

Kang, K.H., and Bier, E. (2010). dHIP14-dependent palmitoylation promotes secretion of the BMP antagonist Sog. *Dev Biol*. **346**:1-10.

Kang, R., Wan, J., Arstikaitis, P., Takahashi, H., Huang, K., Bailey, A.O., Thompson, J.X., Roth, A.F., Drisdel, R.C., Mastro, R., Green, W.N., Yates, J.R., 3rd, Davis, N.G., and El-Husseini, A. (2008). Neural palmitoyl-proteomics reveals dynamic synaptic palmitoylation. *Nature*. **456**:904-909.

Kao, L.R., Peterson, J., Ji, R., Bender, L., and Bender, A. (1996). Interactions between the ankyrin repeat-containing protein Akr1p and the pheromone response pathway in Saccharomyces cerevisiae. *Mol Cell Biol*. **16**:168-178.

Keller, C.A., Yuan, X., Panzanelli, P., Martin, M.L., Alldred, M., Sassoe-Pognetto, M., and Luscher, B. (2004). The gamma2 subunit of GABA(A) receptors is a substrate for palmitoylation by GODZ. *J Neurosci*. **24**:5881-5891.

Kennedy, S., Wang, D., and Ruvkun, G. (2004). A conserved siRNA-degrading RNase negatively regulates RNA interference in C. elegans. *Nature*. **427**:645-649.

Kielar, C., Wishart, T.M., Palmer, A., Dihanich, S., Wong, A.M., Macauley, S.L., Chan, C.H., Sands, M.S., Pearce, D.A., Cooper, J.D., and Gillingwater, T.H. (2009). Molecular correlates of axonal and synaptic pathology in mouse models of Batten disease. *Hum Mol Genet*. **18**:4066-4080.

Kihara, A., Kurotsu, F., Sano, T., Iwaki, S., and Igarashi, Y. (2005). Long-chain base kinase Lcb4 Is anchored to the membrane through its palmitoylation by Akr1. *Mol Cell Biol*. **25**:9189-9197.

Kim, Y.G., Sohn, E.J., Seo, J., Lee, K.J., Lee, H.S., Hwang, I., Whiteway, M., Sacher, M., and Oh, B.H. (2005). Crystal structure of bet3 reveals a novel mechanism for Golgi localization of tethering factor TRAPP. *Nat Struct Mol Biol*. **12**:38-45.

Kokkola, T., Kruse, C., Roy-Pogodzik, E.M., Pekkinen, J., Bauch, C., Honck, H.H., Hennemann, H., and Kreienkamp, H.J. (2011). Somatostatin receptor 5 is palmitoylated by the interacting ZDHHC5 palmitoyltransferase. *FEBS Lett*. **585**:2665-2670.

Korey, C.A., and MacDonald, M.E. (2003). An over-expression system for characterizing Ppt1 function in Drosophila. *BMC Neurosci*. **4**:30.

Korycka, J., Lach, A., Heger, E., Boguslawska, D.M., Wolny, M., Toporkiewicz, M., Augoff, K., Korzeniewski, J., and Sikorski, A.F. (2012). Human DHHC proteins: a spotlight on the hidden player of palmitoylation. *Eur J Cell Biol*. **91**:107-117.

Kraut, R., Menon, K., and Zinn, K. (2001). A gain-of-function screen for genes controlling motor axon guidance and synaptogenesis in Drosophila. *Curr Biol*. **11**:417-430.

Kummel, D., Walter, J., Heck, M., Heinemann, U., and Veit, M. (2010). Characterization of the self-palmitoylation activity of the transport protein particle component Bet3. *Cell Mol Life Sci*. **67**:2653-2664.

Lakkaraju, A.K., Abrami, L., Lemmin, T., Blaskovic, S., Kunz, B., Kihara, A., Dal Peraro, M., and van der Goot, F.G. (2012). Palmitoylated calnexin is a key component of the ribosome-translocon complex. *EMBO J*. **31**:1823-1835.

Lam, K.K., Davey, M., Sun, B., Roth, A.F., Davis, N.G., and Conibear, E. (2006). Palmitoylation by the DHHC protein Pfa4 regulates the ER exit of Chs3. *J Cell Biol*. **174**:19-25.

Lane, S.R., and Liu, Y. (1997). Characterization of the palmitoylation domain of SNAP-25. *J Neurochem*. **69**:1864-1869.

Larance, M., Bailly, A.P., Pourkarimi, E., Hay, R.T., Buchanan, G., Coulthurst, S., Xirodimas, D.P., Gartner, A., and Lamond, A.I. (2011). Stable-isotope labeling with amino acids in nematodes. *Nat Methods*.

Lehtovirta, M., Kyttala, A., Eskelinen, E.L., Hess, M., Heinonen, O., and Jalanko, A. (2001). Palmitoyl protein thioesterase (PPT) localizes into synaptosomes and synaptic vesicles in neurons: implications for infantile neuronal ceroid lipofuscinosis (INCL). *Hum Mol Genet*. **10**:69-75.

Lejeune, F.X., Mesrob, L., Parmentier, F., Bicep, C., Vazquez-Manrique, R.P., Parker, J.A., Vert, J.P., Tourette, C., and Neri, C. (2012). Large-scale functional RNAi screen in C. elegans identifies genes that regulate the dysfunction of mutant polyglutamine neurons. *BMC Genomics*. **13**:91.

Letunic, I., and Bork, P. (2007). Interactive Tree Of Life (iTOL): an online tool for phylogenetic tree display and annotation. *Bioinformatics*. **23**:127-128.

Levental, I., Lingwood, D., Grzybek, M., Coskun, U., and Simons, K. (2010). Palmitoylation regulates raft affinity for the majority of integral raft proteins. *Proc Natl Acad Sci U S A*. **107**:22050-22054.

Levy, A.D., Devignot, V., Fukata, Y., Fukata, M., Sobel, A., and Chauvin, S. (2011). Subcellular Golgi localization of stathmin family proteins is promoted by a specific set of DHHC palmitoyl transferases. *Mol Biol Cell*. **22**:1930-1942.

Li, B., Cong, F., Tan, C.P., Wang, S.X., and Goff, S.P. (2002). Aph2, a protein with a zf-DHHC motif, interacts with c-Abl and has pro-apoptotic activity. *J Biol Chem*. **277**:28870-28876.

Li, W., Bengtson, M.H., Ulbrich, A., Matsuda, A., Reddy, V.A., Orth, A., Chanda, S.K., Batalov, S., and Joazeiro, C.A. (2008). Genome-wide and functional annotation of human E3 ubiquitin ligases identifies MULAN, a mitochondrial E3 that regulates the organelle's dynamics and signaling. *PLoS One*. **3**:e1487.

Li, Y., Hu, J., Hofer, K., Wong, A.M., Cooper, J.D., Birnbaum, S.G., Hammer, R.E., and Hofmann, S.L. (2010). DHHC5 interacts with PDZ domain 3 of post-synaptic density-95 (PSD-95) protein and plays a role in learning and memory. *J Biol Chem*. **285**:13022-13031.

Li, Y., Martin, B.R., Cravatt, B.F., and Hofmann, S.L. (2012). DHHC5 protein palmitoylates flotillin-2 and is rapidly degraded on induction of neuronal differentiation in cultured cells. *J Biol Chem*. **287**:523-530.

Lobo, S., Greentree, W.K., Linder, M.E., and Deschenes, R.J. (2002). Identification of a Ras palmitoyltransferase in Saccharomyces cerevisiae. *J Biol Chem*. **277**:41268-41273.

Lu, D., Sun, H.Q., Wang, H., Barylko, B., Fukata, Y., Fukata, M., Albanesi, J.P., and Yin, H.L. (2012). Phosphatidylinositol 4-kinase IIalpha is palmitoylated by Golgi-localized palmitoyltransferases in cholesterol-dependent manner. *J Biol Chem*. **287**:21856-21865.

Lu, J.Y., Verkruyse, L.A., and Hofmann, S.L. (1996). Lipid thioesters derived from acylated proteins accumulate in infantile neuronal ceroid lipofuscinosis: correction of the defect in lymphoblasts by recombinant palmitoyl-protein thioesterase. *Proc Natl Acad Sci U S A*. **93**:10046-10050.

Lyly, A., von Schantz, C., Salonen, T., Kopra, O., Saarela, J., Jauhiainen, M., Kyttala, A., and Jalanko, A. (2007). Glycosylation, transport, and complex formation of palmitoyl protein thioesterase 1 (PPT1)--distinct characteristics in neurons. *BMC Cell Biol*. **8**:22.

Maduro, M., and Pilgrim, D. (1995). Identification and cloning of unc-119, a gene expressed in the Caenorhabditis elegans nervous system. *Genetics*. **141**:977-988.

Magee, A.I., and Courtneidge, S.A. (1985). Two classes of fatty acid acylated proteins exist in eukaryotic cells. *EMBO J*. **4**:1137-1144.

Manahan, C.L., Patnana, M., Blumer, K.J., and Linder, M.E. (2000). Dual lipid modification motifs in G(alpha) and G(gamma) subunits are required for full activity of the pheromone response pathway in Saccharomyces cerevisiae. *Mol Biol Cell*. **11**:957-968.

Manning, G., Whyte, D.B., Martinez, R., Hunter, T., and Sudarsanam, S. (2002). The protein kinase complement of the human genome. *Science*. **298**:1912-1934.

Mansilla, F., Birkenkamp-Demtroder, K., Kruhoffer, M., Sorensen, F.B., Andersen, C.L., Laiho, P., Aaltonen, L.A., Verspaget, H.W., and Orntoft, T.F. (2007). Differential expression of DHHC9 in microsatellite stable and instable human colorectal cancer subgroups. *Br J Cancer*. **96**:1896-1903.

Mansouri, M.R., Marklund, L., Gustavsson, P., Davey, E., Carlsson, B., Larsson, C., White, I., Gustavson, K.H., and Dahl, N. (2005). Loss of ZDHHC15 expression in a woman with a balanced translocation t(X;15)(q13.3;cen) and severe mental retardation. *Eur J Hum Genet*. **13**:970-977.

Marin, E.P., Derakhshan, B., Lam, T.T., Davalos, A., and Sessa, W.C. (2012). Endothelial cell palmitoylproteomic identifies novel lipid-modified targets and potential substrates for protein acyl transferases. *Circ Res*. **110**:1336-1344.

Martin, B.R., and Cravatt, B.F. (2009). Large-scale profiling of protein palmitoylation in mammalian cells. *Nat Methods*. **6**:135-138.

Martin, B.R., Wang, C., Adibekian, A., Tully, S.E., and Cravatt, B.F. (2012). Global profiling of dynamic protein palmitoylation. *Nat Methods*. **9**:84-89.

Martin, D.D., Beauchamp, E., and Berthiaume, L.G. (2011). Post-translational myristoylation: Fat matters in cellular life and death. *Biochimie*. **93**:18-31.

Maurer-Stroh, S., Eisenhaber, B., and Eisenhaber, F. (2002). N-terminal N-myristoylation of proteins: prediction of substrate proteins from amino acid sequence. *J Mol Biol*. **317**:541-557.

Maurer-Stroh, S., and Eisenhaber, F. (2005). Refinement and prediction of protein prenylation motifs. *Genome Biol*. **6**:R55.

McCormick, P.J., Dumaresq-Doiron, K., Pluviose, A.S., Pichette, V., Tosato, G., and Lefrancois, S. (2008). Palmitoylation controls recycling in lysosomal sorting and trafficking. *Traffic*. **9**:1984-1997.

McIntire, S.L., Garriga, G., White, J., Jacobson, D., and Horvitz, H.R. (1992). Genes necessary for directed axonal elongation or fasciculation in C. elegans. *Neuron*. **8**:307-322.

Merrick, B.A., Dhungana, S., Williams, J.G., Aloor, J.J., Peddada, S., Tomer, K.B., and Fessler, M.B. (2011). Proteomic profiling of S-acylated macrophage proteins identifies a role for palmitoylation in mitochondrial targeting of phospholipid scramblase 3. *Mol Cell Proteomics*. **10**:M110 006007.

Mill, P., Lee, A.W., Fukata, Y., Tsutsumi, R., Fukata, M., Keighren, M., Porter, R.M., McKie, L., Smyth, I., and Jackson, I.J. (2009). Palmitoylation regulates epidermal homeostasis and hair follicle differentiation. *PLoS Genet*. **5**:e1000748.

Miller, K.G., Emerson, M.D., and Rand, J.B. (1999). Goalpha and diacylglycerol kinase negatively regulate the Gqalpha pathway in C. elegans. *Neuron*. **24**:323-333.

Min, K., Kang, J., and Lee, J. (2010). A modified feeding RNAi method for simultaneous knock-down of more than one gene in Caenorhabditis elegans. *Biotechniques*. **48**:229-232.

Mitchell, D.A., Mitchell, G., Ling, Y., Budde, C., and Deschenes, R.J. (2010). Mutational analysis of Saccharomyces cerevisiae Erf2 reveals a two-step reaction mechanism for protein palmitoylation by DHHC enzymes. *J Biol Chem*.

Mitchell, D.A., Vasudevan, A., Linder, M.E., and Deschenes, R.J. (2006). Protein palmitoylation by a family of DHHC protein S-acyltransferases. *J Lipid Res*. **47**:1118-1127.

Mitra, K., Ubarretxena-Belandia, I., Taguchi, T., Warren, G., and Engelman, D.M. (2004). Modulation of the bilayer thickness of exocytic pathway membranes by membrane proteins rather than cholesterol. *Proc Natl Acad Sci U S A*. **101**:4083-4088.

Montell, C. (2003). Mg2+ homeostasis: the Mg2+nificent TRPM chanzymes. *Curr Biol*. **13**:R799-801.

Mukai, J., Dhilla, A., Drew, L.J., Stark, K.L., Cao, L., MacDermott, A.B., Karayiorgou, M., and Gogos, J.A. (2008). Palmitoylation-dependent neurodevelopmental deficits in a mouse model of 22q11 microdeletion. *Nat Neurosci*. **11**:1302-1310.

Mukai, J., Liu, H., Burt, R.A., Swor, D.E., Lai, W.S., Karayiorgou, M., and Gogos, J.A. (2004). Evidence that the gene encoding ZDHHC8 contributes to the risk of schizophrenia. *Nat Genet*. **36**:725-731.

Murray, D., Hermida-Matsumoto, L., Buser, C.A., Tsang, J., Sigal, C.T., Ben-Tal, N., Honig, B., Resh, M.D., and McLaughlin, S. (1998). Electrostatics and the membrane association of Src: theory and experiment. *Biochemistry*. **37**:2145-2159.

Nonet, M.L., Grundahl, K., Meyer, B.J., and Rand, J.B. (1993). Synaptic function is impaired but not eliminated in C. elegans mutants lacking synaptotagmin. *Cell*. **73**:1291-1305.

Noskova, L., Stranecky, V., Hartmannova, H., Pristoupilova, A., Baresova, V., Ivanek, R., Hulkova, H., Jahnova, H., van der Zee, J., Staropoli, J.F., Sims, K.B., Tyynela, J., Van Broeckhoven, C., Nijssen, P.C., Mole, S.E., Elleder, M., and Kmoch, S. (2011). Mutations in DNAJC5, encoding cysteine-string protein alpha, cause autosomal-dominant adult-onset neuronal ceroid lipofuscinosis. *Am J Hum Genet*. **89**:241-252.

O'Dowd, B.F., Hnatowich, M., Caron, M.G., Lefkowitz, R.J., and Bouvier, M. (1989). Palmitoylation of the human beta 2-adrenergic receptor. Mutation of Cys341 in the carboxyl tail leads to an uncoupled nonpalmitoylated form of the receptor. *J Biol Chem*. **264**:7564-7569.

Oh, Y., Jeon, Y.J., Hong, G.S., Kim, I., Woo, H.N., and Jung, Y.K. (2012). Regulation in the targeting of TRAIL receptor 1 to cell surface via GODZ for TRAIL sensitivity in tumor cells. *Cell Death Differ*. **19**:1196-1207.

Ohno, Y., Kashio, A., Ogata, R., Ishitomi, A., Yamazaki, Y., and Kihara, A. (2012). Analysis of substrate specificity of human DHHC protein acyltransferases using a yeast expression system. *Mol Biol Cell*.

Ohno, Y., Kihara, A., Sano, T., and Igarashi, Y. (2006). Intracellular localization and tissue-specific distribution of human and yeast DHHC cysteine-rich domain-containing proteins. *Biochim Biophys Acta*. **1761**:474-483.

Ohyama, T., Verstreken, P., Ly, C.V., Rosenmund, T., Rajan, A., Tien, A.C., Haueter, C., Schulze, K.L., and Bellen, H.J. (2007). Huntingtin-interacting protein 14, a palmitoyl transferase required for exocytosis and targeting of CSP to synaptic vesicles. *J Cell Biol*. **179**:1481-1496.

Omary, M.B., and Trowbridge, I.S. (1981). Covalent binding of fatty acid to the transferrin receptor in cultured human cells. *J Biol Chem*. **256**:4715-4718.

Otani, K., Ujike, H., Tanaka, Y., Morita, Y., Kishimoto, M., Morio, A., Uchida, N., Nomura, A., and Kuroda, S. (2005). The ZDHHC8 gene did not associate with bipolar disorder or schizophrenia. *Neurosci Lett*. **390**:166-170.

Oyama, T., Miyoshi, Y., Koyama, K., Nakagawa, H., Yamori, T., Ito, T., Matsuda, H., Arakawa, H., and Nakamura, Y. (2000). Isolation of a novel gene on 8p21.3-22 whose expression is reduced significantly in human colorectal cancers with liver metastasis. *Genes Chromosomes Cancer*. **29**:9-15.

Parenti, M., Vigano, M.A., Newman, C.M., Milligan, G., and Magee, A.I. (1993). A novel N-terminal motif for palmitoylation of G-protein alpha subunits. *Biochem J*. **291 (Pt 2)**:349-353.

Park, S., Patterson, E.E., Cobb, J., Audhya, A., Gartenberg, M.R., and Fox, C.A. (2011). Palmitoylation controls the dynamics of budding-yeast heterochromatin via the telomere-binding protein Rif1. *Proc Natl Acad Sci U S A*. **108**:14572-14577.

Pasula, S., Chakraborty, S., Choi, J.H., and Kim, J.H. (2010). Role of casein kinase 1 in the glucose sensor-mediated signaling pathway in yeast. *BMC Cell Biol*. **11**:17.

Pedram, A., Razandi, M., Deschenes, R.J., and Levin, E.R. (2012). DHHC-7 and -21 are palmitoylacyltransferases for sex steroid receptors. *Mol Biol Cell*. **23**:188-199.

Peitzsch, R.M., and McLaughlin, S. (1993). Binding of acylated peptides and fatty acids to phospholipid vesicles: pertinence to myristoylated proteins. *Biochemistry*. **32**:10436-10443.

Pepinsky, R.B., Zeng, C., Wen, D., Rayhorn, P., Baker, D.P., Williams, K.P., Bixler, S.A., Ambrose, C.M., Garber, E.A., Miatkowski, K., Taylor, F.R., Wang, E.A., and Galdes, A. (1998). Identification of a palmitic acid-modified form of human Sonic hedgehog. *J Biol Chem*. **273**:14037-14045.

Ponimaskin, E., Dityateva, G., Ruonala, M.O., Fukata, M., Fukata, Y., Kobe, F., Wouters, F.S., Delling, M., Bredt, D.S., Schachner, M., and Dityatev, A. (2008). Fibroblast growth factor-regulated palmitoylation of the neural cell adhesion molecule determines neuronal morphogenesis. *J Neurosci*. **28**:8897-8907.

Porter, M.Y., Turmaine, M., and Mole, S.E. (2005). Identification and characterization of Caenorhabditis elegans palmitoyl protein thioesterase1. *J Neurosci Res*. **79**:836-848.

Prescott, G.R., Gorleku, O.A., Greaves, J., and Chamberlain, L.H. (2009). Palmitoylation of the synaptic vesicle fusion machinery. *J Neurochem*.

Pryciak, P.M., and Hartwell, L.H. (1996). AKR1 encodes a candidate effector of the G beta gamma complex in the Saccharomyces cerevisiae pheromone response pathway and contributes to control of both cell shape and signal transduction. *Mol Cell Biol*. **16**:2614-2626.

Qin, L.X. (2002). Chromosomal aberrations related to metastasis of human solid tumors. *World J Gastroenterol*. **8**:769-776.

Raymond, F.L., Tarpey, P.S., Edkins, S., Tofts, C., O'Meara, S., Teague, J., Butler, A., Stevens, C., Barthorpe, S., Buck, G., Cole, J., Dicks, E., Gray, K., Halliday, K., Hills, K., Hinton, J., Jones, D., Menzies, A., Perry, J., Raine, K., Shepherd, R., Small, A., Varian, J., Widaa, S., Mallya, U., Moon, J., Luo, Y., Shaw, M., Boyle, J., Kerr, B., Turner, G., Quarrell, O., Cole, T., Easton, D.F., Wooster, R., Bobrow, M., Schwartz, C.E., Gecz, J., Stratton, M.R., and Futreal, P.A. (2007). Mutations in ZDHHC9, which encodes a palmitoyltransferase of NRAS and HRAS, cause X-linked mental retardation associated with a Marfanoid habitus. *Am J Hum Genet*. **80**:982-987.

Ren, J., Wen, L., Gao, X., Jin, C., Xue, Y., and Yao, X. (2008). CSS-Palm 2.0: an updated software for palmitoylation sites prediction. *Protein Eng Des Sel*. **21**:639-644.

Resh, M.D. (1999). Fatty acylation of proteins: new insights into membrane targeting of myristoylated and palmitoylated proteins. *Biochim Biophys Acta*. **1451**:1-16.

Resh, M.D. (2006). Trafficking and signaling by fatty-acylated and prenylated proteins. *Nat Chem Biol*. **2**:584-590.

Rinaldi, A., Kwee, I., Poretti, G., Mensah, A., Pruneri, G., Capello, D., Rossi, D., Zucca, E., Ponzoni, M., Catapano, C., Tibiletti, M.G., Paulli, M., Gaidano, G., and Bertoni, F. (2006). Comparative genome-wide profiling of post-transplant lymphoproliferative disorders and diffuse large B-cell lymphomas. *Br J Haematol*. **134**:27-36.

Robert, V.J. (2012). Engineering the Caenorhabditis elegans genome by Mos1-induced transgene-instructed gene conversion. *Methods Mol Biol*. **859**:189-201.

Rocks, O., Peyker, A., Kahms, M., Verveer, P.J., Koerner, C., Lumbierres, M., Kuhlmann, J., Waldmann, H., Wittinghofer, A., and Bastiaens, P.I. (2005). An acylation cycle regulates localization and activity of palmitoylated Ras isoforms. *Science*. **307**:1746-1752.

Roth, A.F., Feng, Y., Chen, L., and Davis, N.G. (2002). The yeast DHHC cysteine-rich domain protein Akr1p is a palmitoyl transferase. *J Cell Biol*. **159**:23-28.

Roth, A.F., Wan, J., Bailey, A.O., Sun, B., Kuchar, J.A., Green, W.N., Phinney, B.S., Yates, J.R., 3rd, and Davis, N.G. (2006). Global analysis of protein palmitoylation in yeast. *Cell*. **125**:1003-1013.

Rual, J.F., Ceron, J., Koreth, J., Hao, T., Nicot, A.S., Hirozane-Kishikawa, T., Vandenhaute, J., Orkin, S.H., Hill, D.E., van den Heuvel, S., and Vidal, M. (2004). Toward improving Caenorhabditis elegans phenome mapping with an ORFeome-based RNAi library. *Genome Res*. **14**:2162-2168.

Rusch, M., Zimmermann, T.J., Burger, M., Dekker, F.J., Gormer, K., Triola, G., Brockmeyer, A., Janning, P., Bottcher, T., Sieber, S.A., Vetter, I.R., Hedberg, C., and Waldmann, H. (2011). Identification of acyl protein thioesterases 1 and 2 as the cellular targets of the ras-signaling modulators palmostatin b and m. *Angew Chem Int Ed Engl*. **50**:9838-9842.

Rush, D.B., Leon, R.T., McCollum, M.H., Treu, R.W., and Wei, J. (2012). Palmitoylation and trafficking of GAD65 are impaired in a cellular model of Huntington's disease. *Biochem J*. **442**:39-48.

Sacco, F., Perfetto, L., Castagnoli, L., and Cesareni, G. (2012). The human phosphatase interactome: An intricate family portrait. *FEBS Lett*. **586**:2732-2739.

Saitoh, F., Tian, Q.B., Okano, A., Sakagami, H., Kondo, H., and Suzuki, T. (2004). NIDD, a novel DHHC-containing protein, targets neuronal nitric-oxide synthase (nNOS) to the synaptic membrane through a PDZ-dependent interaction and regulates nNOS activity. *J Biol Chem*. **279**:29461-29468.

Saja, S., Buff, H., Smith, A.C., Williams, T.S., and Korey, C.A. (2010). Identifying cellular pathways modulated by Drosophila palmitoyl-protein thioesterase 1 function. *Neurobiol Dis*. **40**:135-145.

Satou, M., Nishi, Y., Yoh, J., Hattori, Y., and Sugimoto, H. (2010). Identification and characterization of acyl-protein thioesterase 1/lysophospholipase I as a ghrelin deacylation/lysophospholipid hydrolyzing enzyme in fetal bovine serum and conditioned medium. *Endocrinology*. **151**:4765-4775.

Schmidt, M.F., and Schlesinger, M.J. (1979). Fatty acid binding to vesicular stomatitis virus glycoprotein: a new type of post-translational modification of the viral glycoprotein. *Cell*. **17**:813-819.

Shakes, D.C., and Ward, S. (1989). Mutations that disrupt the morphogenesis and localization of a sperm-specific organelle in Caenorhabditis elegans. *Dev Biol*. **134**:307-316.

Sharma, C., Rabinovitz, I., and Hemler, M.E. (2012). Palmitoylation by DHHC3 is critical for the function, expression, and stability of integrin alpha6beta4. *Cell Mol Life Sci*. **69**:2233-2244.

Sharma, C., Yang, X.H., and Hemler, M.E. (2008). DHHC2 affects palmitoylation, stability, and functions of tetraspanins CD9 and CD151. *Mol Biol Cell*. **19**:3415-3425.

Shin, H.D., Park, B.L., Bae, J.S., Park, T.J., Chun, J.Y., Park, C.S., Sohn, J.W., Kim, B.J., Kang, Y.H., Kim, J.W., Kim, K.H., Shin, T.M., and Woo, S.I. (2010). Association of ZDHHC8 polymorphisms with smooth pursuit eye movement abnormality. *Am J Med Genet B Neuropsychiatr Genet*. **153B**:1167-1172.

Shmueli, A., Segal, M., Sapir, T., Tsutsumi, R., Noritake, J., Bar, A., Sapoznik, S., Fukata, Y., Orr, I., Fukata, M., and Reiner, O. (2010). Ndel1 palmitoylation: a new mean to regulate cytoplasmic dynein activity. *EMBO J*. **29**:107-119.

Sigurdson, D.C., Spanier, G.J., and Herman, R.K. (1984). Caenorhabditis elegans deficiency mapping. *Genetics*. **108**:331-345.

Sijen, T., Fleenor, J., Simmer, F., Thijssen, K.L., Parrish, S., Timmons, L., Plasterk, R.H., and Fire, A. (2001). On the role of RNA amplification in dsRNA-triggered gene silencing. *Cell*. **107**:465-476.

Simmer, F., Moorman, C., van der Linden, A.M., Kuijk, E., van den Berghe, P.V., Kamath, R.S., Fraser, A.G., Ahringer, J., and Plasterk, R.H. (2003). Genome-wide RNAi of C. elegans using the hypersensitive rrf-3 strain reveals novel gene functions. *PLoS Biol*. **1**:E12.

Simmer, F., Tijsterman, M., Parrish, S., Koushika, S.P., Nonet, M.L., Fire, A., Ahringer, J., and Plasterk, R.H. (2002). Loss of the putative RNA-directed RNA polymerase RRF-3 makes C. elegans hypersensitive to RNAi. *Curr Biol*. **12**:1317-1319.

Singaraja, R.R., Hadano, S., Metzler, M., Givan, S., Wellington, C.L., Warby, S., Yanai, A., Gutekunst, C.A., Leavitt, B.R., Yi, H., Fichter, K., Gan, L., McCutcheon, K., Chopra, V., Michel, J., Hersch, S.M., Ikeda, J.E., and Hayden, M.R. (2002). HIP14, a novel ankyrin domain-containing protein, links huntingtin to intracellular trafficking and endocytosis. *Hum Mol Genet*. **11**:2815-2828.

Singaraja, R.R., Huang, K., Sanders, S.S., Milnerwood, A.J., Hines, R., Lerch, J.P., Franciosi, S., Drisdel, R.C., Vaid, K., Young, F.B., Doty, C., Wan, J., Bissada, N., Henkelman, R.M., Green, W.N., Davis, N.G., Raymond, L.A., and Hayden, M.R. (2011). Altered palmitoylation and neuropathological deficits in mice lacking HIP14. *Hum Mol Genet*. **20**:3899-3909.

Singaraja, R.R., Kang, M.H., Vaid, K., Sanders, S.S., Vilas, G.L., Arstikaitis, P., Coutinho, J., Drisdel, R.C., El-Husseini Ael, D., Green, W.N., Berthiaume, L., and Hayden, M.R. (2009). Palmitoylation of ATP-binding cassette transporter A1 is essential for its trafficking and function. *Circ Res*. **105**:138-147.

Skene, J.H., and Virag, I. (1989). Posttranslational membrane attachment and dynamic fatty acylation of a neuronal growth cone protein, GAP-43. *J Cell Biol*. **108**:613-624.

Smardon, A., Spoerke, J.M., Stacey, S.C., Klein, M.E., Mackin, N., and Maine, E.M. (2000). EGO-1 is related to RNA-directed RNA polymerase and functions in germ-line development and RNA interference in C. elegans. *Curr Biol*. **10**:169-178.

Smotrys, J.E., Schoenfish, M.J., Stutz, M.A., and Linder, M.E. (2005). The vacuolar DHHC-CRD protein Pfa3p is a protein acyltransferase for Vac8p. *J Cell Biol*. **170**:1091-1099.

Soyombo, A.A., and Hofmann, S.L. (1997). Molecular cloning and expression of palmitoyl-protein thioesterase 2 (PPT2), a homolog of lysosomal palmitoyl-protein thioesterase with a distinct substrate specificity. *J Biol Chem*. **272**:27456-27463.

Speers, A.E., and Cravatt, B.F. (2004). Profiling enzyme activities in vivo using click chemistry methods. *Chem Biol*. **11**:535-546.

Stowers, R.S., and Isacoff, E.Y. (2007). Drosophila huntingtin-interacting protein 14 is a presynaptic protein required for photoreceptor synaptic transmission and expression of the palmitoylated proteins synaptosome-associated protein 25 and cysteine string protein. *J Neurosci*. **27**:12874-12883.

Strange, K., Christensen, M., and Morrison, R. (2007). Primary culture of Caenorhabditis elegans developing embryo cells for electrophysiological, cell biological and molecular studies. *Nat Protoc*. **2**:1003-1012.

Stryer, L. 1995. Biochemistry. W.H. Freeman and Company.

Sudo, H., Tsuji, A.B., Sugyo, A., Ogawa, Y., Sagara, M., and Saga, T. (2012). ZDHHC8 knockdown enhances radiosensitivity and suppresses tumor growth in a mesothelioma mouse model. *Cancer Sci*. **103**:203-209.

Sulston, J.E., and Horvitz, H.R. (1977). Post-embryonic cell lineages of the nematode, Caenorhabditis elegans. *Dev Biol*. **56**:110-156.

Sutton, L.M., Sanders, S.S., Butland, S.L., Singaraja, R.R., Franciosi, S., Southwell, A.L., Doty, C.N., Schmidt, M.E., Mui, K.K., Kovalik, V., Young, F.B., Zhang, W., and Hayden, M.R. (2012). Hip14l-deficient mice develop neuropathological and behavioural features of Huntington disease. *Hum Mol Genet*.

Swarthout, J.T., Lobo, S., Farh, L., Croke, M.R., Greentree, W.K., Deschenes, R.J., and Linder, M.E. (2005). DHHC9 and GCP16 constitute a human protein fatty acyltransferase with specificity for H- and N-Ras. *J Biol Chem*. **280**:31141-31148.

Tabara, H., Grishok, A., and Mello, C.C. (1998). RNAi in C. elegans: soaking in the genome sequence. *Science*. **282**:430-431.

Takemoto-Kimura, S., Ageta-Ishihara, N., Nonaka, M., Adachi-Morishima, A., Mano, T., Okamura, M., Fujii, H., Fuse, T., Hoshino, M., Suzuki, S., Kojima, M., Mishina, M., Okuno, H., and Bito, H. (2007). Regulation of dendritogenesis via a lipid-raft-associated Ca2+/calmodulin-dependent protein kinase CLICK-III/CaMKIgamma. *Neuron*. **54**:755-770.

Thomas, G.M., Hayashi, T., Chiu, S.L., Chen, C.M., and Huganir, R.L. (2012). Palmitoylation by DHHC5/8 targets GRIP1 to dendritic endosomes to regulate AMPA-R trafficking. *Neuron*. **73**:482-496.

Tian, L., McClafferty, H., Jeffries, O., and Shipston, M.J. (2010). Multiple palmitoyltransferases are required for palmitoylation-dependent regulation of large conductance calcium- and voltage-activated potassium channels. *J Biol Chem*. **285**:23954-23962.

Tian, L., McClafferty, H., Knaus, H.G., Ruth, P., and Shipston, M.J. (2012). Distinct acyl protein transferases and thioesterases control surface expression of calcium-activated potassium channels. *J Biol Chem*. **287**:14718-14725.

Timmons, L., Court, D.L., and Fire, A. (2001). Ingestion of bacterially expressed dsRNAs can produce specific and potent genetic interference in Caenorhabditis elegans. *Gene*. **263**:103-112.

Timmons, L., and Fire, A. (1998). Specific interference by ingested dsRNA. *Nature*. **395**:854.

Topinka, J.R., and Bredt, D.S. (1998). N-terminal palmitoylation of PSD-95 regulates association with cell membranes and interaction with K+ channel Kv1.4. *Neuron*. **20**:125-134.

Tsutsumi, R., Fukata, Y., Noritake, J., Iwanaga, T., Perez, F., and Fukata, M. (2009). Identification of G protein alpha subunit-palmitoylating enzyme. *Mol Cell Biol*. **29**:435-447.

Turnbull, A.P., Kummel, D., Prinz, B., Holz, C., Schultchen, J., Lang, C., Niesen, F.H., Hofmann, K.P., Delbruck, H., Behlke, J., Muller, E.C., Jarosch, E., Sommer, T., and Heinemann, U. (2005). Structure of palmitoylated BET3: insights into TRAPP complex assembly and membrane localization. *EMBO J*. **24**:875-884.

Uemura, T., Mori, H., and Mishina, M. (2002). Isolation and characterization of Golgi apparatus-specific GODZ with the DHHC zinc finger domain. *Biochem Biophys Res Commun*. **296**:492-496.

Uittenbogaard, A., and Smart, E.J. (2000). Palmitoylation of caveolin-1 is required for cholesterol binding, chaperone complex formation, and rapid transport of cholesterol to caveolae. *J Biol Chem*. **275**:25595-25599.

Valdez-Taubas, J., and Pelham, H. (2005). Swf1-dependent palmitoylation of the SNARE Tlg1 prevents its ubiquitination and degradation. *EMBO J*. **24**:2524-2532.

Vallin, E., Gallagher, J., Granger, L., Martin, E., Belougne, J., Maurizio, J., Duverger, Y., Scaglione, S., Borrel, C., Cortier, E., Abouzid, K., Carre-Pierrat, M., Gieseler, K., Segalat, L., Kuwabara, P.E., and Ewbank, J.J. (2012). A genome-wide collection of Mos1 transposon insertion mutants for the C. elegans research community. *PLoS One*. **7**:e30482.

Van Raamsdonk, J.M., and Hekimi, S. (2012). Superoxide dismutase is dispensable for normal animal lifespan. *Proc Natl Acad Sci U S A*. **109**:5785-5790.

Veit, M. (2000). Palmitoylation of the 25-kDa synaptosomal protein (SNAP-25) in vitro occurs in the absence of an enzyme, but is stimulated by binding to syntaxin. *Biochem J*. **345 Pt 1**:145-151.

Veit, M., Becher, A., and Ahnert-Hilger, G. (2000). Synaptobrevin 2 is palmitoylated in synaptic vesicles prepared from adult, but not from embryonic brain. *Mol Cell Neurosci*. **15**:408-416.

Veit, M., Sollner, T.H., and Rothman, J.E. (1996). Multiple palmitoylation of synaptotagmin and the t-SNARE SNAP-25. *FEBS Lett*. **385**:119-123.

Velinov, M., Dolzhanskaya, N., Gonzalez, M., Powell, E., Konidari, I., Hulme, W., Staropoli, J.F., Xin, W., Wen, G.Y., Barone, R., Coppel, S.H., Sims, K., Brown, W.T., and Zuchner, S. (2012). Mutations in the gene DNAJC5 cause autosomal dominant Kufs disease in a proportion of cases: study of the Parry family and 8 other families. *PLoS One*. **7**:e29729.

Verkruyse, L.A., and Hofmann, S.L. (1996). Lysosomal targeting of palmitoyl-protein thioesterase. *J Biol Chem*. **271**:15831-15836.

Vesa, J., Hellsten, E., Verkruyse, L.A., Camp, L.A., Rapola, J., Santavuori, P., Hofmann, S.L., and Peltonen, L. (1995). Mutations in the palmitoyl protein thioesterase gene causing infantile neuronal ceroid lipofuscinosis. *Nature*. **376**:584-587.

Vetrivel, K.S., Meckler, X., Chen, Y., Nguyen, P.D., Seidah, N.G., Vassar, R., Wong, P.C., Fukata, M., Kounnas, M.Z., and Thinakaran, G. (2009). Alzheimer disease Abeta production in the absence of S-palmitoylation-dependent targeting of BACE1 to lipid rafts. *J Biol Chem*. **284**:3793-3803.

Vilinsky, I., Stewart, B.A., Drummond, J., Robinson, I., and Deitcher, D.L. (2002). A Drosophila SNAP-25 null mutant reveals context-dependent redundancy with SNAP-24 in neurotransmission. *Genetics*. **162**:259-271.

Wang, D., Kennedy, S., Conte, D., Jr., Kim, J.K., Gabel, H.W., Kamath, R.S., Mello, C.C., and Ruvkun, G. (2005). Somatic misexpression of germline P granules and enhanced RNA interference in retinoblastoma pathway mutants. *Nature*. **436**:593-597.

Wang, J., Xie, Y., Wolff, D.W., Abel, P.W., and Tu, Y. (2010). DHHC protein-dependent palmitoylation protects regulator of G-protein signaling 4 from proteasome degradation. *FEBS Lett*. **584**:4570-4574.

Wang, X.B., Wu, L.Y., Wang, Y.C., and Deng, N.Y. (2009). Prediction of palmitoylation sites using the composition of k-spaced amino acid pairs. *Protein Eng Des Sel*. **22**:707-712.

Wedegaertner, P.B., and Bourne, H.R. (1994). Activation and depalmitoylation of Gs alpha. *Cell*. **77**:1063-1070.

Winston, W.M., Molodowitch, C., and Hunter, C.P. (2002). Systemic RNAi in C. elegans requires the putative transmembrane protein SID-1. *Science*. **295**:2456-2459.

Wu, H., and Brennwald, P. (2010). The function of two Rho family GTPases is determined by distinct patterns of cell surface localization. *Mol Cell Biol*. **30**:5207-5217.

Xu, M., Clair, D.S., and He, L. (2010). Testing for genetic association between the ZDHHC8 gene locus and susceptibility to schizophrenia: An integrated analysis of multiple datasets. *Am J Med Genet B Neuropsychiatr Genet*. **153B**:1266-1275.

Yamamoto, Y., Chochi, Y., Matsuyama, H., Eguchi, S., Kawauchi, S., Furuya, T., Oga, A., Kang, J.J., Naito, K., and Sasaki, K. (2007). Gain of 5p15.33 is associated with progression of bladder cancer. *Oncology*. **72**:132-138.

Yanai, A., Huang, K., Kang, R., Singaraja, R.R., Arstikaitis, P., Gan, L., Orban, P.C., Mullard, A., Cowan, C.M., Raymond, L.A., Drisdel, R.C., Green, W.N., Ravikumar, B., Rubinsztein, D.C., El-Husseini, A., and Hayden, M.R. (2006). Palmitoylation of huntingtin by HIP14 is essential for its trafficking and function. *Nat Neurosci*. **9**:824-831.

Yang, G., and Cynader, M.S. (2011). Palmitoyl acyltransferase zD17 mediates neuronal responses in acute ischemic brain injury by regulating JNK activation in a signaling module. *J Neurosci*. **31**:11980-11991.

Yang, J., Brown, M.S., Liang, G., Grishin, N.V., and Goldstein, J.L. (2008). Identification of the acyltransferase that octanoylates ghrelin, an appetite-stimulating peptide hormone. *Cell*. **132**:387-396.

Yang, J.S., Nam, H.J., Seo, M., Han, S.K., Choi, Y., Nam, H.G., Lee, S.J., and Kim, S. (2011). OASIS: online application for the survival analysis of lifespan assays performed in aging research. *PLoS One*. **6**:e23525.

Yang, S.H., Shrivastav, A., Kosinski, C., Sharma, R.K., Chen, M.H., Berthiaume, L.G., Peters, L.L., Chuang, P.T., Young, S.G., and Bergo, M.O. (2005). N-myristoyltransferase 1 is essential in early mouse development. *J Biol Chem*. **280**:18990-18995.

Yang, W., Di Vizio, D., Kirchner, M., Steen, H., and Freeman, M.R. (2010). Proteome scale characterization of human S-acylated proteins in lipid raft-enriched and non-raft membranes. *Mol Cell Proteomics*. **9**:54-70.

Yeh, D.C., Duncan, J.A., Yamashita, S., and Michel, T. (1999). Depalmitoylation of endothelial nitric-oxide synthase by acyl-protein thioesterase 1 is potentiated by Ca(2+)-calmodulin. *J Biol Chem*. **274**:33148-33154.

Young, F.B., Franciosi, S., Spreeuw, A., Deng, Y., Sanders, S., Tam, N.C., Huang, K., Singaraja, R.R., Zhang, W., Bissada, N., Kay, C., and Hayden, M.R. (2012). Low levels of human HIP14 are sufficient to rescue neuropathological, behavioural, and enzymatic defects due to loss of murine HIP14 in Hip14-/- mice. *PLoS One*. **7**:e36315.

Yount, J.S., Moltedo, B., Yang, Y.Y., Charron, G., Moran, T.M., Lopez, C.B., and Hang, H.C. (2010). Palmitoylome profiling reveals S-palmitoylation-dependent antiviral activity of IFITM3. *Nat Chem Biol*. **6**:610-614.

Zha, J., Weiler, S., Oh, K.J., Wei, M.C., and Korsmeyer, S.J. (2000). Posttranslational N-myristoylation of BID as a molecular switch for targeting mitochondria and apoptosis. *Science*. **290**:1761-1765.

Zhang, J., Planey, S.L., Ceballos, C., Stevens, S.M., Jr., Keay, S.K., and Zacharias, D.A. (2008). Identification of CKAP4/p63 as a major substrate of the palmitoyl acyltransferase DHHC2, a putative tumor suppressor, using a novel proteomics method. *Mol Cell Proteomics*. **7**:1378-1388.

Zhang, S., Banerjee, D., and Kuhn, J.R. (2011). Isolation and culture of larval cells from C. elegans. *PLoS One*. **6**:e19505.

Zhang, Z., Mandal, A.K., Wang, N., Keck, C.L., Zimonjic, D.B., Popescu, N.C., and Mukherjee, A.B. (1999). Palmitoyl-protein thioesterase gene expression in the developing mouse brain and retina: implications for early loss of vision in infantile neuronal ceroid lipofuscinosis. *Gene*. **231**:203-211.

Zinsmaier, K.E., Eberle, K.K., Buchner, E., Walter, N., and Benzer, S. (1994). Paralysis and early death in cysteine string protein mutants of Drosophila. *Science*. **263**:977-980.

Zou, C., Ellis, B.M., Smith, R.M., Chen, B.B., Zhao, Y., and Mallampalli, R.K. (2011). Acyl-CoA:lysophosphatidylcholine acyltransferase I (Lpcat1) catalyzes histone protein O-palmitoylation to regulate mRNA synthesis. *J Biol Chem*. **286**:28019-28025.